Università degli Studi di Ferrara

DOCTORAL COURSE IN
CHEMICAL
SCIENCES

CYCLE XXXVIII

COORDINATOR Prof. Alessandro Massi

Synthesis and biological evaluation of proteasome modulators for treatment of cancer and neurodegenerative diseases

Scientific/Disciplinary Sector (SDS) CHEM-07/A

Candidate
Ravagli Silvia

Supervisor
Prof. Preti Delia

Co-Supervisor
Prof. Pacifico Salvatore

Years 2022/2025

ABSTRACT

The *ubiquitin–proteasome* system represents a fundamental mechanism for intracellular protein degradation, that has a central role into the mainteanance of cellular homeostasis: this system, that works by two different phases, guarantees the balance of proteomic content of cells, thanks the correct recognition, digestion and elimination of unfolded or mutated proteins.

The proteasome-regulated proteolytic process represents a highly significant pharmaceutical target, as its dysfunction has been implicated in a wide range of pathological conditions. In particular, alterations in proteasome activity have been associated with:

- **Cancer**, notably **acute myeloid leukemia**, which appears to be linked to **excessive proteasome activity**. This multienzymatic complex represents a promising pharmacological target for therapeutic strategies aimed at inhibiting uncontrolled cell proliferation, by mediating the specific and selective degradation of regulatory proteins (CDKs and IκBs).
- **Neurodegenerative disorders**, such as **Alzheimer's disease**, **Parkinson's disease**, and **dementia**. These pathologies share a common feature of proteostasis imbalance: they are characterized by the accumulation of dysfunctional proteins, which leads to oxidative stress and, often, subsequent cell death. Activation of the proteasome represents a promising pharmacological strategy to restore intracellular homeostasis by promoting the degradation of these protein aggregates and thereby preventing neurodegeneration.

Proteasome inhibition has been extensively studied, and several drugs are currently used in the treatment of acute myeloid leukemia. However, many of these compounds, often peptide-based, are limited by rapid metabolism, potential immunogenicity, and adverse effects such as peripheral neuropathy, hematologic, and gastrointestinal toxicities. As a result, ongoing research is focused on the development of novel proteasome inhibitors with improved safety and pharmacological profiles.

Conversely, *positive modulation* of the proteasome represents a relatively recent therapeutic approach, with several small molecules identified as potential activators. These compounds are frequently discovered through high-throughput screening of chemical and/or drug libraries. Nonetheless, the precise molecular mechanisms by which they enhance proteasome activity have not yet been fully elucidated.

This doctoral thesis is focused on the synthesis and biological evaluation of proteasome modulators. Initial work concentrated on the design and preparation of novel non-peptidic proteasome inhibitors, achieved through cyclization of peptidic structures to form a piperazine core, to which functional groups capable of interacting with the proteasome catalytic site were appended. These compounds

were subsequently evaluated in vitro on HeLa cells using two fluorescent peptide-based probes specifically developed for the assays.

In parallel, a biological screening of an internal compound library across four different cell lines was performed to assess both positive and negative modulation of proteasome activity. This screening identified a new class of small molecules containing a 2-oxoquinoxalinic core, which exhibited moderate proteasome inhibition despite the absence of functional groups directly targeting the catalytic site. Furthermore, the screening revealed a compound of particular interest that displayed significant proteasome-activating activity across all tested cell lines. These compounds are currently undergoing secondary assays to elucidate their mechanism of action.

During a research stay at the University of Alcalá, the opportunity arose to explore an alternative therapeutic approach for neurodegenerative diseases. Efforts were directed toward the synthesis of a multivalent molecule designed for the treatment of Alzheimer's and Parkinson's diseases. This strategy represents an innovative symptomatic intervention, integrating multiple pharmacophores that target distinct pathological pathways within a single molecule, with the aim of reducing the need for polypharmacy and minimizing potential side effects. The efficacy of this compound will be assessed through forthcoming in vitro studies.

1 List of contents

1 INTRODUCTION 4
1.1 PROTEIN DEGRADATION 4
1.1.1 UBIQUITIN AS SIGNALING 5
1.1.2 PROTEASOME 8
1.1.3 PROTEASOME BIOGENESIS 9
1.1.4 ACTIVITY 11
2 PROTEASOME AS A PHARMACEUTICAL TARGET 13
2.1 PROTEASOME INHIBITION 13
2.1.1 PROTEASOME INHIBITORS ON THERAPY 16
2.1.2 MECHANISM OF INHIBITION 17
2.1.3 LIMITATIONS OF PROTEASOME INHIBITORS 20
2.2 PROTEASOME ACTIVATION 22
2.2.1 ROLE OF PROTEASOME'S DYSFUNCTION IN NEURODEGENERATIVE DISEASES 23
2.3 Identifying and profiling Proteasome modulators 26
3 PROJECT 1: SYNTHESIS AND BIOLOGICAL EVALUATION OF SMALL MOLECULES AS NEW POTENTIAL PROTEASOME INHIBITORS 30
3.1 AIM OF THE PROJECT 32
3.2 SYNTHESIS 37
3.3 Synthesis of the Diagnostic Probes 56
3.4 BIOLOGICAL EVALUATION 62
3.5 CONCLUSION 67
3.6 EXPERIMENTAL SECTION 70
3.6.1 Materials and Methods 70
3.6.2 General synthetic procedures for synthesis of piperazine core 70
3.6.3 SYNTHESIS FLUORESCENT PROBES 98
3.7 BIOLOGICAL EXPERIMENTAL SECTION 102
3.7.1 Materials and Methods 102
3.7.2 Sample Preparation Procedures 102
3.7.3 Cell Seeding 102
3.7.4 Loading of Compounds 103
3.7.5 Loading of Fluorescent Probes 104
3.7.6 Sample Preparation for FACS Analysis 104
3.7.7 Calculation of Activity Values 105
4 PROJECT 2: BIOLOGICAL SCREENING OF INTERNAL LIBRARY OF COMPOUNDS 108
Lack of Standard Assays for Efficacy Studies 108
4.1 AIM OF THE PROJECT 109

5 PROJECT 2a: SYNTHESIS AND BIOLOGICAL EVALUATION OF PROTEASOME INHIBITORS WITH QUINOXALIN-2-ONE STRUCTURE 113
5.1 AIM OF THE STUDY 117
5.2 SYNTHESIS 119
5.3 BIOLOGICAL TESTS AND RESULTS 123
5.4 CONCLUSIONS 127
5.5 EXPERIMENTAL PROCEDURES 129
5.6 BIOLOGICAL EXPERIMENTAL SECTION 136
5.6.1 Materials and Methods 136
5.6.2 Calculation of Activity Values 136
6 PROJECT 2b. Targeting Proteasome Activation: A New Therapeutic Avenue for Neurodegeneration 139
6.1 AIM OF THE PROJECT 140
6.2 Biological Screening and Evaluation of Proteasome Modulatory Activity 141
6.3 SYNTHESIS 146
6.4 CONCLUSIONS 147
7 Future perspective 149
7.1 Biological Evaluation of Proteasome Modulators 149
Evaluation on Purified 20S Proteasome 149
Apoptosis Assay 150
Western Blot Analysis 150
Quantitative PCR Analysis 150
Photoaffinity Labeling for Mechanistic Elucidation of Proteasome Modulation 151
7.2 EXPERIMENTAL SECTION 154
7.2.1 Materials and Methods 154
7.3 BIOLOGICAL EXPERIMENTAL SECTION 157
7.3.1 Materials and Methods 157
7.3.2 Calculation of Activity Values 157
8 PROJECT 3: SYNTHESIS OF MULTIVALENT MOLECULE FOR A NEW THERAPEUTICAL APPROCH OF NEURODEGENERATIVE DISEASES 160
PHARMACOLOGICAL THERAPIES OF NEURODEGENERATIVE DISEASES 160
8.1 EPIGENETIC MECHANISM 162
8.2 HDAC INHIBITORS 162
8.3 HDACs INHIBITORS IN NEURODEGENERATIVE DISEASES 165
8.3.1 HDACs INHIBITORS IN PARKINSON'S DISEASE 165
8.3.2 HDACs INHIBITORS IN ALZHEIMER'S DISEASE 168
8.4 NEW THERAPEUTICAL STRATEGY FOR NEURODEGENERATIVE DISEASES 173
8.5 AIM OF THE THESIS 176
8.6 SYNTHETIC STRATEGY 180

8.7 CONCLUSIONS 183
8.8 EXPERIMENTAL PROCEDURE 185
8.8.1 Methods and materials 185
9 BIBLIOGRAPHY 189

1 INTRODUCTION

The *ubiquitin–proteasome* system represents a central mechanism for intracellular protein degradation; however, its discovery dates back only to the end of the last century. Its in-depth study followed the discovery of lysosomes, which were initially thought to be solely responsible for intracellular proteolysis. Thanks to various experimental findings, the existence of additional intracellular degradation pathways has been confirmed.

1.1 PROTEIN DEGRADATION

Intracellular protein levels are regulated not only by their rates of synthesis, but also by the efficiency and specificity of their degradation. Protein half-lives within cells can differ significantly, ranging from just a few minutes to several days, underscoring the importance of selective degradation for cellular homeostasis. Proteins that are subject to rapid degradation often play key regulatory roles, such as transcription factors, whose timely turnover is essential to ensure swift cellular responses to external stimuli.

Additionally, certain proteins undergo accelerated degradation upon receiving specific intracellular signals, thereby contributing to the dynamic control of enzymatic activities and broader cellular functions. The prompt removal of aberrant, misfolded, or damaged proteins also serves as a critical quality control mechanism, preventing the accumulation of non-functional or potentially toxic species.
In eukaryotic cells, protein degradation is primarily governed by two distinct and complementary pathways: the *ubiquitin–proteasome system* and *lysosome-mediated proteolysis*. [1]

Extracellular proteins, such as blood coagulation factors, albumin, and peptide hormones, are internalized via pinocytosis or receptor-mediated endocytosis. They are transported in vesicles that subsequently fuse with lysosomes, where they are degraded by **lysosomal proteases**. Throughout this entire process, extracellular self proteins are never exposed to the cytosol.
In contrast, *intracellular* proteins are primarily processed through a highly specific, **non-lysosomal proteolytic** mechanism involving the proteasome, in conjunction with a ubiquitin-based signaling pathway. This type of proteolysis plays a key role in numerous cellular processes, including cell cycle regulation and cell division, DNA repair, cellular stress response, immune response regulation, and antigen processing for presentation via major histocompatibility complex class I (MHC I).

Finally, proteins that are mutated, denatured, or misfolded are efficiently recognized and eliminated by this system.[2]

1.1.1 UBIQUITIN AS SIGNALING

The proteolytic mechanism of the ubiquitin–proteasome system begins with the covalent *labeling* of substrate proteins through the attachment of multiple ubiquitin molecules.
Structurally, *ubiquitin* is a 76-amino acid protein with a C-terminal glycine residue that is essential for conjugation to substrate proteins via a peptide bond with the free amino group. Although lysine is the most common residue involved in this linkage, other amino acids such as cysteine, threonine, and serine can also participate, albeit to a minor extent.

Ubiquitin conjugation occurs through a multi-step, enzyme-mediated cascade:

- **E1** (ubiquitin-activating enzyme) activates ubiquitin in an ATP-dependent manner, generating a high-energy intermediate;
- **E2** (ubiquitin-carrier or conjugating protein) recognizes the activated E1–ubiquitin complex and mediates its transfer;
- **E3** (ubiquitin-protein ligase) catalyzes the final step, facilitating the covalent attachment of ubiquitin to the target substrate.[3]

More recent studies [4] have identified an additional enzyme, **E4**, which appears to be involved in the terminal stage of ubiquitination, specifically in the elongation of the polyubiquitin chain. E4 collaborates with E1, E2, and E3 to assemble polyubiquitin chains by sequentially adding activated ubiquitin units. This process generates a polyubiquitin chain with high binding affinity for the proteasome, thereby ensuring selective substrate recognition.

Notably, E4 can recognize specific regions on substrates that have already been modified with ubiquitin and catalyze the formation of new ubiquitin linkages at those sites. Finally, ubiquitin molecules can be cleaved from the substrate by deubiquitinating enzymes (DUBs) associated with the proteasome and recycled for subsequent rounds of ubiquitination, thereby contributing to a highly efficient biological recycling system.
General process of ubiquitination is illustrated in *Figure 1*.

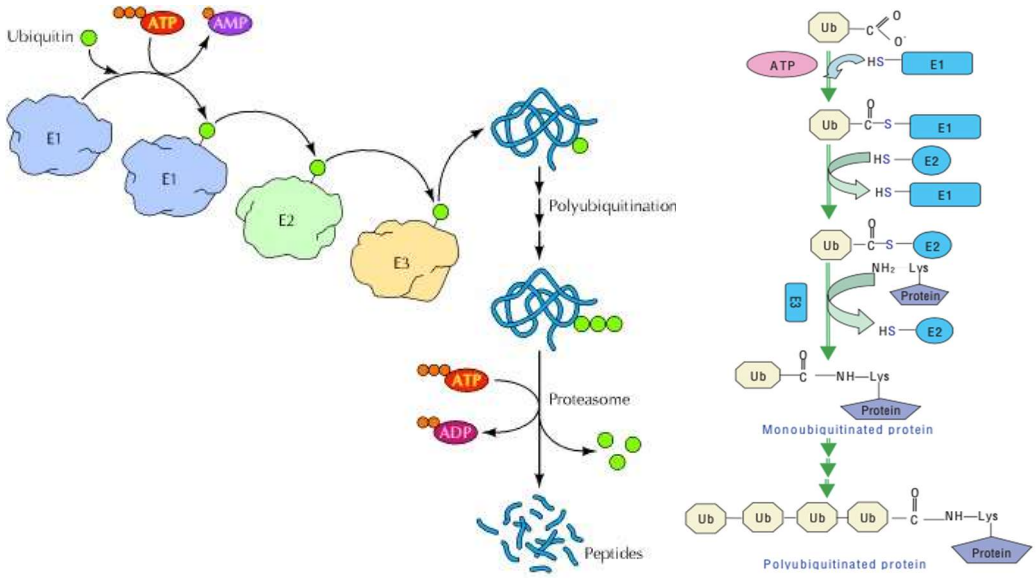

Figure 1. *Ubiquitination process.* On the left,[5] the activation of ubiquitin and its attachment to the target protein is shown, mediated by the action of the enzymes mentioned above. On the right,[6] the process is illustrated from a chemical perspective, highlighting the interaction between the protein and the enzymes involved.

Based on the chemical reactions involved in its biosynthetic pathway, the ubiquitination process can be divided into several stages [7]:

- The initial step is an *adenylation reaction*. Ubiquitin (Ubi) reacts with ATP at the carboxyl terminal glycine residue, releasing pyrophosphate (PPi). A magnesium ion participates in this reaction by reducing electrostatic repulsion between the phosphate groups of ATP and the carboxyl group of ubiquitin (*Figure 2*).

Figure 2. First step of adenylation.

- Subsequently, a reactive thioester bond is formed between the adenylated ubiquitin and the E1 enzyme through the thiol group of a cysteine residue, which performs a nucleophilic attack, resulting in the release of AMP (*Figure 3*).

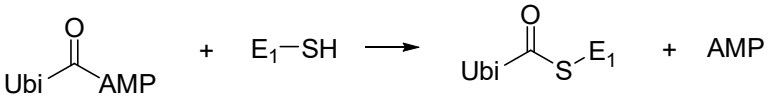

Figure 3. Second step of thioesterification.

- Once the active intermediate is formed, a transthiolation reaction transfers ubiquitin from E1 to the E2 conjugating enzyme, again involving a cysteine thiol. This reaction releases the E1 enzyme, making it available for further rounds of adenylation (*Figure 4*).

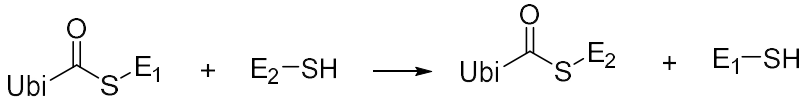

Figure 4. Third step of transthiolation.

These reactions proceed through a conserved mechanism. The determining factor lies in the E3 enzyme: to date, only a single E1 enzyme has been identified, approximately 20 E2 enzymes are known, whereas a considerably larger number of E3 enzymes exist. This hierarchical structure allows for highly specific interactions, which are essential to ensure selective degradation of cellular proteins and thereby promote cell survival.

E3 enzymes can be classified into two main categories [8]:

a. E3 enzymes containing the HECT domain (Homologous to the E6-AP COOH terminus) and a catalytic cysteine residue. These enzymes form a covalent bond with ubiquitin prior to its transfer to the substrate. E3s then catalyze the formation of an isopeptide bond between the C-terminal glycine of ubiquitin and the ε-amino group of a lysine residue on the target protein; if the lysine is absent, the N-terminal amino group can instead be used as the acceptor (*Figure 5*).

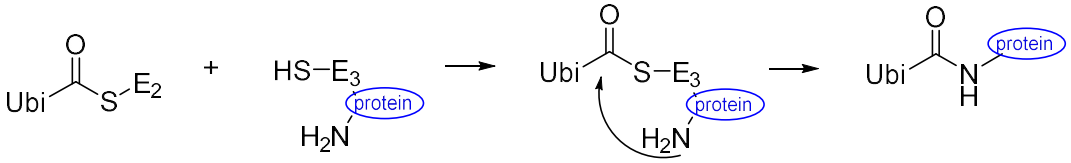

Figure 5. E3 containing the HECT-domain

b. E3 enzymes containing the RING domain (Really Interesting New Gene): these facilitate the transfer of ubiquitin from E2 directly to the target protein without forming a thioester intermediate (*Figure 6*).

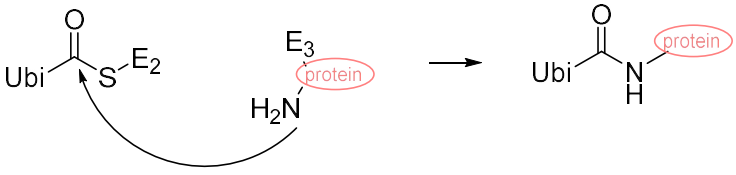

Figure 6. E3 containing the RING domain.

The mono-ubiquitinated protein is subsequently modified by E4 to form a polyubiquitin chain. The bond formed is an amide linkage between the C-terminus of the newly added ubiquitin molecule and the ε-amino group of lysine 48 on the ubiquitin at the end of the chain, a site specifically recognized by E4 [4,8].

The specificity for proteins to be ubiquitinated is conferred by the E3 enzyme, and several hypotheses exist regarding this recognition mechanism. One proposed model suggests that selectivity arises from the interaction with the substrate via short linear sequences, known as PEST motifs. These motifs are predominantly composed of proline, glutamic acid, aspartic acid, serine, and threonine residues and represent regions enriched in phosphorylation signals associated with protein degradation. An alternative mechanism involves substrate recruitment through globular protein folds, which expose distinct and characteristic surface regions. These features facilitate the recognition of misfolded, damaged, or denatured proteins that are readily targeted for degradation. [9,10]

1.1.2 PROTEASOME

The proteasome is a large multicatalytic protease complex found in eukaryotic cells, particularly within the nucleus and the cytosol. It consists of a *core* particle, known as the *20S proteasome*, which is associated with one or two regulatory particles, commonly referred to as the *19S CAP* (or PA700). The core structure has a cylindrical shape, with a central opening approximately 1.3 nm in diameter. This narrow channel is believed to prevent the entry of most proteins that lack the specific recognition signals required for access and gate opening. Furthermore, this structural restriction also contributes to the reduction in size of the degradation products released after proteolysis.

The ***20S proteasome*** is composed of four stacked rings arranged in the sequence α7, β7, β7, and α7, forming a central proteolytic channel. The two α7 rings are positioned at the outer ends, while the two β7 rings occupy the inner positions. Each ring consists of seven subunits. Among the β subunits, β1, β2, and β5 exhibit catalytic activity, whereas the α subunits primarily serve a structural function, stabilizing the β rings and forming the gate that controls substrate entry and the release of degradation products. [11]

The ***19S*** regulatory particle is organized into two distinct subcomplexes. The **lid** comprises nine RPN (Regulatory Particle Non-ATPase) subunits, which lack ATPase activity and are associated with deubiquitinating enzymes. The **base** also contains nine subunits, including six RPT (Regulatory Particle Triple-A ATPase) subunits with ATPase activity and three non-ATPase subunits. Together,

the 20S core particle and the 19S regulatory complex assemble to form the ***26S proteasome***. 26S proteasome general structure is depicted in *Figure 7*.

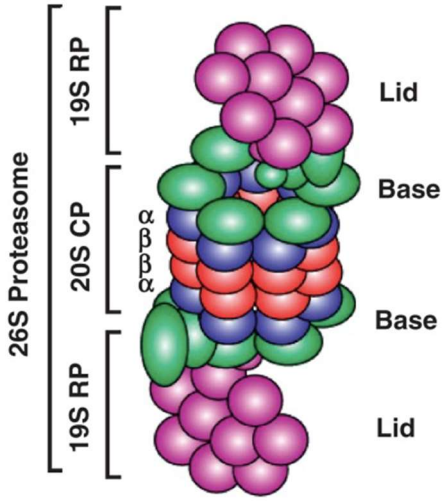

Figure 7. Structure of the 26S proteasome. The 20S core is shown with the seven α subunits in blue, forming the α7 rings, and the seven β subunits in red, forming the β7 rings. The 19S regulatory complex consists of the base (green, 9 subunits) and the lid (purple, 9 subunits).[12]

1.1.3 PROTEASOME BIOGENESIS

Proteasome assembly takes place within the cellular environment. The biosynthetic pathway of the proteasome in mammals has been elucidated using specific antibodies against subunits that serve as precursors to the fully processed structures. This approach enabled the identification of intermediate structures corresponding to proteasome subcomplexes, thereby supporting the hypothesis of a dimerization process in which an α-ring associates with β subunits until the β-ring is also completed.[12] With regard to the synthesis of the α-ring, several proteasome assembly complexes—referred to as **chaperones**—have been identified. These auxiliary factors play a crucial role in guiding biosynthesis, particularly in the assembly of multimeric structures such as the α and β rings of the 20S proteasome. [13]

These chaperones transiently bind α subunits, ensuring correct formation and stabilization of the α-ring. To date, four families of proteasome-dedicated chaperones have been identified: **PBA1, PBA2, PBA3, and PBA4**.

- **PBA1 and PBA2** prevent the aberrant dimerization of two α-rings, as illustrated in *Figure 8*. The precise mechanism by which this is achieved remains unknown. [14]

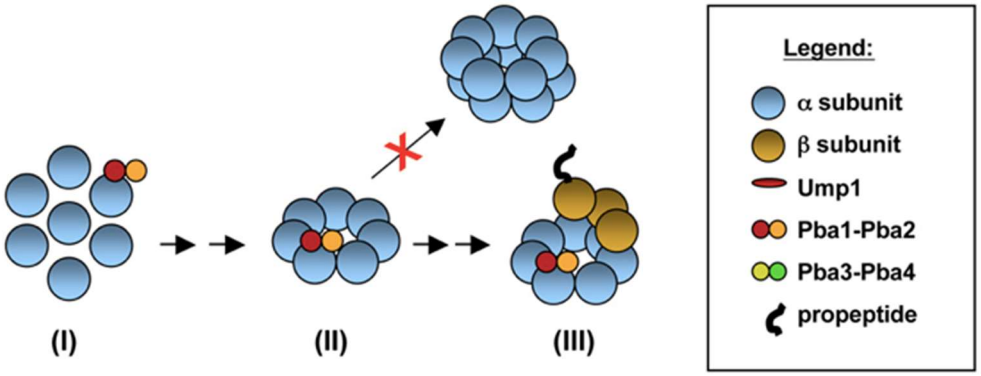

Figure 8. Chaperones PBA1 and PBA2 ensure correct dimerization of the subunits by preventing improper pairing of α subunits.[15]

- **PBA3 and PBA4** specifically bind to α5 subunits and stabilize interactions among the subunits forming the α-ring. As shown in *Figure 9*, the absence of these chaperones leads to incorrect assembly, with multiple α4 subunits competing with α3. This results in structurally defective rings, containing two α4 subunits and lacking α3. [16,17]

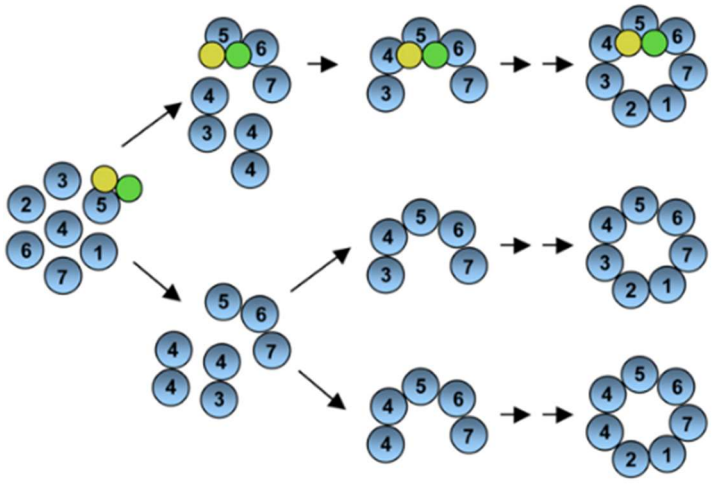

Figure 9. *Top:* PBA3 and PBA4 bind to α5 subunits and stabilize interactions among α-ring subunits. *Bottom:* In the absence of these chaperones, multiple α4 subunits assemble and compete with α3, leading to improper ring formation.[15]

With regard to the β subunits, several studies have demonstrated that their assembly is strictly dependent on the presence of α subunits. Indeed, β subunits require α-ring scaffolding to assemble properly. It is likely that their assembly is also assisted by a dedicated complex composed of molecular chaperones. Among these, **POMP** (Proteasome Maturation Protein, also known as hUP1 or UMP1) plays a fundamental role. In addition to supporting the correct folding and assembly of the structure, POMP protects the N-terminal threonine residue—the catalytic site of the mature complex—from premature reactions that could inactivate it. [18]

This threonine residue becomes exposed through an autocatalytic processing mechanism that occurs within the β1, β2, and β5 subunits .[19]

The first assembly intermediate of the proteasome contains all the α subunits along with a subset of β subunits (β2, β3, and β4), forming a complex known as the **13S particle**. The remaining β subunits are then incorporated sequentially. Finally, upon the addition of the last β subunit (β7), rapid dimerization occurs. At this stage, the propeptides of the β subunits undergo autocatalytic cleavage, completing the assembly of the mature proteasome (*Figure 10*). [20]

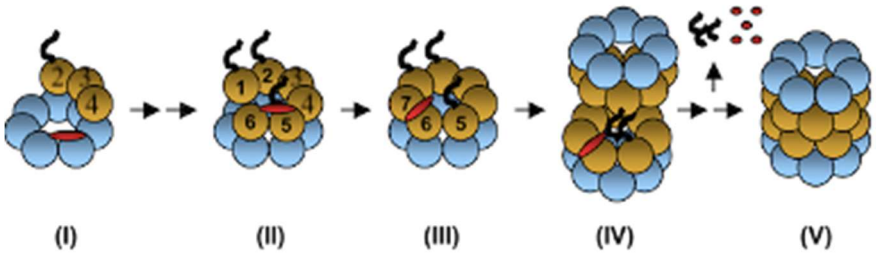

Figure 10. Assembly of the 20S proteasome. (I): A preformed ring of α subunits associated with a subset of β subunits (β1, β2, β4). (II): The presence of UMP1 promotes ring maturation by facilitating the addition of further β subunits and prevents premature dimerization. (III): Addition of β7 subunit. (IV): Dimerization of the half-proteasomes. (V): Removal of the propeptides from the catalytic β subunits.[15]

1.1.4 ACTIVITY

The proteasome discriminates proteins destined for degradation through recognition of the polyubiquitin chain by the 19S regulatory particle, which is associated with specific deubiquitinating enzymes. The lid subunits (RPN) bind the ubiquitylated substrate, enabling the action of proteases that recognize the C-terminal residue of ubiquitin. These enzymes are categorized into two main classes:

- **Ubiquitin C-terminal hydrolases (UCHs)**, which act on ubiquitin adducts with small molecules;
- **Ubiquitin-specific proteases (UBPs)**, which catalyze the release of substrates from polyubiquitin chains. [21]

Once the substrate has been deubiquitinated, the **base of the 19S complex** plays a crucial role in substrate translocation, mainly via the activity of its six ATPase subunits (RPTs), three of which are directly involved in substrate unfolding and translocation. [22]

The adjacent α-ring forms a gate composed of the N-termini of its subunits. The RPTs are responsible for opening this gate and facilitating substrate entry. This is achieved through their **C-terminal tails**,

which contain conserved **HbYX motifs**—regions composed of hydrophobic residues ending with tyrosine. [23]

These motifs insert into intersubunit pockets of the α-ring, inducing conformational changes that open the channel for substrate passage. [24]

As previously mentioned, the actual **catalytic activity** of the proteasome resides in the **β1, β2, and β5** subunits of the inner 20S core. Upon gate opening, the N-terminal threonine residues of these subunits are exposed, enabling proteolytic activity characterized as follows:

- **β1**: Caspase-like activity, cleaving after acidic residues;
- **β2**: Trypsin-like activity, specific for basic residues;
- **β5**: Chymotrypsin-like activity, preferentially cleaving after hydrophobic residues such as phenylalanine, leucine, tryptophan, methionine, and tyrosine.

From a chemical standpoint, the proteolytic process is initiated by a **proton transfer reaction** involving the nitrogen of a **threonine residue** located at the N-terminus, which is present in all catalytic sites—namely β1, β2, and β5. The hydroxyl group of the threonine is deprotonated, thereby increasing its nucleophilicity (*Figure 11*).

This enables efficient nucleophilic attack on the **carbonyl group** of the peptide bond in the protein substrate located within the 20S core channel.

Proteolysis proceeds through a second proton transfer, this time from the nitrogen of threonine to the leaving peptide fragment. The **catalytic site is then regenerated** through the action of a water molecule, completing the catalytic cycle.

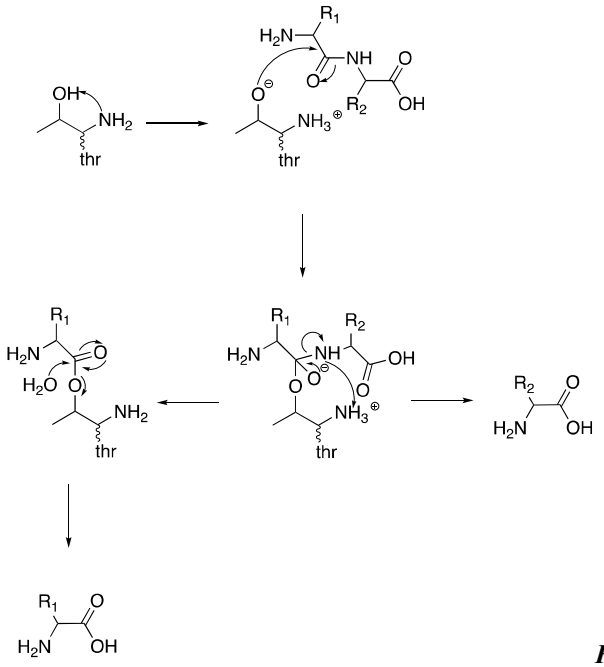

Figure 11. Proteasome-mediated proteolysis.

2 PROTEASOME AS A PHARMACEUTICAL TARGET

Dysregulation of the proteasome-dependent proteolytic machinery has emerged as a highly relevant pharmaceutical target, as impaired proteasome function is implicated in a broad spectrum of pathological conditions. In particular, alterations in proteasome activity have been associated with:

- **Cancer**, notably **acute myeloid leukemia**, which appears to be linked to **excessive proteasome activation**. This overactivation can lead to uncontrolled protein degradation, thereby disrupting cellular homeostasis and promoting tumor progression;
- **Neurodegenerative disorders**, such as **Alzheimer's disease**, **Parkinson's disease**, and **dementia**. These conditions have been associated with **reduced proteasome activity**, leading to the accumulation of misfolded or damaged proteins and contributing to neuronal dysfunction and degeneration.

2.1 PROTEASOME INHIBITION

Given its central role in regulating the selective degradation of key cellular proteins, the proteasome represents a promising pharmacological target for therapeutic strategies aimed at inhibiting uncontrolled cell proliferation, particularly in neoplastic diseases. By mediating the specific and selective degradation of regulatory proteins, the proteasome plays a critical role in the progression of the cell cycle. [25]

Proteasome inhibition primarily acts by interfering with the following key functions:

- **Degradation of CDKs** (Cyclin-Dependent Kinases)**.** *CDKs* are protein kinases whose activity is dependent on cyclins, and they are responsible for phosphorylation events that typically precede ubiquitin-proteasome-mediated degradation.

  Their expression and activity are tightly regulated by the balance between transcriptional regulation and proteasomal turnover. Inhibition of CDKs prevents protein phosphorylation events, thereby blocking subsequent degradation and ultimately leading to cell cycle arrest and apoptosis. Pharmacological studies on proteasome inhibitors have demonstrated that apoptosis is preferentially induced in transformed cells, alleviating concerns regarding potential toxicity to normal, non-mutated cells. For many years, the mechanistic basis for the enhanced sensitivity of cancer cells to proteasome inhibition remained unclear. [26,27]
- **Degradation of IκB proteins.** IκBs are a family of inhibitory proteins that prevent the nuclear translocation of NF-κB, a transcription factor essential for the regulation of immune and inflammatory responses. IκBs can be phosphorylated by IκB kinase (IKK), followed by ubiquitination and subsequent proteasomal degradation. Once IκB proteins are degraded, NF-κB is released and translocates into the nucleus, where it induces the expression of growth

and survival factors. Therefore, **proteasome inhibition** results in **the stabilization of IκB proteins**, preventing NF-κB activation and ultimately blocking the transcriptional induction of nuclear growth-promoting factors.[26,28]

Tumorigenesis involves the deregulation of multiple molecular pathways, several of which are influenced by components of the ubiquitin–proteasome system. Among these, the following have been identified as contributors to tumorigenic progression:[29]

1. **E3 Ubiquitin Ligases and Their Role in Cancer**

   The **Anaphase-Promoting Complex/Cyclosome (APC/C)**, an essential E3 ligase in mitosis, is rarely mutated in cancer. However, its co-activators **CDH1** and **CDC20** are frequently deregulated. CDH1 functions as a tumor suppressor by regulating proteins like BRAF and c-Src, but its activity can be impaired through phosphorylation by ERK, CDK4, or c-Src itself.[30] In contrast, CDC20 is commonly overexpressed in cancers and promotes mitotic exit and cell proliferation, displaying oncogenic properties.[31]

- The **SCF E3 ligase complex**, composed of SKP1, CUL1, and variable F-box proteins, regulates numerous oncogenic pathways. **FBXW7**, a tumor suppressor F-box protein, targets cyclin E, c-Myc, and mTOR for degradation.[32] Its loss or reduced expression is linked to genomic instability, metastasis, and poor prognosis in various cancers.

  Conversely, **SKP2** acts as an oncogene by targeting CDK inhibitors for degradation, promoting uncontrolled proliferation. Pharmacological inhibition of SKP2 restores p27 levels and induces apoptosis in several tumor models.
- **NEDD4-1**, another E3 ligase, exhibits dual roles in cancer. It can promote tumorigenesis via PTEN degradation and AKT activation, yet it also mediates degradation of oncogenic RAS. Its dysregulation contributes to tumor progression, especially in RAS-driven and PTEN-deficient cancers.
- **MDM2**, a well-characterized negative regulator of p53, is often overexpressed in tumors. Its upregulation reduces p53 stability and contributes to chemoresistance, particularly to DNA-damaging agents like cisplatin, by promoting p53 degradation.[33]

2. **Deubiquitinating Enzymes (DUBs) in Oncogenesis**

DUBs counteract the activity of ubiquitin ligases and are critical regulators of cancer-associated pathways. Depending on cellular context, several DUBs function either as oncogenes or tumor suppressors.

- **USP2A** promotes proliferation and drug resistance, particularly in prostate and bladder cancers. However, in glioma cells, it can enhance p53-mediated apoptosis by stabilizing MDM4. [34]
- **USP7** overexpression correlates with increased tumor aggressiveness in prostate, colon, and breast cancers, and promotes Wnt signaling via β-catenin stabilization. [35]
- **CYLD**, a tumor suppressor, inhibits NF-κB signaling by removing ubiquitin chains from key signaling intermediates. Its downregulation in melanoma, hepatocellular carcinoma (HCC), and breast cancer leads to increased cell proliferation and metastasis. [36]
- **A20**, which has both DUB and E3 ligase activities, negatively regulates NF-κB and is often mutated or deleted in lymphomas. In contrast, its overexpression in some solid tumors contributes to therapy resistance.

3. Proteasome-Associated DUBs

Three major DUBs are associated with the 19S regulatory particle: **USP14**, **UCH37**, and **RPN11**. USP14 and UCH37 antagonize proteasomal degradation by trimming ubiquitin chains, while RPN11 promotes substrate degradation by cleaving ubiquitin at the base of the chain.

- **USP14** promotes oncogenesis by stabilizing androgen receptor (AR) and β-catenin, enhancing (epithelial–mesenchymal transition) EMT and Wnt signaling.
- **UCH37** inhibition induces apoptosis in various cancers.[37]
- **RPN11** depletion leads to mitotic arrest and cellular senescence. [38]

2.1.1 PROTEASOME INHIBITORS ON THERAPY

Despite the central role of the *ubiquitin–proteasome system* in maintaining cellular homeostasis, *proteasome inhibitors* (PIs) have demonstrated a favorable safety profile in clinical settings, with a relatively limited spectrum of adverse effects. These agents have shown marked efficacy in hematologic malignancies, particularly *multiple myeloma* and *mantle cell lymphoma*, where they have contributed to significant improvements in both progression-free survival (PFS) and overall survival (OS).

Multiple myeloma represents an especially suitable target for proteasome inhibition due to the high levels of immunoglobulin G (IgG) synthesis characteristic of plasma cells. The elevated protein turnover inherent to myeloma cells creates a therapeutic window in which malignant cells exhibit heightened sensitivity to proteasome inhibition relative to their normal counterparts. [39]

In 2003, the U.S. *Food and Drug Administration* (FDA) approved the first-in-class proteasome inhibitor, ***Bortezomib*** (Velcade, PS-341), for the treatment of relapsed and refractory multiple myeloma. Subsequently, two additional agents—***Carfilzomib*** (Kyprolis) and ***Ixazomib*** (Ninlaro)—have received regulatory approval for the treatment of multiple myeloma.

Among the three, *Ixazomib* is the only orally available compound (administered as a citrate salt), providing a practical advantage in terms of patient compliance due to ease of administration. In contrast, *Bortezomib* and *Carfilzomib* require intravenous administration. [40]

Bortezomib was the first proteasome inhibitor approved for clinical use, exhibiting a unique cytotoxic profile across various tumor cell lines. Preclinical animal models demonstrated a significant capacity to reduce metastasis, thereby providing a strong rationale for clinical investigation. Consequently, several phase I clinical trials were conducted on both solid and hematologic malignancies. In patients with multiple myeloma, promising responses were observed, leading to more targeted phase II studies and ultimately FDA approval. For years, the underlying reason behind the exceptional responsiveness of multiple myeloma to Bortezomib remained unclear, until it was later discovered that the drug inhibits the degradation of IκB.

The success of Bortezomib has sparked widespread interest in targeting the proteasome for cancer therapy. [41]

To date, Ixazomib and Carfilzomib, in addition to Bortezomib, have all been approved by the FDA for the treatment of multiple myeloma.

Furthermore, the indication for *Bortezomib* has been extended to include frontline therapy for both multiple myeloma and mantle cell lymphoma. Additional proteasome inhibitors are currently under

clinical investigation, including ***Marizomib***, which has shown potential therapeutic benefit in patients with glioblastoma.[42]

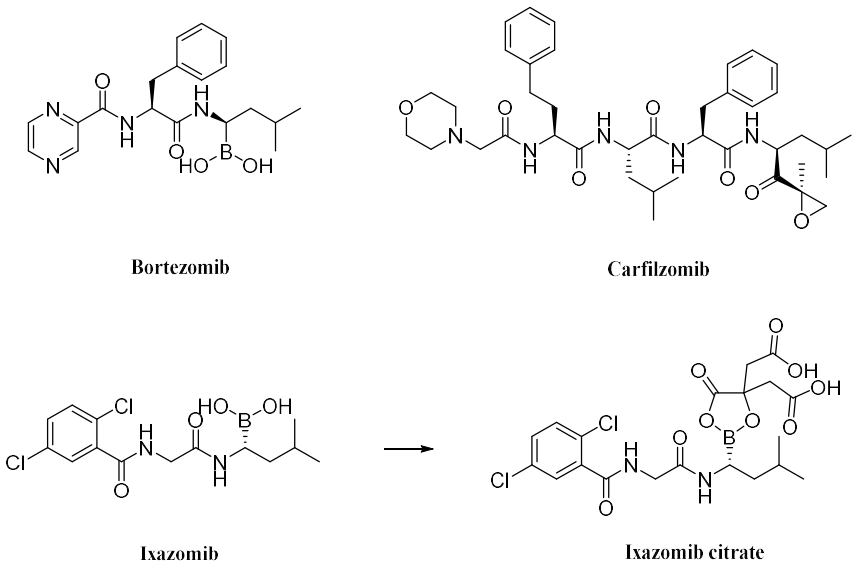

Figure 12. Chemical structures of proteasome inhibitors that are currently approved and used in clinical therapy.

2.1.2 MECHANISM OF INHIBITION

Proteasome inhibitors are commonly categorized according to their binding mechanism, falling into two principal groups: **covalent inhibitors** that form stable interactions with the proteasomal active site, and **non-covalent inhibitors** that associate through reversible, non-covalent forces.

Covalent inhibitors interact with the catalytic threonine residue of the proteasome's β-subunits, forming an adduct whose dissociation rate depends on the stability of the intermediate generated. [43] These synthetic covalent inhibitors are further classified according to the electrophilic warhead they contain**:**

- **Aldehydes:** These compounds inhibit the proteasomes by forming a hemiacetal with the hydroxyl group of the catalytic threonine. An example of this class is MG-132 (*Figure 13A*).
- **Peptide boronates:** These inhibitors form tetrahedral adducts with the active-site threonine, stabilized by a hydrogen bond between the N-terminal amino group of threonine and one of the hydroxyl groups of the boronic acid. Although boronates are generally considered reversible inhibitors, the boronate–proteasome adducts exhibit significantly slower dissociation rates compared to aldehyde–proteasome complexes. A key clinical implication of this slow dissociation, particularly with bortezomib, is that, once the drug binds to the proteasome in red blood cells, it cannot be readily released. In light of this, second-generation boronates have been designed to possess faster off-rates (*Figure 13B*).

- **Epoxyketone peptides:** These are the most potent and specific proteasome inhibitors identified to date. They form a six-membered morpholine ring involving the N-terminal threonine and the epoxide moiety of the inhibitor. Structural studies suggest that the catalytic hydroxyl group first attacks the ketone group of the pharmacophore, followed by nucleophilic attack of the threonine's amino group on the epoxide, completing the adduct formation. A representative compound of this class is carfilzomib, which induces stronger inhibition of chymotrypsin-like activity in patient blood samples than bortezomib (*Figure 13C*).
- **Peptide ketoaldehydes:** These compounds promote the formation of a unique six-membered ring with the N-terminal catalytic threonine. The resulting ring contains both a hemiketal and a Schiff base; the latter is reversible, allowing this class of inhibitors to occupy a distinct niche as covalent yet reversible inhibitors (*Figure 13D*).
- **β-lactones:** These are non-peptidic natural products. The most prominent member of this class is *Marizomib*, a natural compound that esterifies the hydroxyl group of the catalytic threonine. In the presence of a chlorine atom, β-lactone ring opening is followed by the formation of a tetrahydrofuran ring. All β-lactone–proteasome adducts are slowly hydrolyzed by water, resulting in eventual proteasome reactivation, making these inhibitors reversible (*Figure 13E*).
- **Peptide vinyl sulfones:** These synthetic proteasome inhibitors act via Michael addition, wherein the hydroxyl group of the catalytic threonine reacts with the vinyl sulfone double bond. While vinyl sulfones are more synthetically accessible than epoxyketones, they are generally less potent and less specific. Nevertheless, they provide valuable advantages for the development of activity-based probes to assess proteasome function. [44]

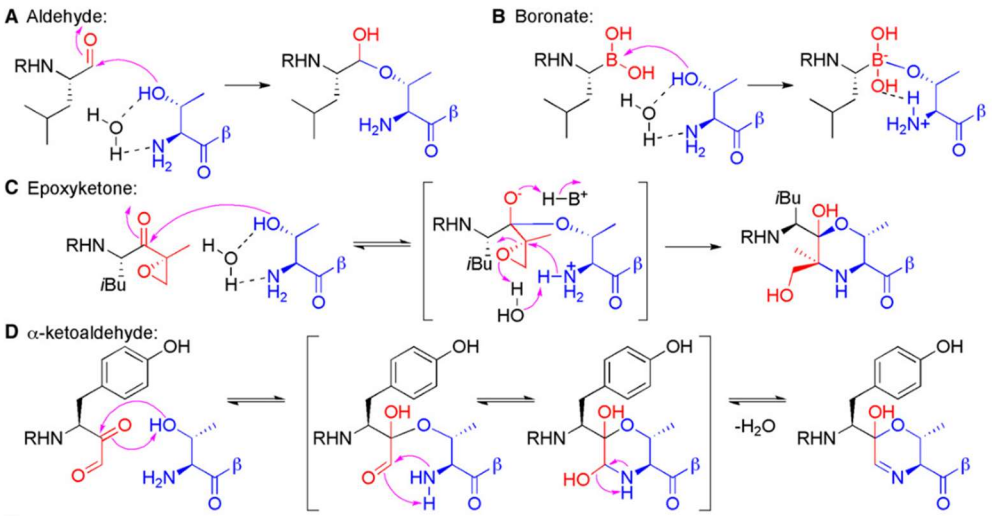

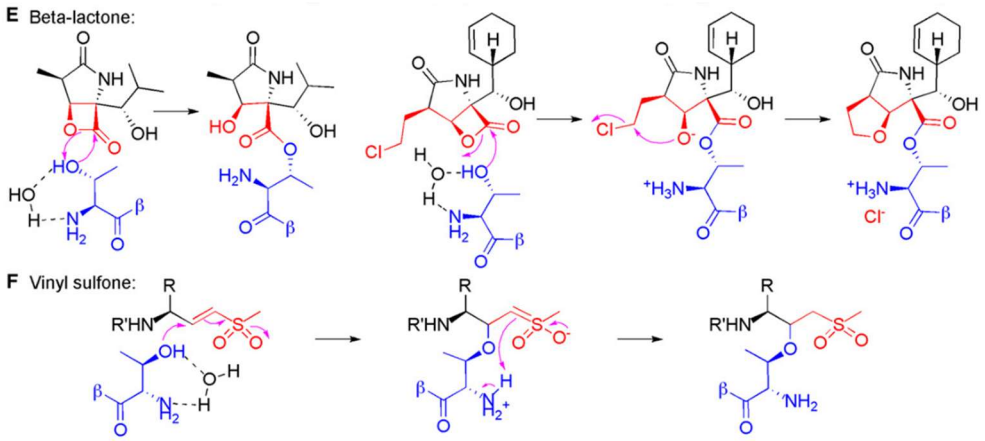

Figure 13A–F. Representative classes of covalent proteasome inhibitors, illustrating their chemical structures and the mode of interaction with the proteasomal active site.[45]

Non-covalent inhibitors are divided into two main classes:

- **Cyclic peptides:** These conformationally constrained molecules bind to all catalytic subunits and primarily act by sterically blocking substrate access to the catalytic threonine residues. The precise mode of binding to the active sites remains to be fully elucidated. A representative example of this class is TMC-95A (*Figure 14*). [46]
- **Acyclic peptides:** These compounds bind to the substrate-binding region by mimicking the upstream polypeptide chain of natural proteasome substrates. The first example in this category was the HIV protease inhibitor Ritonavir. Structural optimization of this compound led to the development of a series of selective inhibitors targeting the chymotrypsin-like site, resulting in the generation of potent dipeptidic inhibitors. [47]

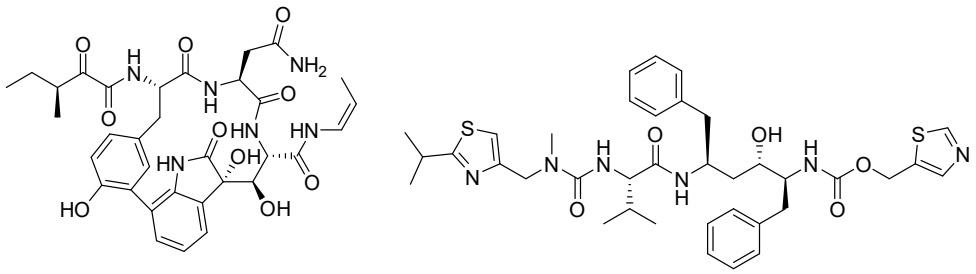

A) **TMC-95** B) **Ritonavir**

Figure 14. Chemical structures of representative non-covalent proteasome inhibitors: (A) TMC-95A and (B) Ritonavir.

2.1.3 LIMITATIONS OF PROTEASOME INHIBITORS

Although proteasome inhibitors have shown significant efficacy in treating multiple myeloma, most clinically approved agents are short peptide-based molecules, which present intrinsic limitations such as poor stability against proteolytic degradation, limited membrane permeability, and low oral bioavailability. [48]

Furthermore, their use has been associated with a range of clinically relevant toxicities, arising either from mechanism-related effects or from drug-specific adverse reactions. The initial safety profile was established through numerous clinical trials involving *Bortezomib*. [49]

It is also important to note that these toxicities occur against the backdrop of a high disease burden typical of multiple myeloma. The acronym **CRAB** summarizes the main complications associated with the disease: **C**alcium elevation (hypercalcemia), **R**enal insufficiency, **A**nemia, and **B**one lesions. [50]

Peripheral neuropathy is among the most debilitating side effects for patients, especially in its painful form. Current research suggests that its pathogenesis may involve multiple mechanisms, including Schwann cell-mediated demyelination, neuronal dysfunction, and glutamate homeostasis imbalance mediated by astrocytes.[51] This adverse event often necessitates dose reduction or discontinuation of bortezomib, thereby limiting therapeutic efficacy in a subset of patients. In contrast, carfilzomib and ixazomib are associated with a substantially lower incidence of peripheral neuropathy.

Hematologic toxicities represent another relevant concern. In early phase III trials with bortezomib, **thrombocytopenia** was observed, which has been attributed to the drug's capacity to increase activation levels of Rho kinase—a negative regulator of proplatelet formation—resulting in reduced platelet counts.[52] Nonetheless, studies have reported very few serious bleeding events or treatment discontinuations attributable to any of the approved proteasome inhibitors, including bortezomib, carfilzomib, and ixazomib.

Gastrointestinal toxicities are also commonly associated with proteasome inhibitors, manifesting as diarrhea, nausea, constipation, and vomiting. These effects are generally manageable. While the precise link between proteasome inhibition and gastrointestinal symptoms remains unclear, it has been hypothesized that the primary pathway contributing to such toxicity may involve **IkB-dependent dysregulation of NF-κB signaling**.[53]

Finally, one of the most clinically significant adverse outcomes is **cardiovascular toxicity**, reported with both bortezomib and carfilzomib. Recent analyses suggest that carfilzomib-associated cardiac events may be mediated by endothelial dysfunction. Ixazomib has also been associated with arrhythmias, hypertension, heart failure, and myocardial infarction.[54]

In conclusion, although several direct proteasome inhibitors have been successfully developed and some have reached clinical use, their associated limitations, including off-target effects and resistance mechanisms, highlight that the proteasome remains an active area of investigation. Moreover, alternative strategies for proteasome inhibition exist, which will be discussed in greater detail in *Project 2*.

2.2 PROTEASOME ACTIVATION

The proteasome has also emerged as an important pharmaceutical target in neurodegenerative diseases, as dysregulation of its activity has been associated with disruptions in cellular homeostasis and, ultimately, neuronal cell death. In fact, the ubiquitin-proteasome system plays a pivotal role in maintaining the regulation of fundamental biological processes vital for cell survival, primarily by facilitating the dynamic turnover of the intracellular proteome.[55] This protein quality control is governed by the **proteostasis network**, which includes the protein synthesis machinery (ribosomes), molecular chaperones responsible for protein folding, and two major proteolytic systems: the **ubiquitin-proteasome system** and the **lysosomal-autophagy pathway**.[56]

Molecular chaperones play an essential role in facilitating the **co-translational folding** of nascent polypeptides at the ribosome, thereby preventing non-productive interactions and protein aggregation.[57] In addition, chaperones identify misfolded or aberrant proteins and assist in their refolding to restore function. Proteins that are irreversibly damaged are targeted for degradation through proteolytic pathways, thus preventing **proteotoxic stress** caused by aggregation or deleterious interactions.[58]

The flexibility and interconnectivity between protein synthesis, folding, and degradation mechanisms ensure the maintenance of proteostasis under various physiological and environmental stress conditions, such as exposure to xenobiotics, oxidative stress, cellular proliferation, and differentiation. The components of the proteostasis network are functionally integrated, and **compensatory mechanisms** are activated to preserve proteostasis whenever one or more systems are compromised.[59,60]

However, during aging, a progressive decline in proteostasis capacity is inevitable. This deterioration perturbs critical signaling pathways and is closely linked to the pathogenesis of various human diseases.[61,62] Targeting intracellular protein levels through modulation of proteolytic systems has emerged as a promising therapeutic strategy for several disorders, including neurodegenerative diseases, cancer, and autoimmune conditions.[63,64]

The proteasome serves as the cell's primary line of defense against proteotoxic stress arising from oxidative damage. The 20S proteasome complex possesses the intrinsic ability to directly degrade oxidatively modified proteins, thereby contributing to cellular detoxification. Reactive oxygen species (ROS), originating from both exogenous sources and endogenous processes such as the mitochondrial respiratory chain and broader cellular metabolism, progressively accumulate with age and cause significant damage to proteins and other macromolecules.[65,66]

Upon oxidative insult, proteins undergo conformational changes that expose hydrophobic residues, predisposing them to aggregation.[67] To mitigate the increasing burden of oxidatively damaged proteins, cells upregulate the 20S proteasome activity, primarily through the disassembly of the 26S proteasome complex.[68,69] However, when the rate of damaged protein accumulation exceeds the degradative capacity of the proteasome, proteostasis becomes disrupted, resulting in proteotoxic stress.[70] This dysregulation is a hallmark of several neurodegenerative diseases, including Parkinson's disease (PD), Alzheimer's disease (AD)[71], Huntington's disease (HD), and amyotrophic lateral sclerosis (ALS, also known as Lou Gehrig's disease).

Moreover, a decline in 26S proteasome activity and accumulation of ubiquitinylated proteins have been observed in post-mortem brain tissues of AD patients.[72] These findings underscore the critical and complementary roles of both the 20S and 26S proteasome complexes in the clearance of aggregation-prone proteins.

2.2.1 ROLE OF PROTEASOME's DYSFUNCTION IN NEURODEGENERATIVE DISEASES

Parkinson's disease

Parkinson's disease is a progressive neurodegenerative disorder characterized by deterioration and loss of dopaminergic neurons in specific brain regions. This neuronal loss leads to hallmark motor symptoms, including bradykinesia, resting tremor, muscular rigidity, and postural instability.[73]

The pathology is histologically characterized by the aggregation of protein inclusions known as Lewy bodies, which result from the misfolding and aggregation of α-synuclein, a presynaptic nerve terminal protein. [74]

For over two decades, it has been well established that neuropathological inclusions in the majority of neurodegenerative disorders consistently contain ubiquitinated proteins, indicating a dysfunction of the ubiquitin-proteasome system (UPS). [75]

Genetic evidence further implicates dysfunction of the ubiquitin system in the pathogenesis of these disorders. Notably, the *parkin* gene—mutated in cases of autosomal recessive juvenile Parkinson's disease—encodes a ubiquitin E3 ligase, highlighting the importance of ubiquitin-mediated protein degradation in maintaining neuronal integrity.[76]

Bedford et al.[77] showed that disruption of ubiquitin-mediated protein degradation leads to the formation of intraneuronal Lewy-like inclusions and widespread neurodegeneration within the

nigrostriatal pathway and forebrain regions. Neuropathological features included the accumulation of ubiquitin and α-synuclein, resembling human Lewy bodies; notably, however, the inclusion bodies also contained mitochondria, suggesting convergence of proteostatic and mitochondrial dysfunction.

Alzheimer's disease

Alzheimer's disease (AD), the most prevalent form of dementia, is neuropathologically defined by the accumulation of insoluble fibrous aggregates in the brain, including intracellular neurofibrillary tangles and extracellular senile plaques. Dysregulation of the UPS has long been proposed as a key mechanism underlying the pathogenesis of AD.[78]

The majority of Alzheimer's disease (AD) cases are sporadic, arising from a complex interplay between genetic predisposition and environmental risk factors. In contrast, familial forms of AD are attributed to pathogenic mutations in genes encoding amyloid precursor protein (APP), presenilins (PS1 and PS2), or other related proteins.[79]

Alzheimer's disease (AD) is neuropathologically defined by the presence of neurofibrillary tangles (NFTs), composed of paired helical filaments (PHFs) derived from aberrantly modified tau protein.[80] In addition, elevated levels of oxidatively damaged proteins have been detected in both the cytoplasm and nuclei of hippocampal neurons from AD patients, relative to age-matched controls.[81] These findings suggest that impairment of intracellular degradation pathways responsible for clearing damaged proteins may contribute to pathological aggregation and progression of neurodegeneration in AD.[82]

Early studies demonstrated that proteasome activity is inhibited in the brains of individuals with Alzheimer's disease (AD), as well as in cell-free assays exposed to amyloid-β (Aβ) peptide.[83] Furthermore, intracellular accumulation of Aβ has been shown to suppress proteasome function in cellular models.[84] In AD brains, abnormal proteasome localization and the accumulation of polyubiquitinated substrates have been linked to the synaptic presence of tau oligomers. Given the critical role of proteasomes in regulating synaptic plasticity, such alterations in proteasome localization and activity are likely to compromise synaptic function and thereby contribute to the cognitive deficits observed in AD.[85]

Given the established correlation between proteasome inhibition and Alzheimer's disease (AD) in neurons, enhancing proteasome activity represents a promising strategy to facilitate the clearance of dysfunctional protein aggregates within neuronal cells.

Multiple sclerosis

Multiple sclerosis (MS) is the most common inflammatory and neurodegenerative disorder of the central nervous system (CNS) in young adults. The disease is primarily driven by autoreactive *T cells* that cross the blood–brain barrier, triggering chronic, low-grade inflammation and ultimately leading to progressive neuronal damage.[86] While the interplay between inflammation and neurodegeneration is a defining feature of MS, neuroinflammation is increasingly recognized as a shared pathogenic mechanism across various neurodegenerative diseases (NDDs) and in the aging brain.[86]
Although immunomodulatory therapies targeting peripheral immune responses have shown efficacy in MS and are under investigation for other NDDs, no current treatments effectively address inflammation intrinsic to the CNS or enhance the capacity of neurons to withstand inflammatory stress.[87]

Notably, MS shares key molecular and cellular features with other NDDs and with aging, such as glutamate-induced excitotoxicity and intracellular accumulation of neuron-specific proteins.[88] Inflammatory CNS conditions also impose high energetic demands on neurons, which have limited metabolic flexibility. **Energy depletion** during neuroinflammation can trigger cell death pathways and has been closely linked to mitochondrial transport deficits in axons, as observed in experimental autoimmune encephalomyelitis (EAE), a widely used animal model of MS.[89,90]

Recent findings further indicate that **persistent glycolysis**, in addition to impaired mitochondrial function, disrupts neuronal homeostasis.[91] Unlike dividing cells, neurons rely on the proteasome to continuously degrade phosphofructo-2-kinase/fructose-2,6-bisphosphatase 3 (PFKFB3),[92] a key glycolytic regulator. This degradation suppresses glycolysis while favoring the pentose phosphate pathway (PPP), which supports antioxidative defenses.[93] Proteasomal dysfunction or glutamate-induced excitotoxicity stabilizes PFKFB3, thereby increasing glycolysis in neurons. Dysfunctional proteasomes also contribute to the accumulation of otherwise short-lived enzymes and signaling proteins, further disturbing neuronal metabolism. Moreover, under certain inflammatory conditions, the catalytic subunits of the proteasome are replaced by inducible isoforms β1i (PSMB9), β2i (PSMB10), and β5i (PSMB8), forming the immunoproteasome.[94] However, the structural and functional consequences of this substitution on neuronal homeostasis remain largely unknown.
Recent transcriptomic and proteomic studies have provided evidence that IFNγ-induced expression of PSMB8 reduces proteasome activity, ultimately contributing to neuronal damage.[95]

2.3 Identifying and profiling Proteasome modulators

As highlighted above, the biological relevance of proteasome modulation makes it essential to evaluate compounds in an assay capable of detecting both inhibitory and stimulatory effects. Conventionally, the activity of proteasome inhibitors is assessed using a fluorogenic assay applied to purified 20S proteasomes in cell lysates [96,97]: this assay employs standard fluorogenic *7-amino-methylcoumarin* (AMC) conjugated small peptide substrates corresponding to the three catalytic sites in the 20S proteasome: **chymotrypsin**-like site (Suc-LLVY-AMC), **caspase**-like site (Z-LLE-AMC), and **trypsin**-like site (Boc-LRR-AMC).[98]

When the small peptide substrate is degraded by the 20S proteasome, the AMC fluorophore is released and quantified

to measure the rate of proteolytic cleavage.[99] In the presence of a proteasome *inhibitor*, fluorescence intensity decreases, as the proteasome is unable to catalyse proteolysis, thereby preventing the release of the fluorogenic moiety of the probe. Conversely, in the presence of an activator, an increase in fluorescence is observed. Nevertheless, this assay is inherently limited to a single mechanism of action, detecting exclusively those compounds that directly engage the proteasome to modulate its catalytic activity.

Indeed, modulation of the proteasome can occur through two primary mechanisms: by interacting with the catalytic threonine residue within the active site, or via **allosteric** effects that induce conformational changes in the proteasome's quaternary structure, thereby limiting exposure of the threonine residue. [100]

Nevertheless, proteasome modulation can occur through various additional mechanisms, as highlighted by recent literature. [101] In particular, proteasome activity may also be modulated indirectly through **alterations** in the **gene expression** of the subunits encoding proteasomal proteins.[102]

For example, Rpn4, originally identified as a protein associated with the 26S proteasome, binds to the conserved sequence motif known as proteasome-associated control element (PACE) in the promoter region of all proteasome subunit genes and some proteasome assembly chaperone genes. [103]

Rpn4 protein is extremely short-lived ($t_{1/2} \approx 2$ min) and is continually degraded by the proteasome. Furthermore, Rpn4 accumulates and promotes proteasome expression in case of proteasomal dysfunction, [104] playing a compensatory role in response to decreased proteasome activity. By contrast, lack of Rpn4 or PACE sequences in yeast decreases proteasome activity and impairs resistance to various stresses, such as DNA damage and oxidative insult. [105]

Other regulatory mechanisms involve modulation of the ubiquitination process itself. In particular, recent evidence indicates that inhibiting E3 ubiquitin-ligase enzymes—which are essential for proper tagging of proteins destined for degradation—can suppress proteolysis by reducing substrate delivery to the proteasome. [106]

In this regard, Leestemaker *et al.* [107] employed an innovative in vitro assay to monitor proteasome activity within the cellular environment, going beyond the assessment of direct enzymatic effects alone. This methodology is particularly noteworthy, as it allows for a comprehensive evaluation of all possible mechanisms by which proteasome activity may be modulated, thereby providing a more holistic understanding of its regulation.

To identify novel small molecules capable of modulating proteasome activity, two fluorescent probes were employed: **BodipyFL-Ahx$_3$L$_3$VS** (*Probe 1*) and **BodipyFL-Ahx$_3$L$_3$S** (*Probe 2*).
Probe 1 covalently binds to the catalytically active subunits of the proteasome in living cells in an activity-dependent manner, whereas *Probe 2* does not interact with the proteasome.

Consequently, treating cells with either positive or negative modulators of proteasome activity followed by probe incubation results in increased or decreased intracellular fluorescence, respectively, which can be quantitatively measured by flow cytometry or SDS-PAGE followed by fluorescence scanning. [108,109]
In intact cells experiments, the cell-permeable nature of the probes enables direct assessment of proteasome activity in a physiological context.

From a structural perspective (*Figure 15*), both probes consist of a tripeptide of leucine residues, followed by three aminohexanoic acid (Ahx) units, with the amino terminus of the terminal Ahx residue functionalized with a Bodipy-FL-NHS ester fluorophore. This design confers equal affinity for all three catalytic subunits of the 20S proteasome. Conversely, the two probes differ in the reactive group responsible for interaction with the enzyme: *Probe 1* incorporates a vinyl sulfone moiety, specifically recognized by the catalytic threonine, whereas *Probe 2* bears a non-reactive sulfone group that does not engage with the enzyme.
Moreover, the observed fluorescence signal not only confirms probe binding but also reflects the consequent inhibition of the enzymatic complex, even in living cell lines. [109]

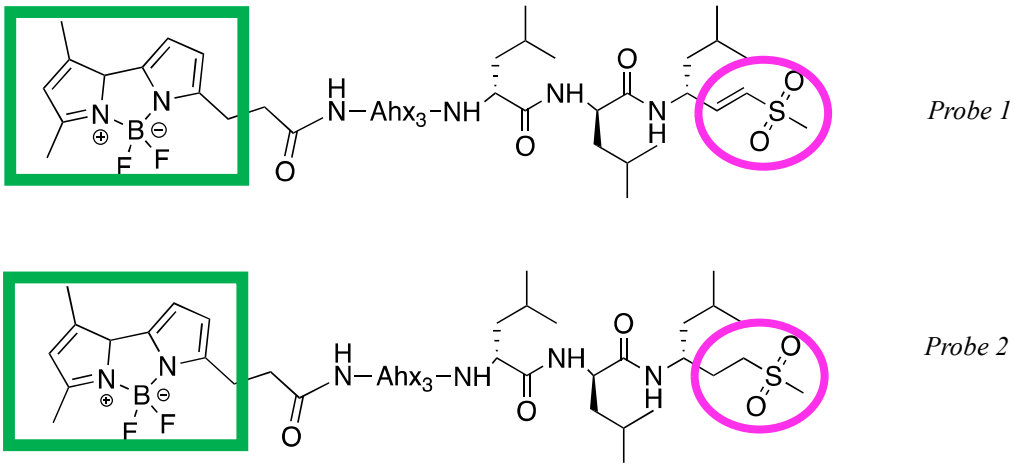

Figure 15. Structures of Probe 1 (top) and Probe 2 (bottom). The Bodipy-FL-NHS ester fluorophore is highlighted in green, while the reactive groups—vinyl sulfone in Probe 1 and sulfone in Probe 2—are shown in pink.

To investigate the probe's binding to the catalytic sites of the 20S proteasome, a human melanoma MEL-JUSO cell line expressing Ub-R-GFP was used. This reporter system, based on GFP-fused proteins containing an N-terminal ubiquitin tag, allows for quantification of proteasome-mediated proteolysis in living cells.[110] The cell line was treated separately with BodipyFL-Ahx$_3$L$_3$VS and with MG-132, a well-characterized aldehyde-based proteasome inhibitor. The percentage of cells responsive to MG-132 was defined as 100%. In cells treated with the fluorescent probe, GFP levels increased over time, along with the fluorescence intensity, which was quantified via flow cytometry. The samples treated with BodipyFL-Ahx$_3$L$_3$VS exhibited significant fluorescence levels, thereby confirming efficient inhibition of the proteasome in cultured cells.

To further confirm this hypothesis, a second experiment was conducted in which MEL-JUSO cells were simultaneously treated with both MG-132 and BodipyFL-Ahx$_3$L$_3$VS. Under these conditions, the probe localized primarily to the plasma membrane and perinuclear region, remaining in an unbound state. This distribution reflects the fact that MG-132, being a more potent inhibitor, saturates all catalytic sites, thereby preventing covalent binding of the vinyl sulfone-containing probe.

These findings suggest that the presence of different inhibitors can influence both the intracellular distribution and the degree of binding of the probe. The distribution pattern correlates directly with changes in fluorescence intensity: when the probe is covalently bound to at least one of the three catalytic threonine residues, an increase in fluorescence is observed; in contrast, when the probe remains unbound and diffusely distributed, a decrease in fluorescence occurs.

This approach represents an innovative methodology for:

- evaluating the activity of newly synthesized compounds by comparing fluorescence levels in cells treated with established proteasome inhibitors and those exposed to candidate modulators.[111]
- assessing proteasome activity directly within the cellular environment, thereby taking into account the complexity of the cellular context and enabling the detection of potential indirect effects of the compounds under investigation; [112]
- simultaneously evaluating both activation and inhibition of the proteasome, making the assay broadly applicable to both therapeutic strategies.
- selecting a limited number of compounds from an internal library, which will subsequently be subjected to more specific assays aimed at elucidating their mechanism of action.

Overall, this assay allows for the evaluation of proteasome activity by monitoring intracellular fluorescence over time. The signal generated by Probe 1 exhibits a linear increase, while the background fluorescence observed with the inactive probe remains stable, demonstrating that Probe 1 provides a reliable measure of the proteasome's enzymatic rate in living cells and enabling the assessment of dynamic modulation under different experimental conditions.[111,112]

3 PROJECT 1: SYNTHESIS AND BIOLOGICAL EVALUATION OF SMALL MOLECULES AS NEW POTENTIAL PROTEASOME INHIBITORS

In light of the therapeutic potential of proteasome inhibition and the limitations associated with currently available drugs, the scientific community continues to seek novel molecules capable of selectively inhibiting proteasome activity, particularly under pathological conditions such as cancer. The initial research project was focused on the identification of novel small molecules capable of modulating proteasome function, with particular emphasis on two key aspects:

- **Elimination of the peptidic scaffold**: all clinically approved proteasome inhibitors currently in use share a peptidic backbone. This structural feature poses several challenges, including restricted routes of administration—limited primarily to parenteral delivery (with the exception of Ixazomib)—as well as an increased risk of autoimmune reactions due to the inherent antigenicity of peptide-based compounds. [113]
- **Introduction of novel electrophilic groups targeting the catalytic threonine residue**, aiming to reduce the toxicity typically associated with current inhibitors.

In 2019, Pacifico et al.[114] reported a new class of dipeptidic and tripeptidic compounds exhibiting significant proteasome inhibitory activity. This effect was attributed to the presence of an **α-ketoamide warhead**, capable of covalently interacting with the proteasome's catalytic sites.[115] Among the compounds tested, the dipeptides exhibited relatively low activity, with the most active example shown in *Figure 16a*.

In contrast, the most potent inhibitor identified was a tripeptide consisting of three leucine residues and bearing an N-terminal benzyloxycarbonyl (Cbz) protecting group, showed in Figure 16b. The α-ketoamide functionality in this molecule was generated by coupling with 1-naphthylamine, which contributed to its enhanced inhibitory activity (**2**).

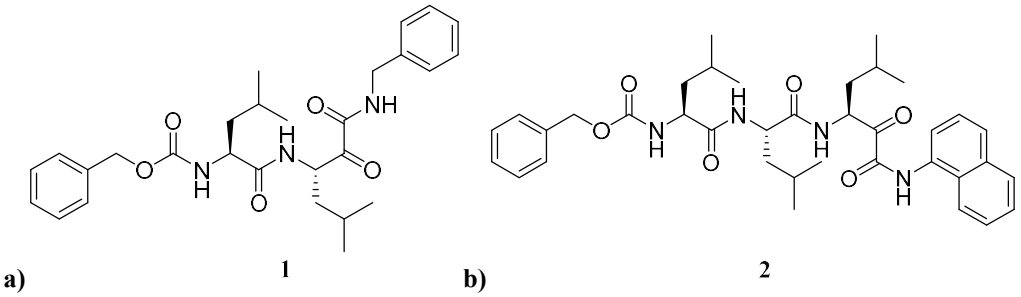

Figure 16. a) Structure of dipeptide (1) with best activity. b) Tripeptide (2) exhibiting the highest activity.

Although these compounds demonstrated promising proteasome-inhibitory activity, their **peptidic nature represents a major limitation**. Indeed, such molecules are highly susceptible to enzymatic degradation by both **endopeptidases and exopeptidases**,[116] which can rapidly cleave them into individual amino acids. This susceptibility significantly compromises their **metabolic stability**, especially when administered through **non-parenteral routes**, potentially resulting in **loss of bioactivity**.[117] Furthermore, the **peptidic backbone** may trigger **immune responses**[118] due to its **antigenic properties**, thus raising concerns regarding both the **efficacy and safety profile** of these compounds.

3.1 AIM OF THE PROJECT

Building upon the peptide-based inhibitors previously reported by Pacifico *et al.*, [114] the first project was aimed at replacing the native peptide backbone with a non-peptidic framework in order to overcome the intrinsic limitations associated with peptide structures. To achieve this goal, the chosen strategy involved the cyclization of a dipeptidic structure, thereby constraining the amino acid side chains within a rigid piperazine scaffold, as illustrated in *Figure 17*.

This design is expected to enhance the overall conformational stability of the molecule, improve its pharmacokinetic properties, and potentially lead to more effective proteasome inhibition.

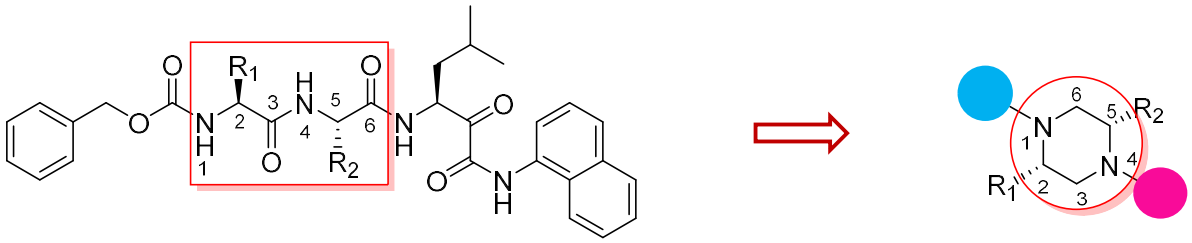

2

Figure 17. Design approach for replacing the peptidic structure of the compounds reported by Pacifico *et al.* through cyclization to a piperazine core.

Another initial objective was to replace the functional group responsible for interacting with the catalytic threonine, to develop molecules with improved target selectivity. This strategy was driven by the evidence that α-ketoamides, although highly potent, tend to exhibit off-target activity toward other enzymes such as proteases, lipases, and calpains.[114]

Based on these considerations, the introduction of a functional group capable of interacting with the proteasome through the formation of a less stable adduct with the catalytic threonine was proposed, with the aim of reducing potential in vivo toxicity. To achieve this goal, a series of compounds was synthesized, sharing a common structural framework and characterized by the following features:

• A **central piperazine scaffold**, generated through the cyclization of a dipeptidic precursor;

• A **bulky substituent** at position 1, either a Cbz group or a pyrazinecarboxylic acid residue—the latter being a structural element also present in Bortezomib;

• An **electrophilic functional group** at position 4, oriented to interact with the proteasome. In these initial derivatives, different moieties such as a diamide, an acrylamide, and an α-hydroxyamide were

introduced, each combined with a recurring naphthalene motif that had previously demonstrated promising activity in the prior study.

The first class of compounds comprises both symmetrical and asymmetrical piperazines, derived from the cyclization of the dipeptides leucine–leucine and phenylalanine–leucine, respectively (figure 18). The selection of these amino acid residues was guided by literature evidence. Specifically, the most active compound reported in our referenced work featured a central dipeptidic motif, whereas one of the most potent known proteasome inhibitors incorporates a phenylalanine–leucine sequence. This rational design approach aims to integrate structural features associated with high biological activity into a more conformationally constrained and metabolically stable scaffold.

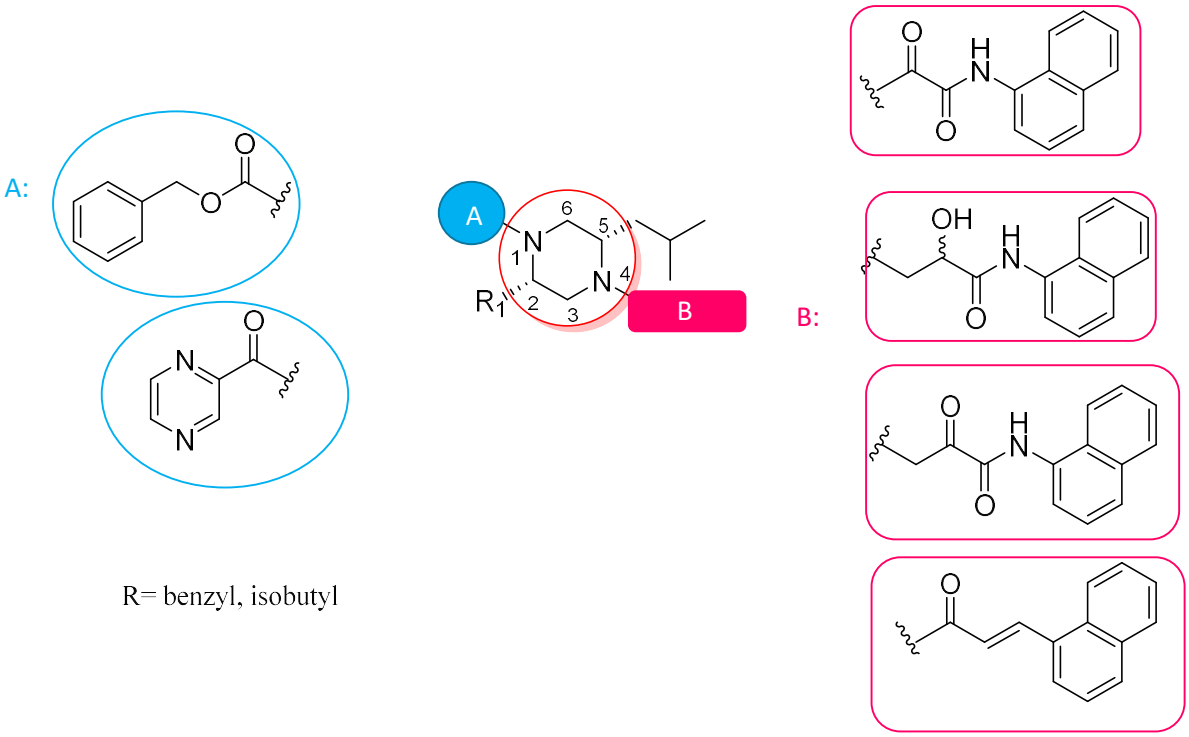

Figure 18. First class of synthesized compounds.

Prompted by the initial biological results, a second class of compounds was conceived, incorporating active functional groups previously reported in the literature. Indeed, the limited success of the first compound class could be attributed, at least in part, to the functional group responsible for activity, which may have lacked sufficient electrophilicity to be efficiently recognized by the catalytic site of the target.

Furthermore, in the naphtil peptide series of the referenced work, the counterpart tripeptidic compound exhibited higher activity than the corresponding dipeptidic analogues. For this reason, another aspect considered in the second generation of new inhibitors was the crucial modification

involving the introduction of an additional leucine-derived aminoacyl residue through the formation of a urea linkage.

This class also retained several key structural features of the original compounds: the carbonyl-oxy group at position 1 was preserved, as were the isobutyl groups at positions 2 and 5.

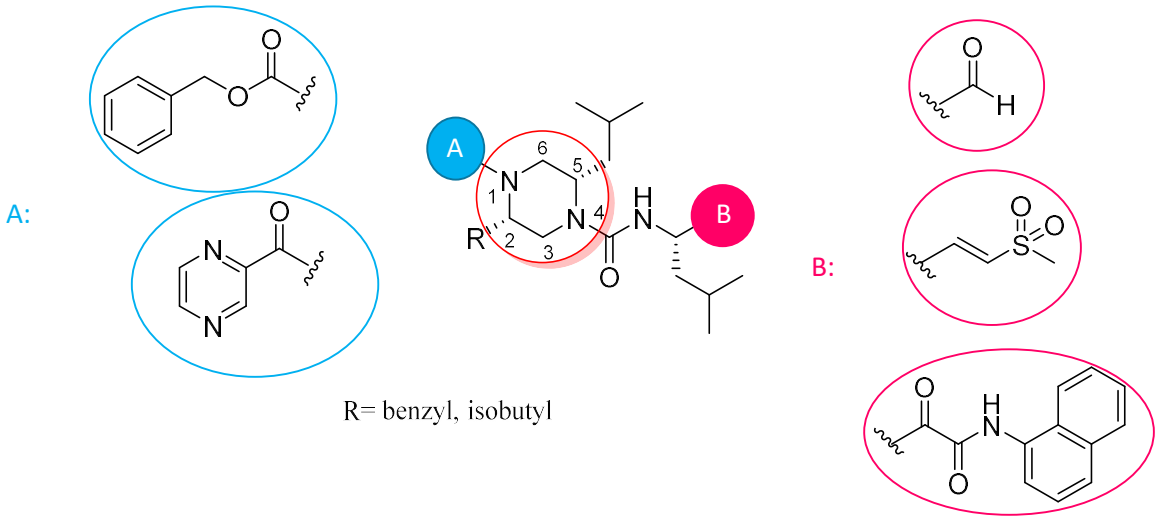

Figure 19. Second class of synthesized compounds.

Figure 20 lists all the final synthesized compounds, encompassing both classes.

FIRST CLASS OF COMPOUNDS

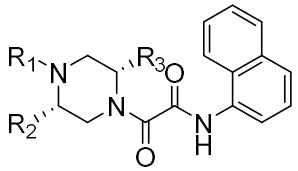

5, R_1= Cbz, R_2=R_3= isobutyl
6, R_1= pyrazinoic acid residue, R_2=R_3= isobutyl
16, R_1= Cbz, R_2= benzyl, R_3= isobutyl
17, R_1= pyrazinoic acid residue, R_2= benzyl, R_3= isobutyl

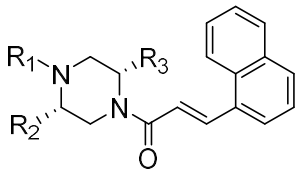

8, R_1= Cbz, R_2=R_3= isobutyl
9, R_1= pyrazinoic acid residue, R_2=R_3= isobutyl
18, R_1= Cbz, R_2= benzyl, R_3= isobutyl
19, R_1= pyrazinoic acid residue, R_2= benzyl, R_3= isobutyl

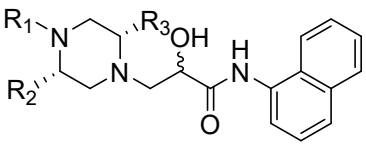

11, R_1= Cbz, R_2=R_3= isobutyl
12, R_1= pyrazinoic acid residue, R_2=R_3= isobutyl
21, R_1= Cbz, R_2= benzyl, R_3= isobutyl
22, R_1= pyrazinoic acid residue, R_2= benzyl, R_3= isobutyl

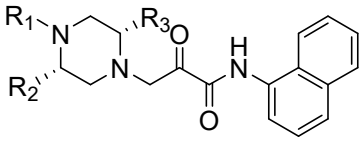

13, R_1= Cbz, R_2=R_3= isobutyl
14, R_1= pyrazinoic acid residue, R_2=R_3= isobutyl
23, R_1= Cbz, R_2= benzyl, R_3= isobutyl
24, R_1= pyrazinoic acid residue, R_2= benzyl, R_3= isobutyl

SECOND CLASS OF COMPOUNDS

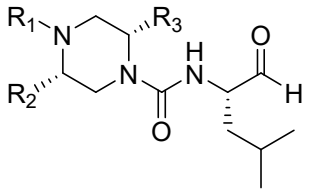

26, R_1= Cbz, R_2=R_3= isobutyl
27, R_1= pyrazinoic acid residue, R_2=R_3= isobutyl
32, R_1= Cbz, R_2= benzyl, R_3= isobutyl
33, R_1= pyrazinoic acid residue, R_2= benzyl, R_3= isobutyl

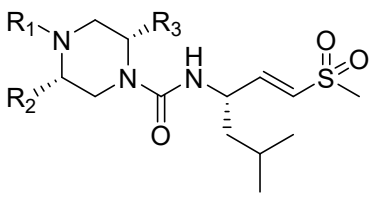

29, R_1= Cbz, R_2=R_3= isobutyl
30, R_1= pyrazinoic acid residue, R_2=R_3= isobutyl
34, R_1= Cbz, R_2= benzyl, R_3= isobutyl
35, R_1= pyrazinoic acid residue, R_2= benzyl, R_3= isobutyl

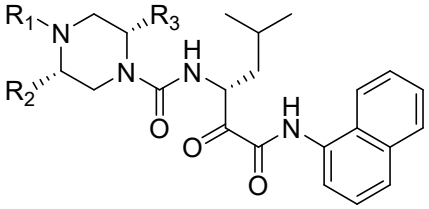

37, R_1= Cbz, R_2=R_3= isobutyl
38, R_1= pyrazinoic acid residue, R_2=R_3= isobutyl
39, R_1= Cbz, R_2= benzyl, R_3= isobutyl
40, R_1= pyrazinoic acid residue, R_2= benzyl, R_3= isobutyl

Figure 20. First and second class of synthesized compounds, comprising symmetrical piperazines with various active substituents.

Both classes of compounds were classified according to the nature of the substitutions on the central piperazine core. **Symmetric piperazines** are characterized by isobutyl chains at positions 2 and 5, derived from the Leucine–Leucine dipeptide, whereas **asymmetric piperazines** bear a benzyl group at position 2 and an isobutyl chain at position 5, originating from the Phenylalanine–Leucine dipeptide.

The first class of compounds can be described as **pseudo-dipeptidic**, as the active functional group responsible for interaction with the target is directly attached to the piperazine nucleus. Within this class, the functional groups vary: compounds **5**, **6**, **16**, and **17** feature a *diamide group*; compounds **8**, **9**, **18**, and **19** incorporate an *acrylamide group*; and compounds **11**, **12**, **21**, and 22 contain an *α-hydroxyamide*, which was subsequently oxidized to yield the corresponding *α-ketoamide* in compounds **13**, **14, 23**, and **24**.
Notably, all these active groups retain the recurring **1-naphthyl motif**, selected and preserved because, in the reference study, the peptide displaying the highest biological activity possessed this

substituent, which appeared to facilitate insertion of the compound into the hydrophobic pocket of the proteasome.

In the second class of compounds, an additional **leucine residue** was introduced via a **urea linkage**, as tripeptides described in the reference study had demonstrated enhanced biological activity. For these derivatives, further active functional groups were incorporated to evaluate whether the piperazine core could serve as an effective scaffold for promoting interaction with the biological target. These included the *aldehyde* (compounds **26**, **27**, **32**, and **33**), *vinyl sulfone* (**29**, **30, 34**, and **35**), and *α-ketoamide* (**37**, **38**, **39**, and **40**) functionalities.

Finally, all compounds were substituted at position 1 with **bulky groups**. Two specific substituents were selected: the **pyrazinoic acid residue**, characteristic of Bortezomib, and the **benzyloxycarbonyl (Cbz) group** present in the peptides described in the reference study. Variability in these substituents was introduced to assess whether either group would modulate biological activity.

3.2 SYNTHESIS

The first class of compounds shares a common synthetic pathway leading to the piperazine core. The specific synthetic strategies employed vary depending on the substituents at positions 2 and 5 of the piperazine ring.

1. SYMMETRICAL PIPERAZINES

a) Preparation of diamide and acrylamide reactive motifs

The synthesis of compounds begins with the construction of the piperazine core, which features two isobutyl chains at positions 2 and 5. This core is subsequently functionalized at position 1 (with either a CBZ group or a pyrazinoic acid residue) and at position 4 with different active groups. The general synthetic route is shown in *Scheme 1*.

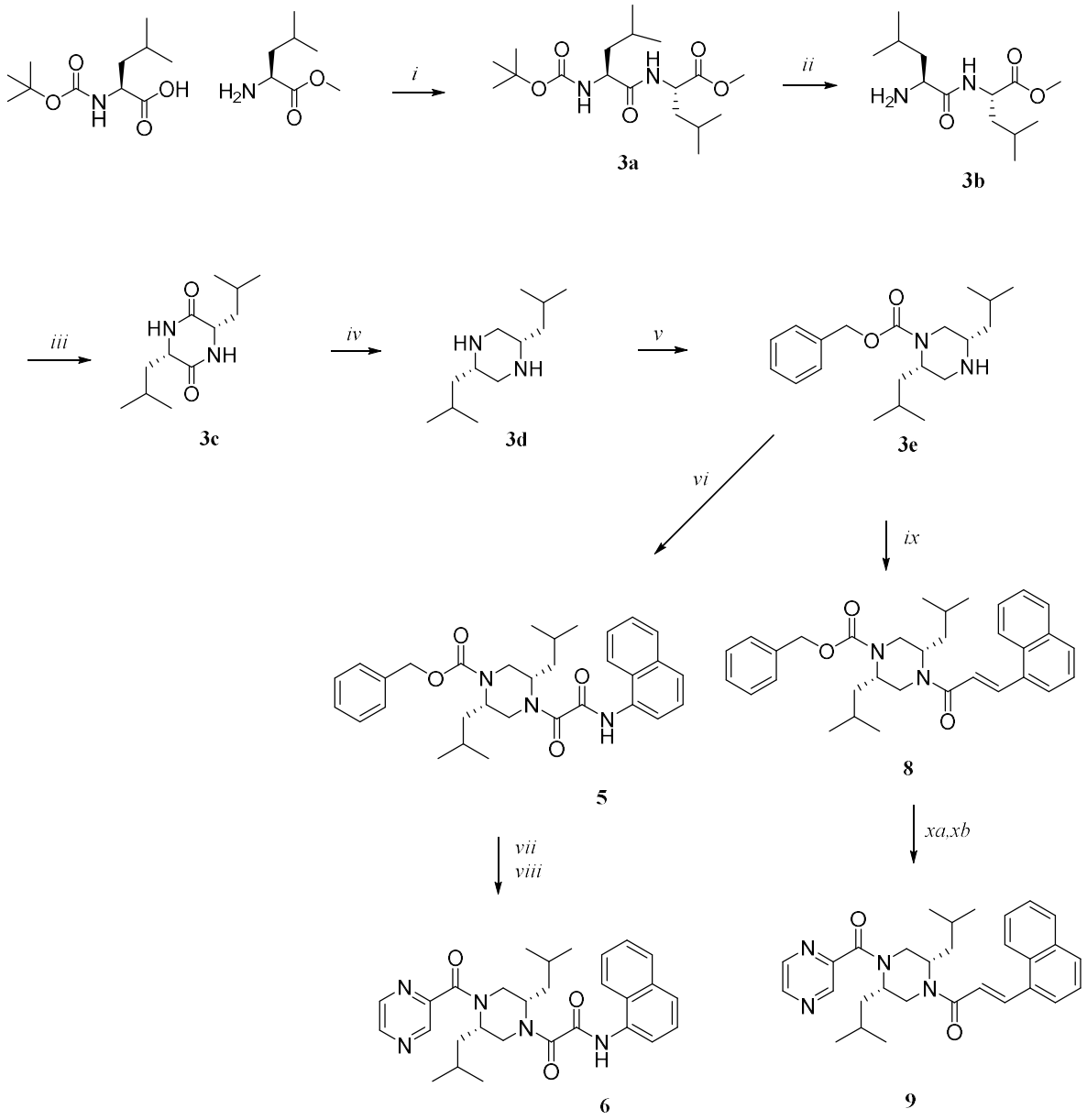

Experimental conditions:

i. WSC, HOBt, TEA, DMF, 16h, rt.

ii. TFA, CH_2Cl_2, 30 min, rt.

iii. *n*-BuOH, toluene, 16h, 120°C.

iv. $LiAlH_4$, anhydrous THF, 2h, 80°C.

v. CBZ-Osu, CH_2Cl_2, 30 min, rt.

vi. 2-(naphthalen-1-ylamino)-2-oxoacetic acid, HATU, DIPEA, DMF, 2h, rt.

vii. H_2, Pd/C 10%, HCl 1M, 16h, rt.

viii. pyrazinoic acid, HATU, DIPEA, DMF, 2h, rt.

ix. (E)-3-(naphthalen-1-yl)acrylic acid, HOBt, WSC, DMF, 2h, rt.

xa. Cbz-Osu, TEA, DCM, 90 min, rt.

xb. pyrazinoic acid, HATU, DIPEA, DMF, 2h, rt.

Scheme 1. Synthetic route for the preparation of compounds presenting symmetrical piperazine scaffold.

The sequence begins with an amide-bond formation between two commercially available amino acids—Boc-L-leucine and leucine methyl ester—affording the linear dipeptide **3a**. The coupling is performed in *N,N*-dimethylformamide (DMF) using water-soluble carbodiimide (WSC) in combination with 1-hydroxybenzotriazole (HOBt), which activate the carboxyl group of Boc-L-leucine and thereby facilitate nucleophilic attack by the amine of the ester.

Upon formation of **3a**, the *N*-terminal Boc protecting group—acid-labile by design—is removed under standard acidic conditions with trifluoroacetic acid (TFA), furnishing the corresponding free amine **3b**.

Cyclization of this deprotected dipeptide then affords the diketopiperazine scaffold **3c**. This reaction is carried out in *n*-butanol/toluene under reflux at 120 °C for 16 h. The reaction mixture is suitably diluted to promote intramolecular ring closure while suppressing competing intermolecular processes.

Finally, reduction of the two carbonyl groups is achieved with lithium aluminum hydride ($LiAlH_4$). Coordination of the carbonyl oxygens to aluminum precedes hydride transfer to the carbonyl carbons, generating the corresponding imine intermediates, which undergo subsequent reduction to produce the fully reduced diamine **3d** (*Scheme 2*).

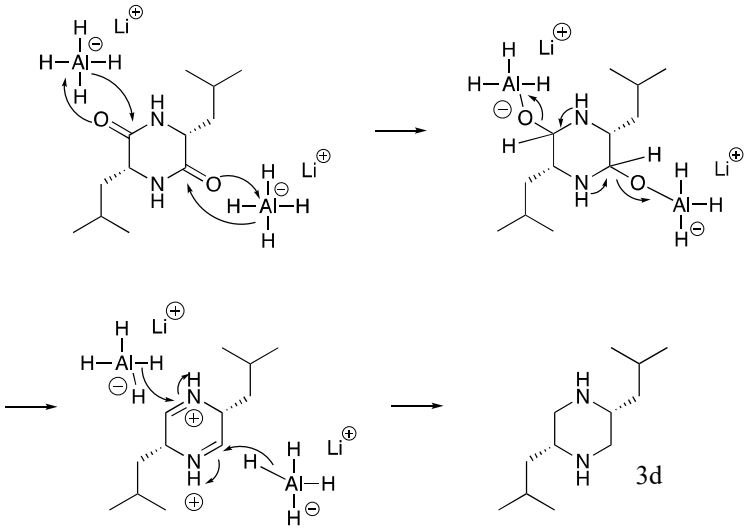

Scheme 2. Mechanism proposed for the $LiAlH_4$-mediated reduction of diketopiperazine.

At this stage, **3d** undergoes selective *N*-monoprotection via nucleophilic substitution with benzyl (2,5-dioxopyrrolidin-1-yl) carbonate (Cbz-Osu). To ensure preferential protection of only one nitrogen atom within the piperazine ring, the Cbz-Osu reagent is introduced incrementally—two successive additions of 0.3 equiv each, followed by a final 0.2 equiv—ultimately affording the monoprotected derivative **3e**.

The latter is subsequently coupled with the previously prepared 2-(naphthalen-1-ylamino)-2-oxoacetic acid **4** to deliver compound **5**. This amidation is mediated by HATU (O-(7-azabenzotriazol-1-yl)-N,N,N',N'-tetramethyluronium hexafluorophosphate) and DIPEA (*N,N*-diisopropylethylamine), which activate the carboxylic acid and promote efficient formation of the amide bond.

To obtain compound **6**, the Cbz protecting group is removed by catalytic hydrogenolysis over palladium on carbon (Pd/C) in methanol under a hydrogen-saturated atmosphere. The resulting free amine is then directly subjected to a final amidation with pyrazinoic acid, again using HATU and DIPEA as coupling agents, affording compound **6**.

In the second pathway, intermediate **3e** is coupled with the previously synthesized (E)-3-(naphthalen-1-yl)acrylic acid to furnish compound **8**. This reaction is carried out with WSC and HOBt as coupling agents.

The (E)-3-(naphthalen-1-yl)acrylic acid **7** itself is prepared via a Doebner condensation between malonic acid and 1-naphthaldehyde in the presence of piperidine and pyridine, as shown in *Scheme 3*.

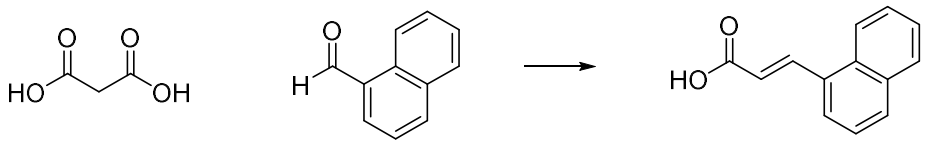

7

Experimental conditions: Piperidine, pyridine, 110°C, 4 hours.

Scheme 3. Synthetic strategy employed for the preparation of compound (E)-3-(naphthalen-1-yl)acrylic acid by Doebner reaction.

The reaction is carried out under basic conditions, using pyridine as the solvent and piperidine as a weak base.

Initially, the α-carbon of malonic acid is deprotonated by piperidine, yielding a resonance-stabilized carbanion (enolate). This intermediate acts as a nucleophile and attacks the carbonyl carbon of the aldehyde, leading to the opening of the double bond and the formation of a hydroxy intermediate. At this stage, a decarboxylation process occurs, accompanied by the loss of a molecule of water, ultimately resulting in the formation of the α,β-unsaturated compound (*Scheme 4*).

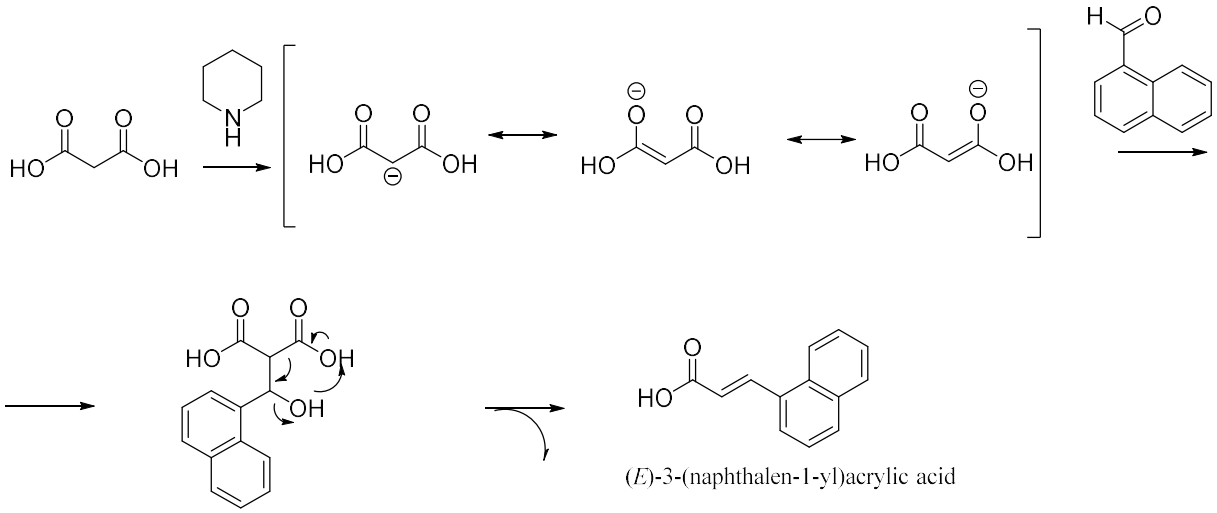

Scheme 4. Proposed mechanistic pathway for the Doebner reaction leading to the formation of (E)-3-(naphthalen-yl)acrylic acid **7**.

Finally, compound **8** is subjected to **catalytic hydrogenolysis** to remove the Cbz protecting group. The reaction is carried out in methanol using **10% Pd/C** and is deliberately limited to ten minutes to prevent reduction of the alkene moiety. The resulting deprotected intermediate is then used directly

in the **amidation** of **3f** with **pyrazinoic acid**, mediated by **HATU** and **DIPEA**, ultimately yielding the first final compound **9**.

b) Preparation of α-hydroxyamide and α-ketoamide active motifs

To obtain the final compounds **11–14**, piperazine **3e** was subjected to a three-step derivatization sequence. First, nucleophilic ring opening of ethyl oxirane-2-carboxylate furnished the corresponding α-hydroxy ester derivative, introducing a methylene spacer on the piperazine ring. Subsequent ester hydrolysis yielded the corresponding carboxylic acid, which was then coupled with 1-naphthylamine through amide-bond formation to afford compound **11**.

At this point, compound **11** diverged into two distinct synthetic pathways. In one route, catalytic hydrogenation removed the Cbz protecting group, enabling subsequent amidic coupling with pyrazinoic acid to deliver compound **12**. In the alternative pathway, oxidation with Dess–Martin periodinane converted the secondary alcohol into the corresponding ketone, affording compound **13**. The same oxidative reaction is performed on compound 12 to afford the final compound **14**.

The synthetic route is showed in *Scheme 5*.

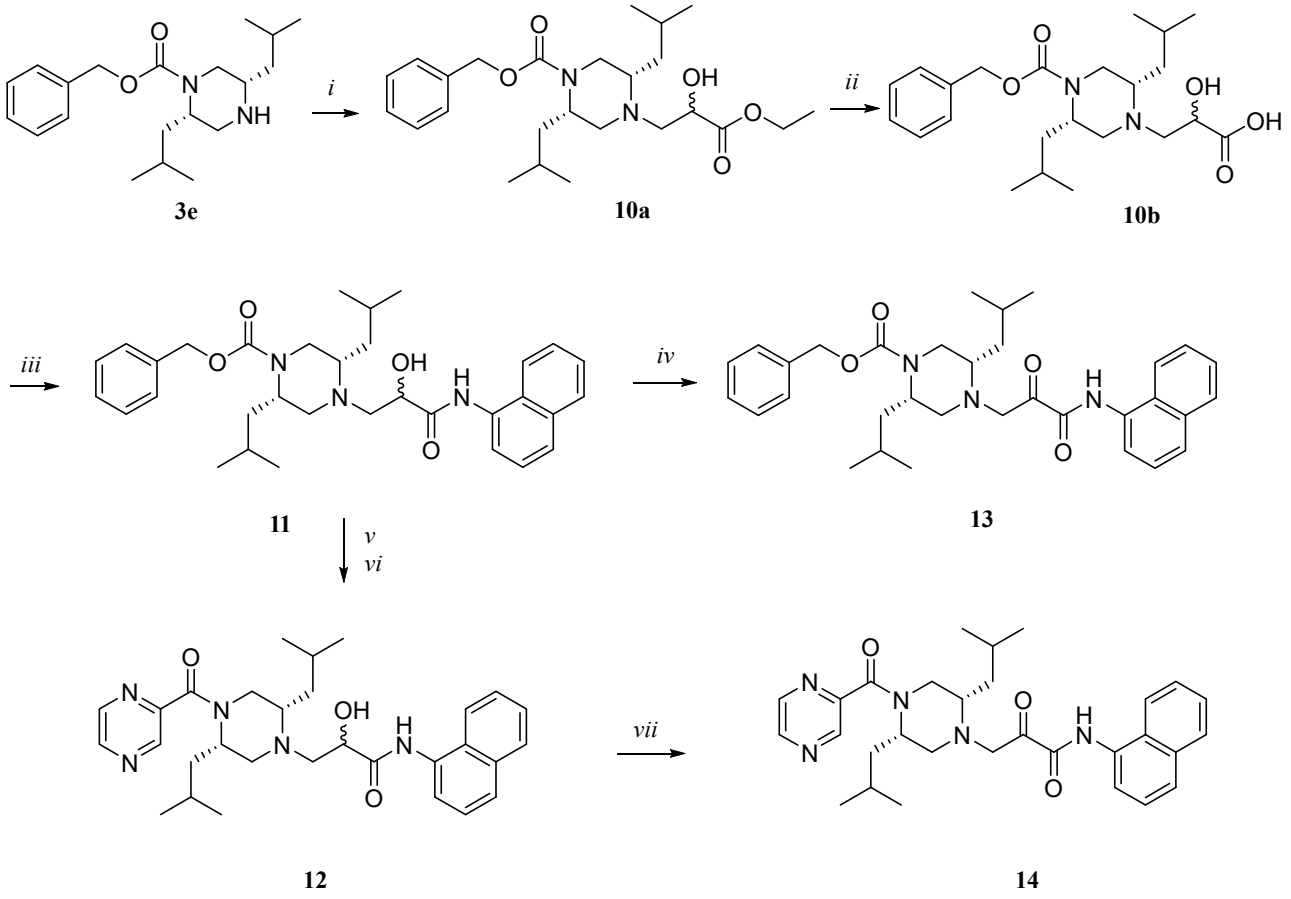

Experimental conditions:

i. *ethyl oxirane-2-carboxylate*, ethanol, 80°C, 48 hours.

ii. KOH 2N, THF/ethanol, rt, 3 hours.

iii. HATU, DIPEA, DMF, 24 hours.

iv, vii. Dess-Martin periodinane, DCM, 2h, rt.

v, H_2, Pd/C, HCl 1M, 16 h, rt.

vi, pyrazinoic acid, HATU, DIPEA, DMF, 2h, rt.

vii. Dess-Martin periodinane, DCM, rt, 20 hours.

Scheme 5. Synthetic strategy for compound **9-12**.

In particular, the *first step* involves the epoxide ring opening with formation of the α-hydroxy ester: the opening occurs preferentially at the C_1 position of ethyl oxirane-2-carboxylate, as this leads to the formation of a more stable final compound.

In this reaction, the secondary amine group of the piperazine core acts as a nucleophile, enhanced by the use of triethylamine, attacking the carbon atom at position 1 of the epoxide ring. This leads to ring opening, resulting in the formation of a new C–N bond and a hydroxyl group in the β-position relative to the piperazine nitrogen. The mechanism is shown in *Scheme 6*.

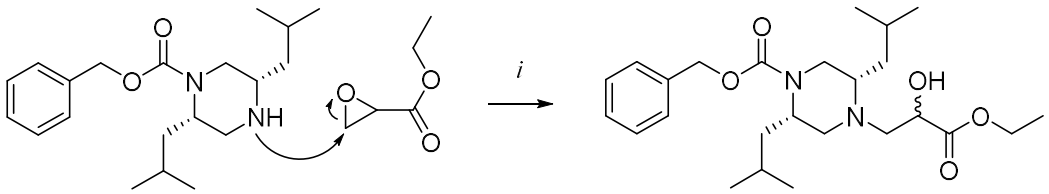

10a

Experimental conditions:

i. ethanol, 80°C, 48 hours.

Scheme 6. Proposed mechanistic pathway for the epoxide ring opening leading to the corresponding α-hydroxy ester.

2. ASYMMETRICAL PIPERAZINES

a) Preparation of diamide and acrylamide reactive motifs

The synthesis of the final asymmetrical piperazines was carried out following a strategy analogous to that used for the symmetric derivatives. The key distinction lies in the cyclization of the dipeptide: due to its asymmetric nature, the amino terminus must be protected with a benzyl group to prevent the formation of regioisomeric mixtures during ring closure. The general synthetic strategy is shown in *Scheme 7*.

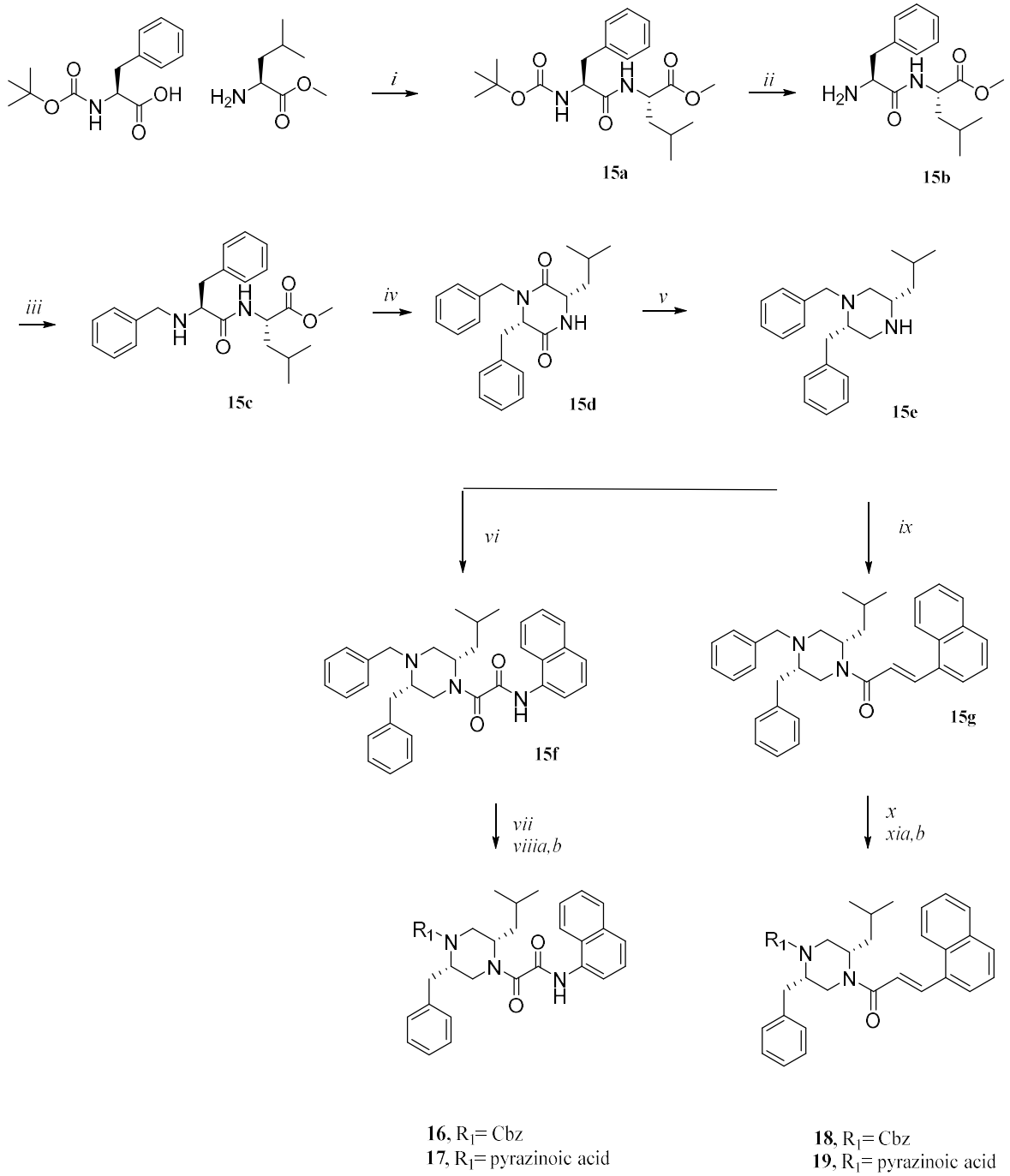

Experimental conditions:

i. WSC, HOBt, TEA, DMF, 16h, rt.

ii. TFA, CH_2Cl_2, 30 min, rt.

iii. C_6H_5CHO, $NaBH_4$, 30 min, rt.

iv. TEA, DMAP, Xylene, 48h, 140°C.

v. $LiAlH_4$, THF anidro, 2h, 80°C.

vi. 2-(naphthalen-1-ylamino)-2-oxoacetic acid, HATU, DIPEA, DMF, 2h, rt..

vii,x. Pd/C, H_2, HCl 1M, MeOH, 16h, rt.

viiia,xia. Cbz-osu, TEA, DCM, 2h, rt.

viiib, xib. pyrazinoic acid, DIPEA, HATU, DMF, 2h, rt.

Scheme 7. Synthetic route for the preparation of compound 16-19.

.

The preparation of compounds **16-19** proceeds through a streamlined elaboration of the Phe–Leu scaffold. The dipeptide **15a** is obtained by coupling Boc-L-phenylalanine with leucine methyl ester in *N,N*-dimethylformamide, with WSC and HOBt employed to activate the carboxyl function. Subsequent cleavage of the Boc protecting group with trifluoroacetic acid furnishes the free amine **15b**.

Introduction of the benzyl moiety is accomplished via reductive amination with benzaldehyde in the presence of triethylamine, which promotes imine formation under mild conditions. Reduction of the resulting imine with sodium borohydride affords the benzylated derivative **15c** in an efficient and controlled manner (*Scheme 8*).

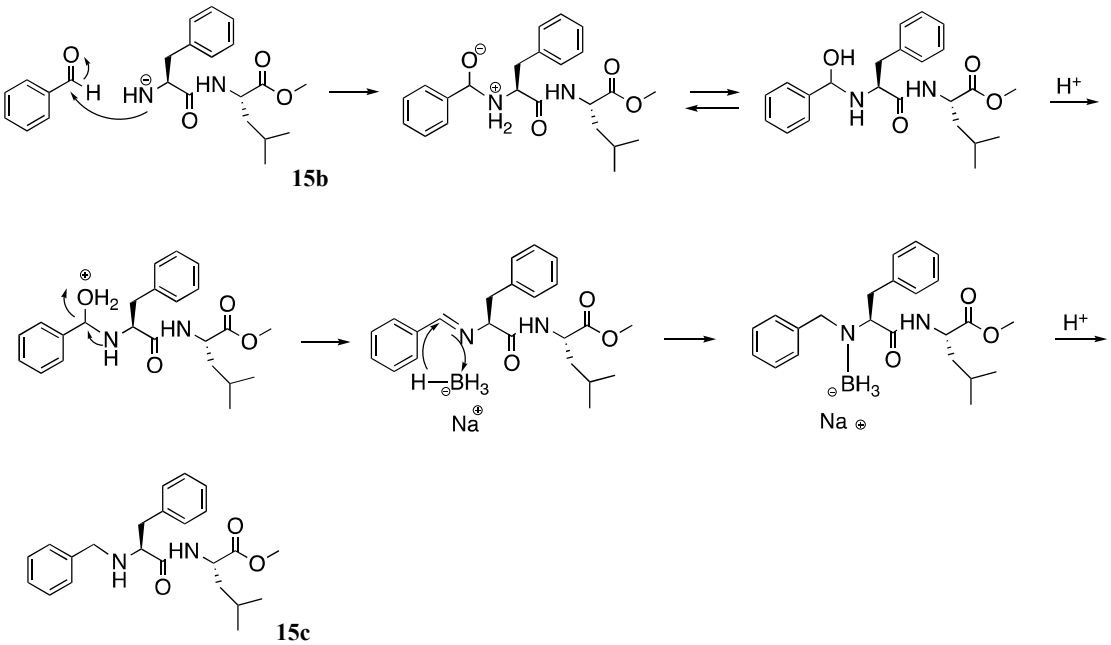

Scheme 8. Mechanistic representation of the reductive amination between a primary amine and an aldehyde under basic conditions.

The *following step* involves cyclization, which in this case requires the use of a catalyst: Compound **15c** is first deprotonated by TEA (triethylamine) to increase the nucleophilicity of the amine. Subsequently, the catalyst DMAP (4-dimethylaminopyridine) is employed: the pyridinic nitrogen performs a nucleophilic attack on the carbonyl carbon of the ester, resulting in the elimination of methanol. This generates a reactive intermediate featuring a good leaving group. Together with the dilution of the compound in xylene under reflux at 140 °C, these conditions favor intramolecular cyclization. DMAP is regenerated, and intermediate **15d** is formed (*Scheme 9*).

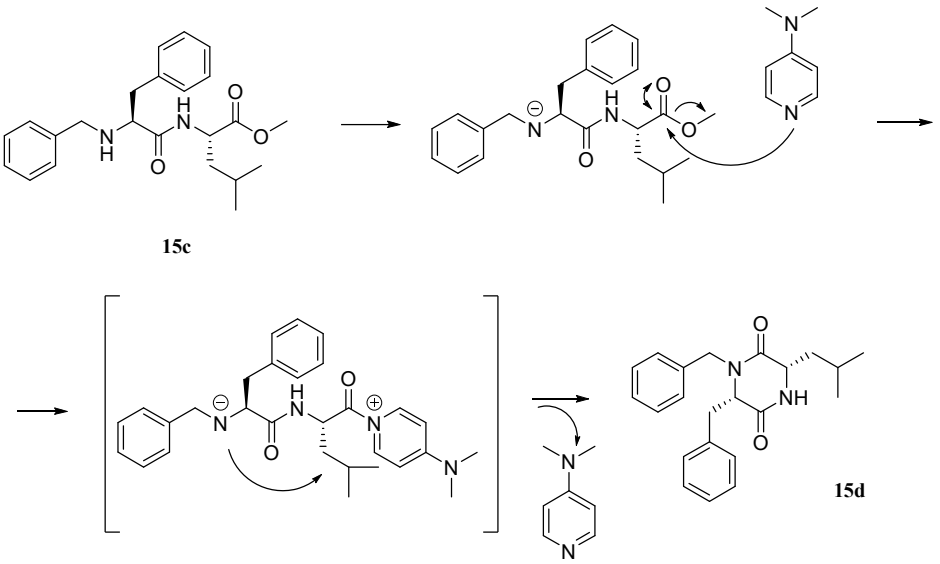

Scheme 9. Proposed mechanistic pathway for the cyclization catalyzed by DMAP and TEA.

At this stage, both amide functionalities of intermediate **15d** are reduced with lithium aluminum hydride ($LiAlH_4$) to furnish the piperazine core. The resulting intermediate then undergoes divergent functionalization pathways.

In one sequence, **15e** is coupled with 2-(naphthalen-1-ylamino)-2-oxoacetic acid via HATU-mediated amide bond formation in the presence of DIPEA, affording compound **15f**.
Catalytic hydrogenation over palladium on carbon (Pd/C) in methanol under a hydrogen-saturated atmosphere subsequently removes the Cbz protecting group, and the resulting free amine is employed directly in reactions with either Cbz-Osu to yield **16**, or with pyrazinoic acid to furnish **17**.

In the alternative pathway, **15e** is coupled with the previously synthesized (E)-3-(naphthalen-1-yl)acrylic acid **7** in the presence of WSC and HOBt. Subsequent catalytic hydrogenation removes the benzyl group, and the resulting intermediate is directly converted either into **18** through reaction with Cbz-Osu, or into **19** via reaction with pyrazinoic acid.

b) Preparation of α-hydroxyamide and α-ketoamide active motifs

The synthetic strategy mirrors that employed for the symmetrical piperazines. Upon reaching intermediates **20c** and **20d**, the benzyl protecting group is removed via catalytic hydrogenation, yielding intermediates that are directly utilized for the preparation of the final compounds **21-24**, as shown in *Scheme 10*.

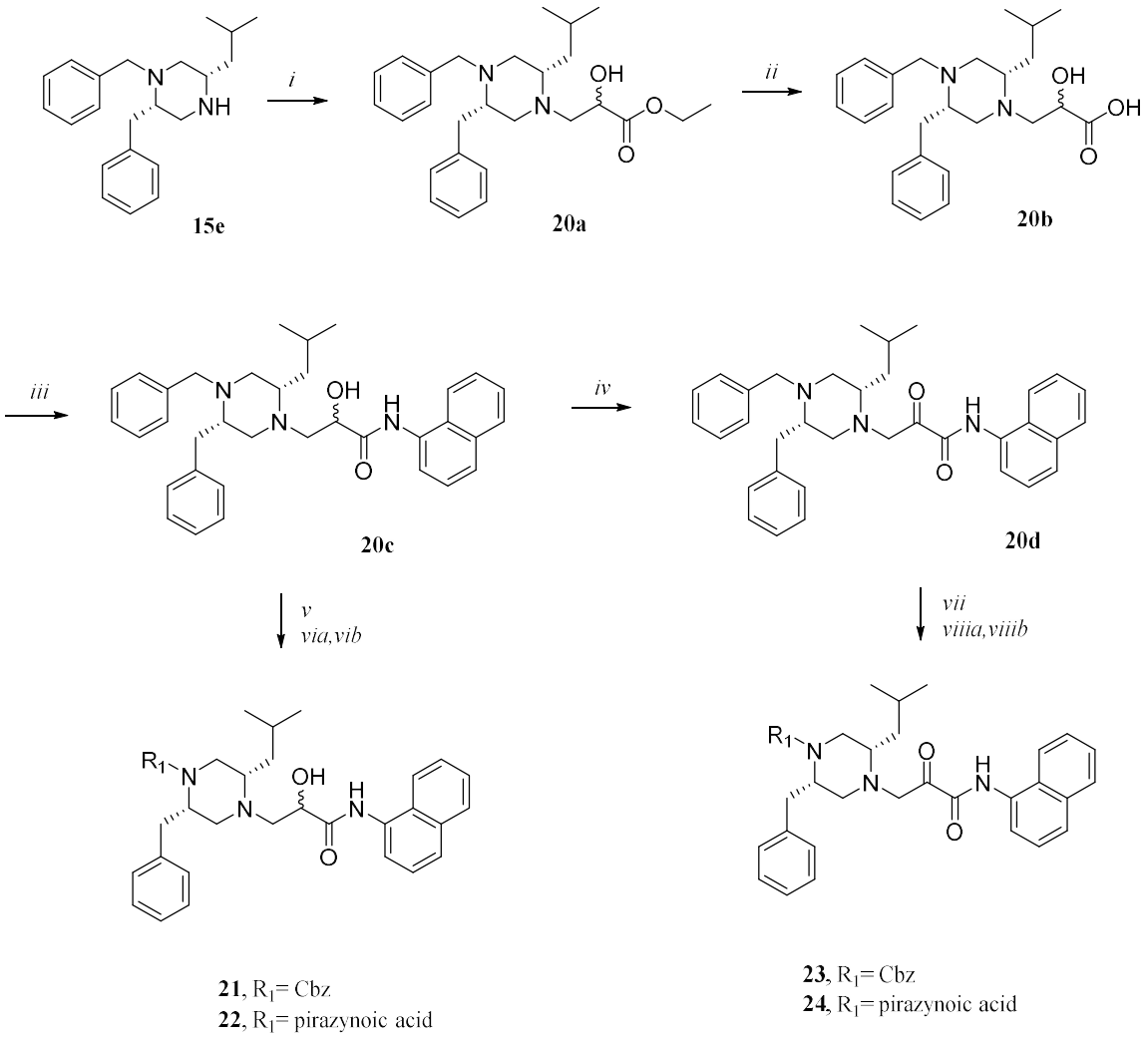

Scheme 10. General synthetic route for synthesis of compounds 21-24.

SYNTHESIS OF SECOND CLASS OF COMPOUNDS

The second class of compounds is distinguished by the incorporation of an additional leucine residue via formation of a urea linkage. This design was guided by the observation reported in a reference article, which indicated that tripeptides display an improved biological activity profile. Furthermore, new reactive functionalities were introduced, including vinyl sulfone, aldehyde, and α-ketoamide moieties, to further explore and modulate the biological properties of these derivatives.

- **SYMMETRICAL PIPERAZINES**

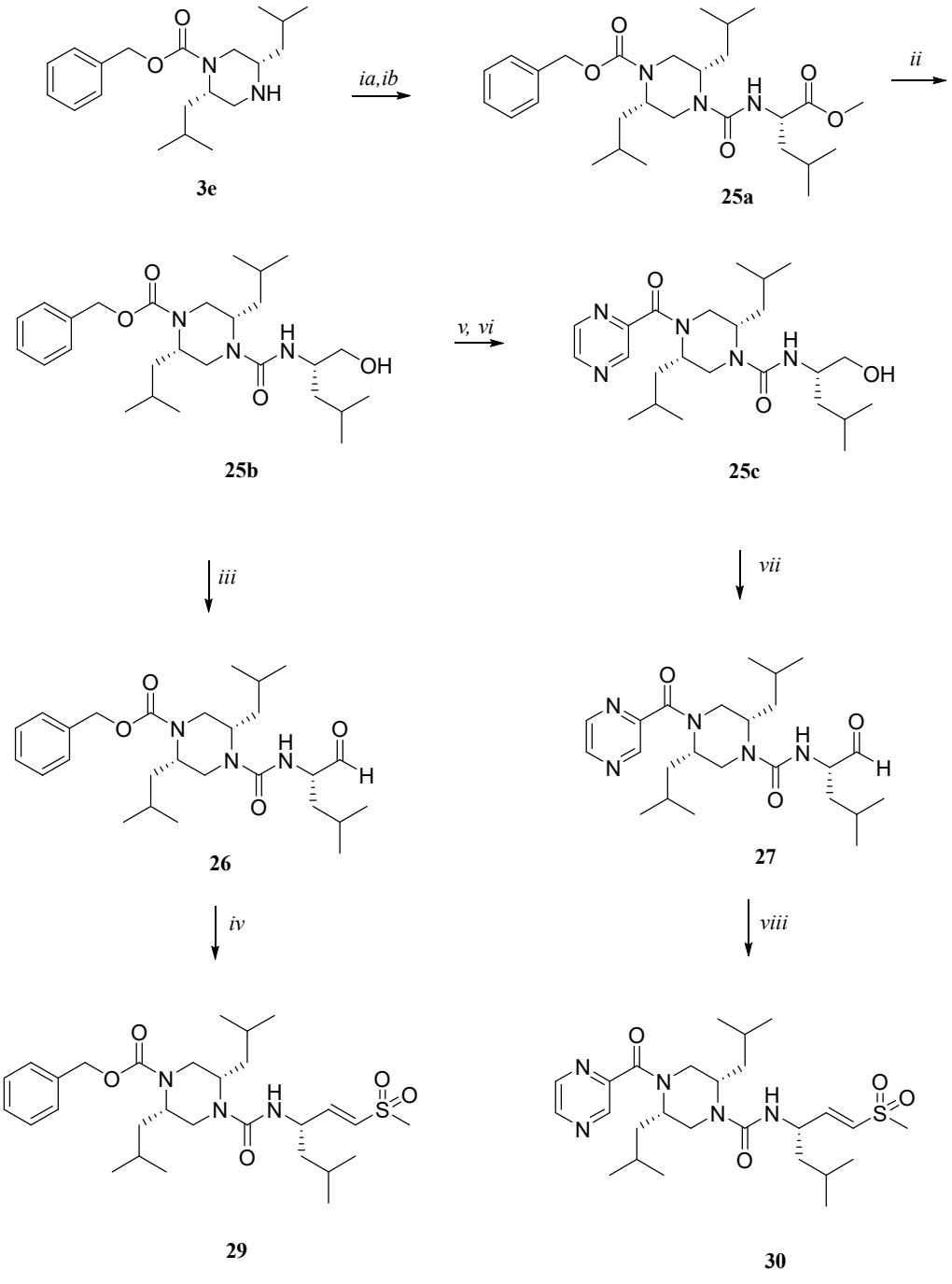

Experimental conditions:
ia. Triphosgene, L-leucine methyl ester hydrochloride, DCM, 0°C, 30 minutes. ib. TEA, CH_2Cl_2, overnight, rt.
ii. $NaBH_4$, anhydrous MeOH, anhydrous THF, overnight, rt.
iii, vii. Dess-Martin periodinane, anhydrous CH_2Cl_2, 3h, rt.
v. H_2, Pd/C 10%, HCl 1M, 16 h, rt.
vi. pyrazinoic acid, HATU, DIPEA, DMF, 2h, rt.
iv, viii. diethyl(methylsulfonyl)methylphosphonate, NaH, anhydrous THF, rt, 50 minutes.

Scheme 11. Synthetic strategy employed for the preparation of the second series of compounds, **26-30.**

The synthesis of this second class of symmetrical piperazines, featuring a tripeptidic framework, commences with the construction of a urea linkage from piperazine **3e**, proceeding through a two-step sequence. Initially, methyl 2-isocyanato-4-methylpentanoate is prepared by reacting L-leucine methyl ester with triphosgene at 0 °C (*Scheme 12*). This isocyanate is then coupled with piperazine **3e** in the presence of TEA, affording the urea-substituted derivative **25a**.

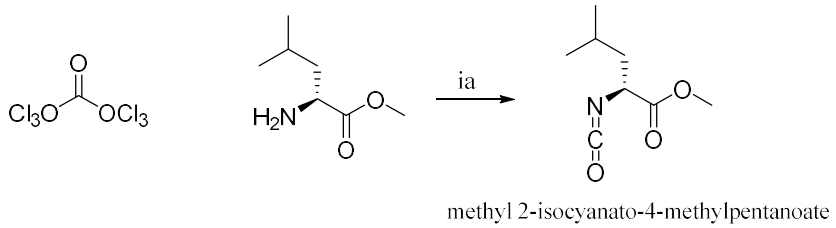

methyl 2-isocyanato-4-methylpentanoate

Experimental conditions:
ia. Triphosgene, L-leucine methyl ester hydrochloride, DCM, 0°C, 30 minutes.

Scheme 12. Synthetic strategy employed for the preparation of methyl 2-isocyanato-4-methylpentanoate.

The second step entails the selective reduction of the terminal ester to a primary alcohol using sodium borohydride ($NaBH_4$). Given the mild reactivity of $NaBH_4$, activation with anhydrous methanol is required to enable ester reduction, which would otherwise terminate at the aldehyde stage, as depicted is Scheme 13.

Methanol coordinates to the boron center via its lone pair, liberating molecular hydrogen and generating sodium methoxyborohydride. This species delivers a hydride to the carbonyl carbon, forming the corresponding alkoxide, which is then protonated to yield the aldehyde intermediate. Owing to the excess of reducing agent, a second hydride transfer and subsequent protonation occur, leading to the formation of the primary alcohol, **25b**.

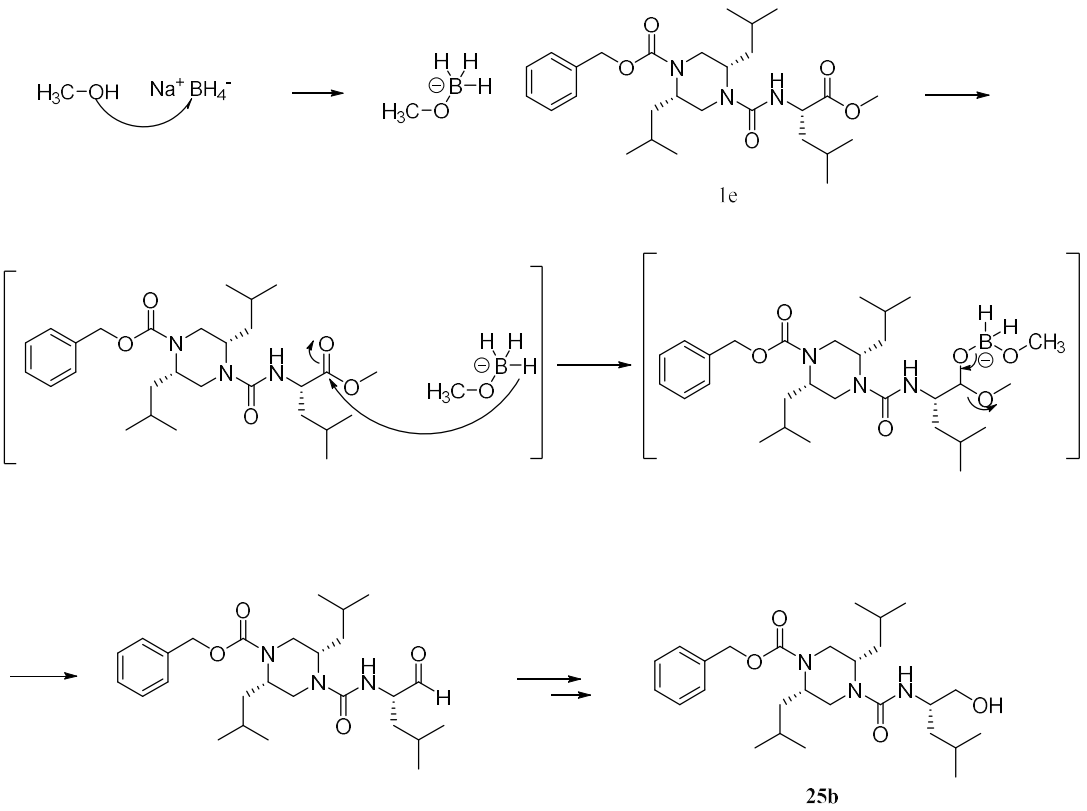

Scheme 13. Proposed mechanism for the reduction of an ester to the corresponding alcohol mediated by sodium borohydride and methanol.

The synthesis of the final compound **26** is accomplished via oxidation of the primary alcohol to the corresponding aldehyde using the mild hypervalent iodine oxidant Dess–Martin periodinane (DMP). In contrast, the preparation of compound **27** involves catalytic hydrogenolysis of the Cbz protecting group in derivative **25b**, affording the free amine, which is subsequently employed directly in an amidation with pyrazinoic acid using HATU and DIPEA as coupling agents.

Compounds **29** and **30** are obtained through further functionalization of **26** and **27**, respectively, via reaction with diethyl (methylsulfonyl)methylphosphonate **28**, effecting the transformation of the aldehyde functionality into a vinyl sulfone moiety (Scheme 14).

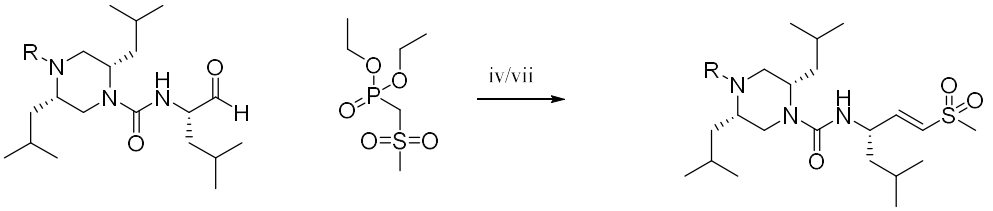

26, R= Cbz
27, R= pyrazinoic acid residue

29, R= Cbz
30, R= pyrazinoic acid residue

Experimental conditions:

iv, vii. NaH, anhydrous THF, rt, 50 minutes.

Scheme 14. Final step in the preparation of compound **4e**.

The reaction begins with an initial step aimed at synthesizing *diethyl(methylsulfonyl)methylphosphonate* **28** through an oxidation reaction using meta-chloroperbenzoic acid (m-CPBA), as shown in Scheme 15.

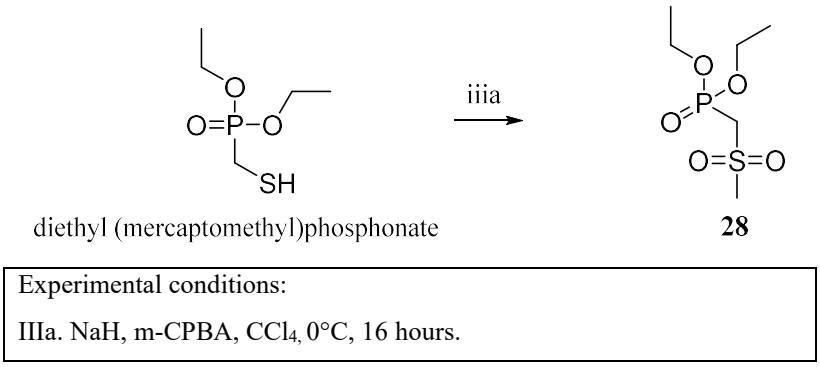

Scheme 15. Synthetic route employed for the preparation of diethyl(methylsulfonyl)methylphosphonate.

The reaction proceeds via a *Horner–Wadsworth–Emmons* (HWE) olefination, as illustrated in *Scheme 16*: initially, deprotonation of the carbon atom in the α-position to the phosphonate occurs through the action of a strong base, *sodium hydride* (NaH), leading to the formation of a stabilized carbanion known as a *phosphonate ylide*. This carbanion then acts as a nucleophile, attacking the aldehyde to form a β-hydroxyphosphonate intermediate.

Finally, the formation of the C=C double bond in the final compound 26 ε 27 takes place via the elimination of a diethyl phosphate molecule.

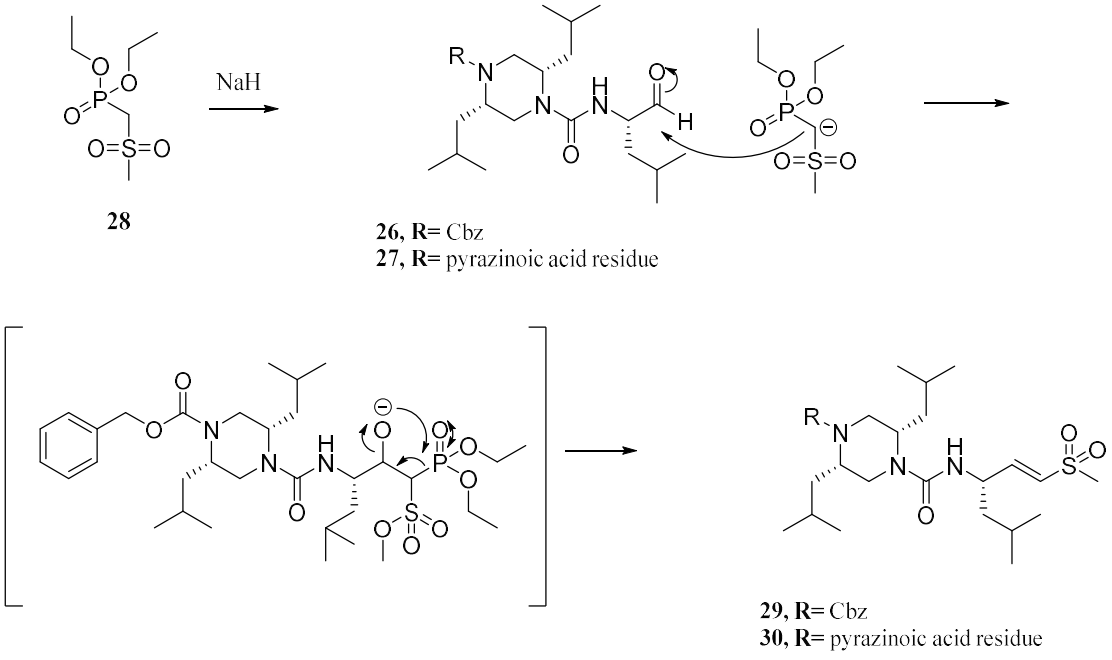

Scheme 16. Mechanism of *Horner–Wadsworth–Emmons* (HWE) olefination.

- **ASYMMETRICAL PIPERAZINES**

In the case of asymmetrical piperazines, the synthetic strategy remains largely analogous, with the distinction that, in step iii, the benzyl protecting group is removed from derivative **31b**, after which the sequence is continued in the same manner as for the symmetrical counterparts, as depicted in *Scheme 17*.

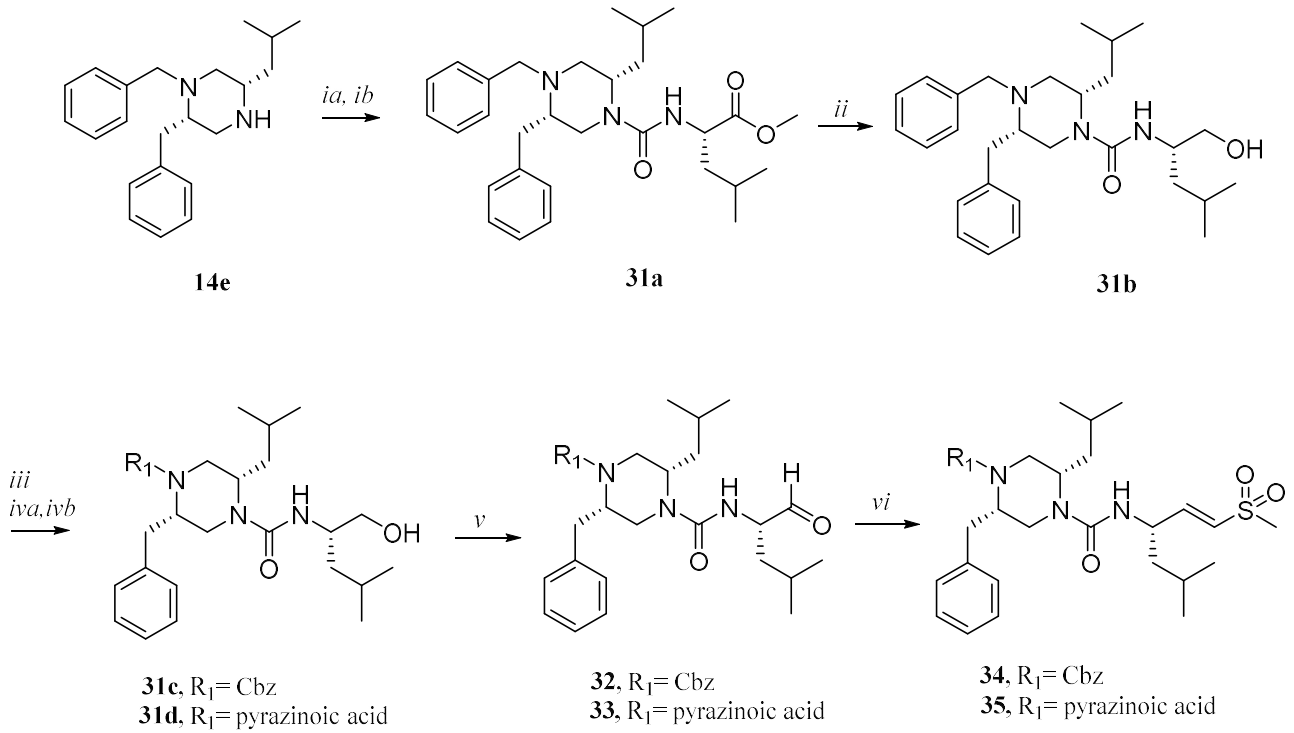

Experimental conditions:

ia. Triphosgene, L-leucine methyl ester hydrochloride, DCM, 0°C, 30 minutes.

ib. TEA, DCM, overnight, rt.

ii. $NaBH_4$, anhydrous MeOH, anhydrous THF, overnight, rt.

iii. H_2, Pd/C 10%, HCl 1M, 16 h, rt.

iva. Cbz-Osu, TEA, DCM, 2 h, rt.

ivb. pyrazinoic acid, HATU, DIPEA, DMF, 2h, rt.

v. Dess-Martin periodinane, anhydrous CH_2Cl_2, 3h, rt.

vi. H_2, Pd/C 10%, HCl 1M, 16 h, rt.

vi. iv, viii. diethyl(methylsulfonyl)methylphosphonate, NaH, anhydrous THF, rt, 50 minutes.

Scheme 17. General synthetic route to aldehyde- and vinyl-sulfone-containing compounds featuring an asymmetrical scaffold.

Synthesis of symmetrical and asymmetrical piperazines with α-ketoamides

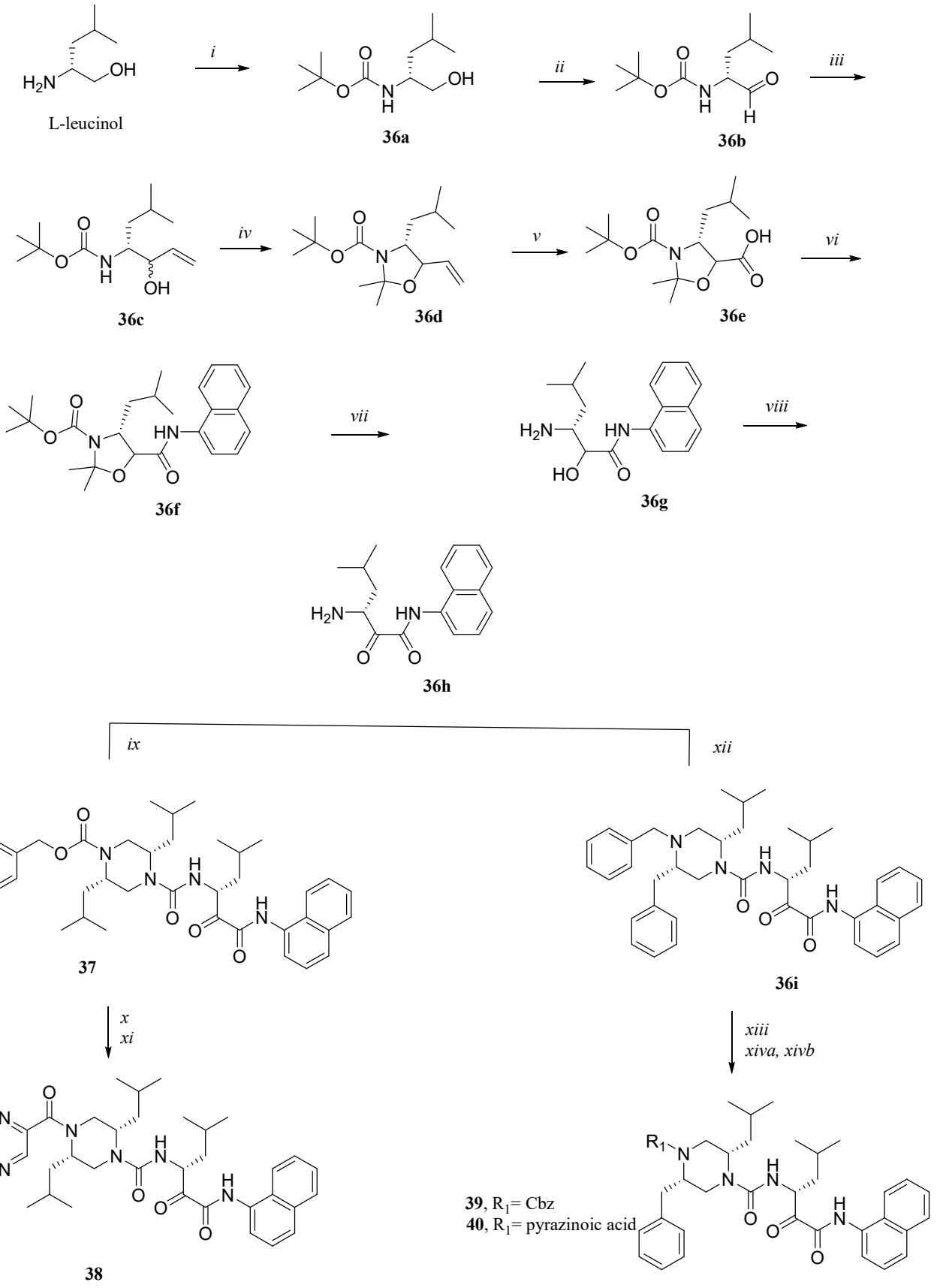

Experimental conditions:

i. Boc_2O, CH_2Cl_2, overnight, rt.

ii. Dess-Martin periodinane, anhydrous CH_2Cl_2, 6h, rt.

iii. C_2H_3MgBr, anhydrous THF, 16 h, rt.

iv. TsOH, $C_5H_{12}O_2$, CH_2Cl_2, 16 h, rt.

v. $NaIO_4$, RuO_2 x H_2O, C_3H_6O e H_2O, 16 h, rt.

vi. $C_{10}H_9N$, HATU, DIPEA, DMF, overnight, rt.

vii. TFA, CH_2Cl_2, 1h, rt.

viii. Dess-Martin periodinano, anhydrous CH_2Cl_2, 3h, rt.

ix,xii. TEA, CH_2Cl_2, overnight, rt.

x, xiii. H_2, Pd/C 10%, HCl 1M, 16 h, rt.

xi, xivb. pyrazinoic acid, HATU, DIPEA, DMF, 2h, rt.

xivb. Cbz-Osu, TEA, DCM, 2h, rt.

Scheme 18. Synthetic strategy employed for the preparation of compounds **37-40**.

A convergent synthetic strategy was selected for the preparation of compounds **37–40** to maximize the overall yield of the ten-step sequence.

L-Leucinol was first protected as its Boc derivative using *di-tert-butyl dicarbonate*. Subsequent oxidation of the resulting primary alcohol to the aldehyde was achieved with Dess–Martin periodinane, affording intermediate **36b**.

The aldehyde **36b** then underwent a Grignard addition with vinylmagnesium bromide. The polarized C–Mg bond renders the vinylic carbon nucleophilic, enabling attack on the aldehydic carbonyl to form a magnesium-coordinated alkoxide intermediate. Acidic work-up protonates this intermediate, yielding the allylic secondary alcohol **36c**. The corresponding mechanism is depicted in *Scheme 19*.

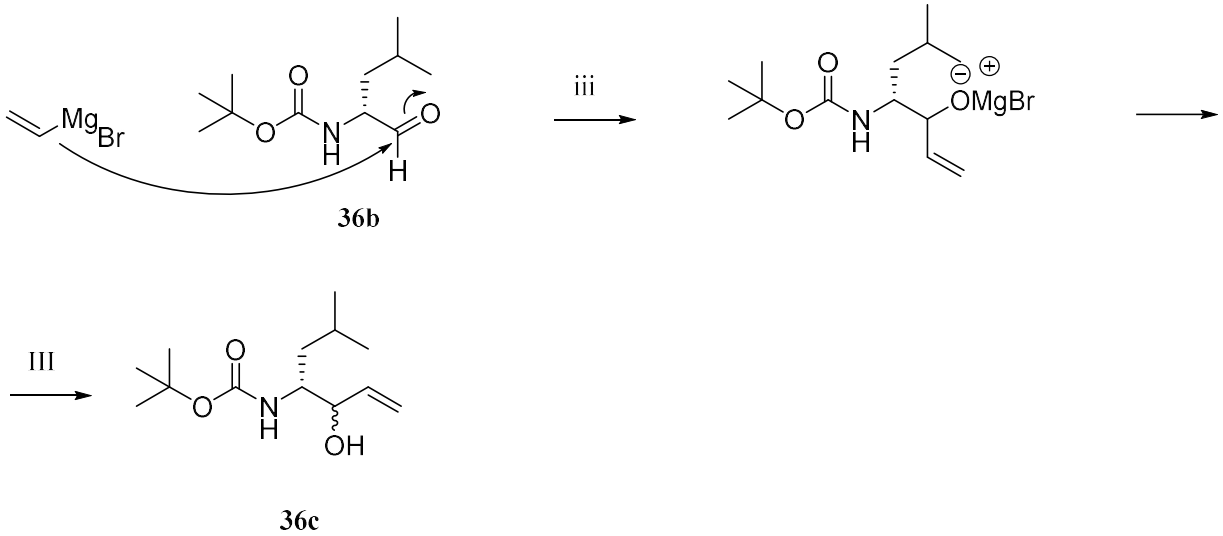

36b

36c

Scheme 19. Proposed mechanism for the Grignard reaction involving vinyl magnesium bromide.

The hydroxyl group was subsequently protected through formation of a **vinyl-oxazolidine** ring via reaction with *p-toluenesulfonic acid* (TsOH) and 2,2-dimethoxypropane. Protonation of one methoxy substituent of 2,2-dimethoxypropane by TsOH generates an oxonium intermediate, thereby enhancing the electrophilicity of the central acetal carbon. Nucleophilic attack by the side-chain hydroxyl group at C-3 on this activated center produces a hemiacetal intermediate with concomitant loss of methanol. The amino nitrogen then engages in intramolecular nucleophilic attack at the same carbon, promoting five-membered ring closure and releasing a second equivalent of methanol. This sequence affords the **oxazolidine** ring, protected by the isopropylidene moiety, corresponding to compound **36d**, as depicted in *Scheme 20*.

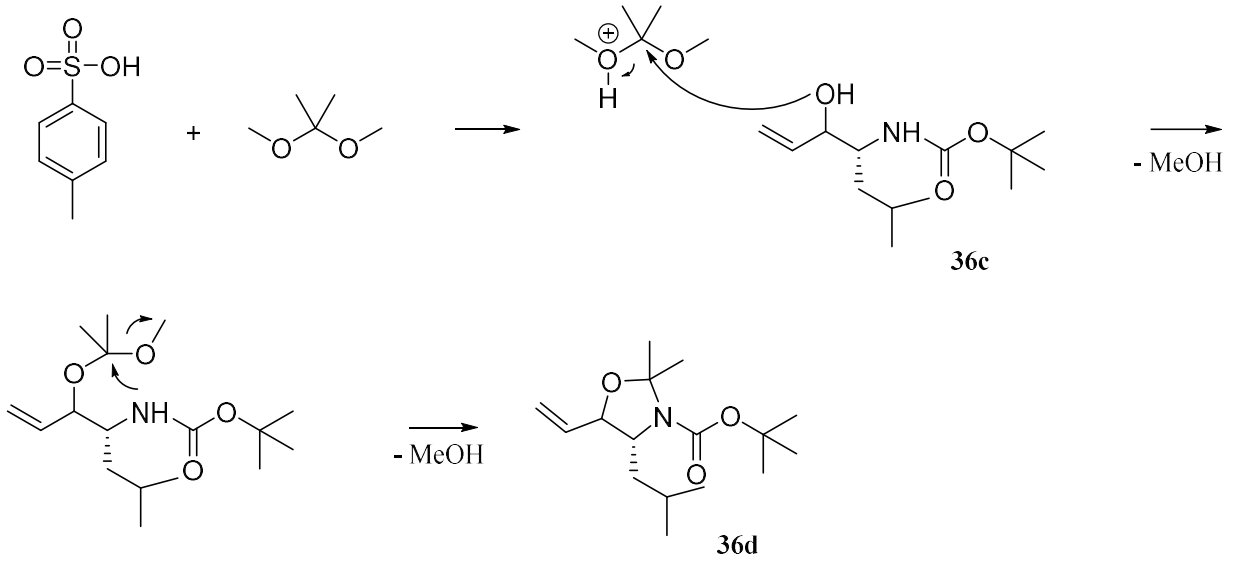

Scheme 20. Proposed mechanistic pathway for the formation of the oxazolidine nucleus.

In the fifth step, compound **36d** undergoes oxidation catalyzed by hydrated ruthenium(IV) oxide ($RuO_2 \cdot H_2O$) in the presence of sodium periodate ($NaIO_4$) as a terminal oxidant. Sodium periodate oxidizes Ru(IV) to Ru(VIII), generating ruthenium tetroxide (RuO_4) *in situ*, which constitutes the active oxidizing species. The vinyl moiety of 36d first engages with RuO_4 to form a transient vicinal diol, which is subsequently cleaved by periodate to yield the corresponding aldehyde. This intermediate then undergoes further oxidation to afford the carboxylic acid. Throughout the process, the ruthenium catalyst is reduced and continuously re-oxidized by sodium periodate, enabling catalytic turnover through sustained regeneration of RuO_4. This sequence furnishes compound **36e**, as illustrated in *Scheme 21*.

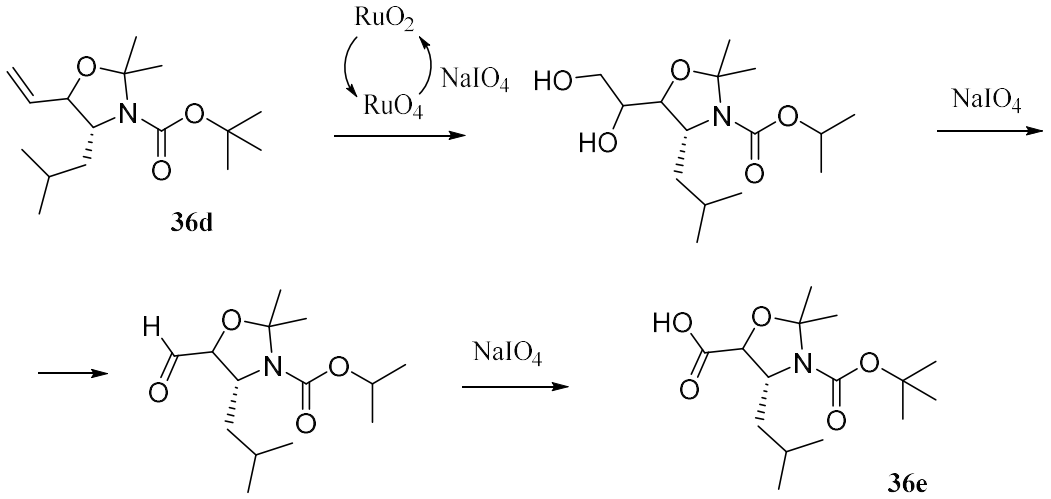

Scheme 21. Oxidation reaction catalyzed by *hydrated ruthenium (IV) oxide* in the presence of sodium periodate.

The sixth step consists of an amide bond formation between the carboxylic acid functionality of compound **36e** and *1-naphthylamine*. The coupling is carried out in DMF using HATU as the activating reagent and DIPEA as the base, yielding the corresponding amide **36f**.

In the seventh step, the oxazolidine protecting group is removed and the Boc group is cleaved under trifluoroacetic acid (TFA), affording **36g**.

The *eighth step* involves oxidation of the secondary alcohol to the corresponding ketone using Dess–Martin periodinane (DMP) **36h**.

The final common step entails formation of a urea moiety by reaction of the α-ketoamide-bearing intermediate with various symmetrical and asymmetrical piperazines, generating the first final compound **37** and the intermediate **36i**. Both species are then subjected to catalytic hydrogenation to remove the Cbz or benzyl protecting groups, respectively. This deprotection enables subsequent introduction of additional substituents, leading to the formation of compounds **38**, **39**, and **40**—the former two incorporating a *pyrazinoic acid* residue, while compound **39** retains the **Cbz** group.

Once all compounds had been synthesized and fully characterized, they were subjected to biological evaluation. This screening required the preparation of two **fluorescent probes**, which were synthesized specifically for use in the corresponding assays.

3.3 Synthesis of the Diagnostic Probes

The diagnostic probes follow a common synthetic route that differs only in one synthetic step, and they share the following structural features:

- A terminal group, either **vinylsulfonic** or **sulfonic** acid, which represents the only difference between the two compounds;
- **Three** sequential **leucine** residues;
- A spacer composed of **three aminohexanoic acid** residues;
- A fluorescent moiety, which in both cases is derived from **Bodipy-FL NHS ester**.

The general chemical structure is illustrated in *Figure 21*.

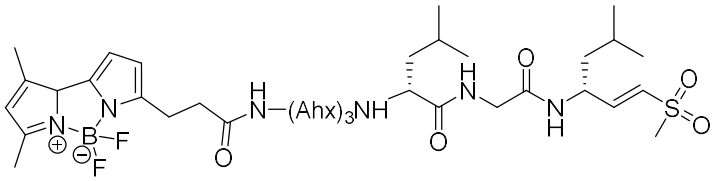

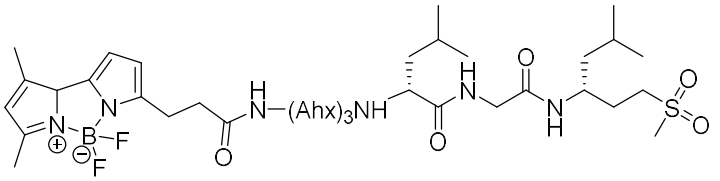

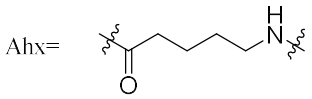

Figure 21. General chemical structures representing the two fluorogenic probes.

The synthesis of the two compounds, was carried out following a procedure reported in the literature,[110] which involves the functionalization of an inhibitory segment generally referred to as NH_2Ahx_3L3VS (similarly, the non-inhibitory segment $NH_2Ahx_3L_3S$ was synthesized) with a fluorophore, in this case represented by the Bodipy-FL NHS ester.

The initial part of the synthesis leading to the formation of compound **41d** was optimized in the liquid phase, in contrast to the procedure described in the literature,[120] allowing us to achieve higher yields of intermediate **41d**.

The general synthetic route is presented in *Scheme 22*.

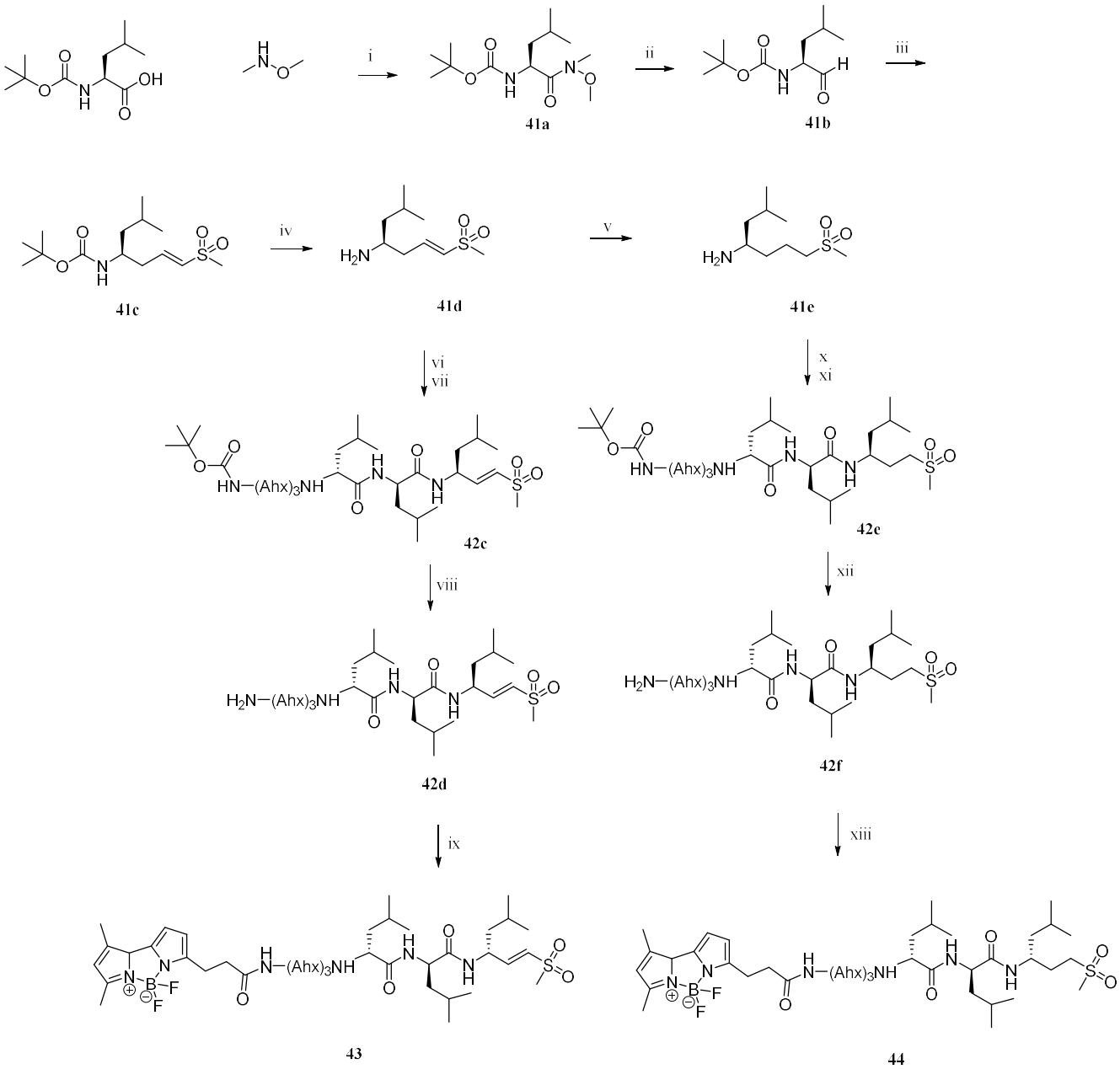

Experimental conditions:
i. WSC, HOBt, TEA, DMF, 16h, rt.
ii. $LiAlH_4$, Et_2O, 30 min, rt.
iii. diethyl(methylsulfonyl)methylphosphonate, anhydrous THF, 50 min, rt.
iv. TFA, CH_2Cl_2, 30 minuti, rt.
v. H_2, Pd/C, methanol, rt, 16 hours.
vi, x. **42b**, DIPEA, HATU, DMF, 16h, rt.
viii, xii. TFA, CH_2Cl_2, 30 min, rt.
ix, xiii. TEA, DCM, rt, 5 min.

Scheme 22. General strategy for the synthesis of fluorescent probes.

Synthesis of active fragments 41d and 41e

The synthesis of the active portions of the probes follows a five-step sequence, in which the first four transformations converge to intermediate **41d**; reduction of this species then affords **41e**, the fragment incorporated into *Probe 2*.

The route begins with an *amide coupling* between *Boc-L-leucine* and *N,O-dimethylhydroxylamine*, carried out in DMF with WSC and HOBt, which facilitates formation of the corresponding Weinreb amide (**41a**).

This intermediate is then subjected to *lithium aluminum hydride* ($LiAlH_4$), whose hydride attack on the amide carbonyl generates the characteristic tetrahedral complex in which the oxygen coordinates to aluminum. Collapse of this intermediate restores the carbonyl functionality and expels the N-methoxy-N-methylamine moiety, yielding the aldehyde **41b** with high chemoselectivity (*Scheme 23*).

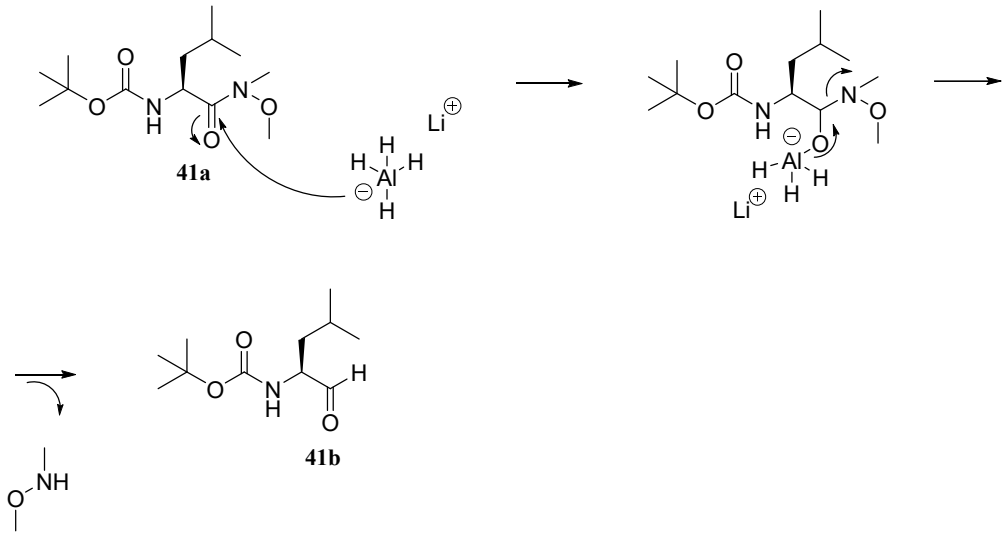

Scheme 23. Mechanistic pathway for the reduction of the Weinreb amide to the corresponding aldehyde, affording compound 41b.

The third step involves the formation of compound **41c** by using the diethyl(methylsulfonyl)methylphosphonate **28**, previously obtained by the oxidation by m-CPBA.

The reaction occurs through a Horner–Wadsworth–Emmons (HWE) olefination, with the mechanism previously examined in the context of the synthesis of compound 29-30 (*Scheme 16*).

During the fourth step of the synthesis, the Boc protecting group was removed to liberate the free amino functionality. This deprotection was achieved by treatment with trifluoroacetic acid (TFA) under standard conditions, leading to the formation of derivative **41d**, for **Probe 1**.

To generate the active fragment incorporated into **Probe 2**, compound **41d** is subjected to catalytic hydrogenolysis over *Pd/C* in methanol. Under these conditions, the vinyl sulfone moiety is selectively reduced, furnishing the corresponding saturated sulfone **41e**.

Once compound **41d** had been obtained, the second part of the synthesis was undertaken, aimed at constructing the inhibitory fragment with the general structure **H_2N–Ahx$_3$–L_3–VS**.
For *Probe 1*, the target segment comprises a vinyl-sulfonic terminus linked to a trileucine motif, followed by three aminohexanoic acid spacers and terminating in a free amino group.
This portion originates from the solid-phase synthesis of the peptide (2-(2-(2-hydrazinylhexanamido) hexanamido)hexanoyl)-D-leucyl-D-leucine (**42a**).

In preparation for the coupling step (vii), the peptide's N-terminus is first protected with a **Boc group** during the sixth step (*Scheme 24*). Only after this protection is installed can the peptide be coupled to residue **41d** via **amide bond formation**, thereby completing assembly of the inhibitory fragment. Specifically, the reaction involves the N-terminal amine of the vinyl-sulfonic derivative and the carboxylic acid group of the previously protected compound. The activation of the carboxylic group is mediated by HATU in the presence of DIPEA. Finally, the Boc protecting group is removed under acidic conditions using trifluoroacetic acid (TFA), affording compound **42d** (*Scheme 24*).

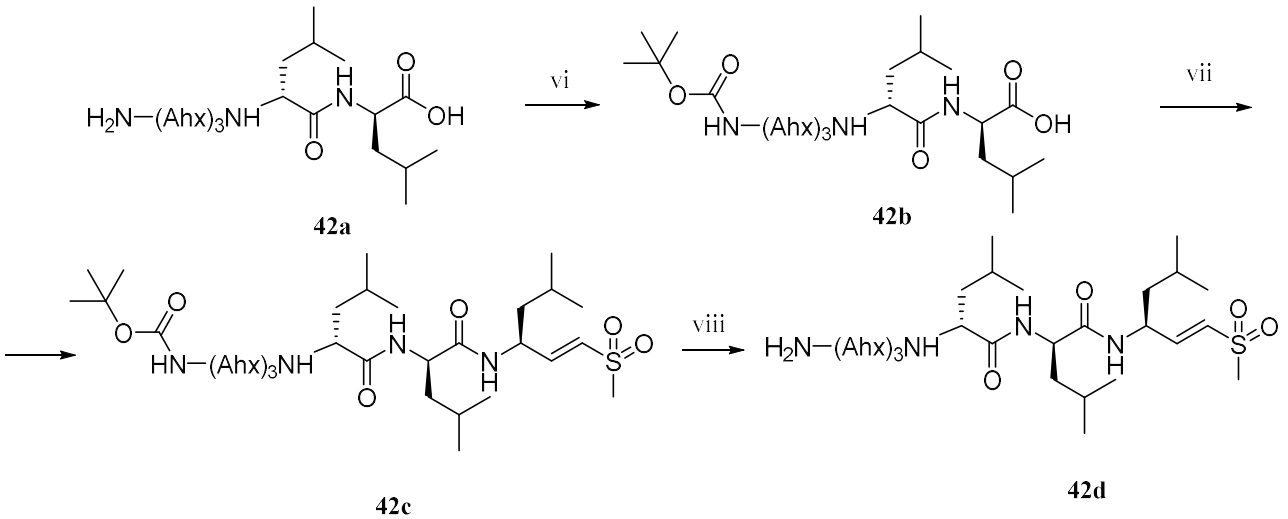

Experimental conditions:
vi. Boc_2O, DIPEA, DMF, 16h, rt.
vii. DIPEA, HATU, DMF, 16h, rt.
viii. TFA, CH_2Cl_2, 30 min, rt.

Scheme 24. Synthetic strategy for the preparation of intermediate 42d in route to Probe 1.

The final stage of the synthesis involves the functionalization of compound **42d** with a fluorophore, specifically Bodipy-FL NHS ester, illustrated in *Scheme 25*. This reaction introduces a fluorescent label through the formation of a stable amide bond between the NHS-activated ester and the free amine. The procedure for this conjugation is well established and has been previously described in the literature.[110]

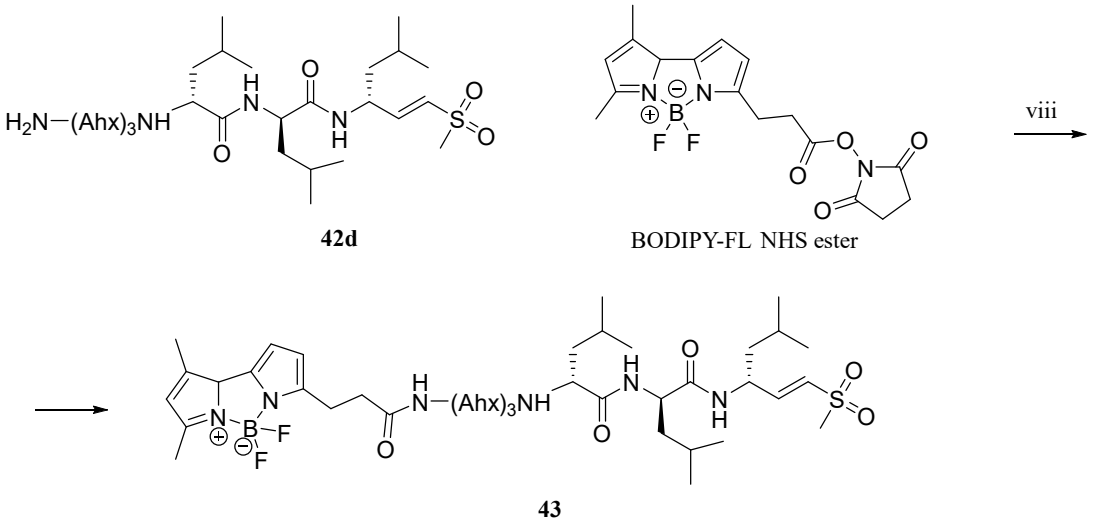

Scheme 25. Last synthetic step to afford *Probe 1* (**43**).

The same procedure is applied to synthesize **Probe 2**, starting from fragment **41e**. A summary of the process is presented in *Scheme 26.*

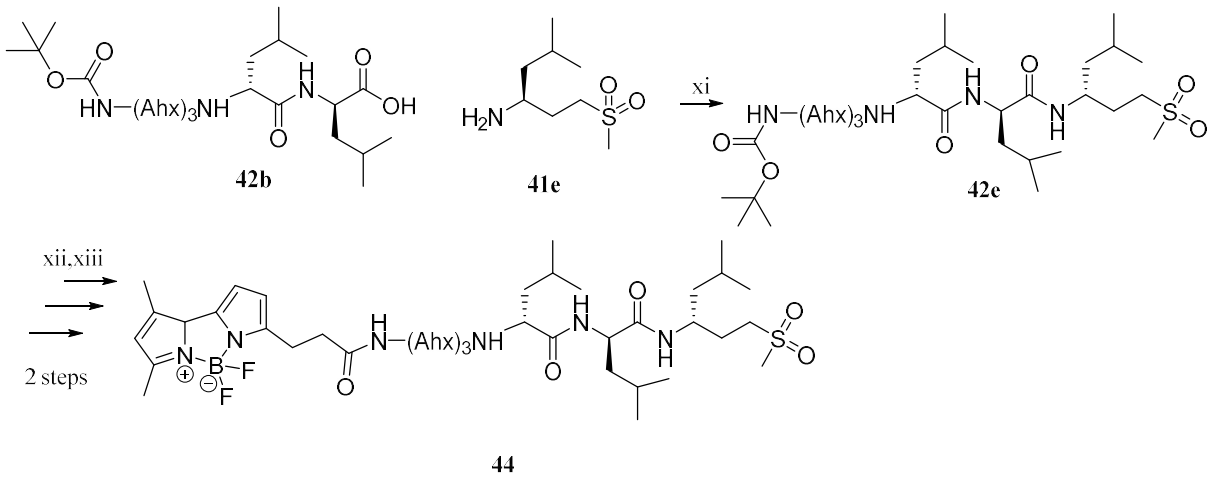

Experimental conditions:
xi. DIPEA, HATU, DMF, 16h, rt.
xii. TFA, CH_2Cl_2, 30 min, rt.
xiii. BODIPY-FL NHS ester, TEA, DCM, 5 min, rt.

Scheme 26. Synthetic pathway for the preparation of *Probe 2* (**44**).

3.4 BIOLOGICAL EVALUATION

All compounds were analyzed using a BD FACS Canto II flow cytometer, in collaboration with Prof. Francesco Nicoli's research group.

The overarching objective of this investigation was to monitor alterations in proteasome activity following the permeation of the synthesized compounds into HeLa cells (cervical cancer cell line) and their subsequent interaction with the proteasome complex.

Although the selected fluorogenic assay does not constitute the classical approach for evaluating the biological activity of proteasome inhibitors, its adoption ultimately proved strategically advantageous. Indeed, the assay's exceptional versatility enabled the simultaneous screening of a compact library of compounds (*Project 2*), allowing the identification of both positive and negative modulators of proteasome function.

This methodological flexibility, in turn, provided a unique opportunity to advance both research projects in parallel, thereby streamlining the experimental workflow and achieving a highly cost-effective strategy without compromising analytical rigor.

The underlying principle of the assay is based on the increase or decrease in fluorescence emitted by specific probes in the presence of the tested molecules. The fluorescence signal, recorded by the instrument as the number of cellular events, is directly proportional to proteasome activity. Therefore, treatment with diagnostic fluorescent probes is essential for the assessment.

- The **vinyl sulfone probe** is capable of interacting with the hydroxyl group of the N-terminal threonine residue in the catalytic β-subunit of the proteasome via its vinyl sulfone moiety. In this case, fluorescence increases linearly with the enzymatic activity of the complex. [110]
- The **sulfone probe**, lacking the vinyl group and containing only a sulfonic moiety, is unable to interact with the aforementioned catalytic subunit. However, it plays a crucial role as it allows for the determination of the fluorescence background, in the absence of proteasome interaction.

The measurement of net proteasome activity is obtained by calculating the difference between the fluorescence detected in the presence of the vinyl sulfone probe and that measured using the sulfone probe:

Net Activity = Vinyl sulfone fluorescence – Sulfone fluorescence

The experiments were conducted using reference compounds with known effects on proteasome activity:

- **MG132**: a known proteasome inhibitor that reduces proteolytic activity, resulting in a corresponding decrease in fluorescence; [121,122]
- **Pimozide**: a known activator that increases proteasome activity and the associated fluorescence signal; [107]
- **DMSO**: used as a solvent for all tested compounds; as it does not modulate the enzymatic complex, associated proteasome activity is considered to represent the baseline (100%).

All compounds were tested in triplicate, and the fluorescence emitted was measured for each replicate. Specifically, each experiment was conducted in a **double-blind** setup for each sample: HeLa cells were treated with culture medium containing the synthesized fluorescent probes. For each compound, two wells of cells were prepared:

- One well in which the cancer cells were treated with the **vinyl sulfone probe** and the compound under investigation;
- A second well in which the cells were treated with the **sulfone probe** and the same compound.

Following an appropriate detachment procedure to release the cells from the well surface, the samples were analyzed using a FACS (Fluorescence-Activated Cell Sorting) flow cytometer.
In this way, the fluorescence values emitted by the cells in the presence of each compound were recorded.

Each compound was tested in **three independent experiments**, and the **percentage of proteasome activity** for each was calculated. These values were then used to compute the **mean activity**. As a reference, compounds classified as proteasome inhibitors exhibit proteasomal activity below the 80% threshold, whereas activators are defined as those inducing proteasomal activity levels exceeding 120%.
The biological data are presented in Graphs 1 and 2, grouped according to the two classes.

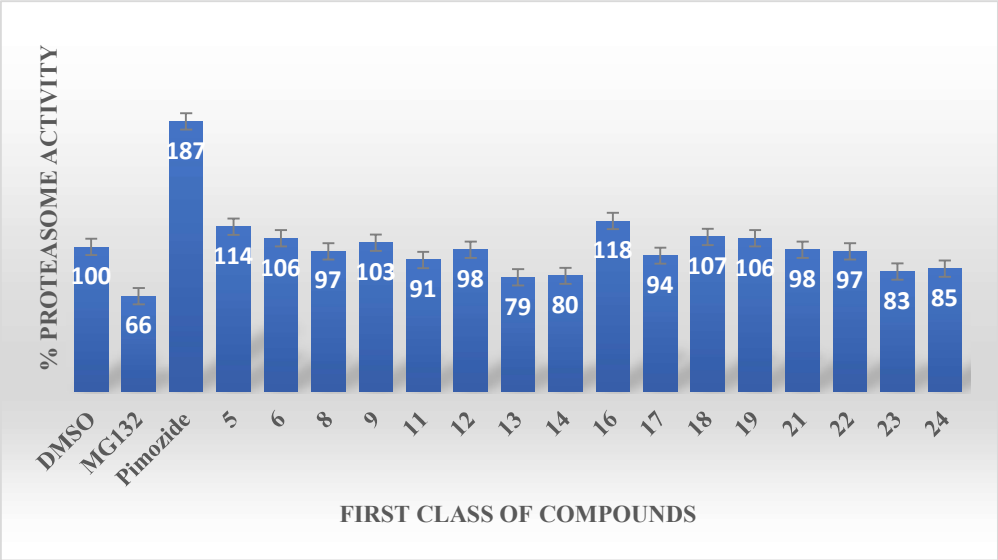

Graph 1. Biological results of the first class of synthesized compounds. Values represent the mean percentage of proteasome activity across all experiments, with DMSO-treated samples considered as the baseline (100% activity).

As illustrated in *Graph 1*, all compounds belonging to the first class exhibited mean proteasome activity values closely aligned with the DMSO baseline. Notably, the derivatives bearing the diamide moiety (**5**, **6**, **13**, and **14**) displayed activity levels exceeding 100%, indicative of a complete absence of inhibitory effect. This behaviour may be attributed to the insufficient electrophilicity of the diamide group, which likely prevents its effective recognition by the proteasome's catalytic site. The diamide functionality had originally been introduced as a substitute for the α-ketoamide group in an attempt to attenuate binding strength and reduce potential toxicity; however, this modification proved unsuccessful.

Similarly, compounds incorporating acrylamide or α-hydroxyamide warheads were also inactive, despite extensive literature describing these moieties as competent electrophilic groups capable of engaging the catalytic threonine residue of the proteasome.

Conversely, compounds featuring the α-ketoamide moiety displayed modestly improved inhibitory behaviour, though still approaching the 100% baseline. Specifically, compounds **13** and **14** showed inhibitory activities of **79%** and **80%**, respectively—slightly below the reference value of 80%—whereas compounds **21** and **22** presented activity levels comparable to the basal condition (~100%). This diminished activity may be attributed to the presence of a benzyl substituent at position 2 of the piperazine ring, whose hydrophobicity and steric bulk likely impede productive engagement with the catalytic site.

Collectively, these results suggest that the direct conjugation of electrophilic warheads to the piperazine core does not constitute a viable strategy for modulating proteasome activity. Indeed, the only derivatives exhibiting even minimal inhibitory effects were those bearing α-ketoamide groups

linked through a methylene spacer, indicating that spatial separation from the piperazine scaffold is critical for activity.

To the other side, in *Graph 2* are reported the data of the second series of compounds.

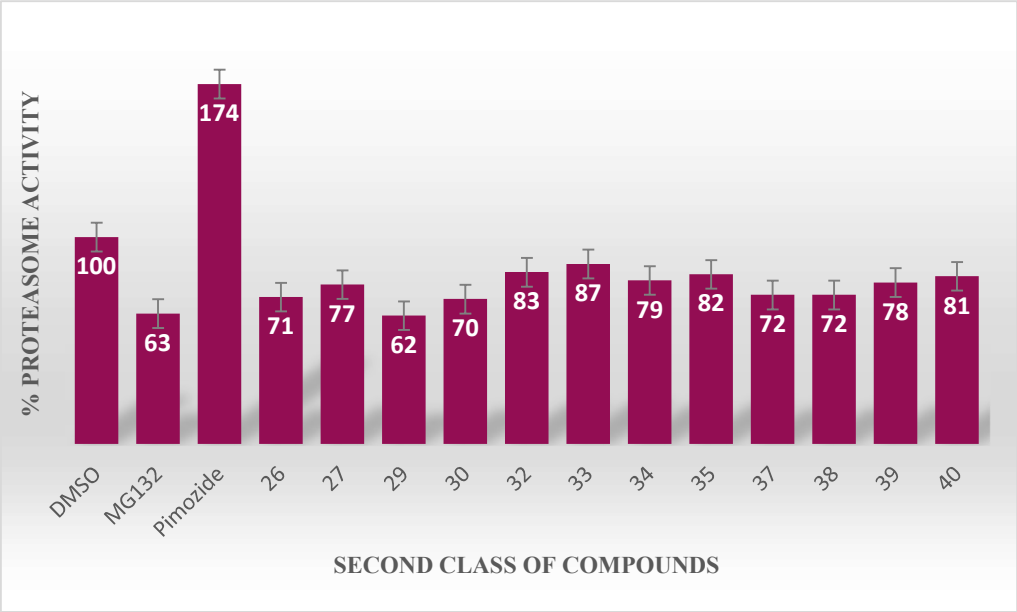

Graph 2. Biological results of the first class of synthesized compounds. Values represent the mean percentage of proteasome activity across all experiments, with DMSO-treated samples considered as the baseline (100% activity).

As illustrated in *Graph 2*, the inhibitory performance of the second class of compounds is markedly enhanced. In particular, compounds **26** and **27**, which feature an aldehyde moiety on a symmetrical piperazine scaffold, exhibited approximately 70% inhibition—slightly lower than inhibitory effect of the reference inhibitor MG132.

In contrast, derivatives bearing a benzyl group at position 2 displayed substantially reduced inhibitory effects, supporting the hypothesis that this substituent diminishes proteasome engagement. A similar trend emerges among the compounds featuring the α-ketoamide moiety: compounds **37** and **38** show superior activity relative to **39** and **40**, both of which include a benzyl substituent at position 2.

The most potent compound within this series is compound **29**, which incorporates a Cbz-protected symmetrical piperazine at position 1 and a vinyl sulfone group attached to the third leucine residue. The vinyl sulfone moiety is well known for its ability to form a covalent bond with the catalytic threonine of the proteasome, thereby conferring strong and irreversible inhibition. Following this, compound **30** displays an activity of approximately 70%, comparable to that of the aldehyde- and ketoamide-based analogues. Conversely, compounds **34** and **35** show significantly weaker inhibition, around 80%.

Overall, compound **29** emerges as the most effective inhibitor of proteasomal activity among all derivatives examined. Beyond the intrinsic reactivity of the vinyl sulfone warhead, the symmetrical piperazine appears to constitute the optimal substitution pattern, a finding consistent with previous studies demonstrating that trileucine-derived scaffolds yield high inhibitory potency. The introduction of an additional leucine residue proximal to the piperazine ring may therefore contribute to enhanced activity.

Finally, compound **29** surpasses its analogue containing a pyrazinoic acid substituent at position 1, possibly due to the ability of the Cbz protecting group to engage in favourable hydrogen-bonding interactions within the proteasome's catalytic environment, thereby facilitating access to—and retention within—the active site.

These findings indicate that the presence of asymmetrical piperazines bearing a benzyl substituent at position 2 appears to be associated with a reduction in inhibitory activity. Moreover, a direct linkage between the piperazine scaffold and the active moiety seems to exert a similar effect, with no substantial differences observed among bulky substituents at position 1. The only compounds exhibiting even minimal inhibitory activity are those in which the α-ketoamide moiety is separated from the piperazine ring by a methylenic spacer.

Compounds incorporating the leucine-derived third residue through a urea linker display enhanced activity, particularly compound 29, which demonstrates superior inhibitory potency compared with the reference inhibitor MG132. This analysis further confirms that benzyl substitution at position 2 correlates with diminished activity, whereas compounds featuring a symmetrical piperazine framework tend to be more active.

3.5 CONCLUSION

The first project was conceived with the objective of identifying new potential proteasome inhibitors, focusing specifically on the synthesis of direct inhibitors in which the conventional peptidic backbone was replaced by a non-peptidic scaffold.

In this context, drawing inspiration from the work of Pacifico et al.[114]—who reported several dipeptides and tripeptides as active proteasome inhibitors—the strategy adopted in this study relied on the cyclization of a dipeptide, thereby enabling the replacement of the classical peptidic framework with a piperazine core. This structural modification was intended to confer increased chemical stability and to reduce susceptibility to enzymatic degradation, while preserving the potential for biological activity.

Within this framework, two distinct series of compounds were designed and synthesized, comprising molecules bearing either symmetrical or asymmetrical piperazine scaffolds. The dipeptides selected for construction of the piperazine core were Leucine–Leucine—identified as the dipeptide most active in the reference study—and Phenylalanine–Leucine, a motif also present in several drugs such as bortezomib and carfilzomib. Furthermore, a bulky substituent was introduced at position 1, represented either by a Cbz group—typical of the peptides described in the reference article—or by a pyrazinoic acid residue, characteristic of bortezomib.

Finally, the two compound classes differ in the position of the active group relative to the piperazine: the first class consists of **pseudo-dipeptidic** derivatives in which the active group is directly attached to the piperazine core, whereas the second class comprises **pseudo-tripeptidic** analogues bearing an additional leucine residue linked to the scaffold through a urea moiety, with the active group located at the C-terminus of this residue.

The first series included molecules in which various functional groups were directly appended to the piperazine ring. Initially, four compounds (**5**, **6**, **16**, and **17**) were prepared, each containing a diamide functional group—an unprecedented motif not previously described in proteasome inhibitors. This substitution was introduced with the aim of replacing the classical α-ketoamide functionality, thereby circumventing its well-known limitations of reduced selectivity and metabolic instability.

Subsequently, additional molecules incorporating active groups previously reported in the literature were synthesized, specifically compounds **8**, **9**, **18**, and **19**, which feature an acrylamide moiety described as an effective pharmacophore for proteasome inhibition.

Moreover, compounds bearing α-hydroxyamide (**11**, **12**, **21**, and **22**) and α-ketoamide (**13**, **14**, **23**, and **24**) groups were prepared to determine whether the inactivity observed in the diamide-containing derivatives was attributable to the piperazine scaffold itself or to the new active group.

The second compound class was obtained by introducing an additional leucine residue connected via a urea spacer. This modification was designed to enhance in vivo stability by reducing peptidase-mediated degradation, thereby potentially improving the bioavailability of the molecules. As in the first series, compounds differed in their active groups, comprising aldehydes (**26**, **27**, **32** and **33**), vinyl sulfone derivatives (**29**, **30**, **34** and **35**), and α-ketoamides (**37–40**). These molecules also varied according to the symmetry or asymmetry of the piperazine scaffold and the nature of the bulky substituent at position 1.
All synthesized compounds were evaluated *in vitro* using a fluorogenic assay performed on HeLa cells. This method required the prior synthesis of two peptide-based fluorescent probes capable of monitoring proteasome activity through emission of a fluorescent signal.

The assay was calibrated using three reference conditions that reflected distinct functional states of the proteasome: *DMSO* as a control representing basal activity, *MG132* as a reference inhibitor indicative of reduced activity, and *pimozide* as a reference activator producing increased activity. These controls ensured the reliability of the assay and provided a robust framework for interpreting the activity of the newly synthesized compounds.

The results revealed clear differences in activity between the two classes of compounds.
Molecules belonging to the first series, in which the active groups were directly attached to the piperazine scaffold, exhibited no significant inhibitory effect and produced proteasome activity values close to 100%, comparable to the DMSO control. Only compounds **13** and **14** demonstrated a modest inhibitory effect, corresponding to symmetrical piperazine derivatives bearing an α-ketoamide moiety positioned at a distance from the scaffold through a methylenic spacer. This finding suggests that direct attachment of the recognition group to the piperazine core is insufficient for effective engagement with the proteasome active site, and that the introduction of a spacer may enhance inhibitory potency.

In contrast, the second series of compounds displayed promising inhibitory activity, with profiles closely resembling that of MG132.

In particular, derivatives bearing aldehyde or α-ketoamide groups exhibited approximately 70% inhibition, slightly less potent than MG132. Within this series, compounds featuring a symmetrical piperazine scaffold demonstrated superior activity, whereas those containing a benzyl group at position 2 showed reduced potency, suggesting that substitution at this position may hinder interaction with the proteasome.

Notably, compounds containing a vinyl sulfone moiety exhibited the most favorable activity. Among them, compound **29**—bearing a symmetrical, Cbz-protected piperazine—displayed 62% activity, exceeding the inhibitory effect of MG132. This result indicates that compound **29** possesses a meaningful capacity to modulate proteasome activity while offering the potential advantage of a non-peptidic structure, which may confer enhanced stability and improved pharmacokinetic properties.

Collectively, these findings underscore the potential of the adopted design strategy to yield novel non-peptidic proteasome inhibitors with promising biological activity.
Despite the variability in activity among the synthesized molecules, the results obtained thus far have enabled the identification of a subset of compounds with potential modulatory effects on the proteasome. Future work will involve a detailed assessment of the most promising candidates using purified proteasome preparations, with the objective of confirming their direct inhibitory potential and clarifying the nature of their biological effects. To this end, these compounds are currently being examined on isolated proteasome complexes to elucidate their mode of interaction with the catalytic threonine residue, the kinetics of binding, and any potential subunit selectivity. Ultimately, this project has established a solid foundation for the rational design of nvel non-peptidic proteasome inhibitors, paving the way for future optimization of structure–activity relationships and for potential applications in proteasome-related therapeutic research.

3.6 EXPERIMENTAL SECTION

3.6.1 Materials and Methods

The progress of the reactions was monitored by Thin Layer Chromatography (TLC) using Macherey-Nagel Poligram SIL/UV 254 silica gel plates (0.25 mm thickness), compatible with ultraviolet detection at 254 nm, and visualized by staining with an aqueous solution of potassium permanganate ($KMnO_4$, 2%).

The molecular weights of the reaction products were verified using an electrospray ionization mass spectrometer (ESI-MS, MICROMASS ZMD 2000). Samples for mass spectrometric analysis were prepared by diluting the reaction mixture in a solution composed of H_2O (40%), CH_3CN (60%), and trifluoroacetic acid (TFA, 0.1%).

Purification of intermediate compounds was carried out via conventional column chromatography using Merck silica gel (230–240 mesh). The eluent phase consisted of mixtures of ethyl acetate and petroleum ether, with proportions adjusted according to the polarity of the compound to be purified.

Final compounds were purified using a preparative HPLC system (DELTA PREP 3000, Waters, USA) equipped with a Delta-Pak C18 300 Å column (30 × 3 cm, 15 µm particle size). Solvent A consisted of H_2O containing 0.1% TFA, while solvent B was a mixture of CH_3CN and H_2O (60:40, v/v) also containing 0.1% TFA. Chromatographic conditions were adjusted based on the retention times of the compounds to be purified.

^1H NMR and ^{13}C NMR (DEPT) spectra were recorded on a VARIAN 400 MHz spectrometer. Samples for NMR analysis were prepared in $CDCl_3$, DMSO-d_6 or MeOD-d_4.

The NMR spectra that are not reported here have already been described in the literature.

3.6.2 General synthetic procedures for synthesis of piperazine core

General procedure for synthesis of dipeptide (3a, 15a)

To a solution of Boc-protected amino acid (1 equiv., 13 mmol) in DMF (10 mL), HOBt (1 equiv., 13 mmol) and WSC (1 equiv., 13 mmol) were added at 0 °C. After complete dissolution, a solution of L-Leucine methyl ester hydrochloride (1.1 equiv., 14.3 mmol) and triethylamine (TEA, 1 equiv., 13 mmol) in DMF was added dropwise. The reaction mixture was stirred at room temperature for 16 hours.

The solvent was then removed under reduced pressure, and the resulting oily residue was diluted with ethyl acetate. The organic layer was sequentially washed with 10% aqueous citric acid, 5% aqueous sodium bicarbonate, and brine. After drying over anhydrous sodium sulfate and filtration, the solvent was removed under vacuum to afford a solid, which was used in subsequent steps without further purification.

Methyl (tert-butoxycarbonyl)-L-leucyl-L-leucinate (3a)

The starting Boc-protected amino acid is the Boc-L-Leucine.

^{1}H NMR (400 MHz, $CDCl_3$) δ 4.93 (s, 1H), 4.2 (s, 1H), 3.71 (s, 3H), 1.63 (m, J = 4.8 Hz, 6H), 1.57 (m, 2H), 1.55 (m, J = 7.6 Hz, 9H), 0.95 (dd, J = 6 Hz, 12 H).

White solid. Yield: 87%. ESI-MS: $[M+H]^+$: 359.43.

Methyl (tert-butoxycarbonyl)-L-phenylalanyl-L-leucinate (15a)

The starting Boc-protected amino acid is the Boc-L-Phenilalanine.

^{1}H NMR (400 MHz, $CDCl_3$) δ 7.30 – 7.18 (m, 5H), 4.55 (dd, J = 8.3 Hz, 1H), 4.34 (d, J = 6.4 Hz, 1H), 3.69 (s, 3H), 3.06 (d, J = 6.9 Hz, 2H), 1.60 – 1.51 (m, 2H), 1.50 – 1.44 (m, 1H). 1.41 (s, 9H), 0.89 (dd, J = 7.6 Hz, 6H).

White solid. Yield: 82%. ESI-MS: $[M+H]^+$: 393.30.

General procedure for Boc deprotection (3b, 15b)

To a solution of compounds **3a** or **15a** (1 equiv., 2.18 mmol) in DCM (7 mL), trifluoroacetic acid (TFA, 4 mL) was added. The reaction mixture was stirred at room temperature for 30 minutes.

The solvent was then removed under reduced pressure. The resulting residue was crystallized by use of diethyl ether, filtered under vacuum, affording compound as a solid.

Methyl L-leucyl-L-leucinate (3b)

^{1}H NMR (400 MHz, $CDCl_3$) δ 4.93 (s, 1H), 4.2 (s, 1H), 3.71 (s, 3H), 1.63 (m, J = 4.8 Hz, 6H), 1.57 (m, 2H), 0.95 (dd, J = 6 Hz, 12 H).

White solid. Yield: 95 %. ESI-MS: $[M+H]^+$: 259.19.

Methyl L-phenylalanyl-L-leucinate (15b)

^{1}H NMR (400 MHz, $CDCl_3$) δ 7.3 – 7.18 (m, 5H), 4.55 (dd, J = 8.3 Hz, 1H), 4.34 (d, J = 6.4 Hz, 1H), 3.69 (s, 3H), 3.06 (d, J = 6.9 Hz, 2H), 1.60 – 1.51 (m, 2H), 1.50 – 1.44 (m, 1H), 0.89 (dd, J = 7.6 Hz, 6H).

White solid. Yield: 98.9 %. ESI-MS: $[M+H]^+$: 293.34.

Synthesis of (3S,6S)-3,6-diisobutylpiperazine-2,5-dione (3c)

A solution of methyl-L-leucyl-L-leucinate (1 equiv., 5.81 mmol) in *n*-butanol (58.5 mL) and toluene (34.5 mL) was heated under reflux at 120 °C for 16 hours. After cooling to room temperature, the solvent was removed under reduced pressure, yielding a colorless oil.

The crude product was crystallized by diethyl ether, filtered under vacuum, affording compound **3c** as a white solid.

^{1}H NMR (400 MHz, $CDCl_3$) δ 6.77 (s, 2H), 3.98 (dt, J = 2.8 Hz, 2H), 1.79 (m, 4H), 1.66 (m, J = 6.4 Hz, 2H), 0.95 (dd, J = 6.4, 12H).

Yield: 98 %. ESI-MS: $[M+H]^+$: 227.19.

Synthesis of methyl benzyl-L-phenylalanyl-L-leucinate (**15c**)

Under anhydrous conditions, to a solution of compound **15b** (1 equiv., 3.4 mmol) in methanol, TEA (1 equiv., 3.4 mmol) and benzaldehyde (1.2 equiv., 4.08 mmol) were added. The reaction mixture was stirred at room temperature for 90 minutes.

The temperature was then lowered to 0 °C, and sodium borohydride (2 equiv., 6.8 mmol) was added in small portions. The reaction was stirred at room temperature for an additional 30 minutes.

The solvent was removed under reduced pressure, and the resulting residue was diluted with ethyl acetate. The mixture was extracted three times with water and washed with brine.

The organic phase was dried over anhydrous Na_2SO_4, filtered, and concentrated under reduced pressure.

The compound was purified by preparative HPLC as a white solid.

^{1}H NMR (400 MHz, $CDCl_3$) δ 7.45 – 6.99 (m, 10H), 4.47 (t, J = 7.7 Hz, 1H), 3.94 (s, 2H), 3.76 (s, 3H), 3.32 (t, J = 7.0 Hz, 1H), 3.07 (dd, J = 12.4 Hz, 1H), 2.68 (dd, J = 12.4 Hz, 1H). 1.87 (t, J = 7.6 Hz, 1H), 1.68 (t, J = 7.6 Hz, 1H), 1.55 – 1.32 (m, 1H), 1.02 (d, J = 6.3 Hz, 6H).

Yield: 91 %. ESI-MS: $[M+H]^+$: 383.12.

Synthesis of (3S,6S)-1,6-dibenzyl-3-isobutylpiperazine-2,5-dione (**15d**)

To a solution of compound **15c** (1 equiv., 0.25 mmol) in xylene (5 mL), TEA (1.2 equiv., 0.3 mmol) was added, and the mixture was stirred for 30 minutes. Catalytic amounts of DMAP were then added, and the reaction was refluxed at 140 °C for 24 hours.

The solvent was removed under reduced pressure, and the residue was purified by column chromatography using a ethyl acetate/petroleum ether mixture (1:9) as the eluent, affording **15d** as a white solid.

^{1}H NMR (400 MHz, DMSO) δ 8.3 (s, 1H), 7.4 – 7.0 (m, 10H), 5.2 (d, J = 14.8, 1H), 3.94 (t, 2H), 3.6 (m, 1H), 3.32 (dd, 1H), 3.1 (dd, 1H), 1.45 (m, 1H), 0.6 (m, J = 2.4 Hz, 8H).

Yield: 72 %. $[M+H]^+$: 351.67.

General procedure for synthesis of piperazine (3d, 15e)

To a suspension of $LiAlH_4$ (10 equiv., 44.2 mmol) in anhydrous THF (15 mL), under anhydrous conditions, a solution of diketopiperazine (1 equiv., 4.42 mmol) in THF was added dropwise. The reaction mixture was then heated under reflux at 80 °C for 2 hours.

The excess reducing agent was quenched by the careful addition of ice. The mixture was filtered through celite, washing with methanol, and the filtrate was concentrated under reduced pressure, affording the compound as an oil.

(2S,5S)-2,5-diisobutylpiperazine (3d)

^1H NMR (400 MHz, $CDCl_3$) δ 2.80 – 2.67 (m, 2H), 2.55 – 2.42 (m, 4H), 1.86 – 1.71 (m, 2H), 1.33 – 1.22 (m, 6H), 1.01 (d, J = 6.3 Hz, 12H).

Yellow oil. Yield: 70 %. ESI-MS: $[M+H]^+$: 199.46.

(2S,5S)-1,2-dibenzyl-5-isobutylpiperazine (15e)

^1H NMR (400 MHz, DMSO) δ 7.40 – 7.15 (m, 10H), 4.0 - 3.7 (dd, 2H), 3.3 (m, 1H), 3.0 (m, 3H), 2.9 (t, J = 6.8 Hz, 2H), 2.7 (d, 2H), 2.6 – 2.4 (m, 3H). 0.8 (m, J = 6 Hz, 6H).

White solid. Yield: 76 %. ESI-MS: $[M+H]^+$: 323.25.

Synthesis of benzyl (2S,5S)-2,5-diisobutylpiperazine-1-carboxylate (3e)

To a solution of compound **3d** (1 equiv., 5.5 mmol) in DCM, *N-(Benzyloxycarbonyloxy)succinimide* (Cbz-Osu) (0.3 equiv., 1.65 mmol) was added, and the mixture was stirred for 30 minutes. Two additional portions of CBZ-Osu (0.3 equiv. and 0.2 equiv., corresponding to 1.65 mmol and 1.1 mmol, respectively) were then added at 30-minute intervals.

After a further 30 minutes of stirring, the solvent was removed under reduced pressure. The residue was diluted with ethyl acetate and extracted with 5% aqueous $NaHCO_3$ and brine. The organic phase was dried over anhydrous Na_2SO_4, filtered, and concentrated under reduced pressure.

The crude product was purified by column chromatography using a 1:3 mixture of ethyl acetate/petroleum ether as the eluent, affording compound **3e** as a yellow oil.

^1H NMR (400 MHz, $CDCl_3$) δ 7.37 – 7.27 (m, 5H), 5.2 (t, J = 7.1 Hz, 2H), 3.15 (m, 4H), 1.7 (t, 2H), 1.5 (m, 4H), 0.9 (m, 14H).

Yield: 89 %. ESI-MS: $[M+H]^+$: 333.24.

Synthesis of final compounds

Synthesis of Ethyl 2-(naphthalen-1-ylamino)-2-oxoacetate (3f)

To a solution of 1-naphthylamine (1 equiv., 4.89 mmol) in DMF, triethylamine (TEA, 1.2 equiv., 5.87 mmol) was added. The reaction mixture was cooled in an ice bath, and a solution of ethyl 2-chloro-2-oxoacetate (1 equiv., 4.89 mmol) in DMF was added dropwise.

The mixture was stirred at room temperature for 16 hours. The solvent was removed under reduced pressure, and the resulting solid residue was diluted with ethyl acetate and extracted with 1 M aqueous HCl and brine.

The organic phase was dried over anhydrous Na_2SO_4, filtered, and concentrated under reduced pressure to afford a white solid, which was used without further purification.

^1H NMR (400 MHz, $CDCl_3$) δ 9.4 (s, 1H), 8.3 - 7.2 (m, 7H), 4.5 (m, J = 7.4 Hz, 2H), 1.5 (t, J = 5.6 Hz, 3H).

Yield: 66 %. ESI-MS: $[M+H]^+$: 243.26.

Synthesis of 2-(Naphthalen-1-ylamino)-2-oxoacetic Acid (4)

To a solution of ethyl 2-(naphthalen-1-ylamino)-2-oxoacetate (1 equiv., 3.19 mmol) in dioxane (5 mL), 1 M NaOH (6.66 mL) was added. The reaction mixture was stirred at room temperature for 16 hours.

The reaction was then neutralized with 1 M HCl, and the solvent was removed under reduced pressure. The resulting solid residue was diluted with ethyl acetate and extracted with water, followed by a wash with brine.

The organic phase was dried over anhydrous Na_2SO_4 and concentrated under reduced pressure to yield a pink solid.

^1H NMR (400 MHz, $CDCl_3$) δ 9.5 (s, 1H), 8.15 - 7.5 (m, 7H).

Yield: 79 %. ESI-MS: $[M+H]^+$: 216.17.

General procedure for amidic coupling (5, 15f)

To a solution of 2-(naphthalen-1-ylamino)-2-oxoacetic acid (1.3 equiv., 0.35 mmol) in DMF at 0 °C, DIPEA (1.3 equiv., 0.35 mmol) and HATU (1.3 equiv., 0.35 mmol) were added. After stirring for 10 minutes, a solution of compound 3e or 15e (1 equiv., 0.27 mmol) in DMF was added dropwise. The reaction mixture was stirred at room temperature for 2 hours.

The solvent was removed under reduced pressure, and the resulting solid residue was diluted with ethyl acetate and sequentially extracted with 10% aqueous citric acid, 5% aqueous $NaHCO_3$, and brine. The organic phase was dried over anhydrous Na_2SO_4, filtered, and concentrated under reduced pressure.

The final compound was purified by preparative HPLC affording the final compound as a solid.

Benzyl (2S,5S)-2,5-diisobutyl-4-(2-(naphthalen-1-ylamino)-2-oxoacetyl)piperazine-1-carboxylate (5)

^{1}H NMR (400 MHz, DMSO) δ 10.9 (s, 1H), 8.0 – 7.1 (m, 12H), 5.2 – 5.0 (dd, 2H), 4.4 – 3.9 (m, 4H), 3.25 – 2.9 (dt, 2H), 1.7 – 1.2 (m, J = 7.2 Hz, 6H), 1.0 – 0.6 (m, J = 12.4 Hz, 12H).

^{13}C NMR (400 MHz, DMSO) δ 161.63 (1C), 159.03 (1C), 157.62 (1C), 128.70 (1C), 128.49 (2C), 128.24 (1C), 128.18 (2C), 127.55 (1C), 127.33 (1C), 127.19 (1C), 126.89 (1C), 125.46 (1C), 124.05 (1C), 119.24 (1C), 67.23 (1C), 51.58 (1C), 50.29 (1C), 48.65 (1C), 47.50 (1C), 40.04 (1C), 39.43 (1C), 25.05 (1C), 22.52 (4C).

White solid. Yield: 47 %. ESI-MS: $[M+H]^+$: 530.57.

2-((2S,5S)-4,5-dibenzyl-2-isobutylpiperazin-1-yl)-N-(naphthalen-1-yl)-2-oxoacetamide (15f)

^{1}H NMR (400 MHz, DMSO) δ 10.6 (d, 1H), 8.5 – 6.75 (m, 17H), 4.4 – 4.2 (m, J = 4.25 Hz, 4H), 3.7 – 3.3 (m, J = 3.48 Hz, 2H), 1.4 – 1.0 (m, J = 1.29 Hz, 6H), 1.0 – 0.8 (m, J = 0.82, 7H).

Brownish solid. Yield: 93 %. ESI-MS: $[M+H]^+$: 520.69.

Synthesis of (E)-3-(naphthalen-1-yl)acrylic acid (7)

To a solution of malonic acid (2 equiv., 2.88 mmol) in pyridine under Argon atmosphere, was cooled to 0 °C and 1-naphthaldehyde (1 equiv., 1.44 mmol) was added. Subsequently, piperidine (0.87 equiv., 1.25 mmol) was added at room temperature, and the reaction mixture was heated at reflux at 110 °C for four hours. The resulting solution was acidified with 37% HCl and the solvent was evaporated under reduced pressure. The product was crystallized by diethyl ether and the solid was collected by under vacuum filtration. *(E)-3-(naphthalen-1-yl)acrylic acid* was afforded as a white solid.

^{1}H NMR (400 MHz, DMSO) δ 12.54 (s, 1H), 8.37 (d, J = 15.7 Hz, 1H), 8.18 (d, J = 8.2 Hz, 1H), 8.03 – 7.90 (m, 3H), 7.66 – 7.50 (m, 3H), 6.58 (d, J = 15.7 Hz, 1H).

Yield: 90%. MS-ESI: $[M+H]^+$ 198.07.

General procedure for synthesis of acrylamide group (8, 15g)

To a solution of *(E)-3-(naphthalen-1-yl)acrylic acid* (1 equiv., 0.15 mmol) in DMF (5 mL) were added, in sequence, HOBt (1 equiv., 0.15 mmol) and WSC (1 equiv., 0.15 mmol) at 0 °C. The reaction mixture was then treated dropwise with a solution of piperazine (1.1 equiv., 0.165 mmol) in DMF, and stirring was continued at room temperature for 4 h.

After completion of the reaction, the solvent was evaporated under reduced pressure, and the resulting oily residue was diluted with DCM. The organic phase was successively washed with 10% aqueous citric acid, 5% aqueous sodium bicarbonate, and brine. The combined organic layers were dried over anhydrous sodium sulfate, filtered, and concentrated under reduced pressure. The crude product was purified by preparative HPLC to afford the compound.

Benzyl (2S,5S)-2,5-diisobutyl-4-((E)-3-(naphthalen-1-yl)acryloyl)piperazine-1-carboxylate (8)

^{1}H NMR (400 MHz, $CDCl_3$) δ 8.31 (d, *J* = 15.1 Hz, 1H), 8.16 (d, 1H), 8.02 – 7.95 (dd, 3H), 7.65 – 7.51 (m, 3H), 7.44-7.36 (m, 1H), 7.28 (m, 5H), 5.06 (s, *J* = 8.7 Hz, 2H), 4.54 (m, 1H), 4.33 (m, 1H), 4.08 (m, 1H), 4.04 (s, 2H), 2.92 (s, 2H), 1.63 – 1.55 (m, 2H), 1.42 (dt, *J* = 13.4, 2H), 1.29 (s, 1H), 0.96 – 0.88 (t, 6H), 0.85 – 0.81 (t, 6H).

^{13}C NMR (500 MHz, $CDCl_3$) δ 165.79 (1C), 140.45 (1C), 133. 97 (1C), 131.46 (1C), 130.25 (1C), 128.35 (3C), 128.09 (1C), 127.96 (1C), 126.77 (1C), 126.18 (1C), 125.43 (1C), 124.74 (1C), 124.52 (1C), 123.74 (1C), 67.31 (1C), 51.75 (1C), 42.19 (1C), 31.97 (1C), 31.35 (1C), 30.31 (1C), 29.78 (3C), 29.42 (1C), 24.57 (1C), 23.78 (1C), 23.24 (1C), 22.67 (1C), 22.30 (1C), 21.69 (1C), 14.08 (1C).

Yellowish white. Yield: 63 %. MS-ESI: $[M+H]^+$ 512.30.

(E)-1-((2S,5S)-4,5-dibenzyl-2-isobutylpiperazin-1-yl)-3-(naphthalen-1-yl)prop-2-en-1-one (15g)

^{1}H NMR (400 MHz, $CDCl_3$) δ 8.08 – 8.01 (m, 1H), 7.93 – 7.83 (m, 2H), 7.71 – 7.64 (m, 2H), 7.56 – 7.45 (m, 3H), 7.33 – 7.16 (m, 7H), 7.24 (m, 1H), 7.19 (d, 2H), 6.51 (d, *J* = 15.9 Hz, 1H), 3.94 (dd, *J* = 10.5, 3.1 Hz, 1H), 3.75 (d, *J* = 12.5 Hz,1H), 3.68-3.56 (m, 2H) 3.52 (d, *J* = 12.4 Hz, 1H), 3.02 – 2.89 (m, 3H), 2.80 (dd, *J* = 10.7, 5.2 Hz, 1H), 2.71 (ddt, *J* = 12.5, 8.1, 0.8 Hz, 1H), 1.73 – 1.61 (m, 1H), 1.51 – 1.42 (m, 1H), 0.98 – 0.90 (m, 7H).

Yellowish solid. Yield: 49%. MS-ESI: $[M+H]^+$ 502.70.

General procedure of catalytic hydrogenation and introduction of pyrazinoic acid residue or Cbz on acrylamide compounds (9, 18, 19)

To a solution of compound Cbz- or benzyl-piperazine (1 equiv., 0.29 mmol) in methanol (3 mL), a few drops of 1 M HCl and 10% palladium on activated carbon (Pd/C) (1 equiv., 0.29 mmol) were

added. The reaction vessel was saturated with hydrogen gas, and the mixture was stirred at room temperature for 30 minutes.
The reaction mixture was filtered through celite, washing with methanol.
The intermediate was directly used for the next step.

Introduction of pyrazinoic acid residue (9,19)

To a solution of 2-pyrazinoic acid (2 equiv., 0.20 mmol) in DMF at 0 °C, DIPEA (2 equiv., 0.20 mmol) and HATU (2 equiv., 0.20 mmol) were added, and the mixture was stirred for 10 minutes. A solution of piperazine (1 equiv., 0.10 mmol) in DMF was then added dropwise, and the reaction mixture was stirred at room temperature for 2 hours.
The solvent was removed under reduced pressure, and the residue was diluted with ethyl acetate. The organic phase was sequentially washed with 10% aqueous citric acid, 5% aqueous $NaHCO_3$, and brine. The organic layer was dried over anhydrous Na_2SO_4, filtered, and concentrated under reduced pressure.
The compound was purified by preparative HPLC.

(E)-1-((2S,5S)-2,5-diisobutyl-4-(pyrazine-2-carbonyl)piperazin-1-yl)-3-(naphthalen-1-yl)prop-2-en-1-one (9)

^{1}H NMR (400 MHz, $CDCl_3$) δ 9.05 (d, *J* = 1.4 Hz, 1H), 8.88 (dd, *J* = 3.6, 1.4 Hz, 1H), 8.79 (d, *J* = 3.5 Hz, 2H), 8.08 – 8.01 (m, 1H), 7.93 – 7.83 (m, 2H), 7.71 – 7.64 (m, 2H), 7.56 – 7.45 (m, 3H), 6.50 (d, *J* = 15.9 Hz, 1H), 4.12 (dd, *J* = 10.8, 2.6 Hz, 1H), 4.09 – 3.99 (m, 2H), 3.92 (tdd, *J* = 8.4, 5.3, 2.7 Hz, 1H), 3.81 (dd, *J* = 10.8, 5.5 Hz, 1H), 3.72 – 3.65 (m, 1H), 1.74 – 1.61 (m, 4H), 1.55 – 1.44 (m, 2H), 0.99 – 0.90 (m, 6H), 0.89 – 0.81 (m, 6H).
^{13}C NMR ($CDCl_3$, 400 MHz) δ 168.32 (1C), 164.56 (1C), 147.97 (2C), 145.74 (1C), 143.65 (1C), 136.48 (1C), 134.44 (1C), 133.27 (1C), 132.71 (1C), 128.39 (3C), 127.06 (1C), 126.15 (1C), 125.18 (1C), 121.42 (1C), 52.44 (1C), 48.67 (2C), 39.61 (2C), 25.12 (2C), 22.27 (4C).
Yellowish oil. Yield: 57%. MS-ESI: $[M+H]^+$ 484.64.

(E)-1-((2S,5S)-5-benzyl-2-isobutyl-4-(pyrazine-2-carbonyl)piperazin-1-yl)-3-(naphthalen-1-yl)prop-2-en-1-one (19)

^{1}H NMR (400 MHz, $CDCl_3$) δ 9.05 (d, *J* = 1.5 Hz, 1H), 8.88 (dd, *J* = 3.6, 1.4 Hz, 1H), 8.79 (d, *J* = 3.5 Hz, 1H), 8.04 (s, 1H), 7.93 – 7.83 (m, 2H), 7.71 – 7.63 (m, 2H), 7.56 – 7.45 (m, 3H), 7.33 – 7.26 (m, 5H), 6.50 (d, *J* = 15.9 Hz, 1H), 4.30 (tdd, *J* = 8.4, 6.4, 3.7 Hz, 1H), 4.16 (dd, *J* = 10.8, 2.8 Hz, 2H), 3.96 – 3.83 (m, 2H), 3.78 (dd, *J* = 10.8, 6.4 Hz, 1H), 3.04 (ddt, *J* = 12.9, 8.6, 0.8 Hz, 1H), 2.82

(ddt, *J* = 12.8, 8.5, 0.8 Hz, 1H), 1.74 – 1.61 (m, 2H), 1.53 – 1.44 (m, 1H), 0.98 – 0.90 (m, 3H), 0.89 – 0.81 (m, 3H).

^{13}C NMR (400 MHz, $CDCl_3$,) δ 168.48 (1C), 164.41 (1C), 148.43 (2C), 145.84 (1C), 143.66 (1C), 136.66 (2C), 134.07 (1C), 133.73 (1C), 132.78 (1C), 128.57 (7C), 126.92 (1C), 126.18 (1C), 125.78 (1C), 125.04 (1C), 121.22 (1C).56.07 (1C), 52.05 (1C), 48.52 (1C), 47.78 (1C), 39.53 (1C), 38.24 (1C), 24.98 (1C), 22.60 (2C).

Brown oil. Yield: 23%. MS-ESI: $[M+H]^+$ 518.66.

General procedure for introduction of Cbz on piperazine (18)

To a solution of piperazine (1 equiv., 0.11 mmol) in DCM, CBZ-OSu (1.1 equiv., 0.12 mmol) was added, and the reaction mixture was stirred at room temperature for 30 minutes.

The solvent was removed under reduced pressure, and the residue was diluted with ethyl acetate and extracted with 5% aqueous $NaHCO_3$ and brine.

The organic layer was dried over anhydrous Na_2SO_4, filtered, and concentrated under reduced pressure.

The compound was purified by preparative HPLC.

benzyl (2S,5S)-2-benzyl-5-isobutyl-4-((E)-3-(naphthalen-1-yl)acryloyl)piperazine-1-carboxylate (18)

^{1}H NMR (400 MHz, $CDCl_3$) δ 8.08 – 8.01 (m, 1H), 7.93 – 7.83 (m, 2H), 7.71 – 7.63 (m, 2H), 7.56 – 7.50 (m, 3H), 7.38 – 7.25 (m, 7H), 7.22-7.15 (m, 4H), 6.50 (d, *J* = 15.9 Hz, 1H), 5.12 (s, 1H), 4.14 (tdd, *J* = 8.4, 6.5, 3.8 Hz, 1H), 4.09 – 3.99 (m, 2H), 3.78-3.72 (M, 1H), 3.72 – 3.61 (m, 2H), 3.02 (ddt, *J* = 12.8, 8.5, 0.9 Hz, 1H), 2.79 (ddt, *J* = 12.8, 8.4, 0.9 Hz, 1H), 1.73 – 1.58 (m, 2H), 1.43 (ddd, *J* = 12.6, 8.4, 7.3 Hz, 1H), 0.94 (d, *J* = 6.9 Hz, 3H), 0.84 (d, *J* = 6.8 Hz, 3H).

^{13}C NMR (400 MHz, $CDCl_3$) δ 168.84 (1C), 156.66 (1C), 136.63 (3C), 137.27 (1C), 133.53 (1C), 132.26 (1C), 128.28 (14C), 127.15 (1C), 126.07 (1C), 125.19 (1C), 121.36 (1C), 66.95 (1C), 55.11 (1C), 52.01 (1C), 48.18 (2C), 39.84 (1C), 38.21 (1C), 24.90 (1C), 22.55 (2C).

Yield: 59%. MS-ESI: $[M+H]^+$ 546.71.

General procedure for the synthesis of the α-hydroxy ester intermediate (10a, 20a)

To a solution of **piperazine** (1 equiv., 0.27 mmol) in anhydrous ethanol, TEA (1 equiv., 0.27 mmol, 40 µL) was added, followed by the dropwise addition of ethyl-2-oxirane carboxylate (6.1 equiv., 1.65 mmol, 0.21 mL). The reaction mixture was refluxed at 80°C for 48 hours. The solvent was then concentrated and the residue diluted with dichloromethane, followed by extraction with deionized

water and brine. The organic phase was dried over anhydrous Na_2SO_4, filtered, and concentrated under reduced pressure. The residue was purified by column chromatography using an eluent mixture of ethyl acetate and petroleum ether, affording the derivative.

Benzyl (2S,5S)-4-(3-ethoxy-2-hydroxy-3-oxopropyl)-2,5-diisobutylpiperazine-1-carboxylate (10a)

The residue was purified by column chromatography using an eluent mixture of ethyl acetate and petroleum ether (6:4), affording the intermediate.

^{1}H NMR (400 MHz, $CDCl_3$) δ 7.40-7.30 (m, *J* = 4.2 Hz, 5H), 5.2 (d, 1H), 5.1 (d,1H), 4.42 (dd, 1H), 4.25 (m, *J* = 7.1 Hz, 3H), 1.65 – 1.48 (m, 4H), 1.32 (m, *J* = 7.2 Hz, 4H), 1.00-0.85 (m, *J* = 6.1 Hz, 14H).

Colourless oil. Yield: 66%. MS-ESI: $[M+H]^+$ 449.44.

Ethyl 3-((2S,5S)-4,5-dibenzyl-2-isobutylpiperazin-1-yl)-2-hydroxypropanoate (20a)

The residue was purified by column chromatography using an eluent mixture of ethyl acetate and petroleum ether (7:3), affording the derivative.

^{1}H NMR (500 MHz, $CDCl_3$) δ 7.33 – 7.23 (m, 7H), 7.22 – 7.16 (m, 3H), 4.31 (q, *J* = 6.3 Hz, 1H), 4.25 – 4.12 (m, 2H), 4.09 (d, J= 4.0 Hz, 1H) 3.76 (d, *J* = 12.4 Hz, 1H), 3.53 (d, *J* = 12.4 Hz, 1H), 3.20 (dd, *J* = 12.1, 6.2 Hz, 1H), 2.99 – 2.86 (m, 4H), 2.77 – 2.55 (m, 5H), 1.71 – 1.59 (m, 2H), 1.48 – 1.39 (m, 1H), 1.09 – 1.03 (m, 3H), 0.99 – 0.90 (m, 7H).

Colourless oil. Yield: 63%. MS-ESI: $[M+H]^+$ 438.61.

General procedure for the synthesis of the α-hydroxy acid intermediate (10b, 20b)

To a solution of **10a** or **20a** (1 equiv., 0.024 mmol) in a 1:1 mixture of THF and absolute ethanol (0.5 mL), 2 N KOH (4 equiv., 0.18 mmol) was added, and the reaction was allowed to proceed at room temperature for 3 hours. The reaction mixture was acidified with 3 M HCl in an ice bath to pH 3–4 and concentrated under reduced pressure. The residue was diluted with methanol and filtered through a Gooch funnel to remove any formed salts. The filtrate was then concentrated, affording compound as a solid.

3-((2S,5S)-4-((benzyloxy)carbonyl)-2,5-diisobutylpiperazin-1-yl)-2-hydroxypropanoic acid (10b)

^{1}H NMR (400 MHz, CD_3OD) δ 7.42 – 7.28 (m, 5H), 5.25-5.20 (d, 1H), 5.15-5.10 (dd, 1H), 1.64 – 1.45 (m, 4H), 1.36 – 1.25 (m, 6H), 1.03 – 0.93 (m, 12H).

White solid. Yield: 74%. ESI-MS: $[M+H]^+$: 421.29.

3-((2S,5S)-4,5-dibenzyl-2-isobutylpiperazin-1-yl)-2-hydroxypropanoic acid (20b)

^{1}H NMR (400 MHz, CD_3OD) δ 7.30 – 7.26 (m, 10H), 4.22 (q, *J* = 5.9 Hz, 1H), 3.70 (d, *J* = 12.4 Hz, 1H), 3.48 (d, *J* = 12.4 Hz, 1H), 3.20 (dd, *J* = 12.0, 5.9 Hz, 1H), 3.02 – 2.88 (m, 4H), 2.84 – 2.66 (m, 4H), 2.62-2.55 (m, 1H), 1.72 – 1.53 (m, 2H), 1.38 (ddd, *J* = 12.3, 8.2, 7.2 Hz, 1H), 0.94 (d, *J* = 6.8 Hz, 3H), 0.84 (d, *J* = 6.8 Hz, 3H).

White solid. Yield: 67%. MS-ESI: $[M+H]^+$ 410.56.

General procedure for the synthesis of the α-hydroxy amide (11, 20c)

To a solution of **acid** (1 equiv., 0.021 mmol) in DMF, DIPEA (5 equiv., 0.105 mmol) and HATU (1 equiv., 0.021 mmol) were added at 0°C and stirred for 20 minutes. A solution of 1-naphthylamine (1 equiv., 0.021 mmol) in DMF was then added dropwise. The reaction mixture was stirred at room temperature for 48 hours. The solvent was concentrated, and the residue was diluted with dichloromethane and extracted sequentially with 10% citric acid solution, 5% aqueous sodium bicarbonate, and brine. The organic phase was dried over anhydrous sodium sulfate, filtered, and concentrated under reduced pressure. The resulting compound was purified by preparative HPLC.

Benzyl (2S,5S)-4-(2-hydroxy-3-(naphthalen-1-ylamino)-3-oxopropyl)-2,5-diisobutylpiperazine-1-carboxylate (11)

^{1}H NMR (400 MHz, $CDCl_3$): δ 8.23 (d, 1H); 7.96 (d, 1H); 7.85 (d, 1H); 7.60-7.50 (m, 3H), 7.36-7.32 (m, 5H), 7.28 (m, 1H), 5.1 (s, 2H), 4.54 (m, 1H), 3.80-3.40 (m, 3H), 3.0-2.80 (m, 3H), 1.72-1.60 (m, 4H), 1.0-0.8 (m, 12H).

^{13}C NMR (400 MHz, $CDCl_3$) δ 174.63 (1C), 156.59 (1C), 137.35 (1C), 136.20 (1C), 128.23 (10C), 123.77 (2C), 117.32 (1C), 68.98 (1C), 66.83 (1C), 58.65 (1C), 56.35 (1C), 55.56 (1C), 51.47 (1C), 46.64 (1C), 40.20 (1C), 39.04 (1C), 25.04 (2C), 22.32 (4C).

Purple oil. Yield: 62%. ESI-MS: $[M+H]^+$ 546.75.

3-((2S,5S)-4,5-dibenzyl-2-isobutylpiperazin-1-yl)-2-hydroxy-N-(naphthalen-1-yl)propenamide (20c)

^{1}H NMR (400 MHz, $CDCl_3$) δ 9.39 (s, 1H), 8.25 – 8.20 (m, 1H), 8.01 – 7.95 (m, 1H), 7.82 (dt, *J* = 7.9, 1.5 Hz, 1H), 7.64 – 7.49 (m, 3H), 7.37 – 7.16 (m, 8H), 7.25-7.17 (m, 2H), 4.91 (d, *J* = 5.5 Hz, 1H), 4.49 (q, *J* = 5.4 Hz, 1H), 3.76 (d, *J* = 12.4 Hz, 1H), 3.53 (d, *J* = 12.3 Hz, 1H), 3.17 (dd, *J* = 12.6,

5.3 Hz, 1H), 2.96 – 2.86 (m, 4H), 2.76 – 2.61 (m, 3H), 2.59-2.52 (m, 2H), 1.71 – 1.59 (m, 2H), 1.48 – 1.39 (m, 1H), 0.99 – 0.90 (m, 7H).
Yield: 52%. MS-ESI: $[M+H]^+$ 535.73.

General procedure of oxidation from α-hydroxyamide to α-ketoamide (13, 20d, 14, 24)

Under an argon atmosphere, Dess–Martin periodinane (1.6 equiv., 0.016 mmol) was added to a solution of the α-hydroxyamide (1 equiv., 0.010 mmol) in dichloromethane. The reaction mixture was stirred at room temperature for 20 hours, after which the solvent was removed under reduced pressure and the crude residue was purified directly by preparative HPLC.

Benzyl (2S,5S)-2,5-diisobutyl-4-(3-(naphthalen-1-ylamino)-2,3-dioxopropyl)piperazine-1-carboxylate (13)

^{1}H NMR (400 MHz, $CDCl_3$)δ 8.08 – 8.02 (m, 1H), 7.88 – 7.82 (m, 1H), 7.75 – 7.67 (m, 2H), 7.59 – 7.48 (m, 2H), 7.38 – 7.31 (m, 5H), 7.32 – 7.20 (m, 2H), 5.12 (s, 2H), 3.94 (d, *J* = 14.6 Hz, 1H), 3.86 – 3.79 (m, 2H), 3.60 (tdd, *J* = 9.0, 5.8, 3.2 Hz, 1H), 3.47 (dd, *J* = 10.8, 5.5 Hz, 1H), 2.93 – 2.80 (m, 3H), 1.73 – 1.54 (m, 4H), 1.42 (dddd, *J* = 19.5, 12.3, 8.6, 7.3 Hz, 2H), 0.95 (dd, *J* = 6.9, 3.7 Hz, 6H), 0.85 (dd, *J* = 6.9, 4.2 Hz, 6H).
^{13}C NMR (400 MHz, $CDCl_3$) δ 199.89 (1C), 162.68 (1C), 156.77 (1C), 136.22 (1C), 133.79 (2C), 128.07 (10C), 125.70 (1C), 124.17 (1C), 118.91 (1C), 67.23 (1C), 57.43 (1C), 55.65 (1C), 53.88 (1C), 51.52 (1C), 46.44 (1C), 39.71 (2C), 25.24 (2C), 22.64 (4C).
Brown oil. Yield. 47%. MS-ESI: $[M+H]^+$ 543.71.

3-((2S,5S)-2,5-diisobutyl-4-(pyrazine-2-carbonyl)piperazin-1-yl)-N-(naphthalen-1-yl)-2-oxopropanamide (14)

^{1}H NMR (400 MHz, $CDCl_3$) δ 9.05 (d, *J* = 1.5 Hz, 1H), 8.88 (dd, *J* = 3.6, 1.4 Hz, 1H), 8.79 (d, *J* = 3.5 Hz, 1H), 8.08 – 8.02 (m, 1H), 7.88 – 7.82 (m, 1H), 7.75 – 7.67 (m, 2H), 7.59 – 7.48 (m, 2H), 7.24 (t, *J* = 7.9 Hz, 1H), 3.99 (dd, *J* = 10.7, 2.7 Hz, 2H), 3.82 (d, *J* = 14.5 Hz, 1H), 3.74 – 3.65 (m, 2H), 3.00 (dd, *J* = 10.9, 3.0 Hz, 1H), 2.96 – 2.87 (m, 2H), 1.67 – 1.56 (m, 4H), 1.54-1.35 (m, 2H), 0.99 – 0.90 (m, 6H), 0.89 – 0.81 (m, 6H).
^{13}C NMR (400 MHz, $CDCl_3$) δ 200.16 (1C), 164.43 (1C), 162.61 (1C), 147.92 (3C), 143.64 (1C), 135.38 (1C), 133.64 (1C), 128.70 (4C), 127.12 (1C), 125.56 (1C), 123.99 (1C), 118.88 (1C), 57.29 (1C), 55.48 (1C), 54.15 (2C), 47.47 (1C), 39.40 (2C), 24.70 (2C), 22.22 (4C).
Purple oil. Yield: 46%. MS-ESI: $[M+H]^+$ 515.66.

3-((2S,5S)-4,5-dibenzyl-2-isobutylpiperazin-1-yl)-N-(naphthalen-1-yl)-2-oxopropanamide (20d)

^{1}H NMR (400 MHz, $CDCl_3$) δ 9.87 (s, 1H), 8.08 – 8.02 (m, 1H), 7.88 – 7.82 (m, 1H), 7.75 – 7.67 (m, 2H), 7.59 – 7.48 (m, 2H), 7.33 – 7.26 (m, 7H), 7.25-7.18 (m, 4H) 3.92 (d, *J* = 14.5 Hz, 1H), 3.84 – 3.73 (m, 2H), 3.53 (d, *J* = 12.3 Hz, 1H), 3.12 – 3.06 (m, 1H), 2.97 – 2.80 (m, 4H), 2.76 – 2.57 (m, 3H), 1.71 – 1.56 (m, 2H), 1.40 (ddd, *J* = 12.3, 8.5, 7.3 Hz, 1H), 0.95 (d, *J* = 6.9 Hz, 3H), 0.85 (d, *J* = 6.8 Hz, 3H).

Yield: 32%. MS-ESI: $[M+H]^+$ 533.72.

benzyl (2S,5S)-2-benzyl-5-isobutyl-4-(3-(naphthalen-1-ylamino)-2,3-dioxopropyl)piperazine-1-carboxylate (23)

^{1}H NMR (400 MHz, $CDCl_3$)δ 8.08 – 8.02 (m, 1H), 7.88 – 7.82 (m, 1H), 7.75 – 7.67 (m, 2H), 7.59 – 7.48 (m, 2H), 7.38 – 7.16 (m, 11H), 5.12 (s, 2H), 3.99 – 3.90 (m, 3H), 3.87 – 3.80 (m, 2H), 3.50 (dd, *J* = 10.8, 5.5 Hz, 1H), 3.26 (dd, *J* = 11.0, 3.7 Hz, 1H), 3.08 (dd, *J* = 11.0, 6.4 Hz, 1H), 2.96 (ddt, *J* = 12.8, 8.6, 0.9 Hz, 2H), 2.87 (tdd, *J* = 8.4, 5.5, 2.7 Hz, 1H), 2.72 (ddt, *J* = 12.9, 8.6, 0.9 Hz, 1H), 1.72 – 1.54 (m, 2H), 1.40 (ddd, *J* = 12.3, 8.4, 7.2 Hz, 1H), 0.95 (d, *J* = 7.0 Hz, 3H), 0.85 (d, *J* = 6.9 Hz, 3H).

^{13}C NMR (400 MHz, $CDCl_3$) δ 174.70 (1C), 156.45 (1C), 137.24 (1C), 136.07 (1C), 134.12 (1C), 128.40 (15C), 123.69 (2C), 116.87 (1C), 69.42 (1C), 67.08 (1C), 58.62 (1C), 55.87 (3C), 46.67 (1C), 39.30 (1C), 38.25 (1C), 25.29 (1C), 22.38 (2C).

Brown oil. Yield: 35%. MS-ESI: $[M+H]^+$ 577.73.

3-((2S,5S)-5-benzyl-2-isobutyl-4-(pyrazine-2-carbonyl)piperazin-1-yl)-N-(naphthalen-1-yl)-2-oxopropanamide (24)

^{1}H NMR (400 MHz, $CDCl_3$) δ 9.05 (d, *J* = 1.5 Hz, 1H), 8.88 (dd, *J* = 3.6, 1.4 Hz, 1H), 8.79 (d, *J* = 3.5 Hz, 1H), 8.08 – 8.02 (m, 1H), 7.88 – 7.82 (m, 1H), 7.75 – 7.67 (m, 2H), 7.59 – 7.48 (m, 2H), 7.33 – 7.16 (m, 6H), 4.11 – 4.01 (m, 2H), 3.94 (d, *J* = 14.6 Hz, 2H), 3.77 (dd, *J* = 10.6, 5.5 Hz, 2H), 3.28 (dd, *J* = 11.0, 3.7 Hz, 1H), 3.11 – 3.00 (m, 2H), 2.92 (tdd, *J* = 8.3, 5.4, 2.7 Hz, 1H), 2.82 (ddt, *J* = 12.8, 8.4, 0.8 Hz, 1H), 1.72 – 1.56 (m, 2H), 1.41 (ddd, *J* = 12.5, 8.5, 7.3 Hz, 1H), 0.95 (d, *J* = 6.9 Hz, 3H), 0.85 (d, *J* = 6.8 Hz, 3H).

^{13}C NMR (400 MHz, $CDCl_3$) δ 174.58 (1C), 164.53 (1C), 148.34 (1C), 147.40 (1C), 145.84 (1C), 143.50 (1C), 137.15 (2C), 133.87 (1C), 128.66 (9C), 126.73 (1C), 123.87 (2C), 117.31 (1C), 69.47 (1C), 58.27 (1C), 55.56 (3C), 48.01 (1C), 38.38 (2C), 25.05 (1C), 22.40 (2C).

Purple oil. Yield. 31%. MS-ESI: 549.68.

General procedure of catalytic hydrogenation and introduction of pyrazinoic acid residue or Cbz (6,12,16,17, 21, 22)

To a solution of compound Cbz- or benzyl-piperazine (1 equiv., 0.29 mmol) in methanol (3 mL), a few drops of 1 M HCl and 10% palladium on activated carbon (Pd/C) (1 equiv., 0.29 mmol) were added. The reaction vessel was saturated with hydrogen gas, and the mixture was stirred at room temperature for 28 hours.

The reaction mixture was filtered through celite, washing with methanol.

The intermediate was directly used for the next step.

Introduction of pyrazinoic acid residue (6,12,17,22)

To a solution of 2-pyrazinoic acid (1.3 equiv., 0.13 mmol) in DMF at 0 °C, DIPEA (1.3 equiv., 0.13 mmol) and HATU (1.3 equiv., 0.13 mmol) were added, and the mixture was stirred for 10 minutes. A solution of piperazine (1 equiv., 0.10 mmol) in DMF was then added dropwise, and the reaction mixture was stirred at room temperature for 2 hours.

The solvent was removed under reduced pressure, and the residue was diluted with ethyl acetate. The organic phase was sequentially washed with 10% aqueous citric acid, 5% aqueous $NaHCO_3$, and brine. The organic layer was dried over anhydrous Na_2SO_4, filtered, and concentrated under reduced pressure.

The compound was purified by preparative HPLC.

2-((2S,5S)-2,5-diisobutyl-4-(pyrazine-2-carbonyl)piperazin-1-yl)-N-(naphthalen-1-yl)-2-oxoacetamide (6)

^{1}H NMR (400 MHz, $CDCl_3$) δ 9.37 (s, 1H), 9.05 (d, *J* = 1.3 Hz, 1H), 8.88 (dd, *J* = 3.6, 1.4 Hz, 1H), 8.79 (d, *J* = 3.5 Hz, 1H), 8.08 – 8.02 (m, 1H), 7.88 – 7.81 (m, 1H), 7.71 (tt, *J* = 6.9, 1.6 Hz, 2H), 7.60 – 7.47 (m, 2H), 7.29 – 7.20 (m, 1H), 4.13 (ddd, *J* = 10.7, 3.1, 2.4 Hz, 2H), 4.02 – 3.88 (m, 2H), 3.82 (ddd, *J* = 11.0, 5.8, 2.0 Hz, 2H), 1.67 (dddd, *J* = 10.8, 7.0, 5.7, 3.8 Hz, 4H), 1.56 – 1.42 (m, 2H), 0.99 – 0.90 (m, 6H), 0.88-0.83 (m, 6H).

^{13}C NMR (400 MHz, $CDCl_3$) δ 164.38 (1C), 161.86 (1C), 158.96 (1C), 148.00 (2C), 145.87 (1C), 143.35 (1C), 135.79 (1C), 133.85 (1C), 128.47 (1C), 125.83 (4C), 125.56 (1C), 123.77 (1C), 118.58 (1C), 52.68 (1C), 51.75 (1C), 48.70 (2C), 39.54 (2C), 24.85 (2C), 22.48 (4C).

White solid. Yield: 60 %. ESI-MS: $[M+H]^+$: 501.63.

3-((2S,5S)-2,5-diisobutyl-4-(pyrazine-2-carbonyl)piperazin-1-yl)-2-hydroxy-N-(naphthalen-1-yl)propenamide (12)

^{1}H NMR (400 MHz, $CDCl_3$) δ 9.39 (s, 1H), 9.05 (d, *J* = 1.5 Hz, 1H), 8.88 (dd, *J* = 3.6, 1.4 Hz, 1H), 8.79 (d, *J* = 3.5 Hz, 1H), 8.25 – 8.20 (m, 1H), 7.98 (dd, *J* = 7.6, 1.1 Hz, 1H), 7.82 (dt, *J* = 7.9, 1.4 Hz, 1H), 7.64 – 7.49 (m, 3H), 7.34 (t, *J* = 7.8 Hz, 1H), 4.91 (d, *J* = 5.7 Hz, 1H), 4.49 (q, *J* = 5.4 Hz, 1H), 3.95 (dd, *J* = 10.6, 2.4 Hz, 1H), 3.73 – 3.59 (m, 2H), 3.17 (dd, *J* = 12.7, 5.4 Hz, 1H), 2.96 – 2.87 (m, 2H), 2.87 – 2.72 (m, 2H), 1.74 – 1.58 (m, 4H), 1.54 – 1.39 (m, 2H), 1.00 – 0.91 (m, 6H), 0.89 – 0.81 (m, 6H).

^{13}C NMR (400 MHz, $CDCl_3$) δ 174.84 (1C), 164.39 (1C), 148.38 (2C), 145.82 (1C), 143.63 (1C), 137.13 (1C), 134.13 (1C), 128.80 (1C), 126.83 (4C), 123.89 (2C), 117.17 (1C), 69.10 (1C), 58.21 (1C), 56.45 (1C), 55.65 (1C), 53.68 (1C), 47.76 (1C), 39.86 (1C), 38.84 (1C), 25.02 (2C), 22.47 (4C).

Yield: 28%. MS-ESI: $[M+H]^+$: 517.67.

2-((2S,5S)-5-benzyl-2-isobutyl-4-(pyrazine-2-carbonyl)piperazin-1-yl)-N-(naphthalen-1-yl)-2-oxoacetamide (17)

^{1}H NMR (400 MHz, $CDCl_3$) δ 9.8 (d, 1H), 8.0 – 7.0 (m, 15H), 1.40 – 1.35 (m, J = 1.38 Hz, 2H), 1.33 – 1.25 (m, J = 1.29 Hz, 4H), 1.12 – 1.0 (m, J = 1.07 Hz, 4H), 0.93 – 0.85 (m, J = 0.88 Hz, 7H).

^{13}C NMR (400 MHz, $CDCl_3$) δ 164.41 (1C), 161.55 (1C), 158.90 (1C), 148.12 (1C), 145.67 (1C), 143.37 (1C), 137.35 (1C), 135.81 (1C), 134.12 (1C), 128.82 (8C),127.13 (2C), 125.60 (1C), 123.71 (1C), 119.16 (1C), 56.15 (1C), 51.81 (1C), 48.95 (2C), 39.50 (1C), 38.02 (1C), 24.94 (1C), 22.65 (2C).

White solid. Yield: 81 %. ESI-MS: $[M+H]^+$: 535.65.

3-((2S,5S)-5-benzyl-2-isobutyl-4-(pyrazine-2-carbonyl)piperazin-1-yl)-2-hydroxy-N-(naphthalen-1-yl)propenamide (22)

^{1}H NMR (500 MHz, $CDCl_3$) δ 9.39 (s, 1H), 9.05 (d, *J* = 1.5 Hz, 1H), 8.88 (dd, *J* = 3.6, 1.4 Hz, 1H), 8.79 (d, *J* = 3.5 Hz, 1H), 8.25 – 8.20 (m, 1H), 8.01 – 7.95 (m, 1H), 7.82 (dt, *J* = 8.0, 1.4 Hz, 1H), 7.64 – 7.49 (m, 3H), 7.37 – 7.16 (m, 6H), 4.91 (d, *J* = 5.7 Hz, 1H), 4.49 (q, *J* = 5.4 Hz, 1H), 4.13 – 4.00 (m, 2H), 3.75 (dd, *J* = 10.7, 5.2 Hz, 1H), 3.21 – 3.13 (m, 2H), 3.04 (ddt, *J* = 12.8, 8.4, 0.8 Hz, 1H), 2.97 – 2.88 (m, 3H), 2.87 – 2.77 (m, 2H), 1.72 – 1.58 (m, 2H), 1.48 – 1.39 (m, 1H), 0.95 (d, *J* = 6.8 Hz, 3H), 0.88 – 0.81 (m, 3H).

^{13}C NMR (500 MHz, $CDCl_3$) δ 174.42 (1C), 164.52 (1C), 148.28 (2C), 146.12 (1C), 143.38 (1C), 137.16 (2C), 133.83 (1C), 128.73 (9C), 126.78 (1C), 124.25 (2C), 117.03 (1C), 69.01 (1C), 58.25 (1C), 55.51 (3C), 47.71 (1C), 38.54 (2C), 25.26 (1C), 22.31 (2C).
Yield: 36%. MS-ESI: 551.69.

General procedure for introduction of Cbz on piperazine (16, 21)

To a solution of piperazine (1 equiv., 5.5 mmol) in DCM, CBZ-OSu (1.1 equiv., 6.05 mmol) was added, and the reaction mixture was stirred at room temperature for 30 minutes.
The solvent was removed under reduced pressure, and the residue was diluted with ethyl acetate and extracted with 5% aqueous $NaHCO_3$ and brine.
The organic layer was dried over anhydrous Na_2SO_4, filtered, and concentrated under reduced pressure.
The compound was purified by preparative HPLC.

benzyl (2S,5S)-2-benzyl-5-isobutyl-4-(2-(naphthalen-1-ylamino)-2-oxoacetyl)piperazine-1-carboxylate (16)

^{1}H NMR (400 MHz, $CDCl_3$) δ 7.77 – 7.60 (m, 2H), 7.46 – 7.29 (m, 4H), 7.28 – 7.15 (m, 10H), 7.12 (dd, J= 6.6 Hz, 1H), 6.59 (dd, J=7.2 Hz, 1H), 5.37 (s, 2H), 4.65 – 4.55 (m, 1H), 4.12 (tt, J=7.0, 4.4 Hz, 1H), 3.98 (dd, J=12.3, 6.9 Hz, 1H), 3.78 (dd, J=12.5, 2.9 Hz, 1H), 3.36 (dd, J=12.4, 6.8 Hz, 1H), 3.16 (dd, J=12.4, 2.8 Hz, 1H), 3.02 (dd, J=12.5, 6.7 Hz, 1H), 2.77 (dd, J=12.4, 6.8 Hz, 1H), 2.39 – 2.11 (m, 1H), 1.41 (dd, J=6.8, 4.3 Hz, 2H), 1.04 (d, J=6.3 Hz, 6H).
^{13}C NMR (400 MHz, $CDCl_3$) δ 161.47 (1C), 159.14 (1C), 156.41 (1C), 137.48 (1C), 135.88 (2C), 133.88 (1C), 128.48 (13C), 127.41 (1C), 126.67 (1C), 125.22 (1C), 123.95 (1C), 119.09 (1C), 67.17 (1C), 54.37 (1C), 52.03 (1C), 48.24 (1C), 47.50 (1C), 39.57 (1C), 37.96 (1C), 24.78 (1C), 22.30 (2C).
White solid. Yield: 75 %. ESI-MS: $[M+H]^+$: 563.70.

benzyl (2S,5S)-2-benzyl-4-(2-hydroxy-3-(naphthalen-1-ylamino)-3-oxopropyl)-5-isobutylpiperazine-1-carboxylate (21)

^{1}H NMR (400 MHz, $CDCl_3$) δ 9.39 (s, 1H), 8.25 – 8.20 (m, 1H), 8.01 – 7.95 (m, 1H), 7.82 (dt, *J* = 7.9, 1.4 Hz, 1H), 7.64 – 7.49 (m, 3H), 7.38 – 7.25 (m, 8H), 7.23-7.14 (m, 4H), 5.12 (s, 2H), 4.91 (d, *J* = 5.7 Hz, 1H), 4.49 (q, *J* = 5.4 Hz, 1H), 3.92 (tdd, *J* = 8.4, 6.6, 3.8 Hz, 1H), 3.80 (dd, *J* = 10.6, 2.6 Hz, 1H), 3.48 (dd, *J* = 10.8, 5.3 Hz, 1H), 3.17 (dd, *J* = 12.7, 5.4 Hz, 1H), 3.05 (dd, *J* = 10.6, 3.8 Hz, 1H), 3.00 – 2.88 (m, 2H), 2.79 – 2.68 (m, 3H), 1.72 – 1.56 (m, 2H), 1.42 (ddd, *J* = 12.4, 8.3, 7.3 Hz, 1H), 0.95 (d, *J* = 6.8 Hz, 3H), 0.85 (d, *J* = 6.8 Hz, 3H).

^{13}C NMR (400 MHz, $CDCl_3$) δ 174.20 (1C), 156.23 (1C), 137.16 (1C), 136.38 (1C), 134.46 (1C), 128.25 (14C), 126.90 (1C), 124.04 (2C), 117.27 (1C), 69.40 (1C), 66.90 (1C), 58.62 (1C), 56.27 (1C), 55.33 (2C), 46.42 (1C), 39.50 (1C), 38.15 (1C), 25.22 (1C), 22.31 (2C).
Yield: 64%. MS-ESI: $[M+H]^+$: 579.74.

General procedure for synthesis of second class of compounds

Synthesis methyl 2-isocyanato-4-methylpentanoate

Leucine methyl ester hydrochloride (3 equiv., 1.10 mmol) was dissolved in a saturated solution of $NaHCO_3$ and dichloromethane (DCM) (1:1, 3 mL) at 0 °C. A solution of triphosgene in DCM was then added dropwise, and the reaction mixture was stirred at 0 °C for 40 minutes. After this time, the mixture was diluted with DCM and the organic layer was separated from the aqueous phase by extraction. The organic phase was washed with brine, dried over anhydrous sodium sulfate, filtered, and concentrated under reduced pressure to afford a colourless oil. The crude product was used directly in the next step without further purification.

General procedure for introduction of urea bond (25a, 31a)

To a solution of methyl 2-isocyanato-4-methylpentanoate (1 equiv., 1.11 mmol) in DCM, a solution of piperazine (1 equiv., 1.11 mmol) in DCM was added dropwise, followed by triethylamine (TEA, 1.1 equiv., 1.22 mmol). The reaction mixture was stirred at room temperature for 48 hours. After completion, the reaction was diluted with DCM and washed with 10% aqueous citric acid and brine. The organic layer was separated, dried over anhydrous sodium sulfate, filtered, and concentrated under reduced pressure.

benzyl (2S,5S)-2,5-diisobutyl-4-(((S)-1-methoxy-4-methyl-1-oxopentan-2-yl)carbamoyl)piperazine-1-carboxylate (25a)

The crude product was purified by column chromatography (ethyl acetate/petroleum ether, 1.5:8.5) to afford the desired compound as a yellow oil.
^{1}H NMR (400 MHz, $CDCl_3$) δ 7.36 – 7.17 (m, 5H), 5.10 (d, 1H), 5.00 (d, 1H), 4.69 (d, J = 7.9 Hz, 1H), 4.43 (td, J = 8.2, 1H), 4.10 (d, J = 16.3 Hz, 3H), 3.90 (m, 1H), 3.65 (s, 3H), 2.68 – 2.47 (m, 2H), 1.66 – 1.23 (m, 6H), 1.40-1.28 (m, 3H), 0.87 (dd, J = 6.5, 3.6 Hz, 12H), 0.78 (d, 6H).
Yield: 61%. ESI-MS: $[M+H]^+$: 504.72.

methyl ((2S,5S)-4,5-dibenzyl-2-isobutylpiperazine-1-carbonyl)-L-leucinate (31a)

The crude product was purified by column chromatography (ethyl acetate/petroleum ether, 1:9) to afford the desired compound as a colourless oil.

^{1}H NMR (400 MHz, $CDCl_3$) δ 7.33 – 7.16 (m, 10H), 4.24 (dt, *J* = 8.3, 7.2 Hz, 1H), 3.88 (dd, *J* = 11.4, 3.2 Hz, 1H), 3.75 (d, *J* = 12.4 Hz, 1H), 3.62 – 3.49 (m, 4H), 3.03 – 2.90 (m, 3H), 2.84 (dd, *J* = 10.8, 5.5 Hz, 3H), 2.71 (ddt, *J* = 12.6, 8.1, 0.9 Hz, 1H), 1.74 – 1.58 (m, 4H), 1.50 – 1.40 (m, 2H), 0.93 (dd, *J* = 10.3, 6.7 Hz, 6H), 0.85 (dd, *J* = 6.6, 4.5 Hz, 6H).

Yield: 58%. MS-ESI: 493.69.

General procedure for synthesis of alcohol group (25b, 31b)

Under anhydrous conditions, a solution of compound 25a and 31a (1 eq, 1.146 mmol) in dry THF (2 mL) was cooled to 0 °C. sodium borohydride ($NaBH_4$, 10 equiv., 11.46 mmol) was added, and the reaction mixture was heated at reflux at 80 °C for 15 minutes. After cooling to room temperature, anhydrous methanol was added dropwise, and the mixture was stirred overnight at room temperature. The reaction was then acidified on ice with 3 M HCl until pH 3–4 was reached, and the solvent was removed under reduced pressure. The residue was diluted with dichloromethane and washed with water and brine. The organic layer was dried over anhydrous Na_2SO_4, filtered, and concentrated under reduced pressure.

benzyl (2S,5S)-4-(((S)-1-hydroxy-4-methylpentan-2-yl)carbamoyl)-2,5-diisobutylpiperazine-1-carboxylate (25b)

The crude product was purified by column chromatography using ethyl acetate/petroleum ether (4:6) as the eluent.

^{1}H NMR (400 MHz, $CDCl_3$) δ 7.34 (m, *J* = 4.1 Hz, 5H), 5.59 (d, *J* = 8.2 Hz, 1H), 5.12 (s, 2H), 4.03-3.95 (m, 2H); 3.83 – 3.58 (m, 5H), 3.51 – 3.39 (m, 2H), 1.75 – 1.56 (m, 5H), 1.00 – 0.91 (m, 10H), 0.90-0.81 (m, 8H).

Yield: 60%. ESI-MS: $[M+H]^+$: 476.64.

(2S,5S)-4,5-dibenzyl-N-((S)-1-hydroxy-4-methylpentan-2-yl)-2-isobutylpiperazine-1-carboxamide (31b)

The product was directly used for the next step without purification.

^{1}H NMR (400 MHz, $CDCl_3$) δ 7.35 – 7.15 (m, 10H), 5.59 (d, *J* = 8.2 Hz, 1H), 3.85 – 3.62 (m, 4H), 3.61-3.52 (m, 3H), 3.52 – 3.39 (m, 2H), 3.04 – 2.89 (m, 3H), 2.84 (dd, *J* = 10.7, 5.4 Hz, 1H), 2.71 (m, 1H), 1.75 – 1.56 (m, 3H), 1.54 – 1.33 (m, 2H), 1.26 (m, 1H), 0.94 (d, *J* = 6.6 Hz, 6H), 0.85 (t, *J* = 6.6 Hz, 6H).

Yield: 65%. MS-ESI: $[M+H]^+$: 465.68.

General procedure of catalytic hydrogenation and introduction of pyrazinoic acid residue or Cbz (25c, 31c, 31d)

To a solution of compound Cbz- or benzyl-piperazine (1 equiv., 0.29 mmol) in methanol (3 mL), a few drops of 1 M HCl and 10% palladium on activated carbon (Pd/C) (1 equiv., 0.29 mmol) were added. The reaction vessel was saturated with hydrogen gas, and the mixture was stirred at room temperature for 28 hours.

The reaction mixture was filtered through celite, washing with methanol.

The intermediates were directly used for introduction of pyrazinoic acid residue (see in procedure for synthesis of 6,12,17,22) and Cbz (see in procedure for 16,21).

The intermediates were directly used for the next step.

General procedure for synthesis of aldehyde (26,27, 32 and 33)

To a suspension of Dess–Martin periodinane (2 equiv., 0.09 mmol) in anhydrous CH_2Cl_2, a solution of alcohol (1 equiv., 0.05 mmol) in CH_2Cl_2 was added dropwise under anhydrous conditions. The reaction mixture was stirred at room temperature for 3 hours. After completion, the solvent was removed under reduced pressure. The resulting residue was diluted with CH_2Cl_2 and extracted sequentially with 5% aqueous $NaHCO_3$, 10% aqueous Na_2SO_3, and brine. The organic phase was dried over anhydrous Na_2SO_4, filtered, and concentrated under reduced pressure. The crude product was purified by preparative HPLC.

Benzyl (2S,5S)-2,5-diisobutyl-4-(((S)-4-methyl-1-oxopentan-2-yl)carbamoyl)piperazine-1-carboxylate (26)

The compound **26** is afforded as a brown oil.

^{1}H NMR (500 MHz, $CDCl_3$) δ 9.59 (d, 1H), 7.34 (q, J = 2.9 Hz, 5H), 5.17 (dd, J = 12.3, 4.9 Hz, 1H), 5.08 (d, J = 12.1 Hz, 1H), 4.86 (d, J = 6.3 Hz, 1H), 4.43 (d, J = 6.6 Hz, 1H), 4.19 (m, 4H), 3.90 (s, 1H), 1.48 – 1.36 (m, 5H), 1.30 – 1.16 (m, 4H), 1.02 – 0.81 (m, 18H).

^{13}C NMR (500 MHz, $CDCl_3$) δ 198.28 (1C), 159.00 (1C), 157.63 (1C), 136.35 (1C), 128.20 (5C), 50.10 (1C), 48.66 (1C), 47.59 (1C), 40.64 (1C), 40.14 (1C), 39.57 (1C), 25.41 (1C), 25.04 (1C), 24.97 (1C), 22. 56 (1C), 22.48 (5C).

Yield: 32%. ESI-MS: $[M+H]^+$: 474.51.

(2S,5S)-2,5-diisobutyl-N-((S)-4-methyl-1-oxopentan-2-yl)-4-(pyrazine-2-carbonyl)piperazine-1-carboxamide (27)

^{1}H NMR (500 MHz, $CDCl_3$) δ 9.60 (dt, *J* = 6.4, 0.9 Hz, 1H), 9.05 (d, *J* = 1.4 Hz, 1H), 8.88 (dd, *J* = 3.6, 1.4 Hz, 1H), 8.79 (d, *J* = 3.5 Hz, 1H), 6.04 (d, *J* = 7.9 Hz, 1H), 4.36 – 4.27 (m, 1H), 4.10 (dd, *J* = 10.9, 2.8 Hz, 1H), 4.02 – 3.89 (m, 3H), 3.77 (dd, *J* = 10.9, 5.6 Hz, 1H), 3.67 – 3.60 (m, 1H), 1.76 – 1.61 (m, 6H), 1.55 – 1.41 (m, 3H), 0.98 – 0.90 (m, 9H), 0.89 – 0.80 (m, 9H).

^{13}C NMR (500 MHz, $CDCl_3$) δ 198.14 (1C), 163.29 (1C), 159.50 (1C), 148.72 (2C), 145.35 (1C), 143.37 (1C), 55.12 (1C), 52.72 (2C), 48.64 (2C), 40.74 (1C), 40.02 (2C), 24.61 (3C), 22.19 (6C).

Yield: 25%. MS-ESI: 445.61.

benzyl (2S,5S)-2-benzyl-5-isobutyl-4-(((S)-4-methyl-1-oxopentan-2-yl)carbamoyl)piperazine-1-carboxylate (32)

^{1}H NMR (500 MHz, $CDCl_3$) δ 9.60 (dt, *J* = 6.4, 0.9 Hz, 1H), 7.38 – 7.16 (m, 10H), 5.32 (s, 2H), 4.36 – 4.27 (m, 1H), 4.22 (tdd, *J* = 8.6, 6.6, 3.8 Hz, 1H), 4.07 – 3.96 (m, 2H), 3.79 – 3.63 (m, 3H), 3.02 (ddt, *J* = 12.8, 8.4, 0.8 Hz, 1H), 2.79 (ddt, *J* = 12.8, 8.4, 1.0 Hz, 1H), 1.76 – 1.59 (m, 4H), 1.50 – 1.39 (m, 2H), 0.98 – 0.90 (m, 6H), 0.89 – 0.80 (m, 6H).

^{13}C NMR (500 MHz, $CDCl_3$) δ 198.50 (1C), 159.11 (1C), 156.51 (1C), 137.84 (1C), 136.34 (1C), 128.80 (10C), 67.40 (1C), 56.38 (1C), 54.88 (1C), 52.83 (1C), 49.03 (1C), 47.63 (1C), 40.86 (1C), 39.43 (1C), 37.93 (1C), 25.31 (1C), 22.81 (5C).

Yield: 29%. MS-ESI: $[M+H]^+$: 507.68.

(2S,5S)-5-benzyl-2-isobutyl-N-((S)-4-methyl-1-oxopentan-2-yl)-4-(pyrazine-2-carbonyl)piperazine-1-carboxamide (33)

^{1}H NMR (500 MHz, $CDCl_3$) δ 9.60 (dt, *J* = 6.4, 0.9 Hz, 1H), 9.05 (d, *J* = 1.4 Hz, 1H), 8.88 (dd, *J* = 3.6, 1.4 Hz, 1H), 8.79 (d, *J* = 3.5 Hz, 1H), 7.33 – 7.16 (m, 5H), 4.36 – 4.25 (m, 2H), 4.15 (dd, *J* = 10.9, 2.8 Hz, 1H), 4.06 (dd, *J* = 11.6, 3.8 Hz, 1H), 3.92 (tdd, *J* = 8.6, 5.5, 2.7 Hz, 1H), 3.84 (dd, *J* = 10.8, 5.5 Hz, 1H), 3.75 (dd, *J* = 11.6, 6.5 Hz, 1H), 3.04 (ddt, *J* = 12.8, 8.4, 1.0 Hz, 1H), 2.81 (ddt, *J* = 13.0, 8.6, 0.9 Hz, 1H), 1.76 – 1.61 (m, 4H), 1.51 – 1.41 (m, 2H), 0.99 – 0.90 (m, 6H), 0.89 – 0.80 (m, 6H).

^{13}C NMR (500 MHz, $CDCl_3$) δ 198.52 (1C), 164.63 (1C), 158.56 (1C), 147.78 (3C), 145.41 (1C), 143.67 (1C), 138.08 (1C), 128.47 (5C), 126.97 (1C), 55.74 (2C), 52.83 (1C), 48.50 (2C), 39.99 (2C), 38.26 (1C), 25.09 (1C), 22.81 (4C).

Yield: 36%. Molecular Weight: 479.63.

Synthesis diethyl ((methylsulfonyl)methyl)phosphonate (28)

To a solution of diethyl (methylthio)methylphosphonate (1 equiv., 2.5 mmol) in CCl_4 (2 mL) under an inert atmosphere at 0 °C, a solution of m-chloroperbenzoic acid (m-CPBA, 2.2 equiv., 5.5 mmol) in CCl_4 (5 mL) was added. The reaction mixture was stirred at 0 °C for 16 hours. After completion, the reaction mixture was filtered through a Gooch crucible to afford compound 28 as a white solid.

^{1}H NMR (400 MHz, $CDCl_3$) δ 4.23 (dqd, *J* = 8.1, 4H), 3.58 (dd, *J* = 16.4, 2H), 3.20 (s, 3H), 1.43 – 1.32 (m, 6H).

Yield: 80%. MS-ESI: 230.04.

General synthesis of vinyl-sulfone (29,30,34 and 35)

To a solution of *diethyl (methylsulfonyl)methylphosphonate* (1 equiv, 0.019 mmol) in dry THF at 0 °C under anhydrous conditions, sodium hydride (NaH, 2 equiv, 0.038 mmol) was added. Subsequently, a solution of aldehyde (1 equiv, 0.019 mmol) in dry THF (200 µL) was added dropwise. The reaction mixture was stirred at room temperature for 50 minutes. After completion, the solvent was removed under reduced pressure. The residue was diluted with ethyl acetate and extracted successively with 10% aqueous citric acid, 5% aqueous $NaHCO_3$, and brine. The organic phase was dried over anhydrous Na_2SO_4, filtered, and concentrated under reduced pressure. The crude product was purified by preparative HPLC.

benzyl (2S,5S)-2,5-diisobutyl-4-(((S,E)-5-methyl-1-(methylsulfonyl)hex-1-en-3-yl)carbamoyl)piperazine-1-carboxylate (29)

The compound is afforded as a brown oil.

^{1}H NMR (500 MHz, $CDCl_3$) δ 7.38 – 7.29 (m, 5H), 6.81 (dd, *J* = 15.0, 5.0 Hz, 1H), 6.37 (d, *J* = 15.2 Hz, 1H), 5.35 (d, *J* = 5.1 Hz, 1H), 5.20 (d, *J* = 12.1 Hz, 1H), 5.12 (m, 1H), 4.62 (s, 1H), 4.18 (d, *J* = 9.1 Hz, 3H), 3.82 (m, 1H), 3.71 (dd, *J* = 10.3, 6.5 Hz, 2H), 3.14 (ddt, *J* = 14.8, 11.4, 7.2 Hz, 2H), 2.94 (s, 3H), 2.73 – 2.64 (m, 2H), 2.62 – 2.53 (m, 2H), 2.24 (t, *J* = 7.7 Hz, 2H), 0.94 (dd, *J* = 6.8, 5.2 Hz, 11H), 0.88 (t, *J* = 6.6 Hz, 6H).

^{13}C NMR (500 MHz, $CDCl_3$) δ 167.75 (1C), 156.58 (1C), 138.17 (1C), 128.66 (5C), 62.66 (2C), 53.77 (1C), 52.07 (1C), 49.53 (1C), 42. 76 (1C), 29.53 (1C), 24.98 (1C), 24.78 (1C), 24.51 (1C), 23.14 (1C), 22.78 (1C), 22.33 (1C), 22.02 (1C); 18.88 (1C), 18.60 (1C), 17.45 (1C), 14.10 (1C),11.83 (1C), 8.52 (3C).

Yield: 56%. ESI-MS: $[M+H]^+$:550.71.

(2S,5S)-2,5-diisobutyl-N-((S,E)-5-methyl-1-(methylsulfonyl)hex-1-en-3-yl)-4-(pyrazine-2-carbonyl)piperazine-1-carboxamide (30)

The compound is afforded as a brown oil.

^{1}H NMR (500 MHz, $CDCl_3$) δ 9.05 (d, *J* = 1.4 Hz, 1H), 8.88 (dd, *J* = 3.6, 1.4 Hz, 1H), 8.79 (d, *J* = 3.5 Hz, 1H), 6.55 (dp, *J* = 18.7, 1.1 Hz, 1H), 6.28 (ddt, *J* = 18.7, 7.3, 0.9 Hz, 1H), 4.40 – 4.31 (m, 1H), 4.10 (dd, *J* = 10.8, 2.9 Hz, 1H), 4.02 – 3.89 (m, 2H), 3.77 (dd, *J* = 10.8, 5.5 Hz, 1H), 3.67 – 3.60 (m, 1H), 3.00 (s, 3H), 1.74 – 1.57 (m, 6H), 1.55 – 1.42 (m, 2H), 1.36 (dddd, *J* = 12.8, 7.9, 6.8, 0.9 Hz, 1H), 0.98 – 0.90 (m, 9H), 0.89 – 0.80 (m, 9H).

^{13}C NMR (500 MHz, $CDCl_3$) δ 165.11 (1C), 158.82 (1C), 148.31 (2C), 145.63 (1C), 143.20 (1C), 140 51 (1C), 136.61 (1C), 52.97 (1C), 52.44 (1C), 50.48 (1C), 48.72 (2C), 43.04 (2C), 39.89 (2C), 25. 56 (3C), 22.17 (6C).

Yield: 64%. MS-ESI: $[M+H]^+$: 521.72.

benzyl (2S,5S)-2-benzyl-5-isobutyl-4-(((S,E)-5-methyl-1- (methylsulfonyl) hex-1-en-3-yl) carbamoyl)piperazine-1-carboxylate (34)

The compound is afforded as a brown oil.

^{1}H NMR (500 MHz, $CDCl_3$) δ 7.38 – 7.16 (m, 10H), 6.55 (dp, *J* = 18.7, 1.1 Hz, 1H), 6.28 (ddt, *J* = 18.7, 7.3, 0.9 Hz, 1H), 5.64 (d, *J* = 7.7 Hz, 1H), 5.16 (s, 2H), 4.40 – 4.31 (m, 1H), 4.22 (tdd, *J* = 8.6, 6.6, 3.8 Hz, 1H), 4.07 – 3.96 (m, 2H), 3.79 – 3.63 (m, 3H), 3.06 – 2.98 (m, 3H), 2.79 (ddt, *J* = 12.8, 8.4, 0.9 Hz, 1H), 1.73 – 1.57 (m, 4H), 1.49 – 1.31 (m, 2H), 0.94 (dd, *J* = 6.5, 1.4 Hz, 6H), 0.88 – 0.81 (m, 6H).

^{13}C NMR (500 MHz, $CDCl_3$) δ 159.30 (1C), 156.99 (1C), 140.69 (1C), 136.98 (3C), 128.39 (10C), 67.12 (1C), 54.77 (1C), 52.80 (1C), 50.33 (1C), 48.50 (1C), 47.44 (1C), 43.01 (2C), 39.59 (1C), 37.80 (1C), 24.93 (2C), 22.48 (4C).

Yield: 53%. MS-ESI: $[M+H]^+$: 583.79.

(2S,5S)-5-benzyl-2-isobutyl-N-((S,E)-5-methyl-1-(methylsulfonyl)hex-1-en-3-yl)-4-(pyrazine-2-carbonyl)piperazine-1-carboxamide (35)

The compound is afforded as a brown oil.

^{1}H NMR (500 MHz, $CDCl_3$) δ 9.05 (d, *J* = 1.5 Hz, 1H), 8.88 (dd, *J* = 3.6, 1.4 Hz, 1H), 8.77 (d, *J* = 3.5 Hz, 1H), 7.33 – 7.16 (m, 5H), 6.55 (dp, *J* = 18.7, 1.1 Hz, H), 6.28 (ddt, *J* = 18.7, 7.3, 0.9 Hz, 1H), 4.40 – 4.25 (m, 2H), 4.15 (dd, *J* = 10.9, 2.8 Hz, 1H), 4.06 (dd, *J* = 11.6, 3.8 Hz, 1H), 3.94 (tdd, *J* = 8.6, 5.6, 2.8 Hz, 1H), 3.84 (dd, *J* = 10.8, 5.5 Hz, 1H), 3.75 (dd, *J* = 11.6, 6.5 Hz, 1H), 3.08 – 2.98 (m,

4H), 2.81 (ddt, *J* = 13.0, 8.6, 0.9 Hz, 1H), 1.73 – 1.57 (m, 4H), 1.51 – 1.42 (m, 4H), 1.36 (dddd, *J* = 12.8, 7.9, 6.8, 0.9 Hz, 2H), 0.94 (dd, *J* = 6.6, 2.2 Hz, 6H), 0.85 (dd, *J* = 6.6, 5.2 Hz, 6H).
^{13}C NMR (500 MHz, $CDCl_3$) δ 164.50 (1C), 159.66 (1C), 147.95 (2C), 146.04 (1C), 143.67 (1C), 140.88 (1C), 138.13 (1C), 136.74 (1C), 129.02 (5C), 56.11 (1C), 53.18 (1C), 50.25 (1C), 48.39 (2C), 43.04 (2C), 39.60 (1C), 38.20 (1C), 25.47 (2C), 22.68 (4C).
Yield: 47%. MS-ESI: $[M+H]^+$: 555.74.

Synthesis tert-butyl (R)-(1-hydroxy-4-methylpentan-2-yl)carbamate (36a)

To a solution of L-leucinol (1 equiv., 1.71 mmol) in anhydrous CH_2Cl_2 under anhydrous conditions, a solution of di-tert-butyl dicarbonate (Boc_2O, 1 equiv., 1.71 mmol) in anhydrous CH_2Cl_2 was added. The reaction mixture was stirred at room temperature overnight. After completion, the solvent was removed under reduced pressure, and the crude product was purified by column chromatography using ethyl acetate/petroleum ether (3:7) as the eluent, affording **36a** as a colourless oil.
^{1}H NMR (400 MHz, $CDCl_3$) δ 4.58 (s, *J* = 7.6 Hz, 1H), 3.75-3.63 (m, 1H), 3.54-3.47 (dt, *J* = 11.0, 5.5 Hz, 1H), 1.73-1.60 (m, 1H), 1.45 (s, 9H), 1.35-1.26 (m, 2H), 0.93 (dd, *J* = 6.6, 1.8 Hz, 7H).
Yield: 99%. ESI-MS: $[M+H]^+$: 218.17.

Synthesis tert-butyl (R)-(4-methyl-1-oxopentan-2-yl)carbamate (36b)

Under Argon atmosphere, a solution of **36a** (1 equiv., 7.63 mmol) in anhydrous CH_2Cl_2 was added dropwise to a suspension of Dess–Martin periodinane (DMP, 2 equiv., 15.2 mmol) in anhydrous CH_2Cl_2. The reaction mixture was stirred at room temperature for 4 hours. After completion, the solvent was removed under reduced pressure. The residue was diluted with CH_2Cl_2 and extracted with 5% aqueous $NaHCO_3$ and brine. The organic layer was dried over anhydrous Na_2SO_4, filtered, and concentrated under reduced pressure. The crude product was purified by column chromatography using ethyl acetate/petroleum ether (2:8) as the eluent, affording **36b** as a yellow oil.
^{1}H NMR (400 MHz, DMSO) δ 9.40 (s, 1H), 3.83 (m, *J* = 10.1, 7.5, 4.6 Hz,1H), 1.69 – 1.54 (m, 1H), 1.88-1.41 (m, 1H), 1.37 (s, 9H), 0.85 (dd, *J* = 10.1, 6.6 Hz, 7H).
Yield: 57%. ESI-MS: $[M+H]^+$: 216.1.

Synthesis tert-butyl ((4R)-3-hydroxy-6-methylhept-1-en-4-yl)carbamate (36c)

Under argon atmosphere, to a solution of compound **36b** (1 equiv., 4.18 mmol) in anhydrous THF, that was stirred on ice under anhydrous conditions for 5 minutes, vinylmagnesium bromide (1 equiv., 4.18 mmol) was added dropwise, and the reaction mixture was stirred at room temperature for 3 hours. The solvent was removed under reduced pressure, and the residue was diluted with

ethyl acetate, resulting in the formation of a white precipitate. The suspension was stirred at 0 °C for 15 minutes and then filtered through a Gooch crucible, washing with ethyl acetate. The filtrate was concentrated as a yellow oil and purified by column chromatography using ethyl acetate/petroleum ether (1.5:8.5) as the eluent, to afford **36c** as a yellowish oil.

^{1}H NMR (400 MHz, $CDCl_3$) δ 5.93-5.78 (m, *J* = 23.4, 17.2, 10.5, 5.7 Hz, 1H), 5.37 – 5.15 (m, 2H), 4.63-4.44 (m, *J* = 8.8 Hz, 1H), 4.04 (s, 1H), 2.99 (d, *J* = 5.6 Hz, 1H), 1.75 – 1.57 (m, 2H), 1.51-1.47 (m, 1H), 1.53 – 1.43 (m, 9H), 1.30 – 1.19 (m, 1H), 1.00 – 0.86 (m, 6H).

Yield: 73%. MS-ESI: 243.35.

Synthesis tert-butyl (4R)-4-isobutyl-2,2-dimethyl-5-vinyloxazolidine-3-carboxylate (36d)

To a solution of compound 36c (1 equiv., 0.35 mmol) in CH_2Cl_2 (4 mL), p-toluenesulfonic acid (0.04 equiv., 0.014 mmol) was added under stirring at room temperature. After 5 minutes, 2,2-dimethoxypropane (3.5 equiv., 1.22 mmol) was added, and the reaction mixture was stirred overnight at room temperature. Upon completion, the mixture was diluted with CH_2Cl_2 and extracted with 5% aqueous $NaHCO_3$ and brine. The organic phase was dried over anhydrous Na_2SO_4, filtered, and concentrated under reduced pressure to obtain the compound 36d, without using any further purification as a yellow oil.

Yield: 65%. MS-ESI: $[M+H]^+$: 283.21.

Synthesis (4R)-3-(tert-butoxycarbonyl)-4-isobutyl-2,2-dimethyloxazolidine-5-carboxylic acid (36e)

To a suspension of Ru (IV) oxide hydrate (0.075 eq, 0.016 mmol) in water/acetone (1:1) cooled to 0°C, $NaIO_4$ (6.5 eq, 1.38 mmol) was added. Then, 36d (1 eq, 0.21 mmol) dissolved in acetone was added dropwise and the reaction was stirred for four hours at room temperature. Then, the mixture was filtered on celite and washed by acetone. The filtrate was concentrated and subsequently diluted by dichloromethane and filtered off to remove the white solid. The filtrate was then washed by citric acid solution 10% and brine. Finally, it was dried over anhydrous sodium solfate, filtered and concentrated under vacuum. The residue was directly used for the next step.

Yield: 80%. MS-ESI: $[M+H]^+$: 301.19.

Synthesis tert-butyl (4R)-4-isobutyl-2,2-dimethyl-5-(naphthalen-1-ylcarbamoyl)oxazolidine-3-carboxylate (36f)

To a solution of 36e (1 eq, 0.13 mmol) in DMF, DIPEA (1.1 eq, 0.15 mmol, 0.026 mL) and HBTU (1.1 eq, 0.15 mmol) were added at 0 °C and the mixture was stirred for 5 minutes. A solution of 1-

naphthylamine (1 eq, 0.13 mmol) in DMF was then added dropwise. The reaction mixture was stirred at room temperature for 16 hours. The solvent was evaporated under reduced pressure, and the residue was diluted with dichloromethane and washed successively with 10% aqueous citric acid, 5% $NaHCO_3$ solution, and brine. The organic phase was dried over anhydrous sodium sulfate, filtered, and concentrated under reduced pressure.
Yield: 62%. ESI-MS: $[M+H]^+$: 427.25.

Synthesis (4R)-3-(tert-butoxycarbonyl)-4-isobutyl-2,2-dimethyloxazolidine-5-carboxylic acid (36g)

To a solution of **36f** (1 eq, 0.11 mmol) in CH_2Cl_2, trifluoroacetic acid (10 eq, 0.8 mL) was added. The reaction mixture was stirred at room temperature for 48 hours. The solvent was then removed under reduced pressure using a rotary evaporator. The resulting residue was filtered under vacuum and washed with diethyl ether. Finally, the compound was purified by preparative HPLC to afford a light yellow solid.
^{1}H NMR (400 MHz, $CDCl_3$) δ 9.41 (s, 1H), 8.01 (s, 2H), 7.80 – 7.73 (m, 3H), 7.64 (d, *J* = 8.2 Hz, 1H), 7.53 (dd, *J* = 14.0, 8.7 Hz, 1H), 7.48 – 7.38 (m, 2H), 4.82 (s, 1H), 3.97 (s, 1H), 1.62 (d, *J* = 23.0 Hz, 2H), 1.43 (d, *J* = 1.8 Hz, 3H), 0.85 (dd, *J* = 13.9, 9.1 Hz, 6H).
Yield: 73%. ESI-MS: $[M+H]^+$: 287.17.

Synthesis (R)-3-amino-5-methyl-N-(naphthalen-1-yl)-2-oxohexanamide (36h)

Under an argon atmosphere, Dess–Martin periodinane (1.6 equiv., 0.028 mmol) was added to a solution of compound **36g** (1 equiv., 0.017 mmol) in dichloromethane. The reaction mixture was stirred at room temperature for 20 h and then concentrated under reduced pressure. The crude product was purified by preparative HPLC to afford compound **36h**.
^{1}H NMR (400 MHz, $CDCl_3$) δ 9.99 (s, 1H), 8.08 – 8.02 (m, 1H), 7.89 – 7.82 (m, 1H), 7.76 – 7.66 (m, 2H), 7.60 – 7.47 (m, 2H), 7.24 (t, *J* = 8.0 Hz, 1H), 4.26 – 4.20 (m, 2H), 4.18 – 4.07 (m, 1H), 1.80 – 1.64 (m, 2H), 1.60 – 1.48 (m, 1H), 1.02 – 0.91 (m, 3H), 0.91 – 0.81 (m, 3H).
Yield: 46%. ESI-MS: $[M+H]^+$: 284.36.

Synthesis 3-isocyanato-5-methyl-N-(naphthalen-1-yl)-2-oxohexanamide

To afford 3-isocyanato-5-methyl-N-(naphthalen-1-yl)-2-oxohexanamide, compound **36h** was treated with triphosgene according to the experimental procedure used for the synthesis of methyl 2-isocyanato-4-methylpentanoate (see Synthesis second class of compounds).

General procedure of introduction of urea bond (37, 36i)

To a solution of 3-isocyanato-5-methyl-N-(naphthalen-1-yl)-2-oxohexanamide (1 equiv., 0.10 mmol) in DCM, a solution of piperazine (1 equiv., 0.10 mmol) in DCM was added dropwise, followed by triethylamine (TEA, 1.1 equiv., 0.11 mmol). The reaction mixture was stirred at room temperature for 48 hours. After completion, the reaction was diluted with DCM and washed with 10% aqueous citric acid and brine. The organic layer was separated, dried over anhydrous sodium sulfate, filtered, and concentrated under reduced pressure. The crude product was purified by column chromatography (ethyl acetate/petroleum ether, 1.5:8.5) to afford the desired compound.

benzyl (2S,5S)-2,5-diisobutyl-4-(((R)-5-methyl-1-(naphthalen-1-ylamino)-1,2-dioxohexan-3-yl)carbamoyl)piperazine-1-carboxylate (37)

^{1}H NMR (500 MHz, $CDCl_3$) δ 8.08 – 8.02 (m, 1H), 7.88 – 7.83 (m, 1H), 7.71 (ddt, *J* = 9.7, 8.9, 1.5 Hz, 2H), 7.59 – 7.48 (m, 2H), 7.38 – 7.33 (m, 4H), 7.31 – 7.21 (m, 2H), 6.83 (d, *J* = 8.2 Hz, 1H), 5.10 (s, 2H), 4.66 (dt, *J* = 8.0, 7.0 Hz, 1H), 4.06 – 3.95 (m, 2H), 3.93 – 3.84 (m, 2H), 3.75 (tdd, *J* = 8.6, 5.7, 2.9 Hz, 1H), 3.70 – 3.59 (m, 3H), 1.80 –1.57 (m, 6H), 1.54 – 1.37 (m, 3H), 0.98– 0.75 (m, 18H).

^{13}C NMR (500 MHz, $CDCl_3$) δ 190.96 (1C), 162.70 (1C), 159.00 (1C), 157.42 (1C), 136.03 (2C), 134.48 (1C), 128.11 (10C), 125.90 (1C), 124.13 (1C), 118.83 (1C), 67.47 (1C), 55.98 (1C), 52.48 (1C), 50.04 (1C), 48.31 (2C), 40.34 (3C), 24.93 (2C), 22.30 (6C).

Brown oil. Yield: 27%. MS-ESI: 642,84.

(2S,5S)-4,5-dibenzyl-2-isobutyl-N-((R)-5-methyl-1-(naphthalen-1-ylamino)-1,2-dioxohexan-3-yl)piperazine-1-carboxamide (36i)

^{1}H NMR (500 MHz, $CDCl_3$) δ 8.08 – 8.02 (m, 1H), 7.88 – 7.82 (m, 1H), 7.71 (ddt, *J* = 9.7, 8.8, 1.6 Hz, 2H), 7.59 – 7.48 (m, 2H), 7.33 – 7.16 (m, 11H), 6.83 (d, *J* = 8.2 Hz, 1H), 4.66 (dt, *J* = 8.0, 7.0 Hz, 1H), 3.88 (dd, *J* = 11.4, 3.2 Hz, 1H), 3.75 (d, *J* = 12.4 Hz, 1H), 3.62 – 3.49 (m, 3H), 3.03 – 2.90 (m, 3H), 2.84 (dd, *J* = 10.8, 5.5 Hz, 1H), 2.71 (ddt, *J* = 12.6, 8.0, 0.9 Hz, 1H), 1.80 – 1.59 (m, 4H), 1.54 – 1.40 (m, 2H), 0.98 – 0.77 (m, 12H).

White solid. Yield: 31%. MS-ESI: 632,85.

General procedure of catalytic hydrogenation and introduction of pyrazinoic acid residue or Cbz (38, 39, 40)

To a solution of compound Cbz- or benzyl-piperazine (1 equiv., 0.29 mmol) in methanol (3 mL), a few drops of 1 M HCl and 10% palladium on activated carbon (Pd/C) (1 equiv., 0.29 mmol) were

added. The reaction vessel was saturated with hydrogen gas, and the mixture was stirred at room temperature for 28 hours.
The reaction mixture was filtered through celite, washing with methanol.
The intermediates were directly used for the next step.

Introduction of pyrazinoic acid residue (38,40)

To a solution of 2-pyrazinoic acid (1.3 equiv., 0.13 mmol) in DMF at 0 °C, DIPEA (1.3 equiv., 0.13 mmol) and HATU (1.3 equiv., 0.13 mmol) were added, and the mixture was stirred for 10 minutes. A solution of piperazine (1 equiv., 0.10 mmol) in DMF was then added dropwise, and the reaction mixture was stirred at room temperature for 2 hours.
The solvent was removed under reduced pressure, and the residue was diluted with ethyl acetate. The organic phase was sequentially washed with 10% aqueous citric acid, 5% aqueous $NaHCO_3$, and brine. The organic layer was dried over anhydrous Na_2SO_4, filtered, and concentrated under reduced pressure.
The compound was purified by preparative HPLC.

(2S,5S)-2,5-diisobutyl-N-((R)-5-methyl-1-(naphthalen-1-ylamino)-1,2-dioxohexan-3-yl)-4-(pyrazine-2-carbonyl)piperazine-1-carboxamide (38)

^{1}H NMR (500 MHz, $CDCl_3$) δ 9.05 (d, *J* = 1.4 Hz, 1H), 8.88 (dd, *J* = 3.6, 1.4 Hz, 1H), 8.79 (d, *J* = 3.5 Hz, 1H), 8.08 – 8.02 (m, 1H), 7.88 – 7.82 (m, 2H), 7.71 (ddt, *J* = 9.7, 8.8, 1.6 Hz, 1H), 7.59 – 7.48 (m, 1H), 7.23 (s, 1H), 6.83 (d, *J* = 8.2 Hz, 1H), 4.66 (dt, *J* = 8.0, 7.0 Hz, 1H), 4.10 (dd, *J* = 10.9, 2.8 Hz, 1H), 4.02 – 3.89 (m, 3H), 3.77 (dd, *J* = 10.9, 5.6 Hz, 1H), 3.67 – 3.60 (m, 1H), 1.73 – 1.61 (m, 6H), 1.55 – 1.42 (m, 3H), 1.00 – 0.75 (m, 18H).
^{13}C NMR (500 MHz, $CDCl_3$) δ 190.80 (1C), 164.44 (1C), 163.13 (1C), 158.88 (1C), 148.48 (2C), 146.03 (1C), 143.82 (1C), 136.11 (1C), 134.07 (1C), 127.02 (7C), 119.25 (1C), 55.87 (1C), 53.00 (1C), 52.11 (1C), 48.17 (2C), 39.73 (3C), 24.67 (3C), 22.22 (6C).
Brown oil. Yield: 27%. MS-ESI: 614,79.

(2S,5S)-5-benzyl-2-isobutyl-N-((R)-5-methyl-1-(naphthalen-1-ylamino)-1,2-dioxohexan-3-yl)-4-(pyrazine-2-carbonyl)piperazine-1-carboxamide (40)

^{1}H NMR (500 MHz, $CDCl_3$) δ 9.05 (d, *J* = 1.5 Hz, 1H), 8.86 (dd, *J* = 3.6, 1.4 Hz, 1H), 8.79 (d, *J* = 3.5 Hz, 1H), 8.08 – 8.01 (m, 1H), 7.87 – 7.82 (m, 1H), 7.75 – 7.67 (m, 2H), 7.60 – 7.48 (m, 2H), 7.35 – 7.19 (m, 6H), 6.85 (d, *J* = 8.2 Hz, 1H), 4.60 (dt, *J* = 8.0, 7.1 Hz, 1H), 4.30 (tdd, *J* = 8.4, 6.4, 3.7 Hz, 1H), 4.15 (dd, *J* = 10.9, 2.9 Hz, 1H), 4.06 (dd, *J* = 11.6, 3.8 Hz, 1H), 3.92 (tdd, *J* = 8.6, 5.5,

2.7 Hz, 1H), 3.84 (dd, *J* = 10.8, 5.5 Hz, 1H), 3.75 (dd, *J* = 11.6, 6.5 Hz, 1H), 3.05 (ddt, *J* = 12.8, 8.4, 0.9 Hz, 1H), 2.81 (ddt, *J* = 13.0, 8.6, 0.9 Hz, 1H), 1.76 – 1.63 (m, 4H), 1.54 – 1.42 (m, 2H), 0.82 – 0.74 (m, 12H).

^{13}C NMR (500 MHz, $CDCl_3$) δ 190.27 (1C), 164.86 (1C), 162.98 (1C), 159.11 (1C), 148.44 (2C), 146.00 (1C), 143.34 (1C), 137.80 (1C), 136.17 (1C), 134.32 (1C), 128.96 (10C), 125.45 (1C), 124.02 (1C), 119.32 (1C), 56.17 (1C), 53.29 (1C), 48.14 (2C), 41.18 (1C), 39.78 (1C), 37.90 (1C), 24.79 (2C), 22.13 (4C).

Yield: 26%. MS-ESI: 648,81

General procedure for introduction of Cbz on piperazine (39)

To a solution of piperazine (1 equiv., 0.07 mmol) in DCM, CBZ-OSu (1.1 equiv., 0.07 mmol) was added, and the reaction mixture was stirred at room temperature for 30 minutes.

The solvent was removed under reduced pressure, and the residue was diluted with ethyl acetate and extracted with 5% aqueous $NaHCO_3$ and brine.

The organic layer was dried over anhydrous Na_2SO_4, filtered, and concentrated under reduced pressure.

The compound was purified by preparative HPLC.

Benzyl (2S,5S)-2-benzyl-5-isobutyl-4-((R)-5-methyl-1-(naphthalen-1-ylamino)-1,2-dioxohexan-3-yl)carbamoyl)piperazine-1-carboxylate (39)

^{1}H NMR (500 MHz, $CDCl_3$) δ 8.10 – 8.04 (m, 1H), 7.85 – 7.81 (m, 1H), 7.69 (ddt, *J* = 9.7, 8.8, 1.5 Hz, 2H), 7.59 – 7.47 (m, 2H), 7.38 – 7.16 (m, 11H), 6.80 (d, *J* = 8.2 Hz, 1H), 4.99 (s, 2H), 4.65 (dt, *J* = 8.0, 7.0 Hz, 1H), 4.22 (tdd, *J* = 8.6, 6.6, 3.8 Hz, 1H), 4.07 – 3.93 (m, 2H), 3.79 – 3.63 (m, 3H), 3.03 (ddt, *J* = 12.8, 8.4, 0.8 Hz, 1H), 2.85 – 2.77 (m, 1H), 1.80 – 1.56 (m, 4H), 1.54 – 1.39 (m, 2H), 0.98 – 0.69 (m, 12H).

^{13}C NMR (500 MHz, $CDCl_3$) δ 190.99 (1C), 163.12 (1C), 158.98 (1C), 157.29 (1C), 136.05 (3C), 133.89 (1C), 129.17 (15C), 125.91 (1C), 124.21 (1C), 119.43 (1C), 67.18 (1C), 56.16 (1C), 54.81 (1C), 52.25 (1C), 48.81 (1C), 47.46 (1C), 40.99 (1C), 39.30 (1C), 37.78 (1C), 24.78 (2C), 22. 62 (4C).

Yield: 38%. MS-ESI: 676.86.

3.6.3 SYNTHESIS FLUORESCENT PROBES

Synthesis 41a

To a solution of Boc-L-leucine (1 equiv., 4.33 mmol) in DMF at 0 °C were added HOBt (1 equiv., 4.33 mmol) and WSC (1 equiv., 4.33 mmol). A solution of N,O-dimethylhydroxylamine hydrochloride (1.1 equiv., 4.76 mmol) and TEA (1 equiv., 4.33 mmol) in DMF was then added dropwise, and the mixture was stirred at room temperature for 16 h. The solvent was evaporated under reduced pressure, and the residue was diluted with ethyl acetate and successively washed with 10% aqueous citric acid, 5% aqueous $NaHCO_3$, and brine. The organic layer was dried over anhydrous Na_2SO_4, filtered, and concentrated under reduced pressure. The crude product was purified by column chromatography using ethyl acetate/petroleum ether (1:4) as eluent (Rf = 0.4), affording a clear oil.

^{1}H NMR (400 MHz, DMSO): δ 6.9 (d, 1H), 4.4 (t, 1H), 3.7 (s, 3H), 3.13 (s, 3H), 1.6 (s, 1H), 1.3 (s, 9H), 0.8 (m, J = 4 Hz, 7H).

Yield: 91%. ESI-MS: $[M + H]^+$ = 275.24.

Synthesis 41b

To a suspension of $LiAlH_4$ (5 equiv., 18.2 mmol) in anhydrous diethyl ether (15 mL) at 0 °C, a solution of compound **41a** (1 equiv., 3.64 mmol) in diethyl ether (5 mL) was added dropwise. The reaction mixture was stirred for 30 min at room temperature. The excess reducing agent was quenched with ice, and the mixture was filtered through Celite, washing with diethyl ether. The filtrate was concentrated under reduced pressure, and the crude residue was purified by column chromatography using ethyl acetate/petroleum ether (1:4) as eluent (Rf = 0.7), affording compound **41b** as a yellow oil.

^{1}H NMR (400 MHz, DMSO): δ 9.4 (s, 1H), 7.25 (s, 1H), 2.05 (s, 2H), 1.4–1.3 (d, J = 1.36 Hz, 9H), 1.10–1.04 (t, J = 1.07 Hz, 2H), 0.89–0.78 (m, J = 0.83 Hz, 6H).

Yield: 42%. ESI-MS: $[M + H]^+$ = 216.48.

Synthesis 41c

To a solution of diethyl (methylsulfonyl)methylphosphonate **28** (1 equiv., 0.67 mmol) in anhydrous THF (5 mL) under inert atmosphere at 0 °C was added NaH (2 equiv., 1.34 mmol), followed by a solution of compound **41b** (1 equiv., 0.67 mmol) in anhydrous THF (5 mL). The reaction mixture was stirred at room temperature for 50 min, then diluted with ethyl acetate and successively washed with 1 M HCl, saturated $NaHCO_3$, and brine. The organic phase was dried over anhydrous Na_2SO_4,

filtered, and concentrated. The residue was purified by column chromatography using ethyl acetate/petroleum ether (1:4) as eluent (Rf = 0.3), affording compound **41c** as a brown oil.
Yield: 69%. ESI-MS: $[M + H]^+$ = 292.11.

Synthesis 41d

To a solution of compound **41c** (1 equiv., 0.45 mmol) in CH_2Cl_2 (1.3 mL) was added trifluoroacetic acid (0.9 mL), and the mixture was stirred at room temperature for 30 min. The solvent was evaporated under reduced pressure to afford a brown oil, which was used without further purification.
Yield: 98%. ESI-MS: $[M + H]^+$ = 192.25.

Synthesis 41e

To a solution of compound **41d** (10 equiv., 0.52 mmol) in methanol (2.5 mL) were added 1 M HCl and 10% Pd/C (1 equiv., 0.052 mmol). The atmosphere was saturated with hydrogen, and the reaction mixture was stirred for 16 h at room temperature. The catalyst was removed by filtration through Celite, washing with methanol.
Yield: 22%. ESI-MS: $[M + H]^+$ = 194.23.

Synthesis 42b

To a solution of $H_2N(Ahx)_3$-Leu-Leu-OH **42a** (1 equiv., 0.27 mmol, previously obtained in solid phase) in DMF (5 mL) were added DIPEA (5 equiv., 1.35 mmol) and di-tert-butyl dicarbonate (1.2 equiv., 0.32 mmol). The reaction mixture was stirred at room temperature for 16 h, and the solvent was evaporated without further purification, affording compound **42b** as a brown oil.

General procedure of amidic coupling (42c, 42e)

To a solution of compound 42b (1.3 equiv., 0.13 mmol) in DMF (5 mL) at 0 °C were added DIPEA (1.3 equiv., 0.13 mmol) and HATU (1.3 equiv., 0.13 mmol). After 10 min, a solution of compound 41 d and 41e (1 equiv., 0.10 mmol) in DMF (1.7 mL) was added dropwise, and the mixture was stirred at room temperature for 16 h. The solvent was removed, and the residue was diluted with ethyl acetate and washed successively with 10% aqueous citric acid, 5% aqueous $NaHCO_3$, and brine. The organic phase was dried over anhydrous Na_2SO_4, filtered, and concentrated.
The crude product were purified by preparative HPLC.

tert-butyl (13R,16R,19S)-4,7,10-tributyl-13,16-diisobutyl-21-methyl-19-((E)-2-(methylsulfonyl)vinyl)-5,8,11,14,17-pentaoxo-2,3,6,9,12,15,18-heptaazadocosanoate (42c)
Yield: 38%. ESI-MS: $[M + H]^+$ = 857.98.

tert-butyl (13R,16R,19S)-4,7,10-tributyl-13,16-diisobutyl-21-methyl-19-(2-(methylsulfonyl)ethyl)-5,8,11,14,17-pentaoxo-2,3,6,9,12,15,18-heptaazadocosanoate (42e)
Yield: 10%. ESI-MS: $[M + H]^+$ = 859.34.

Synthesis 42d and 42f

To a solution of compound 42c or 42e (1 equiv., 0.05 mmol) in dichloromethane (1 mL) was added trifluoroacetic acid (0.5 mL), and the reaction mixture was stirred for 30 min at room temperature. The solvent was removed under reduced pressure, and the residue was filtered through a Gooch filter, washing with diethyl ether. The compound was used without further purification.

N-((4S,7R,10R)-13-butyl-7,10-diisobutyl-2-methyl-4-((E)-2-(methylsulfonyl)vinyl)-6,9,12,15-tetraoxo-5,8,11,14-tetraazaicosan-16-yl)-2-hydrazinylhexanamide (42d)
Yield: 56%. ESI-MS: $[M + H]^+$ = 757.93.

N-((4S,7R,10R)-13-butyl-7,10-diisobutyl-2-methyl-4-(2-(methylsulfonyl)ethyl)-6,9,12,15-tetraoxo-5,8,11,14-tetraazaicosan-16-yl)-2-hydrazinylhexanamide (42f)
Yield: 67%. ESI-MS: $[M + H]^+$ = 759.54.

General procedure of synthesis of final probes 43 and 44

To a solution of compound 8g (1.1 equiv., 0.0036 mmol) in CH_3CN (0.5 mL) and H_2O (0.5 mL) was added TEA (1.1 equiv., 0.0036 mmol). A solution of Bodipy NHS ester (1 equiv., 0.0033 mmol) in CH_3CN (1.5 mL) was then added dropwise, and the mixture was stirred for 10 min at room temperature. The solvent was evaporated, and the crude product was purified by preparative HPLC.

N-((4R,7R,10R)-13-butyl-7,10-diisobutyl-2-methyl-4-((E)-2-(methylsulfonyl)vinyl)-6,9,12,15-tetraoxo-5,8,11,14-tetraazaicosan-16-yl)-2-(2-(3-(5,5-difluoro-7,9-dimethyl-5,9a-dihydro-

5l4,6l4-dipyrrolo[1,2-c:2',1'-e][1,3,2]diazaborol-3-yl)propanoyl)hydrazinyl)hexanamide (43)

Probe 1

The final probe was afforded as a orange-red solid.

Yield: 56%. ESI-MS: $[M + H]^+$ = 1031.69. HPLC: t_R= 14.50 min.

N-((4R,7R,10R)-13-butyl-7,10-diisobutyl-2-methyl-4-(2-(methylsulfonyl)ethyl)-6,9,12,15-tetraoxo-5,8,11,14-tetraazaicosan-16-yl)-2-(2-(3-(5,5-difluoro-7,9-dimethyl-5,9a-dihydro-5l4,6l4-dipyrrolo[1,2-c:2',1'-e][1,3,2]diazaborol-3-yl)propanoyl)hydrazinyl)hexanamide (44)

Probe 2

The second probe was afforded as a yellow-orange solid.

Yield: 67%. ESI-MS: $[M + H]^+$ = 1033.46. HPLC: t_R= 20.10 min.

3.7 BIOLOGICAL EXPERIMENTAL SECTION

3.7.1 Materials and Methods

For *in vitro* assays, HeLa cell lines—immortalized and highly stable human cervical cancer cells—were employed.

Cells were cultured in Dulbecco's Modified Eagle Medium (DMEM) supplemented with 10% fetal bovine serum (FBS), penicillin, and streptomycin to promote cell growth and prevent bacterial contamination.

Phosphate-buffered saline (PBS) was used for washing the cultures, while cell counting was performed using Trypan Blue dye and a Bürker counting chamber.

Plasticware employed included filter-cap flasks for cell culture and growth, Eppendorf tubes and micropipettes of various volumes for cell transfer, and multiwell plates for biological testing. As reference compounds, MG132, Pimozide, and DMSO were used. Fluorogenic diagnostic probes B1 and B2, synthesized in-house, were employed to assess proteasome activity. Fluorescence analysis was carried out using a BD FACSCanto II flow cytometer.

3.7.2 Sample Preparation Procedures

Each experiment was repeated several times to ensure reproducibility and statistical reliability; results were standardized by calculating the arithmetic mean of the obtained values. All procedures and dilutions were performed under identical conditions in each trial.

3.7.3 Cell Seeding

Initially, the density of HeLa cells cultured in flasks was evaluated under an optical microscope. When confluency was reached, the culture medium was removed, and the cells were washed with 4 mL of PBS. Then, 0.5 mL of trypsin was added, and the flask was incubated for 5 min at 37 °C. After incubation, 5.5 mL of fresh medium was added to neutralize trypsin activity.

Cell counting was performed using a Bürker chamber: 50 µL of the cell suspension was mixed with 50 µL of Trypan Blue, and 50 µL of this mixture was loaded into the chamber. Representative cell counts were as follows:

Upper right chamber: 69 cells

Lower left chamber: 44 cells

$$\bar{x} = \frac{69 + 44}{2} = 56.5$$

To ensure accuracy, the procedure was repeated, yielding the following counts:

Upper right chamber: 67 cells

Lower left chamber: 44 cells

$$\bar{x} = \frac{67 + 44}{2} = 55.5$$

The arithmetic mean of all four measurements was calculated and used to determine the cell concentration according to the Bürker formula, resulting in **1.12×10^6 cells/mL**.
Based on this concentration, the volume of the mother suspension required to obtain **200,000 cells per well** was calculated.

Considering 13 wells, the total number of cells needed was **2.6×10^6 cells**.
Since each well required 2 mL of suspension, a total of 25 mL was necessary for seeding. Accordingly, **2.32 mL** of the original cell suspension was diluted to a final volume of 25 mL with fresh medium, and **12 wells** were seeded with 2 mL each.
The seeded plate was incubated at 37 °C for approximately 5 hours.

3.7.4 Loading of Compounds

After 5 hours of incubation, the wells were treated with the reference compounds.

- In the first two wells, **1 µL of sterile DMSO** was added to each as a control.
- The reference compounds **MG132** and **Pimozide** were diluted at a **1:10 ratio** in the vehicle (DMSO), and **1 µL** of each solution was added per well.
- The **test compounds**, according to the established protocol, were added to the wells at a **final concentration of 10 mM**. The corresponding dilution in DMSO was prepared using the following formula:

n mol: x mL = 0.01: 100 mL

3.7.5 Loading of Fluorescent Probes

After 16 hours of incubation, the fluorescent probes were loaded into the wells. In this experiment, 6 wells were assigned to the vinyl-sulfonic probe and 6 wells to the sulfonic probe. According to the protocol, both compounds were diluted 1:400 in the selected growth medium.

To calculate the total volume of medium required for the dilution: given the 1:400 dilution, 1 µL of probe is required per well. Therefore, 6 µL of the vinyl-sulfonic probe were dissolved in 2.4 mL of medium, and 6 µL of the sulfonic probe were dissolved in a separate 2.4 mL of medium.

Prior to adding the probes, the previous medium was removed, and the wells were washed with PBS. Subsequently, 400 µL of the diluted probe solution was added to each well. The plate was then incubated for 2 hours.

3.7.6 Sample Preparation for FACS Analysis

At the end of the incubation, samples were prepared for analysis using a flow cytometer. The culture medium was removed, and each well was rinsed with 0.5 mL of PBS. Subsequently, 0.5 mL of PBS was added, and the plate was incubated for 30 minutes. After incubation, the PBS was removed, and 3 drops of trypsin were added to each well, followed by a 5-minute incubation. Fresh growth medium was then added, and the cells were transferred to appropriate FACS tubes. Samples were centrifuged for 5 minutes at 1500 rpm. After centrifugation, the supernatant was discarded, and 150 µL of PBS was added to each sample.

3.7.7 Calculation of Activity Values

Each compound was tested in triplicate. The activity percentages were calculated as the arithmetic mean of the three values obtained for each experiment and each compound. The activity of the proteasome in the presence of DMSO was considered as 100%, and all other values were normalized relative to this reference.

Compounds	**Fluorescence values measured in the presence of the vinyl-sulfonic probe**			**Fluorescence values measured in the presence of the sulfonic probe.**		
	First experiment	*Second experiment*	*Third experiment*	*First experiment*	*Second experiment*	*Third experiment*
DMSO	179	196	65	74	76	35
MG132	126	139	46	83	78	34
Pimozide	314	306	88	103	59	30
5	193	190	65	77	66	26
6	206	199	74	80	79	34
8	96	188	107	54	62	57
9	135	151	140	47	56	52
11	147	161	148	67	70	65
12	132	137	110	53	49	56
13	140	140	175	68	77	97
14	144	142	136	77	74	64
16	179	188	69	74	75	31
17	183	195	73	77	80	35
18	130	160	130	42	65	43
19	170	139	152	84	47	60
21	173	151	110	94	62	58
22	142	179	138	67	94	50
23	146	165	156	80	74	64
24	140	150	120	64	87	46

Table 1. Fluorescence measurements obtained for the first class of compounds in all experimental runs.

COMPOUNDS	**Average proteasome activity percentages**
DMSO	100
MG132	66
Pimozide	187
5	114

6	106
8	97
9	103
11	91
12	98
13	79
14	80
16	118
17	94
18	107
19	106
21	98
22	97
23	83
24	85

Table 2. Mean values of % proteasome activity for the first class of compounds in all experimental runs.

Compounds	**Fluorescence values measured in the presence of the vinyl-sulfonic probe**			**Fluorescence values measured in the presence of the sulfonic probe.**		
	First experiment	*Second experiment*	*Third experiment*	*First experiment*	*Second experiment*	*Third experiment*
DMSO	179	196	65	74	76	35
MG132	126	139	46	83	78	34
Pimozide	314	306	88	103	59	30
26	193	190	65	77	66	26
27	206	199	74	80	79	34
29	96	188	107	54	62	57
30	135	151	140	47	56	52
32	147	161	148	67	70	65
33	132	137	110	53	49	56
34	140	140	175	68	77	97
35	144	142	136	77	74	64
37	179	188	69	74	75	31
38	183	195	73	77	80	35
39	130	160	130	42	65	43
40	170	139	152	84	47	60
23	146	165	156	80	74	64
24	140	150	120	64	87	46

Table 3. Fluorescence measurements obtained for the second class of compounds in all experimental runs.

COMPOUNDS	Average proteasome activity percentages
DMSO	100
MG132	81
Pimozide	187
26	71
27	77
29	62
30	70
32	83
33	87
34	79
35	82
37	72
38	72
39	78
40	81

Table 4. Mean values of % proteasome activity for the second class of compounds in all experimental runs.

4 PROJECT 2: BIOLOGICAL SCREENING OF INTERNAL LIBRARY OF COMPOUNDS

The field of developing new proteasome modulators remains highly dynamic, owing to the growing therapeutic interest in this target. On one hand, the search for improved proteasome inhibitors is still crucial, particularly in light of the limitations associated with currently available drugs.
On the other hand, the exploration of proteasome activators has become increasingly compelling. Indeed, the study of proteasome activation represents a potential paradigm shift in the treatment of neurodegenerative disorders, driving efforts to identify molecules capable of enhancing proteasome function.

To date, the principal approach for identifying small-molecule proteasome activators has relied on screening clinically relevant drug libraries.[123-126]
Hits emerging from these collections are typically subjected to medicinal chemistry optimization to eliminate activity at their original targets while retaining, or improving, efficacy toward the proteasome. [127]

A potentially more effective strategy would involve defining the true binding pockets of current 20S activators through proteomic or crystallographic techniques. Although seemingly straightforward in theory, this effort is complicated by the presence of multiple potential binding sites and numerous activation mechanisms within the large 2.5-MDa proteasome complex.

Lack of Standard Assays for Efficacy Studies [128]

Canonical proteasome activity assays employ peptide substrates specific for each of the proteasome's catalytic sites (CT-L: Suc-LLVY-AMC; Tryp-L: Boc-LRR-AMC; Casp-L: Z-LLE-AMC), each carrying a C-terminal fluorophore that becomes fluorescent upon proteasomal cleavage. [129]
Although widely used, these assays present intrinsic limitations. On the one hand, the small size of these peptides allows them to pass through the narrow gate of the latent 20S proteasome, leading to elevated and variable baseline activity, which can compromise assay reliability. On the other hand, these primary screens rely on purified 20S proteasome and fluorogenic peptides that are specific to individual catalytic sites, thereby neglecting the allosteric interaction between the three catalytic sites that collectively orchestrates protein degradation. [130] Consequently, compounds that selectively stimulate the other catalytic sites or act upstream of the proteasome are likely to be missed in these assays.

The search for proteasome agonists has driven the development of innovative assays designed to overcome existing limitations and validate the therapeutic potential of targeting proteotoxic disorders. These include IDP-based biochemical assays employing physiologically relevant substrates, mass spectrometry-based assays that eliminate non-bona fide activators, peptide-FRET reporters to minimize background activity, and proteasome activity-based probes for high-throughput cellular screening. [131, 123, 125, 126]

4.1 AIM OF THE PROJECT

As previously discussed, the pursuit of novel proteasome activators by direct targeting of the site responsible for their modulation remains challenging, as the precise binding sites of these small molecules within the proteasome have yet to be identified.

In line with the approaches commonly adopted in this field, an in vitro biological assay was developed to facilitate the screening of an internal compound library.

The choice of the assay was a critical step, as the overarching goal was to efficiently identify a subset of compounds capable of modulating proteasome activity. Importantly, the selected assay allowed for the *simultaneous assessment of both positive and negative modulatory effects*, thereby providing a comprehensive evaluation of compound activity.

Another essential requirement was the ability to evaluate proteasome activity within *a cellular context*, thereby allowing detection of all potential modes of compound-mediated modulation. Indeed, reliance on purified proteasome complexes would have precluded the identification of compounds capable of exerting allosteric effects or modulating the transcriptional regulation of proteasome-encoding genes.

To meet these criteria and building upon the work of Leestemaker et al.[126], an in vitro fluorogenic assay was developed and fully standardized, employing two fluorogenic probes. The emitted fluorescence was measured to enable precise quantification of proteasome activity in the presence of the tested compounds.

The activity of the probes is described in *Paragraph 3.4* and their synthesis is detailed in *Paragraph 3.3*.

A preliminary screening was performed using the **HeLa** cell line (*human cervical carcinoma*), starting from an internal library of 200 compounds. This library included synthetic intermediates,

derivatives originally designed for other pharmacological targets—some of which were inactive—as well as peptides primarily acting on GPCR receptors, such as NOP.

The choice of this cell line for the initial screening was driven both by practical considerations, given the exploratory nature of the assay, and by the need to employ a well-established model system for investigating fundamental aspects of cellular physiology. [132-134]

Each compound was tested in triplicate, and the biological effect was expressed as the percentage of proteasome activity relative to three reference treatments: **DMSO**, which does not affect proteasomal function and therefore represents basal activity; **MG132**, a well-established proteasome inhibitor; and **pimozide**, a known proteasome activator.

Graph 3 illustrates the molecules that exhibited a measurable modulatory effect on proteasome activity:

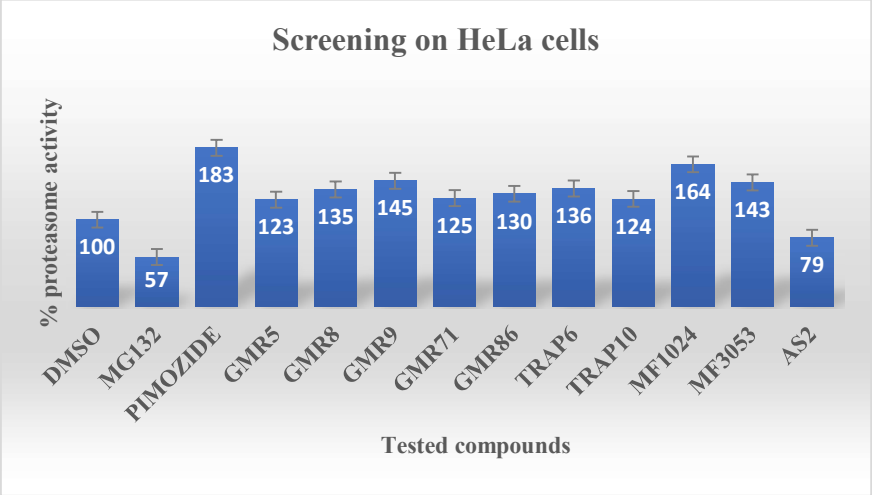

Graph 3. Effects of compounds exhibiting modulatory activity on the proteasome in the preliminary screening conducted on HeLa cells.

The preliminary screening enabled the identification of ten compounds that exerted modulatory effects on the proteasome. Of these, nine emerged as positive modulators, exhibiting an average activity above 120%, while a single compound, **AS2**, showed modest inhibitory properties. The general chemical scaffolds of the active compounds are summarized in *Figure 22*, providing a visual overview of the structural diversity associated with proteasome modulation.

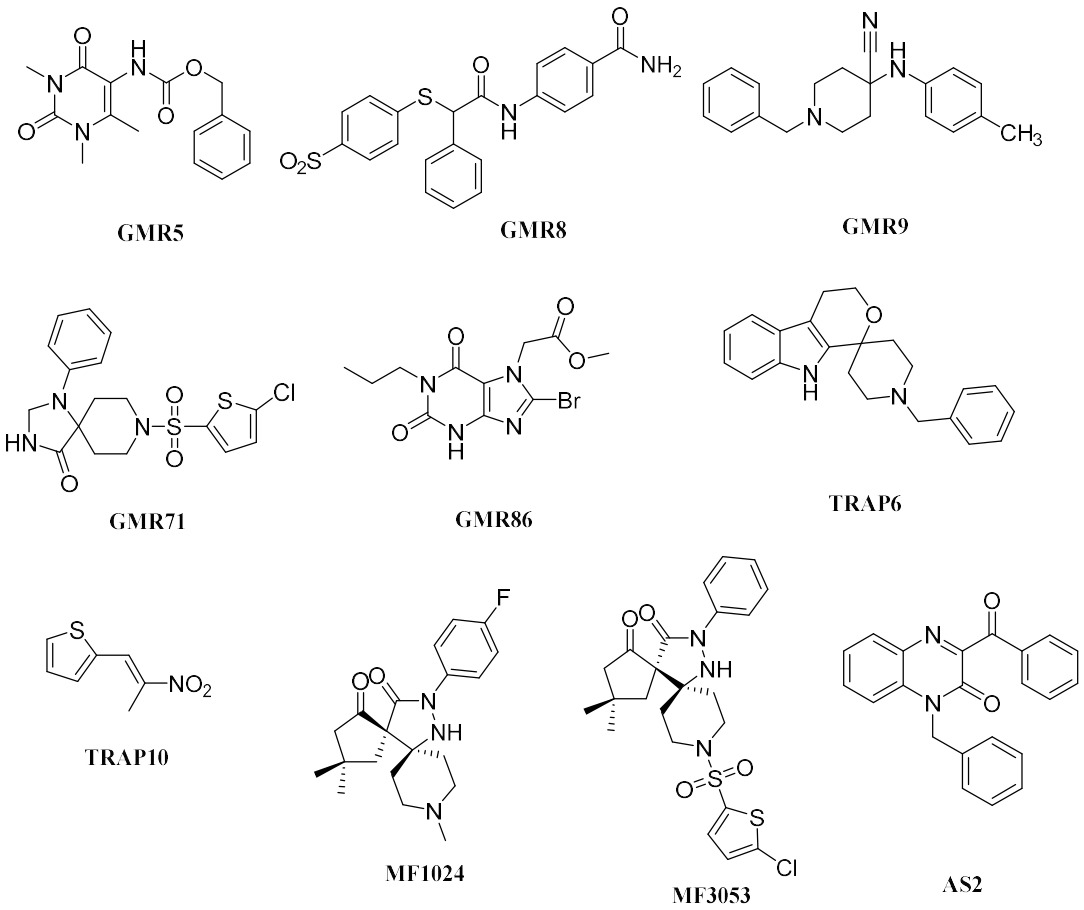

Figure 22. General chemical structures of the ten compounds exhibiting notable modulatory activity in HeLa cells.

Among the nine compounds that demonstrated positive modulation of the proteasome, a diverse array of central scaffolds was observed, including pyrimidinedione (**GMR5**), triazaspiro (**GMR71**, **MF1024**, and **MF3053**), dihydropurine (**GMR86**), spiroindole (**TRAP6**), and thiophene-based cores (**TRAP10**), reflecting notable structural diversity among the active modulators.

By contrast, the single compound exhibiting mild inhibitory activity against the proteasome is characterized by a quinoxalinone core (**AS2**), highlighting a distinct chemical framework associated with proteasome inhibition.

The compounds previously identified as exhibiting biological activity on the proteasome were subjected to a subsequent screening step across three additional cell lines: **MDA-MB-231** (*human breast adenocarcinoma*), **HCT116** (*human colorectal carcinoma*), and **HaCat** (*immortalized human keratinocytes*).

The decision to extend the screening to four cell lines was motivated by the need to determine whether compound activity is consistent across distinct cellular contexts, taking into account both differences in cellular origin and variability in the protein composition of the ubiquitin–proteasome system.

The corresponding biological results are presented and discussed separately in the sections “Project 2a” and “Project 2b.”

5 PROJECT 2a: SYNTHESIS AND BIOLOGICAL EVALUATION OF PROTEASOME INHIBITORS WITH QUINOXALIN-2-ONE STRUCTURE

The aformentioned screening campaign on HeLa cells has led to the identification of a compound, designated **AS2**, depicted in *Figure 23*, that exhibits a marked capacity to modulate proteasome activity. Notably, this molecule has demonstrated promising inhibitory effects on the proteasome.

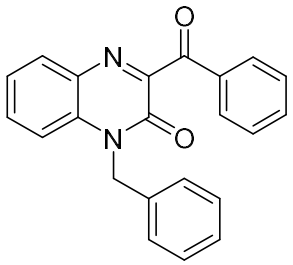

Figure 23. Structure of compound AS2.

AS2 is characterized by a quinoxalin-2-one scaffold, bearing a benzyl substituent at the N_1 position and an anilide moiety at position 3. As evident from its structure, the molecule lacks any reactive functional group capable of interacting with the well-characterized catalytic site of the proteasome. This observation suggests the possibility of an alternative mechanism underlying its inhibitory activity.

Indeed, several noncanonical pathways of proteasome downregulation have been reported in the literature, although none have yet yielded therapeutically approved agents.

Among the mechanisms recurrently highlighted in the literature, the most prominent non-canonical pathways implicated in the attenuation of proteasomal activity are outlined below.

a) Modulation of E3 ubiquitin ligases

E3 ubiquitin ligases constitute a pivotal class of enzymes responsible for conferring substrate specificity during protein ubiquitination, thereby directing selected proteins toward degradation.[135]

Targeted protein degradation through small molecules has emerged as a powerful therapeutic approach, as evidenced by the clinical success of thalidomide analogues in treating hematologic malignancies. Compounds such as lenalidomide and pomalidomide function by modulating the activity of the *$CRL4^{CRBN}$ E3 ubiquitin ligase* complex (comprising CUL4, RBX1, DDB1, and CRBN), thereby promoting recruitment and ubiquitination of neo-substrates such as IKZF1, IKZF3, and CK1α. This process ultimately results in their proteasomal degradation.[136]

Furthermore, quantitative proteomics revealed that lenalidomide selectively induces ubiquitination and subsequent degradation of two lymphoid transcription factors, IKZF1 and IKZF3, through the CRBN–CRL4 E3 ubiquitin ligase complex. These transcription factors are essential regulators in multiple myeloma. A single amino acid substitution in IKZF3 was found to confer resistance to lenalidomide-induced degradation, thereby preventing the associated inhibition of cell proliferation. Moreover, the lenalidomide-induced interleukin-2 (IL-2) production in T cells was attributed to IKZF1 and IKZF3 depletion. Collectively, these findings highlight a novel mechanism of action in which modulation of E3 ubiquitin ligase activity results in selective degradation of disease-relevant proteins (*Figure 24)*.[137]

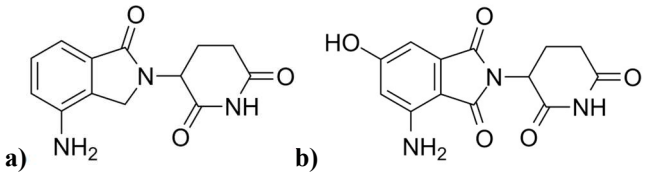

Figure 24. Structure of Lenalidomide (a) and Pomalidomide (b).

b) Mutations on catalytic site of enzyme E2 CDC34

Despite the extensive focus on ubiquitin ligases (E3s) and deubiquitinating enzymes (DUBs), largely due to their substrate specificity, the roles of most ubiquitin-conjugating enzymes (E2s) remain comparatively underexplored. While it is established that E2 enzymes transport activated ubiquitin and form complexes with E3 ligases, their broader functional contributions are not fully elucidated. For instance, the E2 enzyme CDC34 is known to promote degradation of downstream targets via the ubiquitin–proteasome system (UPS), yet its non-catalytic roles remain largely elusive. [138]

Indeed, although ubiquitination specificity has traditionally been ascribed predominantly to E3 ligases, growing evidence indicates that E2 enzymes also exert pivotal influence over substrate selection and determine the architecture of ubiquitin chains during this process.[139]

Silencing **CDC34** has been demonstrated to decrease the degradation of **$p27^{Kip1}$** and to impede cell proliferation, an effect most likely attributable to compromised ubiquitination and the ensuing stabilization of the target protein.[140]

Elevated CDC34 expression levels have been reported in various tumors, including T-cell acute lymphoblastic leukemia[141], multiple myeloma[142], and hepatocellular carcinoma cell lines[143], suggesting that CDC34 may represent a promising therapeutic target in cancer treatment.

A small molecule, termed CC0651, shown in *Figure 24*, has been identified as a selective inhibitor of human CDC34 (hCDC34). Structural studies revealed that CC0651 binds to a cryptic allosteric pocket on hCDC34, distal to the catalytic site, inducing subtle yet widespread conformational changes in secondary structural elements of the E2 enzyme.

Analogues of CC0651 have been shown to inhibit the proliferation of human cancer cell lines and promote the accumulation of $p27^{Kip1}$, a known substrate of the SCF^{Skp2} ubiquitin ligase complex.[144]

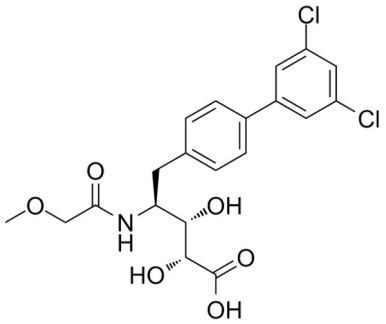

Figure 25. Chemical structure of CC0651.

c) Noncompetitive modulators

Another mechanism of target modulation that has gained attention is referred to as ***noncompetitive modulation***. Noncompetitive modulators bind to sites distinct from the catalytic core, altering enzyme behavior without directly competing with substrates. [145]

Owing to its complex composition of multiple subunits, diverse enzymatic activities, and associated regulatory proteins, the proteasome represents an ideal target for allosteric modulation.[146]

First, proper proteasome function requires tightly coordinated action among all catalytic subunits, achieved either through direct molecular interactions or through auxiliary regulatory interfaces—to ensure the full execution of proteolytic activity. Moreover, in the quiescent core particle, the sophisticated gating structure constituted by the α-rings effectively occludes the entrance to the central channel and the catalytic chamber. Increasing evidence suggests that allosteric signaling is a major mechanism by which this gate can be transitioned from a closed to an open conformation.[147] Therefore, it is conceivable that compounds regulating the proteasome activity in an allosteric manner may offer an alternative type of discriminating capabilities between healthy and mutated cells.[148]

It is acknowledged that the 19S CAP and PA28 activator allosterically regulate gate dynamics, independently of their ability to physically clear the substrate entry path. [149] Conversely, genetic

deletion of gate elements induces permanent opening and results in severe physiological consequences. [150]

Several examples of nonpeptidic noncovalent proteasome modulators have been reported, including phakellins[151], oxadiazoles,[152] hydroxyureas,[153] imidazolines[154,155] sulfone or piperazine agents,[156] and tamoxifen derivatives.[157]

Furthermore, substituted quinolines and a novel series of **naphthoquinone** derivatives, identified and optimized by Lawrence and colleagues, represent promising classes of non-peptidic, non-covalent inhibitors of the proteasome. [158]

Notably, the quinoxalinone core has also emerged as a promising non-competitive inhibitor of the proteasome: 5-amino-8-hydroxyquinoline (5-AHQ, *Figure 25*) has been reported as a non-competitive inhibitor of the human proteasome.[159]

Furthermore, 5-AHQ demonstrated efficacy against bortezomib-resistant cell lines, highlighting a key advantage of employing mechanistically distinct classes of proteasome inhibitors. [160]

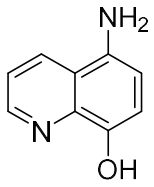

5-amino-8-hydroxyquinoline

Figure 26. Structure of 5-AHQ.

Quinoxalines display a wide array of pharmaceutical activities such as anticancer [161], antimicrobial [162], and anti-inflammatory properties[163,164], and were identified as non-covalent proteasome inhibitors by Tepe et al.[165]

Beyond its potential to overcome acquired resistance to active-site inhibitors, noncompetitive modulation of enzyme activity may also offer the advantage of reduced off-target interactions - and associated toxicities- and improved tolerability. Nevertheless, small-molecule noncompetitive inhibitors of the proteasome remain limited, and those identified to date generally exhibit activity only at high or non-physiological concentrations.

5.1 AIM OF THE STUDY

In recent years, quinoxaline derivatives have received considerable attention owing to their diverse biological properties and broad pharmaceutical potential.[166]

In particular, over the past two decades, numerous 2-oxo and 2,3-dioxo quinoxaline derivatives have been reported, along with studies detailing their biological activities.[167]

Carta and colleagues escribed the synthesis and biological evaluation of more than 150 quinolin-2-one derivatives, many of which exhibited noteworthy antimicrobial activity. [168-172]

Across several studies, variations at positions 1 and 3 of the quinolin-2-one scaffold—particularly the introduction of CF_3, Cl, and CH_2Br substituents—were shown to produce differential biological effects against various bacterial strains.

Moreover, several quinoxalinone derivatives with promising antiviral profiles have been designed by exploiting structural features of of Efavirenz[173-176] and GW-420867X[177,178], two well-known non-nucleoside HIV-1 reverse transcriptase inhibitors (NNRTIs).

Another promising area of application for this scaffold lies in the development of dipeptidyl peptidase-IV (DPP-IV) inhibitors, a validated therapeutic approach for the treatment of type 2 diabetes.[179] Hwang et al. conducted preliminary structure–activity relationship (SAR) study on a series of N-ureido and N-thioureido quinoxalinediones, identified through high-throughput screening.[180]

Besides, a series of quinoxalinone derivatives, variously substituted on the benzene ring and bearing different aminoalkyl chains at position 1, were synthesized by Sparatore and colleagues and evaluated for their deconditioning, analgesic, and antispastic activities.[181-184] The authors also investigated the interaction with D_1 and D_2 receptors, concluding that the observed biological activity was not mediated by dopaminergic pathways, thereby hypothesizing involvement of alternative receptor systems.[184]

Additional medicinal applications include the development of antithrombotic agents, in which Ries et al.[185] and Edmunds et al.[186] demonstrated that introduction of an ethylbenzimidamide moiety at position 3 enhanced pharmacological potency.

Finally, from the 1980s to recent years, several quinoxalinone derivatives have been identified with anticancer properties, demonstrating notable antiproliferative activity[171]. In 2021, Eissa et al.

synthesized and reported a new class of quinoxaline-2(1H)-one-based inhibitors targeting VEGFR-2, further underscoring the therapeutic versatility of this chemotype.[187]

Despite the extensive body of literature describing the diverse therapeutic activities associated with the quinoxaline scaffold, its potential application as a proteasome inhibitor has not previously been explored.

In light of recent biological screening results identifying compound A2 as a promising proteasome inhibitor, further investigation was undertaken to assess the feasibility of extending the therapeutic scope of core structure. This objective aligns with the broader aim of establishing an alternative strategy for proteasome inhibition using a novel chemotype.

Given the therapeutic potential associated with the well-established applicability of the quinoxaline core, a series of seven final compounds was synthesized through systematic modifications of the central scaffold, with particular focus on structural variations at positions 1 and 3.

Specifically, efforts were directed toward the introduction of substituents with varying electronic and steric properties—such as halogens and methoxy groups—at the para position of the benzyl moiety at position 1. At position 3, various para-substituted anilines and a benzylamine group were introduced to further expand the molecular framework (*Figure 27*).

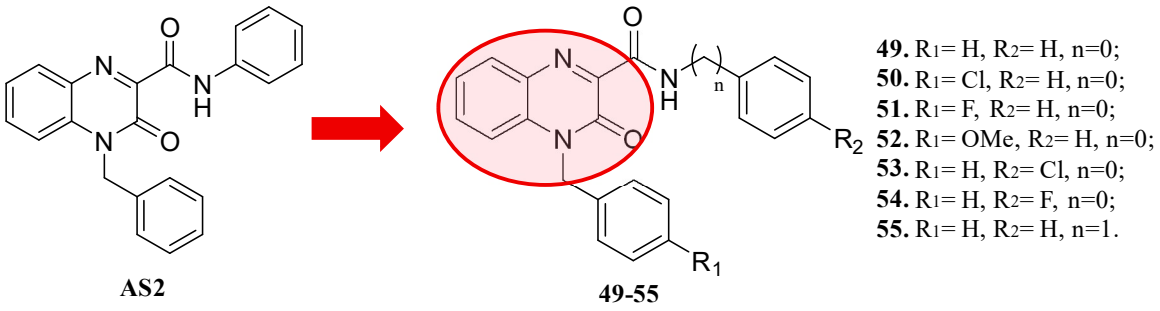

Figure 27. General modifications introduced on the quinoxalin-2-one scaffold to investigate their impact on proteasome activity.

5.2 SYNTHESIS

The series of compounds **48-54** were synthesized using a four-step synthetic procedure, described in *Scheme 27*.

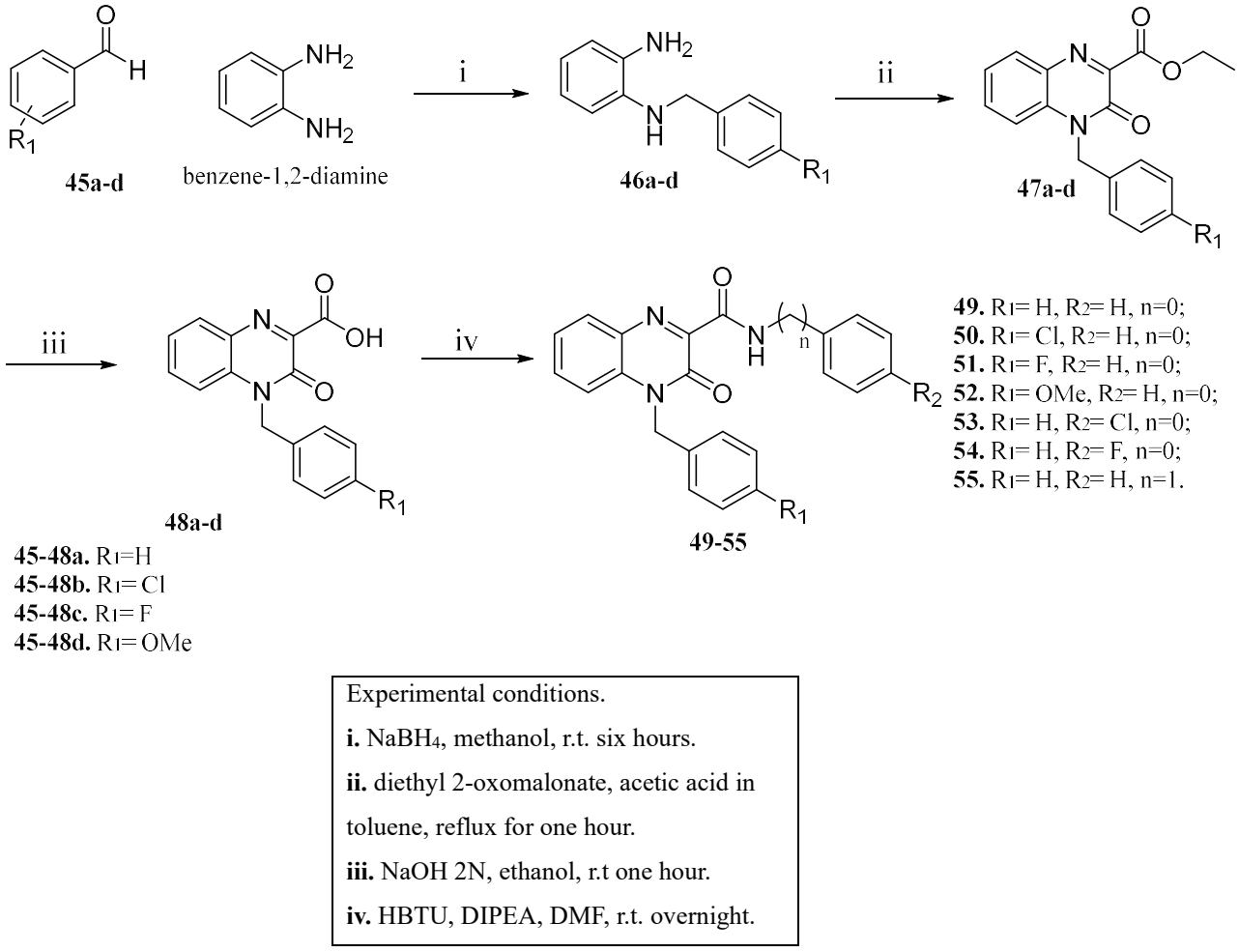

Scheme 27. General synthetic strategy for the preparation of compounds 49-55.

The synthesis begins with a *reductive amination* between 1,2-phenylenediamine and the appropriate para-substituted benzaldehydes (R_1), affording intermediates **46a–d**, using sodium boro hydride as reductive agent in methanol. Subsequent cyclization in refluxing toluene in the presence of glacial acetic acid furnishes the 2-oxoquinoxaline core, yielding intermediates **47a–d** (*Scheme 28*).

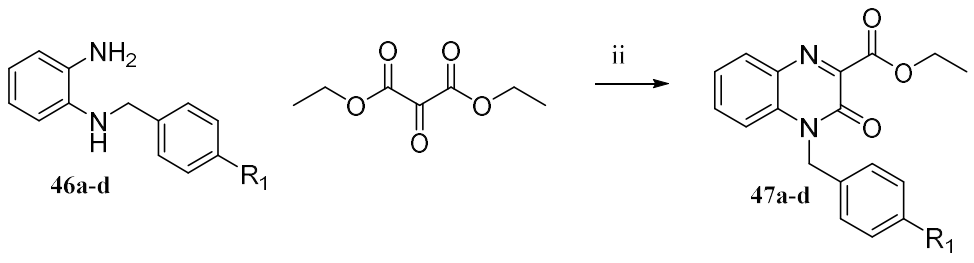

Scheme 28. Representation of the second reaction step.

The presence of acetic acid promotes the protonation of the ketonic carbonyl oxygen, thereby facilitating the nucleophilic attack by the primary amine. Upon heating, a molecule of water is eliminated, and the other amino group attacks the ester carbon, enabling ring formation and extension of conjugation. The mechanism is depicted in *Scheme 29*.

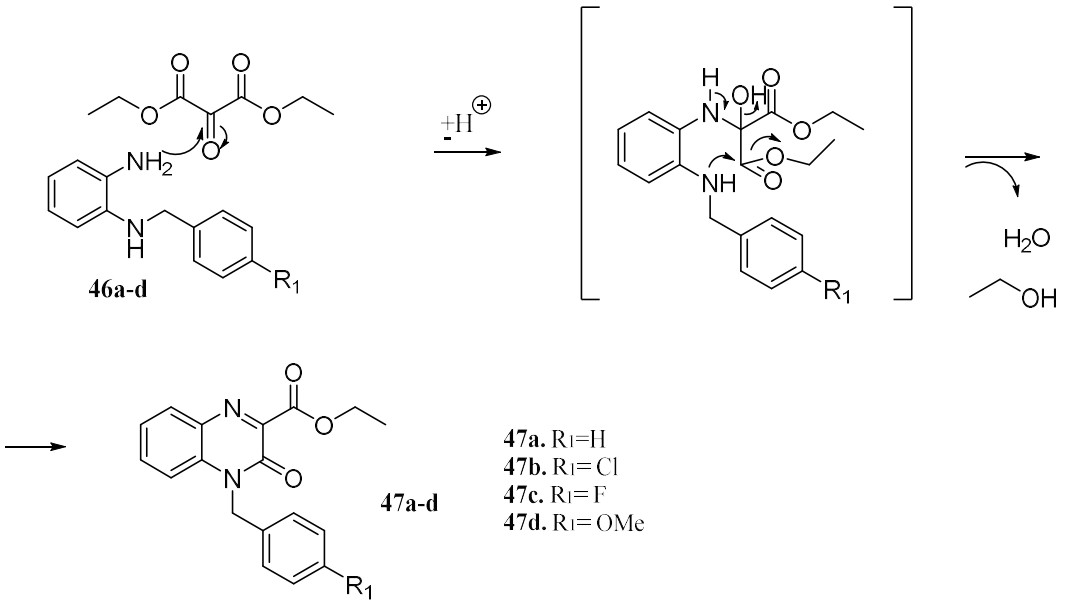

Scheme 29. Mechanistic pathway of the reaction's second step.

The synthesis then proceeds with hydrolysis of the ester functionality in the presence of sodium hydroxide in ethanol, affording the corresponding carboxylic acid derivatives **48a–d**. The final transformation entails amide-bond formation between compounds 48a-d and the appropriately substituted anilines or benzylamine. This coupling, carried out in DMF using HBTU and DIPEA, ultimately furnishes the final compounds **49–55**.

Finally, an additional compound was synthesized based on the modification of intermediate **47c**. In this case, an analogue was prepared in which the 4-fluorobenzene moiety was distanced from the central quinoxalin-2-one core through a propylene linker, as depicted in *Scheme 30*. This structural alteration was designed to investigate potential changes in biological activity by increasing the separation of the aromatic ring at position 1, ultimately leading to the synthesis of compound **57**.

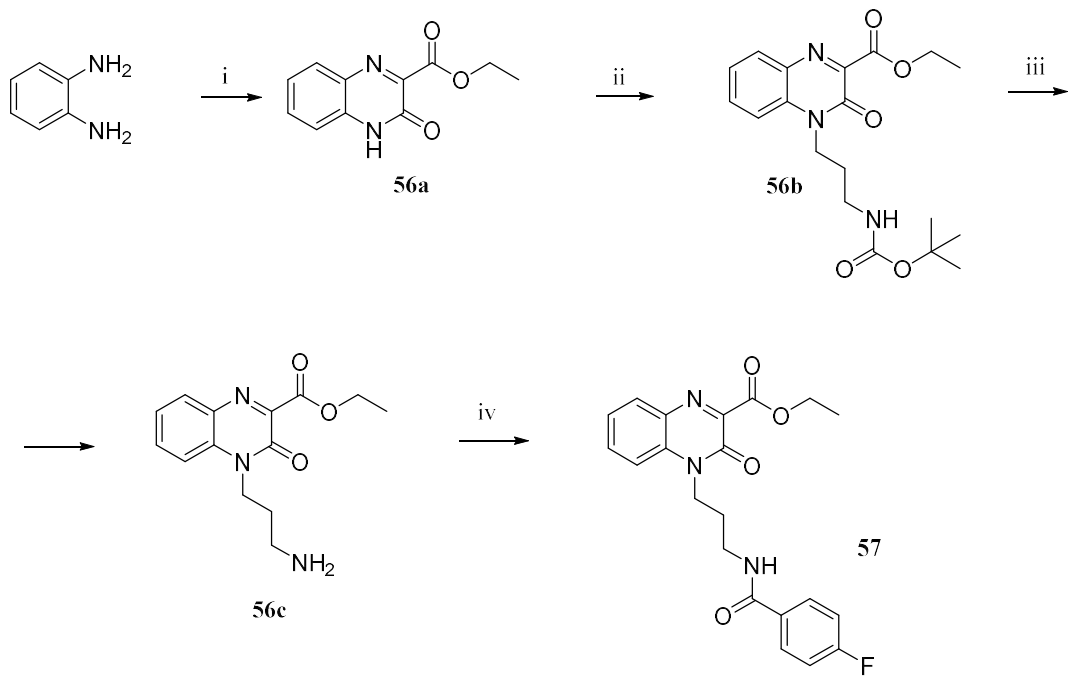

Experimental conditions.
i. diethyl 2-oxomalonate, acetic acid, toluene, 130°C, one hour.
ii. tert-butyl (3-bromopropyl)carbamate, K_2CO_3, DMF, rt, 16 hours.
iii. TFA, DCM, rt, one hour.
iv. HBTU, DIPEA, DMF, r.t. overnight.

Scheme 30. General synthetic strategy for the preparation of compound **57**.

The synthetic sequence begins with the cyclization of ortho-aminoaniline to generate the 2-oxoquinoxaline core, leading to derivative **56a**. This transformation is carried out in toluene under reflux in the presence of glacial acetic acid, following the same protocol employed for the preparation of compounds **47a-d**. Under these conditions, the diamine undergoes intramolecular condensation to afford the heterocyclic scaffold in high efficiency, thereby establishing the structural framework required for subsequent derivatization.

The following step involves a nucleophilic substitution at the N1 position using tert-butyl (3-bromopropyl)carbamate as the electrophilic partner to obtain the intermediate **56b**. This reaction is carried out under basic conditions with potassium carbonate, which serves to deprotonate the N1 nitrogen, thereby enabling its nucleophilic attack on the alkylating agent (*Scheme 31*).

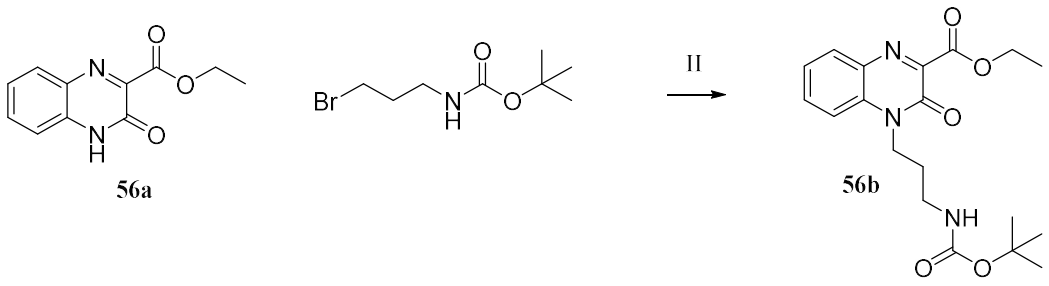

Scheme 31. Representation of the second reaction step.

The *third step* requires the removal of the Boc protecting group under acidic conditions using trifluoroacetic acid, to afford the intermediate **56c**.

Finally, compound **56c** was reacted with 4-fluorobenzoic acid to afford the final compound **57** through an amide coupling reaction. The reaction was carried out using HBTU and DIPEA as coupling agents.

5.3 BIOLOGICAL TESTS AND RESULTS

The final compounds, together with the corresponding intermediates, were evaluated using the previously described fluorescent biological assay. The initial screening was carried out in *HeLa cells* employing the same fluorescent probes in order to assess potential modulatory effects on proteasome function.

Graph 3 summarizes the outcomes of these experiments, expressed as the percentage of residual proteasome activity following treatment with each compound; the reported values correspond to the mean percentage obtained from three independent assays. The compounds were analyzed alongside established reference controls: **DMSO**, which does not affect proteasomal function and therefore reflects basal activity; **MG132**, a well-characterized proteasome inhibitor; and **Pimozide**, a known proteasome activator. As illustrated in *Graph 4*, the values associated with each compound represent the averaged results from all experimental replicates.

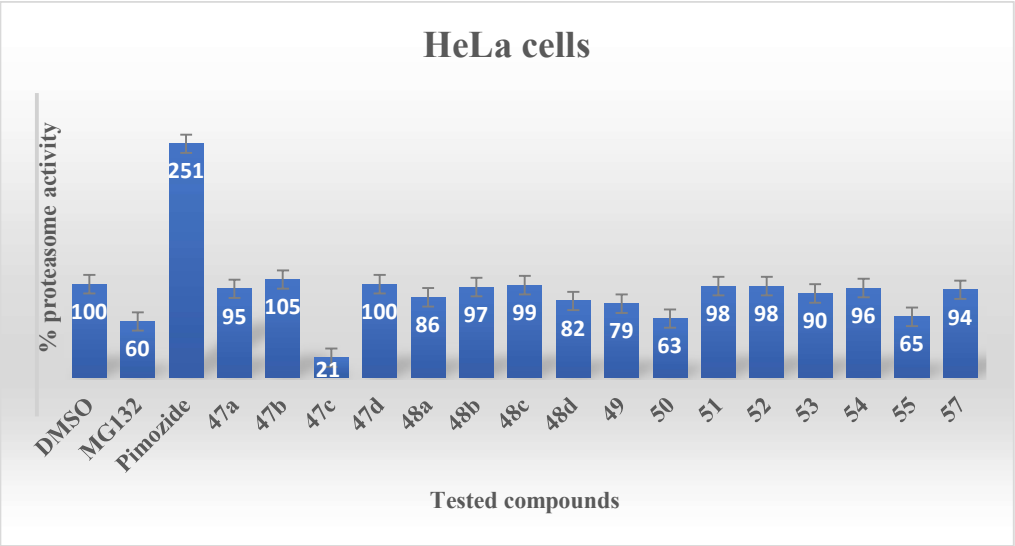

Graph 4. Biological activity of the compounds evaluated in HeLa cells.

Among the tested molecules, only three displayed measurable inhibitory activity. In particular, compounds **50** and **55** showed comparable average residual activities—63% and 65%, respectively—calculated from three independent experiments. Although similar in their overall biological profiles, these two derivatives differ structurally in notable ways. At position 1, compound 50 carries a para-chloro substituent on the benzene ring, whereas compound 55 lacks substitution at this position. At position 3, compound 50 features an aniline-derived amide, while compound 55 bears an amide originating from benzylamine.

In contrast, intermediate **47c** exhibited a remarkably strong inhibitory effect, with only 21% residual proteasome activity. This compound also displayed an intriguing peculiarity: during the biological

assays, both fluorescent probes produced unusually high signal intensities. This observation suggests the need for further investigation to determine whether the enhanced fluorescence originates from intrinsic photophysical properties of the compound or is instead the result of a specific cellular response triggered upon treatment.

The compounds exhibiting significant activity were subsequently evaluated in additional cell lines—including two cancer models (*MDA-MB-231* and *HCT116*) and a non-tumorigenic line (*HaCat*)—to explore possible variations in their biological effects across different cellular contexts.

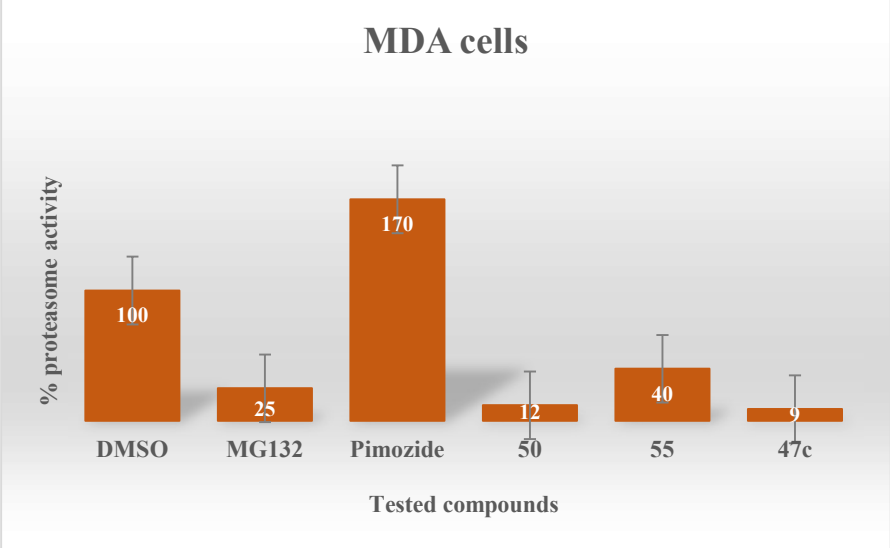

Graph 5. Results of tests on MDA cells.

As illustrated in *Graph 5*, compounds **50** and **55** displayed notable proteasome inhibitory activity in HeLa cells. Compound **50**, in particular, produced a markedly stronger inhibition than the reference inhibitor MG132, reducing proteasome activity to 12% residual activity. Compound **55** exhibited a milder effect, reaching approximately 40% residual activity, slightly below the inhibition achieved with MG132. Intermediate **47c** maintained an exceptionally strong inhibitory profile, with an average residual activity of 9%.

In contrast, when tested on HCT116 and HaCat cells, compounds **50** and **55** did not display inhibitory activity, yielding proteasome activity levels comparable to the basal condition. Conversely, intermediate **47c** continued to exert a noteworthy inhibitory effect in these cell lines, although its potency was markedly reduced compared to that observed in HeLa cells. The last results are shown in *Graph 6* and *7*.

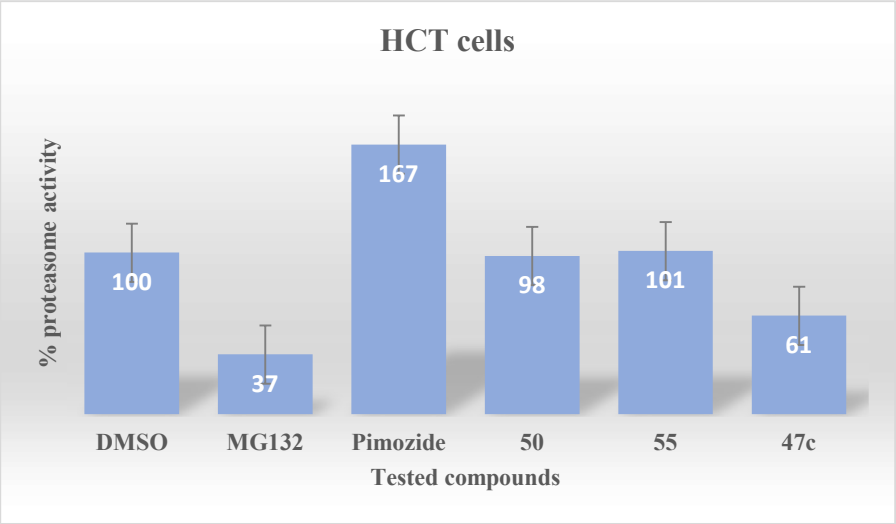

Graph 6. Results on HCT-116 cells.

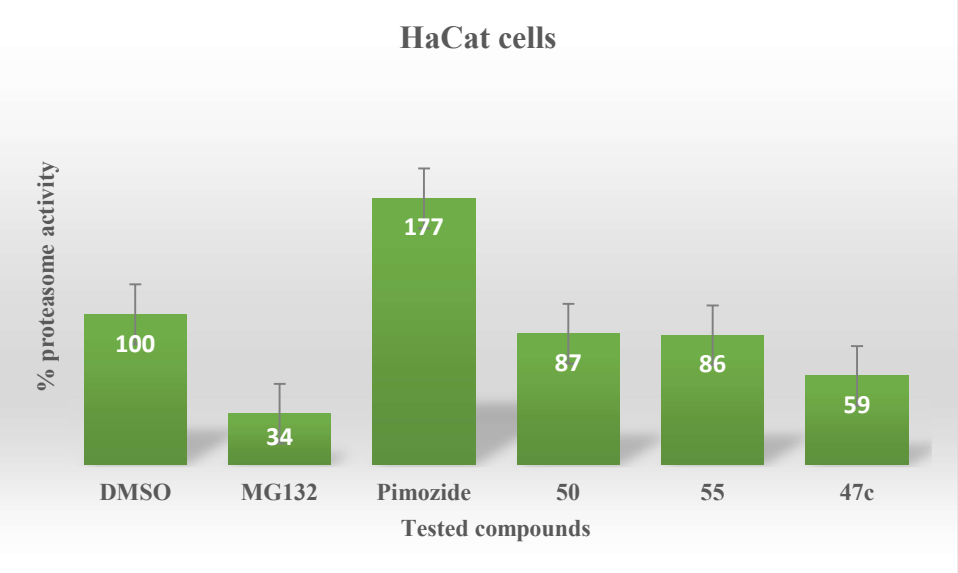

Graph 7. Results on HaCat cells.

The observed reduction in activity is likely attributable to structural and morphological differences among the cell lines, as revealed by experimental analyses. The data indicate that the compounds may selectively target a proteasome subtype that is more abundant, accessible, or sensitive in HeLa cells compared to HCT cells.

HeLa cells were found to express a distinct combination of proteasomal subunits—such as intermediate or asymmetric proteasomes—potentially underlying their heightened susceptibility to inhibition.

In contrast, HCT cells exhibited a different subunit composition, corresponding to a lower sensitivity to proteasome inhibition. Conversely, HCT cells demonstrated a more rapid compensatory response in proteasome recovery relative to MDA cells, as indicated by the experimental findings.[188,189]

Finally, HeLa cells have been reported to undergo apoptosis upon treatment with proteasome inhibitors. The observed differences in sensitivity between HeLa and HCT cells may reflect their differential tolerance to proteotoxic stress.[190]

In contrast, HaCat cells, as the only keratinocyte-derived line in the study, exhibited features consistent with their unique cellular identity. [191]

This observation may suggest a degree of selectivity of the compounds toward specific cell types.

5.4 CONCLUSIONS

In this second project, an alternative mode of proteasome inhibition was investigated, focusing on mechanisms that do not involve direct targeting of the catalytic active site. This approach was prompted by the observation of compound AS2 from our internal library, which demonstrated notable proteasome inhibition despite lacking any functional group conventionally capable of interacting with the catalytic site. While classical inhibition mechanisms are well characterized in the literature, non-competitive pathways have also been reported. Notably, quinoxaline cores have shown considerable activity as non-competitive proteasome modulators, interacting with currently unidentified binding sites to induce inhibition. [165]

The quinoxalin-2-one core at the center of compound AS2 has not previously been described as a proteasome inhibitor. However, its other pharmacological properties—including antimicrobial [168-172], DPP(IV) inhibitory [179], analgesic, and antispasmodic activities [181-184]—have been extensively documented. These findings suggest that this scaffold, appropriately substituted, could serve as a versatile platform for the development of novel small molecules capable of inducing proteasome inhibition through alternative mechanisms, potentially avoiding the adverse effects commonly associated with classical inhibitors.

To explore this potential, a series of seven derivatives was synthesized, introducing systematic variations via substituents with differing electronic and steric properties, such as halogens and methoxy groups at the para position of the benzyl moiety in position 1. Additionally, various para-substituted anilines and a benzylamine group were incorporated at position 3 to further diversify the molecular framework. Subsequently, a further derivative was synthesized from compound 3l, introducing a propylenic spacer to increase the distance between the quinoxalin-2-one core and the aromatic ring in position 1, based on preliminary promising activity.

All synthesized compounds were evaluated using a fluorogenic assay employing two fluorescent probes, allowing quantitative assessment of proteasome activity as a percentage. This approach enabled the detection of proteasome modulation via any potential mechanism affecting activity.
Initial screening was performed in HeLa cells, a well-established tumor cell model, which allowed the selection of three compounds exhibiting significant inhibitory activity. Compounds **50** and **55**, differing minimally in structure, displayed approximately 65% inhibition (63% and 65%, respectively). Remarkably, intermediate **47c**, containing a para-fluoro benzyl group at position 1 and an ethyl ester at position 3, exhibited potent inhibition with only 21% residual proteasome activity,

highlighting its potential as a strong proteasome inhibitor. In contrast, compound **57**, designed with a propylenic spacer to further separate the aromatic group from the quinoxalin-2-one core, showed markedly reduced activity (93% residual activity), indicating a loss of inhibitory potential.

The most active compounds were subsequently tested in three additional cell lines to assess potential selectivity: *MDA-MB-231* (human breast adenocarcinoma), *HCT-116* (human colorectal carcinoma), and *HaCat* (immortalized human keratinocytes). Compounds **50** and **55** showed a better inhibitory activity in MDA-MB-231 cells as observed in HeLa cells, with compound 50 exhibiting even stronger inhibition than the reference compound MG132 (residual activity 12%). To the other side, the intermediate **47c** showed an incredible inhibitory potential, with a mean percentage of 9%.
In contrast, all compounds exhibited markedly reduced activity in HCT116 and HaCaT cells. Compounds **50** and **55** showed a complete loss of inhibitory effect, with values comparable to those of the DMSO control, indicating basal proteasome activity. Even compound **47c**, while still active, displayed a substantial decrease in potency, yielding residual activity levels of approximately 60%.
This differential response may be attributed to variations in proteasomal subunit composition, such as the presence of intermediate or asymmetric proteasomes in HeLa cells, which likely confer heightened susceptibility to inhibition.[171-172]
The distinction between HaCat cells and the tumor-derived HeLa, MDA-MB-231, and HCT-116 lines lies primarily in cellular origin. HaCat cells are non-tumorigenic keratinocytes derived from normal epithelial tissue, whereas the other lines originate from malignant epithelial tumors. This fundamental difference between non-tumoral and tumoral cells likely contributes to the observed variations in response.[191]

Overall, the screening highlights the quinoxalin-2-one core as a promising scaffold for proteasome modulation. Among the synthesized derivatives, three compounds demonstrated potent inhibitory activity with variable selectivity across cell lines, suggesting potential for targeted modulation.

As the precise mechanism of action of these compounds has not yet been fully elucidated, they will be subjected to a series of complementary assays aimed at determining the specific stage of the proteasomal pathway at which they exert their effects. At present, the compounds are being evaluated using the purified 20S proteasome to assess whether they interact directly with the target and to investigate potential selectivity toward the different catalytic subunits. Subsequently, they will undergo Western blot analysis to determine whether their activity also influences the transcriptional regulation of the genes encoding the proteasome subunits.

5.5 EXPERIMENTAL PROCEDURES

For Material and Methods: *Paragraph 3.6.1.*

General procedures for synthesis of 46a-d

Under an argon atmosphere, a solution of 1,2-phenylenediamine (4 equiv.) and the appropriate benzaldehyde (1 equiv.) in methanol was cooled to 0 °C and stirred for 2 hours. Sodium borohydride (1.4 equiv.) was then added portionwise. The reaction mixture was stirred at room temperature for 6 hours. Subsequently, the suspension was concentrated under reduced pressure, and the resulting residue was diluted with dichloromethane, inducing precipitation. The suspension was filtered under vacuum, and the filtrate was concentrated to afford a crude oil. The oily residue was purified by column chromatography using an appropriate mixture of ethyl acetate and petroleum ether as eluent.

N^1-benzylbenzene-1,2-diamine (46a)

Purified by column chromatography using ethyl acetate/ petroleum ether 1:9, affording the compound as a white solid.

^{1}H NMR (400 MHz, DMSO) δ 7.42 – 7.35 (d, 2H), 7.34-7.30 (t, 2H), 7.27 – 7.21 (t, 1H), 7.01 (d, *J* = 7.7, 1H), 6.94 (t, 1H), 6.60 (t, *J* = 7.2 Hz, 2H), 4.33 (s, 2H).

Yield: 78%. MS-ESI: 198.27. HPLC t_R: 13.46.

N^1-(4-chlorobenzyl)benzene-1,2-diamine (46b)

Purified by column chromatography using ethyl acetate/ petroleum ether 1.5:8.5, affording the compound as an orange oil.

^{1}H NMR (400 MHz, DMSO) δ 7.45-7.39 (m, J= 5.2 Hz, 2.8 Hz, 2H), 7.20-7.14 (m, J=8.4 Hz, 1H), 7.08-7.04 (dd, *J* = 7.7, 1.5 Hz, 1H), 6.94 (td, *J* = 7.7, 1.6 Hz, 1H), 6.65-6.60 (m, 2H), 4.36 (s, 2H).

Yield: 64%. MS-ESI: 232.71. HPLC t_R: 12.86.

N^1-(4-fluorobenzyl)benzene-1,2-diamine (46c)

Purified by column chromatography using ethyl acetate/ petroleum ether 1:9, affording the compound as a brown solid.

^{1}H NMR (400 MHz, DMSO) δ 7.44 – 7.39 (m, J= 6.0 Hz, 2.8 Hz, 2H), 7.18 – 7.11 (m, J=8.8 Hz, 2H), 7.04 (dd, *J* = 7.7, 1.5 Hz, 1H), 6.95 (dt, *J* = 7.7, 1.6 Hz, 1H), 6.63 – 6.56 (m, 2H), 4.33 (s, 2H).

Yield: 67%. MS-ESI: 216.26. HPLC t_R: 13.17.

N^1-(4-methoxybenzyl)benzene-1,2-diamine (46d)

Purified by column chromatography using ethyl acetate/ petroleum ether from 1:9 to 1:4, affording the compound as a yellowish white solid.

^{1}H NMR (400 MHz, DMSO) δ 7.30 (m, 2H), 7.01 (m, 1H), 6.94 (m, 1H), 6.91-6.84 (m, 2H), 6.62 (t, *J* = 7.5 Hz, 2H), 4.25 (s, 2H), 3.71 (s, 3H).
Yield: 63%. MS-ESI: 228.30. HPLC t_R: 14.63.

General procedures for synthesis of 47a-d

Under an argon atmosphere, a solution of the appropriate compound **46a-d** (1 equiv.) in toluene and glacial acetic acid (1.1 equiv.) was added. The mixture was then refluxed at 130 °C for one hour. After cooling to room temperature, the solvent was concentrated under reduced pressure. The resulting residue was diluted with dichloromethane (DCM) and washed successively with saturated aqueous sodium bicarbonate and brine. The organic layer was then dried over anhydrous sodium sulfate, filtered, and concentrated under reduced pressure.

Ethyl 4-benzyl-3-oxo-3,4-dihydroquinoxaline-2-carboxylate (47a)

Purified by preparative HPLC, affording the compound as a brown oil.
^{1}H NMR (400 MHz, $CDCl_3$) δ 7.75 (d, J= 8.1 Hz, 1H), 7.52 (t, J= 7.9 Hz, 1H), 7.38-7.24 (m, 7H), 5.51 (s, 2H), 4.53 (q, *J*= 7.2 Hz, 2H), 1.46 (t, J= 7.1 Hz, 3H).
Yield: 85%. MS-ESI: 308.34. HPLC t_R: 17.95.

Ethyl 4-(4-chlorobenzyl)-3-oxo-3,4-dihydroquinoxaline-2-carboxylate (47b)

Purified by preparative HPLC, affording the compound as a brown oil.
^{1}H NMR (400 MHz, $CDCl_3$) δ 7.96 (m, 1H), 7.54 (t, *J* = 8.0 Hz, 1H), 7.37 (m, 1H), 7.31-7.17 (m, 5H) 5.47 (s, 2H), 4.53 (q, *J* = 7.1 Hz, 2H), 1.46 (t, *J* = 7.1 Hz, 3H).
Yield: 89%. MS-ESI: 342.78. HPLC t_R: 19.29.

Ethyl 4-(4-fluorobenzyl)-3-oxo-3,4-dihydroquinoxaline-2-carboxylate (47c)

Purified by preparative HPLC, affording the compound as a brown oil.
^{1}H NMR (400 MHz, $CDCl_3$) δ 7.96 (dd, *J* = 8.0 Hz, 1H), 7.56 (dt, *J* = 8.6, 7.2, 1.6 Hz, 1H), 7.39 – 7.34 (dt, 1H), 7.31-7.24 (m, 3H), 7.04 – 6.97 (m, 2H), 5.47 (s, 2H), 4.53 (q, *J* = 7.1 Hz, 2H), 1.46 (t, *J* = 7.2 Hz, 3H).
Yield: 72%. MS-ESI: 326.33. HPLC t_R: 20.87.

Ethyl 4-(4-methoxybenzyl)-3-oxo-3,4-dihydroquinoxaline-2-carboxylate (47d)

Purified by preparative HPLC, affording the compound as a brown oil.

^{1}H NMR (400 MHz, $CDCl_3$) δ 7.95 (dd, *J* = 8.0, 1.5 Hz, 1H), 7.55 (ddd, *J* = 8.6, 7.2, 1.6 Hz, 1H), 7.39 – 7.31 (m, 2H), 7.26 – 7.20 (m, 3H), 6.91 – 6.80 (m, 2H), 5.45 (s, 2H), 4.52 (q, *J* = 7.1 Hz, 2H), 3.76 (s, 3H), 1.46 (t, *J* = 7.2 Hz, 3H).
Yield: 64%. MS-ESI: 338.36. HPLC t_R: 23.55.

General procedures for synthesis of 48a-d

To a solution of the appropriate compound **47a-d** (1 equiv) in ethanol, an aqueous solution of NaOH 2 N (3 equiv) was added dropwise. The reaction mixture was stirred at room temperature for one hour. The solvent was then concentrated under reduced pressure, and the resulting residue was acidified with 1 N HCl to acidic pH and diluted with dichloromethane (DCM). The organic phase was washed with water and brine, then dried over anhydrous sodium sulfate, filtered, and concentrated under vacuum.

4-benzyl-3-oxo-3,4-dihydroquinoxaline-2-carboxylic acid (48a)

Purified by preparative HPLC, affording the compound as an orange solid.
^{1}H NMR (400 MHz, DMSO) δ 12.1 (s, 1H), 7.89 (dd, *J* = 16 Hz, 0H), 7.63 (ddd, *J* = 24 Hz, 1H), 7.52 (dd, *J* = 16 Hz, 1H), 7.41 (ddd, *J* = 20 Hz, 1H), 7.36 – 7.20 (m, 5H), 5.52 (s, 2H).
Yield: 87%. MS-ESI: 280.28. HPLC t_R: 15.71.

4-(4-chlorobenzyl)-3-oxo-3,4-dihydroquinoxaline-2-carboxylic acid (48b)

Purified by preparative HPLC, affording the compound as an orange oil.
^{1}H NMR (400 MHz, DMSO) δ 12.05 (s, 1H)8.11 (dd, *J* = 8.5, 1.2 Hz, 1H), 7.87 (ddd, *J* = 8.7, 7.1, 1.7 Hz, 1H), 7.58 – 7.47 (m, 2H), 7.37 (dt, J= 8.0 Hz, 2H) 7.30 (dt, *J* = 8.3, 0.8 Hz, 2H), 5.35 (s, 2H).
Yield: 82%. MS-ESI: 314.73. HPLC t_R: 16.13.

4-(4-fluorobenzyl)-3-oxo-3,4-dihydroquinoxaline-2-carboxylic acid (48c)

Purified by preparative HPLC, affording the compound as a yellow oil.
^{1}H NMR (400 MHz, DMSO) δ 12.1 (s, 1H), 8.11 (dd, *J* = 8.5, 1.2 Hz, 1H), 7.87 (ddd, *J* = 8.7, 7.1, 1.7 Hz, 1H), 7.58 – 7.47 (m, 2H), 7.36 (ddt, *J* = 8.1, 3.4, 0.9 Hz, 2H), 7.31 (ddt, *J* = 8.1, 2H), 5.35 (s, 2H).
Yield: 78%. MS-ESI: 298,27. HPLC t_R: 17.78.

4-(4-methoxybenzyl)-3-oxo-3,4-dihydroquinoxaline-2-carboxylic acid (48d)

Purified by preparative HPLC, affording the compound as a yellow oil.

^{1}H NMR (400 MHz, DMSO) δ 12.51 (s, 1H), 8.11 (dd, *J* = 8.5, 1.2 Hz, 1H), 7.87 (ddd, *J* = 8.5, 7.0, 1.6 Hz, 1H), 7.58 – 7.47 (m, 2H), 7.18 (dt, *J* = 8.6, 0.9 Hz, 2H), 6.86 – 6.78 (m, 2H), 5.35 (s, 2H), 3.78 (s, 3H).

Yield: 67%. MS-ESI: 310,31. HPLC t_R: 21.52.

General procedures for synthesis of 49-55

To a solution of the appropriate **48a-d** in DMF at 0 °C, DIPEA (1 equiv.) and HBTU (1 equiv.) were added. Then, a solution of the appropriate aniline or benzylamine (1.1 equiv.) in DMF was added dropwise. The reaction mixture was stirred at room temperature for 16 h. Afterwards, the solvent was removed under reduced pressure, and the residue was diluted with DCM and washed sequentially with 10 % aqueous citric acid, 5 % aqueous $NaHCO_3$, and brine. The organic phase was collected, dried over anhydrous sodium sulfate, filtered, and concentrated. The crude product was purified by preparative HPLC.

4-benzyl-3-oxo-N-phenyl-3,4-dihydroquinoxaline-2-carboxamide (49)

The residue was purified by preparative HPLC, affording **49** as a yellow solid.

Yield: 43%. MS-ESI: 355.40. HPLC t_R: 20.10.

^{1}H NMR (400 MHz, $CDCl_3$) δ 11.98 (s, 1H), 8.26 – 8.21 (m, 1H), 7.83 (d, *J* = 7.8 Hz, 2H), 7.63 (t, *J* = 7.9 Hz, 1H), 7.53-7.21 (m, 9H), 7.18 (t, *J* = 32 Hz, 1H), 5.64 (s, 2H).

^{13}C NMR (400 MHz, $CDCl_3$) δ 159.38 (1C), 155.61 (1C), 137.60 (1C), 134.11 (1C), 133. 65 (1C), 133.22 (1C), 132.63 (1C), 129.15 (4C), 128.20 (2C), 125.08 (2C), 120.63 (2C), 114.90 (1C), 46.58 (1C).

4-(4-chlorobenzyl)-3-oxo-N-phenyl-3,4-dihydroquinoxaline-2-carboxamide (50)

The residue was purified by preparative HPLC, affording **50** as a yellow solid.

Yield: 33%. MS-ESI: 389,84. HPLC t_R: 20.56.

^{1}H NMR (400 MHz, $CDCl_3$) δ 11.83 (s, 1H), 8.26 (s, 1H), 7.83 (d, *J* = 28 Hz, 2H), 7.64 (t, *J* = 24 Hz, 1H), 7.53-7.46 (m, 5H), 7.25 – 7.15 (m, 3H), 5.59 (s, 2H).

^{13}C NMR (400 MHz, $CDCl_3$) δ 144.19 (1C), 137.58 (1C), 133.97 (1C), 133.35 (1C), 132.98 (1C), 132.73 (1C), 132.50 (1C), 129.33 (1C), 129.13 (1C), 129.03 (1C), 128.81 (1C), 128.54 (1C), 128.13 (1C), 127.96 (1C), 127.77 (1C), 125.43 (1C), 125.33 (1C), 125.12 (1C), 125.08 (1C),124.73 (1C), 120.39 (1C), 45.68 (1C).

4-(4-fluorobenzyl)-3-oxo-N-phenyl-3,4-dihydroquinoxaline-2-carboxamide (51)

The residue was purified by preparative HPLC, affording **51** as a brown-purple solid.

Yield: 33%. MS-ESI: 373,39. HPLC t_R: 21.74.

^{1}H NMR (500 MHz, $CDCl_3$) δ 11.85 (s, 1H), 10.90 (s, 1H), 8.28 (d, *J* = 8.0 Hz, 1H), 7.84 (d, *J* = 8.0 Hz, 2H), 7.66 (t, *J* = 7.8 Hz, 1H), 7.52 – 7.46 (m, 2H), 7.43 – 7.31 (m, 4H), 7.21 – 7.12 (m, 2H), 7.08-7.03 (m, 2H), 5.60 (s, 2H).

^{13}C NMR (400 MHz, $CDCl_3$) δ 144.15 (1C), 137.75 (1C), 133.55 (1C), 132.81 (3C), 129.52 (1C), 129.32 (3C), 128.97 (2C), 128.35 (2C), 128.10 (1C), 125.18 (4C), 120.68 (3C), 46.13 (1C).

4-(4-methoxybenzyl)-3-oxo-N-phenyl-3,4-dihydroquinoxaline-2-carboxamide (52)

The residue was purified by preparative HPLC, affording **52** as a yellow solid.

Yield: 54%. MS-ESI: 385,42. HPLC t_R: 22.37.

^{1}H NMR (400 MHz, $CDCl_3$) δ 11.97 (s, 1H), 8.23 (s, 1H), 7.82 (s, 2H), 7.64 (t, *J* = 7.9 Hz, 1H), 7.48-7.42 (m, 2H), 7.39 (t, *J* = 7.7 Hz, 2H), 7.20 (dd, *J* = 18.6, 7.8 Hz, 2H), 7.17 (t, *J*= 8.0 Hz, 1H), 6.88 (d, *J* = 8.6 Hz, 2H), 5.57 (s, 2H), 3.78 (s, 3H).

^{13}C NMR (400 MHz, $CDCl_3$) δ 159.19 (1C), 155.73 (1C), 143.52 (1C), 138.02 (1C), 133.52 (2C), 132.66 (1C), 129.15 (2C), 128.16 (2C), 126.31 (1C), 125.14 (1C), 120.64 (2C), 114.46 (3C), 55.40 (1C), 46.03 (1C).

4-benzyl-N-(4-chlorophenyl)-3-oxo-3,4-dihydroquinoxaline-2-carboxamide (53)

The residue was purified by preparative HPLC, affording **53** as a yellow solid.

Yield: 63%. MS-ESI: 389.84. HPLC t_R: 20.56.

^{1}H NMR (400 MHz, $CDCl_3$) δ 11.99 (s, 1H), 8.26 (dd, *J* = 8.1, 1.5 Hz, 1H), 7.84 – 7.73 (m, 2H), 7.66 – 7.56 (dt, J= 8.6, 7.3, 1.5 Hz, 1H), 7.41 – 7.19 (m, 6H), 7. 26- 7.21 (m, 4H), 5.63 (s, 2H).

^{13}C NMR (400 MHz, $CDCl_3$) δ 159.02 (1C), 155.65 (1C), 144.02 (1C), 136.56 (1C), 134.04 (1C), 133.68 (1C), 133.20 (1C), 132.84 (1C), 132.69 (1C), 129.85 (1C), 129.36 (2C), 129.02 (2C), 126.83 (1C), 126.60 (1C), 125.38 (1C), 125.13 (1C), 121.73 (2C), 114.82 (1C), 46.43 (1C).

4-benzyl-N-(4-fluorophenyl)-3-oxo-3,4-dihydroquinoxaline-2-carboxamide (54)

The residue was purified by preparative HPLC, affording **54** as a yellow solid.

Yield: 63%. MS-ESI: 373.79. HPLC t_R: 19.77.

^{1}H NMR (400 MHz, $CDCl_3$) δ 11.96 (s, 1H), 8.26 (d, *J* = 8.1 Hz, 1H), 7.81 (dd, *J* = 8.8, 4.8 Hz, 2H), 7.64 (t, *J* = 7.8 Hz, 1H), 7.49 (dd, *J*= 7.5 Hz, 1H), 7.43 – 7.27 (m, *J*= 17.6, 9.3 Hz, 4H), 7.24 (m, 5H), 7.08 (t, *J* = 8.5 Hz, 2H), 5.63 (s, 2H).

^{13}C NMR (400 MHz, $CDCl_3$) δ 155.47 (1C), 144.16 (1C), 134.19 (1C), 133.52 (1C), 133.02 (1C), 132.53 (1C), 129.41 (1C), 129.10 (1C), 128.21 (1C), 128.06 (1C), 126.79 (2C), 126.54 (1C), 125.16 (1C), 122.26 (3C), 115.95 (1C), 115.72 (1C), 114.93 (1C), 114.52 (1C), 47.08 (1C).

N,4-dibenzyl-3-oxo-3,4-dihydroquinoxaline-2-carboxamide (55)

The residue was purified by preparative HPLC, affording **55** as a red solid.

Yield: 67%. MS-ESI: 369.42. HPLC t_R: 20.53.

^{1}H NMR (400 MHz, $CDCl_3$) δ 10.29 (s, 1H), 8.13 (d, *J* = 7.9 Hz, 1H), 7.61 (t, *J* = 7.8 Hz, 1H), 7.49 – 7.23 (m, 10H), 7.20 (d, *J* = 8.0 Hz, 2H), 5.56 (s, 2H), 4.77 (d, 2H).

^{13}C NMR (400 MHz, $CDCl_3$) δ 162.14 (1C), 155.53 (1C), 143.81 (1C), 137.65 (1C), 134.37 (1C), 133.53 (1C), 133.28 (1C), 133. 17 (1C), 132.87 (1C), 132.36 (1C), 129.27 (1C), 129.04 (1C), 128.92 (1C), 128.81 (1C), 128.69 (1C), 128.21 (1C), 128.15 (1C), 127.98 (1C), 127.93 (1C), 127.64 (1C), 127.57 (1C), 126.93 (1C), 126.72 (1C), 126.48 (1C), 126.08 (1C), 125.22 (1C), 125.09 (1C), 114.37 (1C), 46.90 (1C), 44.23 (1C).

General procedure of synthesis of ethyl 3-oxo-3,4-dihydroquinoxaline-2-carboxylate (56a)

To a solution of benzene-1,2-diamine (1 equiv., 2.86 mmol) in toluene, acetic acid (1.1 equiv., 3.14 mmol) and diethyl 2-oxomalonate (1.1 equiv., 3.14 mmol) were added dropwise in succession. The reaction mixture was then refluxed at 130 °C for one hour. Upon completion, the solvent was removed under reduced pressure, and the resulting residue was diluted with dichloromethane (DCM) and washed sequentially with a 5% aqueous sodium bicarbonate solution and brine. The organic layer was dried over anhydrous sodium sulfate, filtered, and concentrated under reduced pressure. The crude product was not subjected to further purification and was used directly in the subsequent reaction step.

^{1}H NMR (400 MHz, DMSO) δ 7.81 (ddd, *J* = 7.9, 1.4, 0.7 Hz, 1H), 7.67 – 7.58 (m, 1H), 7.41 – 7.28 (m, 2H), 6.51 – 6.42 (m, 1H), 6.39 – 6.30 (m, 1H), 5.73 (s, 1H), 4.35 (q, *J* = 7.1 Hz, 2H), 1.30 (t, *J* = 7.2 Hz, 3H).

Yield: 81%. MS-ESI: 218.21. HPLC t_R: 12.80.

General procedure of synthesis of 56b

To a solution of compound **1n** (1.0 equiv, 0.33 mmol) in DMF, K_2CO_3 (1.2 equiv, 0.40 mmol) was added. Subsequently, tert-butyl (3-bromopropyl)carbamate (1.6 equiv, 0.53 mmol) was added dropwise, and the reaction mixture was stirred at room temperature for 16 hours. The solvent was then removed under reduced pressure, and the resulting residue was diluted with a 10% aqueous

solution of **citric acid** until the pH reached 3. The mixture was extracted with ethyl acetate (3 ×), and the combined organic layers were washed with brine, dried over anhydrous sodium sulfate, filtered, and concentrated under reduced pressure. The crude product was purified by column chromatography using a gradient of ethyl acetate/petroleum ether from 20% to 50%, affording compound **2n** as a yellow oil.

^{1}H NMR (400 MHz, $CDCl_3$) δ 7.98 (dd, *J* = 8.0 Hz, 1H), 7.67 (ddd, *J* = 8.0 Hz, 1H), 7.44 – 7.37 (m, J= 8.0 Hz, 2H), 5.41 (s, 1H), 4.51 (q, *J* = 5.3 Hz, 2H), 4.36 (t, *J* = 8.0 Hz, 2H), 3.42 (d, *J* = 8.0 Hz, 1H), 1.98 (t, J= 6.0 Hz, 2H), 1.44 (m, 14H).

Yield: 75%. MS-ESI: 375.43. HPLC t_R: 23.97.

General procedure of synthesis of 56c

To a solution of compound **2n** (1.0 equiv, 1.06 mmol) in dichloromethane (DCM), trifluoroacetic acid (2.8 mL) was added dropwise, and the reaction mixture was stirred at room temperature for 3 hours. The solvent was then removed under reduced pressure, and the crude residue was washed with diethyl ether, affording compound **3n** as a yellow oil without further purification.

General procedure of synthesis of 57

To a solution of 4-fluorobenzoic acid (1 equiv., 0.11 mmol) in DMF at 0 °C, DIPEA (1.1 equiv., 0.12 mmol) and HBTU (1.1 equiv., 12 mmol) were added. Then, a solution of compound 3n (1.1 equiv., 0.12 mmol) in DMF was added dropwise. The reaction mixture was stirred at room temperature for 16 h. Afterwards, the solvent was removed under reduced pressure, and the residue was diluted with DCM and washed sequentially with 10 % aqueous citric acid, 5 % aqueous $NaHCO_3$, and brine. The organic phase was collected, dried over anhydrous sodium sulfate, filtered, and concentrated. The crude product was purified by preparative HPLC, affording a yellow oil.

^{1}H NMR (400 MHz, $CDCl_3$) δ 8.02 (dd, J= 4.0 Hz, 1H), 7.96- 7.89 (m, 2H)7.82-7.75 (m, 1H), 7.75–7.68 (m, 1H), 7.50 – 7.41 (m, 2H), 7.15 (t, *J* = 10.0 Hz, 2H), 4.53 (q, *J* = 6.0 Hz, 2H), 4.46 (t, *J* = 6.6 Hz, 2H), 3.45 (q, *J* = 5.5 Hz, 2H), 2.21 – 2.10 (m, 2H), 1.46 (t, *J* = 6.0 Hz, 1H).

^{13}C NMR (400 MHz, $CDCl_3$) δ 167.56 (1C), 166.22 (1C)163.96 (1C), 153.27 (1C), 148.13 1C), 132.50 (2C), 131.73 (1C), 129.68 (3C), 125.25 (1C), 115.95 (3C), 114.05 (2C), 62.66 (1C), 39.84 (1C), 36.29 (1C), 27.05 (1C), 14.11 (1C).

Yield: 58%. MS-ESI: 397.41. HPLC t_R: 21.03.

5.6 BIOLOGICAL EXPERIMENTAL SECTION

5.6.1 Materials and Methods

For *in vitro* experiments, HeLa (human cervical carcinoma), MDA-MB-231 (human breast adenocarcinoma), HCT116 (human colorectal carcinoma), and HaCaT (immortalized human keratinocyte) cell lines were employed. Cells were maintained in Dulbecco's Modified Eagle Medium (DMEM) supplemented with 10% fetal bovine serum (FBS), 100 U/mL penicillin, and 100 µg/mL streptomycin to support optimal growth and prevent bacterial contamination. Cultures were routinely washed with phosphate-buffered saline (PBS), and cell viability and counting were assessed using Trypan Blue exclusion in conjunction with a Bürker counting chamber. All cell lines were cultured under standard conditions at 37 °C in a humidified atmosphere containing 5% CO_2.

Plasticware employed included filter-cap flasks for cell culture and growth, Eppendorf tubes and micropipettes of various volumes for cell transfer, and multiwell plates for biological testing. As reference compounds, MG132, Pimozide, and DMSO were used. Fluorogenic diagnostic probes B1 and B2, synthesized in-house, were employed to assess proteasome activity. Fluorescence analysis was carried out using a BD FACSCanto II flow cytometer.

5.6.2 Calculation of Activity Values

Each compound was tested in triplicate. The activity percentages were calculated as the arithmetic mean of the three values obtained for each experiment and each compound. The activity of the proteasome in the presence of DMSO was considered as 100%, and all other values were normalized relative to this reference.

Compounds	**Fluorescence values measured in the presence of the vinyl-sulfonic probe**			**Fluorescence values measured in the presence of the sulfonic probe.**		
	First experiment	*Second experiment*	*Third experiment*	*First experiment*	*Second experiment*	*Third experiment*
DMSO	163	139	120	70	55	64
MG132	107	122	111	56	70	76
Pimozide	302	277	234	90	57	86
47a	128	111	151	40	30	65
47b	144	153	113	89	101	56
47c	348	388	316	352	415	289
47d	128	118	111	64	66	58
48a	112	132	177	60	53	137

48b	151	133	135	56	58	47
48c	88	200	99	60	70	59
48d	96	97	90	54	60	46
49	140	145	150	66	71	70
50	175	150	141	117	100	104
51	95	195	90	59	72	59
52	130	129	144	78	73	86
53	119	130	147	67	80	67
54	110	144	113	57	86	47
55	140	136	146	77	81	112
57	142	151	184	68	56	136

Table 5. Fluorescence measurements obtained for the first class of compounds in all experimental runs on HeLa cells.

Compounds	**Fluorescence values measured in the presence of the vinyl-sulfonic probe**			**Fluorescence values measured in the presence of the sulfonic probe.**		
	First experiment	*Second experiment*	*Third experiment*	*First experiment*	*Second experiment*	*Third experiment*
DMSO	10527	23169	21101	6122	11319	13361
MG132	7756	11093	9676	6195	10521	8826
Pimozide	56599	8954	18762	23923	8227	8237
50	6409	13846	9723	6499	12461	8324
55	56599	8954	8624	32676	8227	7946
47c	6467	14811	7654	6221	10968	7650

Table 6. Fluorescence measurements obtained for the first class of compounds in all experimental runs on MDA cells.

Compounds	**Fluorescence values measured in the presence of the vinyl-sulfonic probe**			**Fluorescence values measured in the presence of the sulfonic probe.**		
	First experiment	*Second experiment*	*Third experiment*	*First experiment*	*Second experiment*	*Third experiment*
DMSO	9079	8640	8534	5699	2561	3300
MG132	5359	5131	4682	5034	2960	3796
Pimozide	17571	17800	18904	11129	14820	15088
50	9079	9798	8543	6006	3784	3522

55	9774	11003	8922	6370	4985	3877
47c	7592	8754	9647	5159	7256	5984

Table 7. Fluorescence measurements obtained for the first class of compounds in all experimental runs on HCT cells.

Compounds	**Fluorescence values measured in the presence of the vinyl-sulfonic probe**			**Fluorescence values measured in the presence of the sulfonic probe.**		
	First experiment	*Second experiment*	*Third experiment*	*First experiment*	*Second experiment*	*Third experiment*
DMSO	47686	36545	15563	27183	17888	10243
MG132	32285	27162	13426	31105	19632	9587
Pimozide	88598	59344	18965	52462	36888	10532
50	39776	31245	14325	23032	15574	9591
55	49404	28612	14356	33453	12754	9728
47c	34114	48677	18976	20187	36924	14348

Table 8. Fluorescence measurements obtained for the first class of compounds in all experimental runs on HaCat cells.

6 PROJECT 2b. Targeting Proteasome Activation: A New Therapeutic Avenue for Neurodegeneration

As previously noted, the proteasome represents the cell's primary defence against the accumulation of proteotoxic stress resulting from oxidative damage. In particular, the 20S proteasome complex can directly recognize and degrade oxidatively modified proteins, thereby contributing to cellular detoxification. [192-194]

During aging, multiple intracellular mechanisms contribute to the progressive accumulation of oxidative damage. In response to such insults, proteins often unfold and expose hydrophobic regions, making them particularly susceptible to aggregation. To counter the increasing burden of oxidatively modified proteins, cells enhance the abundance of the 20S proteasome, predominantly through disassembly of the 26S complex. [195,196]

However, when the accumulation of damaged proteins exceeds the degradative capacity of the proteasome, proteostasis becomes dysregulated and proteotoxic stress ensues. These events constitute key pathological features of several neurodegenerative disorders, including Parkinson's disease (PD), Alzheimer's disease (AD), Huntington's disease (HD), and amyotrophic lateral sclerosis (ALS, also known as Lou Gehrig's disease).

Genetic manipulation of proteasomal proteolytic systems in animal models of various neurodegenerative disorders has shown that enhancing these systems can mitigate disease-associated pathology, suggesting that stimulation of proteasomal activity may represent an effective therapeutic strategy.[197,198]

Consequently, the search for novel molecules capable of activating the proteasome has gained considerable interest. Such compounds could offer a new therapeutic avenue by promoting the clearance of protein aggregates and thereby preventing the downstream signaling events that ultimately lead to neuronal death.

As already outlined in the previous section, the molecular basis underlying positive proteasome modulation remains largely unresolved. What is known to date, however, is that several clinically approved drugs—originally developed for unrelated pathological conditions—have unexpectedly demonstrated the ability to enhance proteasome activity.

Consequently, research in this pharmacological domain is currently oriented primarily toward the biological screening of drug libraries and structurally diverse small-molecule collections, with the aim of identifying novel proteasome-activating agents.

6.1 AIM OF THE PROJECT

The investigation of proteasome modulation has emerged as a promising avenue for the development of innovative therapeutic strategies for neurodegenerative disorders, many of which are characterized by impaired proteostasis and the accumulation of misfolded or damaged proteins. Enhancing proteasome activity, in particular, represents a potentially transformative approach, thereby motivating the search for small molecules capable of restoring or augmenting proteolytic function.

As previously discussed, the rational design of novel proteasome activators remains a considerable challenge. This difficulty stems primarily from the fact that the precise binding sites and modes of interaction of small-molecule activators within the 26S proteasome have not yet been conclusively defined. Consequently, direct targeting of the proteasomal subunits or regulatory interfaces responsible for functional modulation is highly complex, and empirical screening strategies continue to represent a crucial component of discovery efforts in this field.

In accordance with current methodologies, an **in vitro cellular assay** was developed to enable the systematic screening of an internal compound library. The assay was specifically selected for its capacity to identify both inhibitors and activators of proteasome activity within a physiologically relevant cellular environment. This feature was essential not only for capturing direct modulatory interactions with the proteasome itself, but also for detecting indirect mechanisms of action—such as allosteric regulation or transcriptional modulation of proteasome-related genes—that would be undetectable using purified proteasome complexes.

The initial preliminary screening performed in **HeLa cells** allowed the identification of **nine molecules** exhibiting pronounced proteasome-activating properties. Importantly, these compounds were not intermediates arising from synthetic sequences but rather fully elaborated molecules previously designed for unrelated pharmacological targets. Several structural analogues of these compounds were also evaluated but failed to display notable proteasome modulation, suggesting that the specific substitution patterns present in the active molecules may play a crucial role in conferring biological activity.

Following this initial selection, the nine hit compounds were subjected to a broader evaluation across three distinct cell lines: **MDA-MB-231** (human breast adenocarcinoma), **HCT-116** (human colorectal carcinoma), and **HaCat** (immortalized human keratinocytes).

The decision to expand the screening across multiple cellular backgrounds was motivated by the need to determine whether modulatory activity was cell-line dependent. This consideration is particularly relevant given the heterogeneity in proteasome composition, regulation, and activity across different tissues and cancer types, as well as the intrinsic variability of the ubiquitin–proteasome system between transformed and non-transformed cells.
Together, these investigations laid the foundation for a more comprehensive assessment of structure–activity relationships and provided valuable insight into the context-dependent nature of proteasome modulation.

6.2 Biological Screening and Evaluation of Proteasome Modulatory Activity

As previously detailed in *Paragraph 4*, the biological assay required the use of fluorescent probes which, through their interaction with the proteasome, enabled quantification of proteasome activity expressed as a percentage.

To this end, three reference compounds were employed: **DMSO**, representing basal activity (100%); **MG132**, a well-established proteasome inhibitor; and **Pimozide**, a proteasome activator first reported by Leestemaker et al.[126]

The inclusion of both an inhibitor and an activator was essential for assay validation. As expected, MG132 decreased proteasome activity, as indicated by reduced fluorescence detected with the vinyl sulfone probe, whereas Pimozide induced an increase in fluorescence, corresponding to enhanced proteasome activity.
A comprehensive description of the assay workflow and its underlying mechanisms is provided in *Paragraph 3.4*.

As illustrated in *Graph 8*, the screening of the nine molecules displaying measurable proteasome-activating properties demonstrated that each compound maintained activation levels exceeding 120%. Among these, compound **MF3053** emerged as particularly remarkable, exhibiting a **288% increase in proteasome activity**, thereby surpassing the performance of the reference activator **Pimozide** by a substantial margin.

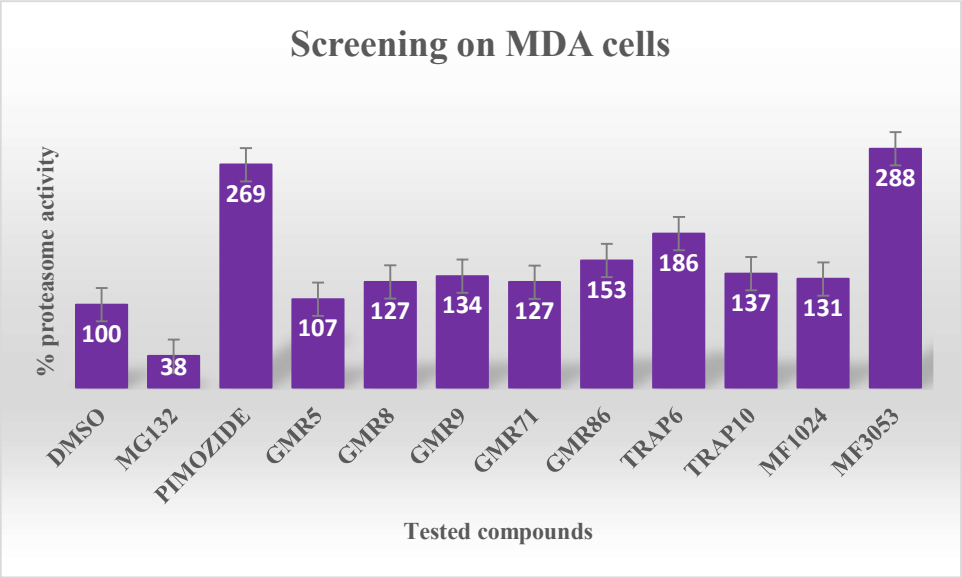

Graph 8. Results of the biological screening conducted in MDA cells.

Accordingly, all aforementioned molecules were subsequently assessed in the remaining two cellular lines: results are shown in *Graph 9* and *10*.

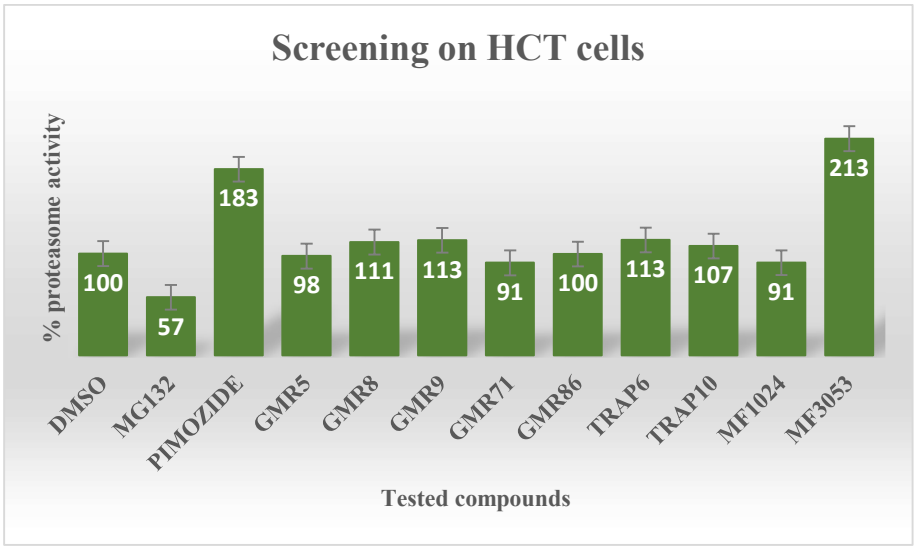

Graph 9. Results of the biological screening conducted in HCT cells.

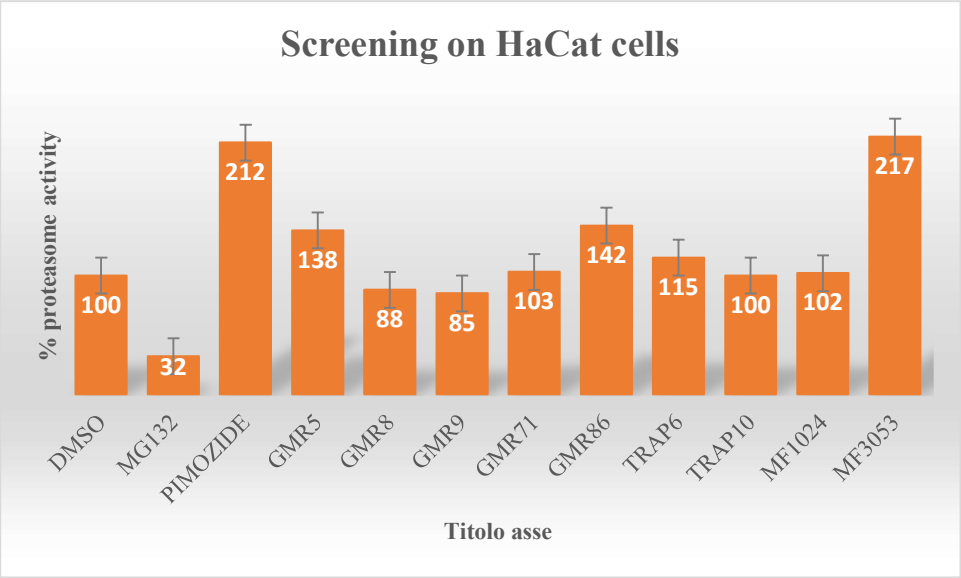

Graph 10. Results of the biological screening conducted in HaCat cells.

As evidenced in the two graphs, the majority of the compounds exhibited a marked reduction in activity. In HCT-116 cells, all tested molecules showed a pronounced loss of potency, with mean proteasome-activity values approaching basal levels. Only **compound MF3053** retained substantial activity, displaying an average value of **213%**, which remained consistently higher than that of the reference activator.

Conversely, in the HaCat cell line, compounds **GMR5** and **GMR86** preserved a modest degree of positive modulatory activity, although their effects were markedly weaker than those observed during the initial screening in HeLa cells. The only molecule that consistently maintained robust activity was **MF3053**, which reached **217% proteasome activity**, again exceeding the performance of **Pimozide**. Structurally, compounds **MF1024** and **MF3053** share a common dispiropiperidinic core, bearing variable substituents at positions 9 and 13. Specifically, **MF1024** features a methyl group at position 9 and a para-fluorobenzyl substituent at position 13. In contrast, **MF3053** incorporates a more elaborated architecture, with a (5-chlorothiophen-2-yl)sulfonyl group at position 9 and a benzyl moiety at position 13. The general structures of both compounds are depicted in **Figure 28**.

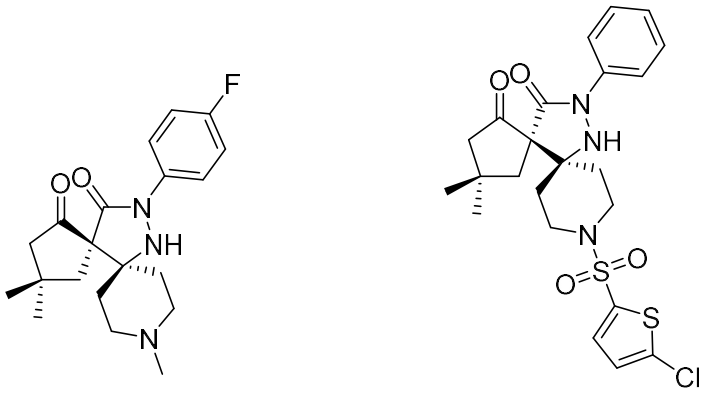

MF1024 **MF3053**

Figure 28. Chemical structure of compounds MF1024 and MF3053.

In recent work, Tepe and colleagues reported that fluspirilene and a series of its derivatives, characterized by a spiropiperidinic scaffold, exhibit significant proteasome-activating properties.
In particular, they identified fluspirilene as a molecule capable of enhancing the activity of all three catalytic subunits of the 20S proteasome, without activating the 26S complex. Subsequent structure–activity relationship (SAR) optimization, achieved through the introduction of an acyl substituent on the fluspirilene scaffold, led to the development of two derivatives that facilitated the clearance of α-synuclein—an important finding given the pathological accumulation of this protein observed in Alzheimer's disease (*Figure 29*).[198]

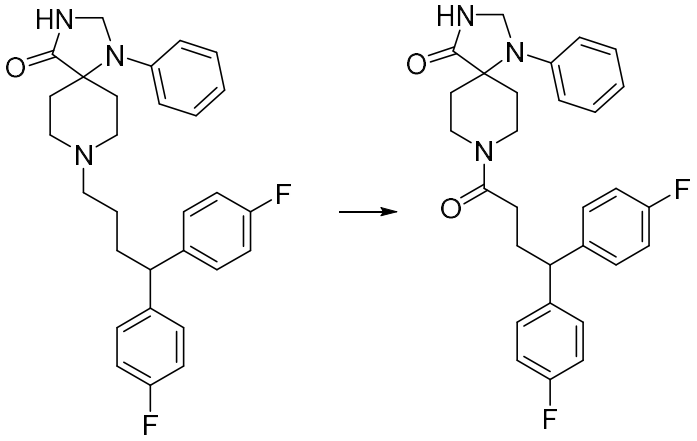

Fluspirilene **N-acylated Fluspirilene**

Figure 29. Chemical structure of fluspirilene and its N-acylated derivative obtained through SAR studies.

In view of the structural similarity between their central scaffolds and that of fluspirilene, these compounds may share recurring structural features with the reference ligand. During the biological screening campaign, additional molecules bearing the same core scaffold—differentially substituted at positions 9 and 13—were evaluated. Notably, the introduction of either a benzyl or a methyl group

at position 9 resulted in a marked loss of modulatory activity. This observation suggests that the **2-chloro-5-(methylsulfonyl)thiophene** substituent at position 9 may play a pivotal role in defining the biological activity of the series.
By contrast, position 13 appears to be a more promising site for further structural exploration. Modifying the benzyl substituent at this position while retaining the crucial 2-chloro-5-(methylsulfonyl)thiophene group at position 9 could enable a deeper investigation into the contribution of position 13 to the overall activity profile.

Compound **MF3053** was originally conceived and synthesized by our research group within the framework of a broader effort to identify novel modulators of the mitochondrial permeability transition pore, with the ultimate aim of developing therapeutic agents for ischaemia–reperfusion injury (IRI). Although its structural features were rationally designed to confer inhibitory potential in this context, the compound did not exhibit the anticipated biological activity. Nevertheless, its unexpectedly favorable profile in proteasome activation renders it an intriguing scaffold, meriting further exploration beyond its initial therapeutic rationale.[199]

This compound may therefore constitute an excellent model for elucidating the mechanisms underlying proteasome activation, particularly given the absence of any other known molecular targets that could confound its biological profile.

6.3 SYNTHESIS

The synthetic approach to the obtainment of the target compounds involves a known microwave-assisted strategy realized in a short time and with an excellent control of the diastereoselectivity. The 1,3-dipolar cycloaddition reaction was performed starting from different carbonyl compounds, piperidine (*Scheme 32*). Especially, N-benzyl-4-piperidone was commercially available. Carbonyl compound was initially reacted with N-methylhydrazine to realize the corresponding hydrazone intermediate.

In addition, for all the synthesized derivatives we employed the same diazo compound, synthesized through a standard liquid-phase reaction between dimedone, a 1,3-diketone, and the p-toluenesulfonyl azide in the presence of potassium carbonate (K_2CO_3).

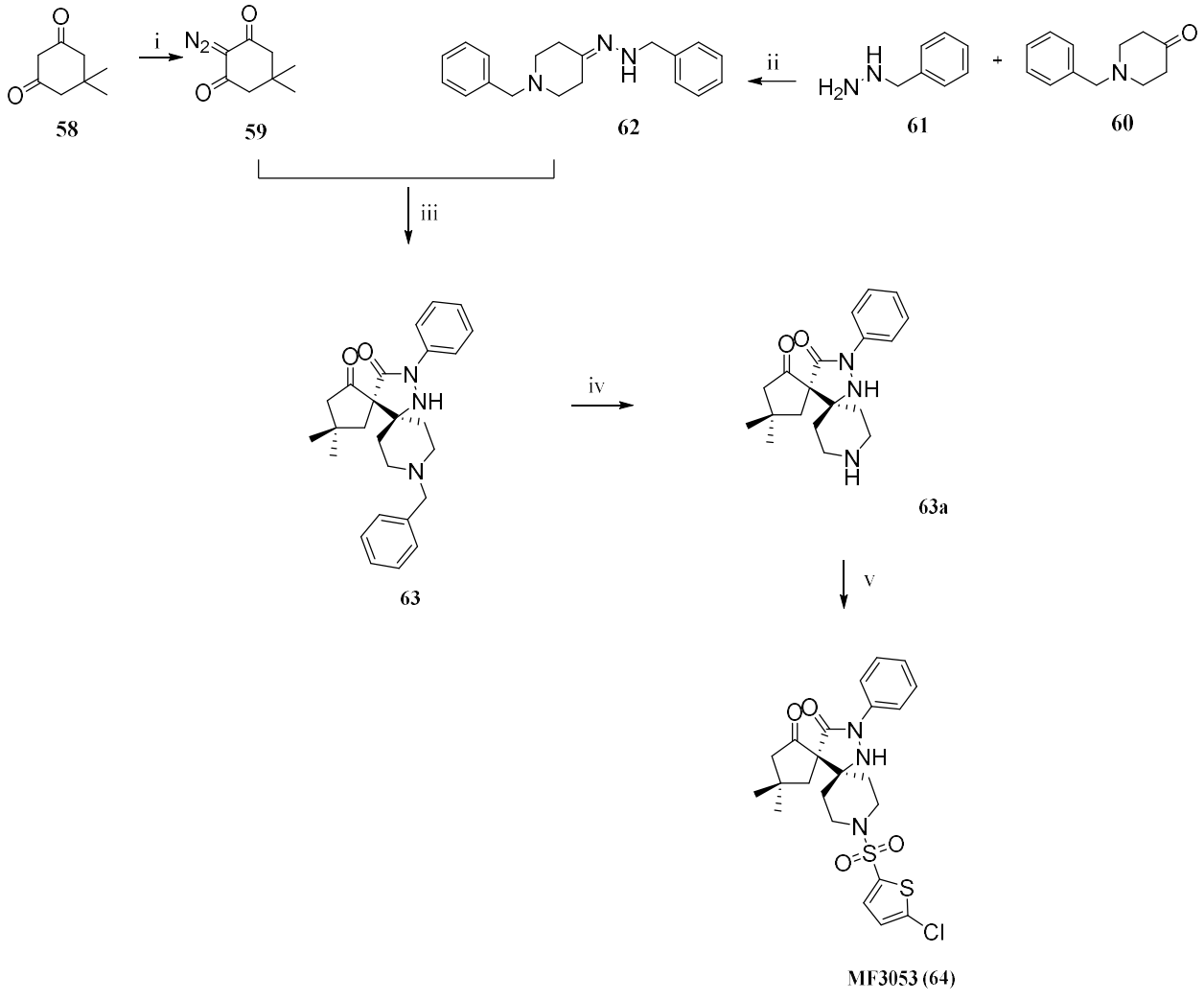

Experimental conditions.
i. TsN_3, K_2CO_3, MeCN, 0°C to rt 2h;
ii. Toluene, microwave 140°C 15 min;
iii. Toluene, microwave 140°C 15 min;
iv. H_2, 10% C/Pd, EtOH, AcOH;
v. 5-Cl-thiophen-2-yl-SO2Cl, DIPEA, THF, rt 2h.

Scheme 32. Overview of the general synthetic approach employed for the synthesis of compound MF3053.

6.4 CONCLUSIONS

Proteasome activation has emerged as one of the most promising and innovative strategies for the prevention of neurodegenerative disorders. These pathologies are frequently characterized by the accumulation of misfolded or aggregated proteins, which initiates a cascade of pathogenic events ultimately culminating in neuronal death. A substantial body of evidence suggests that such accumulation is, at least in part, attributable to impaired proteasomal function—an essential cellular machinery responsible for the selective degradation of intracellular proteins. Accordingly, enhancing proteasomal activity represents a compelling therapeutic avenue for mitigating, or potentially preventing, neurodegeneration.

To date, only a limited number of small molecules—primarily drugs already approved for other therapeutic indications—have been identified as capable of increasing proteasome activity. Such discoveries typically arise from high-throughput screening of pharmacological libraries.

In the context of the present project, which focuses on positive modulation of proteasomal function, we conducted a biological screening of an internal library comprising one hundred compounds. The evaluation employed a fluorogenic assay capable of quantifying proteasomal activity within a cellular environment, thereby integrating all cellular processes that might contribute to enhanced proteasome function.

A preliminary screen in HeLa cells enabled the identification of ten compounds exhibiting appreciable activatory properties.
Among these, two stood out owing to their shared dispiropiperidinic central scaffold, reminiscent of the core structure of fluspirilene—a compound previously reported to activate all three catalytic subunits of the proteasome. These structural considerations prompted further investigation of the two candidates across three additional cellular lines.

The ensuing biological results revealed that compound **MF3053** displayed particularly marked proteasome-activating activity, in several cases surpassing that of the reference agent Pimozide.
Interestingly, **MF3053** had originally been designed as a potential therapeutic agent for ischaemia–reperfusion injury but proved inactive in that context. This lack of activity against its intended target renders the compound especially valuable for mechanistic studies of proteasome activation, as it reduces the likelihood of confounding off-target effects.

MF3053 is currently being evaluated on purified 20S proteasome preparations to determine whether its activatory effect arises from a direct interaction with the proteasome and to assess its potential selectivity toward specific catalytic subunits.

7 Future perspective

7.1 Biological Evaluation of Proteasome Modulators

The compounds emerging from *Projects 1* and *2* that demonstrated modulatory activity toward the proteasome will be subjected to an extensive series of biological investigations. These studies aim to elucidate the mechanism of action, the specificity of modulation, the cytotoxic profile, and the molecular consequences of proteasome perturbation. The combination of biochemical, cellular, and molecular techniques will provide a comprehensive evaluation of both inhibitory and activating behaviours of the newly synthesized molecules.

Evaluation on Purified 20S Proteasome [114]

In the first stage, the selected compounds will be assessed using purified 20S proteasomes in order to determine their direct modulatory effects on the catalytic core particle. This assay enables precise characterization of both the temporal profile of modulation (with particular interest in sustained negative modulation) and the selectivity toward the three principal catalytic activities—chymotrypsin-like, trypsin-like, and caspase-like.

Proteasomal activities will be quantified using fluorogenic substrates specific for each catalytic site: **Suc-LLVY-AMC** for the chymotrypsin-like activity, **Boc-LRR-AMC** for the trypsin-like activity, and **Z-LLE-AMC** for the caspase-like activity. Upon cleavage, these substrates release AMC, whose fluorescence intensity directly correlates with proteasome activity. Increased fluorescence indicates the presence of an activator, whereas decreased fluorescence denotes an inhibitory effect.

Purified proteasomes will be incubated with increasing concentrations of each compound (0.01–100 μM), and the extent of inhibition will be expressed as **IC_{50} values**. A lower IC_{50} is indicative of a more potent inhibitor. Moreover, activity will be monitored over extended incubation times (up to 72 h) to determine the reversibility of binding: a decrease in inhibitory effect over time suggests reversible interaction.

Control references—including *DMSO, MG132*, and *Pimozide*—will be employed to contextualize the activity of the new compounds.

Apoptosis Assay [114]

To investigate the potential cytotoxicity associated with proteasome modulation, the compounds will be evaluated through an *Annexin V/Propidium Iodide apoptosis assay*. Annexin V binds phosphatidylserine, which becomes exposed on the outer leaflet of the plasma membrane during early apoptosis (Annexin V^+/PI^-), whereas PI stains cells that have lost membrane integrity, identifying late apoptotic or necrotic cells (Annexin V^+/PI^+).

Assays will be carried out at 48 h and 72 h, allowing assessment of both the onset and progression of cytotoxic effects. This analysis will provide insight into whether proteasome modulation translates into pro-apoptotic signaling in cancer cells.

Western Blot Analysis [200]

Western blotting will be employed to characterize how proteasome modulators influence the expression, abundance, and post-translational modification of proteasome-related proteins. This technique enables:

- *Quantification* of protein levels, allowing assessment of up- or down-regulation of specific substrates or regulatory components.
- *Detection of post-translational modifications*, such as ubiquitination, which reflects proteostatic stress and impaired proteasomal degradation.
- *Assessment of expression changes*, for example in proteasome subunits or regulatory proteins.
- Analysis of *protein stability*, revealing whether modulation alters the half-life of proteasome substrates.

Collectively, these data will contribute to a molecular understanding of the cellular response to proteasome modulation.

Quantitative PCR Analysis [201]

Quantitative PCR will be used to assess transcriptional responses triggered by proteasome modulation. This technique is particularly informative because the proteasome plays a fundamental role in maintaining proteostasis; therefore, its inhibition or activation leads to *predictable transcriptional adjustments*.

- **Proteasome inhibition** results in accumulation of ubiquitinated proteins, activating stress-response pathways—most notably the unfolded protein response (UPR). Upregulated transcripts typically include:
    - *ATF4*, *DDIT3/CHOP*, *XBP1s* (UPR markers)
    - *HSPA5 (BiP/GRP78)*, *HSP70*, *HSP90*, *ERdj4*, *HERPUD1* (proteostasis-related genes)
    - Proteasome subunit genes (*PSMA*, *PSMB*, *PSMC*, *PSMD*), reflecting compensatory upregulation.
- **Proteasome activation**, conversely, reduces proteotoxic stress and is associated with decreased expression of these transcripts.

Thus, qPCR will allow precise quantification of transcriptional signatures characteristic of either inhibitory or activating modulation.

Photoaffinity Labeling for Mechanistic Elucidation of Proteasome Modulation [202]

Photoaffinity labeling (PAL) is a validated chemoproteomic strategy widely used in drug discovery for target identification and for mapping ligand–protein interactions. First introduced in the early 1960s by Westheimer's group [203], PAL has been revitalized through modern proteomic workflows that enable comprehensive identification of photolabeled targets. Traditionally employed to profile proteins bound by a given probe, PAL is now increasingly applied to pinpoint binding sites and to characterize structural or conformational features of proteins. As a photocrosslinking-based approach, it offers a unique means to identify unknown targets, elucidate protein function, and reveal alternative or cryptic binding pockets.

PAL employs multifunctional ligands capable of covalently attaching to their protein targets upon UV irradiation[204]. The ligand contains an affinity or specificity motif responsible for reversible binding, coupled to a photoreactive "warhead" that forms a covalent adduct upon activation.[205] Probes may also incorporate a reporter or purification tag to facilitate detection and enrichment of the PAL–protein complexes, allowing applications both with isolated proteins and in live-cell contexts. As illustrated in Figure 30, photoaffinity probes (PAPs) typically consist of three modules: a bioactive ligand, a photoreactive group, and a tag. [206]

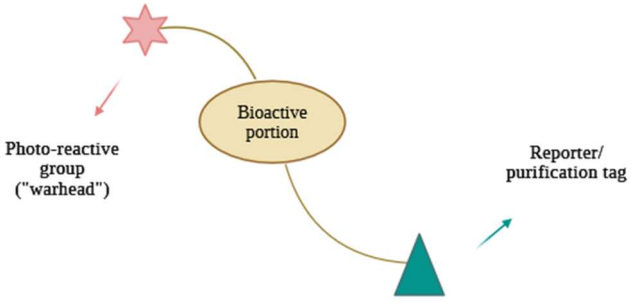

Figure 30. General structure of PAPs.

Rational PAP design generally requires extensive structure–activity relationship (SAR) studies to ensure that the photoreactive group is positioned without compromising affinity. The length and composition of linker elements are also critical: overly short linkers can promote intramolecular crosslinking, whereas excessively long ones may reduce photolabeling efficiency. Because conventional reporter tags often reduce cell permeability, a common strategy is to introduce the tag post-labeling via click chemistry. [207] In such designs, the probe contains only the pharmacophore, the photogroup, and a bioorthogonal handle (usually an alkyne or azide), enabling cell entry. Following lysis, the complementary azide- or alkyne-modified reporter is attached through copper-catalyzed azide–alkyne cycloaddition.

Developing an optimal PAP requires balancing multiple features, including chemical stability in the dark, minimal perturbation of the parent compound's activity, and synthetic accessibility. Selection of the photoreactive group is likewise guided by considerations such as activation wavelength (ideally avoiding protein-damaging UV ranges at 200 and 280 nm), reactivity, and structural compactness. The principal groups employed are phenylazides, phenyldiazirines, and benzophenones, which generate nitrenes, carbenes, and diradicals, respectively, upon irradiation. [206]

For downstream analysis, reporter tags are incorporated directly or indirectly into PAPs. Biotin is widely used due to its exceptionally high affinity for avidin, enabling efficient enrichment of labeled proteins and facilitating target or binding-site identification. Fluorophores, which offer a broad range of spectral properties, are commonly used for visualization by in-gel fluorescence or imaging. [208]

In light of these considerations, for the compounds identified as modulators of the proteasome—namely **47c** as an inhibitor and **MF3053** as an activator—specific molecular designs were developed to enable their application in PAL experiments (*Figure 31*). These structures incorporate an alkyne and an azide functional group, which together provide suitable handles for photocrosslinking and subsequent tagging following UV irradiation. Once synthesized, the compounds will be evaluated to confirm both their modulatory activity and their suitability for PAL studies.

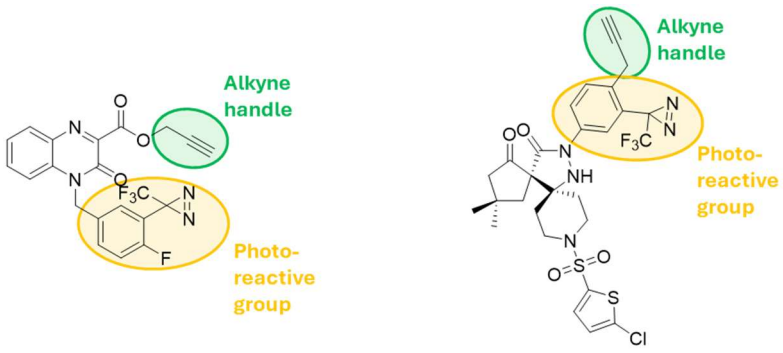

Figure 31. General structure of molecules designed for the application of photoaffinity labeling.

7.2 EXPERIMENTAL SECTION

7.2.1 Materials and Methods

Reagents and solvents were purchased by BLD, Fluorochem and Sigma Aldrich. Microwave-assisted three-component reactions were conducted with a Biotage® Initiator+. Reaction progress and product mixture were monitored by thin-layer chromatography (TLC) on pre-coated F254 Macherey-Nagel plates of silica gel, visualized with a UV lamp (254 nm light source), and/or by ESI MICROMASS ZMD 2000 electrospray mass spectrometer, after dissolution of compounds in a solution composed by 40:60:0.1 of H2O:CH3CN:TFA. Derivatives were purified by, flash chromatography or via reverse-phase purification using a Waters Delta 600 high-performance liquid chromatography (HPLC) system with a Jupiter column C18 (250 × 30 mm, 300 Å, 15 μm spherical particle size), using a binary mobile

phase consisting of solution A (100% H2O, 0. 1% v/v TFA) and solution B (40% H2O, 60% CH3CN, 0.1% v/v TFA) at a flow rate of 20 mL/min. Gradient was established individually considering the analytical HPLC profile of the crude product. Analytical HPLC was performed with a Beckman 126 liquid chromatograph furnished of a UV detector Beckman

168 and equipped with KARAT32 software. The purity of all the derivatives was assessed with an Agilent Zorbax C18 column (4.6 × 150 mm, 3.5 μm particle size) at a flow rate of 0.7 mL/min using a linear gradient from 100% of A (water + 0.1% TFA) to 100% of B (acetonitrile + 0.1% TFA) over a period of 25 min. All final compounds were monitored at

220 nm showing ≥ 96% purity. 1H NMR and 13C NMR spectra were performed on a Varian Mercury Plus 400 MHz spectrometer. The signals were referenced to residual 1H shift of the deuterated solvents (respectively δ H 7.26 for CDCl3;δ H 2.50 for DMSO-d6). Chemical shifts (δ) are expressed in parts per million (ppm) using the peak of deuterated solvents as an internal standard, while values of coupling constants (J) are reported in Hertz (Hz). Splitting patterns are designed as s, singlet; d, doublet; dd, double doublet; t, triplet; m, multiplet; and bs, broad signal. Melting points for purified products were determined in a glass capillary on a Stuart Scientific electrothermal apparatus SMP30.

Preparation of 2-diazo-5,5-dimethylcyclohexane-1,3-dione 59.

To a solution of dimedone 58 (1 equiv., 7.13 mmol) in MeCN (15 mL) were added tosyl azide (1 equiv.) and K2CO3 (1.1 equiv.) at 0°C. The mixture was stirred at 0°C for 1h and then at room temperature for 3h. Upon completion, as indicated by TLC, the volatile fraction was evaporated under reduced pressure. The resulting crude material was directly purified by flash chromatography (EtOAc/PE as the eluent) to yield derivative 17 as pale white solid (stored at -25°C).

Pale yellow solid (yield 97%).
1H NMR (400 MHz, DMSO-d6) δ 2.42 (s, 2H), 1.01 (s, 3H).
13C NMR (101 MHz, DMSO-d6) δ 189.91, 49.50, 30.64, 27.57. MS (ESI) [M+H]+ 167.08.

General procedure for the preparation of 9-benzyl-3,3-dimethyl-13-phenyl-9,12,13-triazadispiro[4.0.56.35]tetradecane-1,14-dione (63).

To a solution of 1-benzylpiperidin-4-one **60** (1 equiv., 0.80 mmol) in toluene (3 mL), in a specific vial, was added benzylhydrazine **61** (2 equiv.). The reaction mixture was sealed and irradiate with microwaves (400 W) at 140 °C for 15 min and then cooled down to 50°C by airflow. When the hydrazone intermediate was achieved, as indicated by MS(ESI), the diazo compound (2.5 equiv.) was added to the resulting mixture, which was sealed again, irradiate with microwaves (400 W) at 140 °C for 15 min and then cooled down to 50°C by airflow. Upon completion, as indicated by MS (ESI), the solvent was evaporated and the obtained crude material was directly purified by semi-preparative HPLC, to yield derivative 5 as white solid.
White solid (yield 43%). mp 68-70°C.
^{1}H NMR (400 MHz, DMSO-d6) δ 9.76 (bs, 1H), 7.82 (dd, J = 8.6, 0.9 Hz, 2H), 7.56-7.46 (m, 5H), 7.44-7.36 (m, 2H), 7.16 (t, J = 7.4 Hz, 1H), 6.24 (s, 1H), 4.41 (s, 2H), 3.46-3.06 (m, 4H), 2.39 (d, J = 17.0 Hz, 1H), 2.24-1.98 (m, 3H), 1.87-1.71 (m, 2H), 1.73 (d, J = 14.0 Hz, 1H), 1.48 (d, J = 15.0 Hz, 1H), 1.20 (s, 3H), 1.08 (s, 3H).
^{13}C NMR (101 MHz, DMSO-d6) δ 212.66, 169.44, 138.90, 131.06, 129.80, 129.53, 128.81, 128.55, 124.27, 118.39, 67.41, 60.79, 58.81, 53.75, 47.60, 47.34, 39.54, 32.89, 29.33, 28.05, 26.33, 25.03.
MS (ESI) [M+H]+ 418.2489; HPLC: t_R = 18.26 min.

General procedure for the preparation of 3,3-dimethyl-13-phenyl-9,12,13-triazadispiro[4.0.56.35]tetradecane-1,14-dione (63a)

A solution of dispiro-piperidine derivative **63** (1 eq, 0.45 mmol) in EtOH (5 mL) and glacial AcOH (1 mL) was treated with a catalytic amount (0.045 mmol) of palladium on activated charcoal (10% Pd basis) in an atmosphere of hydrogen. Upon completion, as indicated by TLC and MS (ESI), the mixture was filtered through celite, washed with fresh EtOH and then concentrated under reduced pressure. The resulting solid residue was directly purified by semi-preparative HPLC to yield the final derivative 63c as a white solid.
White solid (yield 40%). mp 52-53°C.

1H NMR (400 MHz, DMSO-d6) δ 8.70 (bs, 1H), 8.49 (bs, 1H), 7.83-7.77 (m, 2H), 7.44-7.35 (m, 2H), 7.17-7.12 (m, 1H), 6.21 (s, 1H), 3.29-3.19 (m, 3H), 3.12-2.99 (m, 1H), 2.41 (d, J = 17.0 Hz, 1H), 2.22-1.98 (m, 3H), 1.83-1.72 (m, 3H), 1.41 (d, J = 15.2 Hz, 1H), 1.22 (s, 3H), 1.09 (s, 3H).
13C NMR (101 MHz, DMSO-d6) δ 212.74, 169.45, 138.88, 128.57, 124.17, 118.18, 67.83, 61.01, 53.79, 39.56, 39.54, 39.14, 32.89, 29.35, 28.05, 25.64, 24.48. MS (ESI) [M+H]+ 328.2020; HPLC: tR = 15.31 min.

General procedure for the preparation of (S)-9-((5-chlorothiophen-2-yl)sulfonyl)-3,3-dimethyl-13-phenyl-9,12,13-triazadispiro[4.0.56.35]tetradecane-1,14-dione (64)

To a solution of dispiro-piperidine derivative 7 (1 equiv., 0.60 mmol) in THF (8 mL) were added DIPEA (1 equiv.) and the appropriate sulfonyl chloride (1.2 equiv.). The resulting mixture was stirred at room temperature 2-3h. Upon completion, as indicated by TLC and MS (ESI), the solvent was evaporated under reduce pressure. The resulting solid residue was extracted with EtOAc (3x15 mL) and the combined organic layers were washed with water (1x15 mL), brine (1x10 mL), and then dried over Na2SO4. The volatile fraction was then evaporated and the crude solid was purified by semi-preparative HPLC to yield derivative 8 as a white solid.

White solid (yield 51%). mp 166-168°C.

^{1}H NMR (400 MHz, DMSO-d6) δ 7.70-7.65 (m, 2H), 7.61 (d, J = 4.0 Hz, 1H), 7.42 (d, J = 4.0 Hz, 1H), 7.38-7.31 (m, 2H), 7.14-7.08 (m, 1H), 5.99 (s, 1H), 3.59-3.54 (m, 2H), 2.90-2.81 (m, 1H), 2.74-2.63 (m, 1H), 2.38 (d, J = 16.6 Hz, 1H), 2.13-1.94 (m, 3H), 1.86 (d, J = 13.9 Hz, 1H), 1.70-1.58 (m, 2H), 1.34 (d, J =13.7 Hz, 1H), 1.22 (s, 3H), 1.05 (s, 3H).

^{13}C NMR (101 MHz, DMSO-d6) δ 212.85, 169.89, 138.93, 135.42, 134.26, 132.83, 128.73, 128.51, 124.05, 118.15, 67.78, 61.87, 53.75, 42.03, 41.48, 39.26, 32.94, 28.93, 28.06, 27.97, 26.78.

MS (ESI) [M+H]+ 508,1126. HPLC: t_R = 26.16 min.

7.3 BIOLOGICAL EXPERIMENTAL SECTION

7.3.1 Materials and Methods

For *in vitro* experiments, HeLa (human cervical carcinoma), MDA-MB-231 (human breast adenocarcinoma), HCT116 (human colorectal carcinoma), and HaCat (immortalized human keratinocyte) cell lines were employed. Cells were maintained in Dulbecco's Modified Eagle Medium (DMEM) supplemented with 10% fetal bovine serum (FBS), 100 U/mL penicillin, and 100 µg/mL streptomycin to support optimal growth and prevent bacterial contamination. Cultures were routinely washed with phosphate-buffered saline (PBS), and cell viability and counting were assessed using Trypan Blue exclusion in conjunction with a Bürker counting chamber. All cell lines were cultured under standard conditions at 37 °C in a humidified atmosphere containing 5% CO_2.

Plasticware employed included filter-cap flasks for cell culture and growth, Eppendorf tubes and micropipettes of various volumes for cell transfer, and multiwell plates for biological testing. As reference compounds, MG132, Pimozide, and DMSO were used. Fluorogenic diagnostic probes B1 and B2, synthesized in-house, were employed to assess proteasome activity. Fluorescence analysis was carried out using a BD FACSCanto II flow cytometer.

7.3.2 Calculation of Activity Values

Each compound was tested in triplicate. The activity percentages were calculated as the arithmetic mean of the three values obtained for each experiment and each compound. The activity of the proteasome in the presence of DMSO was considered as 100%, and all other values were normalized relative to this reference. In this case, the percentage values obtained from the runs are reported directly in the tables, as they were originally provided in this format.

Compounds	**% proteasome activity calculated for every experiment**			
	First experiment	*Second experiment*	*Third experiment*	*Dev. ST*
GMR5	144	125	110	17,03917
GMR8	159	107	140	26,31223
GMR9	186	117	132	36,29049
GMR71	128	116	130	7,571878
GMR86	110	133	146	18,23001
TRAP6	129	162	117	23,30236
TRAP10	140	111	120	14,84363

MF1024	190	185	117	40,7799
MF3053	139	146	148	4,7258

Table 9. % proteasome activity obtained for the first class of compounds in all experimental runs on HeLa cells.

Compounds	**% proteasome activity calculated for every experiment**			
	First experiment	*Second experiment*	*Third experiment*	*Dev. ST*
GMR5	*122*	*102*	*96*	13,61372
GMR8	*124*	*161*	*117*	23,64318
GMR9	*142*	*127*	*108*	17,03917
GNR71	*137*	*112*	*132*	13,22876
GMR86	*154*	*153*	*143*	6,082763
TRAP6	*190*	*182*	*133*	30,8599
TRAP10	*147*	*131*	*146*	8,962886
MF1024	*122*	*152*	*120*	17,92577
MF3053	*395*	*288*	*228*	84,59511

Table 10. % proteasome activity obtained for the first class of compounds in all experimental runs on MDA cells.

Compounds	**% proteasome activity calculated for every experiment**			
	First experiment	*Second experiment*	*Third experiment*	*Dev. ST*
GMR5	88	95	120	16,8226
GMR8	113	89	136	23,50177
GMR9	142	137	104	20,64784
GMR71	123	77	80	25,73584
GMR86	111	109	104	3,605551
TRAP6	124	136	155	15,63117
TRAP10	104	138	199	48,13523
MF1024	125	120	119	3,21455
MF3053	183	217	238	27,75488

Table 11. % proteasome activity obtained for the first class of compounds in all experimental runs on HCT cells.

Compounds	**% proteasome activity calculated for every experiment**			
	First experiment	*Second experiment*	*Third experiment*	*Dev. ST*
GMR5	160	116	150	31,3529
GMR8	80	96	143	10,93034
GMR9	68	101	86	23,64832
GMR71	106	100	142	4,77064
GMR86	104	151	123	69,42268
TRAP6	142	88	110	38,1259
TRAP10	90	109	163	13,19779
MF1024	93	101	122	14,97776
MF3053	226	208	455	137,7038

Table 12. % proteasome activity obtained for the first class of compounds in all experimental runs on HaCat cells.

8 PROJECT 3: SYNTHESIS OF MULTIVALENT MOLECULE FOR A NEW THERAPEUTICAL APPROCH OF NEURODEGENERATIVE DISEASES

During the second year of the doctoral program, a research stay was carried out at the laboratory of the Universidad de Alcalá, where it was possible to investigate a novel potential therapeutic approach for the treatment of neurodegenerative diseases.

Although **Alzheimer's disease** (AD) and **Parkinson's disease** (PD) have different origins and characteristics, both are neurodegenerative disorders that affect cognitive and motor functions, leading to the *progressive loss of cholinergic and dopaminergic neurons*.[209] These diseases involve the *abnormal accumulation of proteins* in the brain and are influenced by both *genetic* and *environmental factors*.[210] They also share a **multifactorial nature**,[211] which makes multitarget drug strategies a promising therapeutic approach. However, most importantly, no cure is currently available; existing treatments can only **alleviate symptoms**.[212]

PHARMACOLOGICAL THERAPIES OF NEURODEGENERATIVE DISEASES [213]

Current therapeutic strategies for *Alzheimer's disease* (AD) and *Parkinson's disease* (PD) primarily aim to manage symptoms rather than modify the underlying disease processes.

In AD, two main classes of drugs have received regulatory approval: **cholinesterase inhibitors**—which include naturally derived, synthetic, and hybrid analogues—and **N-methyl-D-aspartate (NMDA) receptor antagonists**.[214]

Specifically, the first class is designed to inhibit the degradation of acetylcholine (ACh), a crucial neurotransmitter in the central nervous system, whose transmission is markedly reduced under pathological conditions, including the progression of Alzheimer's disease.[215] Indeed, the cholinergic system—which encompasses nicotinic and muscarinic ACh receptors, the vesicular ACh transporter, butyrylcholinesterase (BuChE), acetylcholinesterase (AChE), and choline acetyltransferase—undergoes significant alterations during aging and in various age-related disorders, particularly AD.[216]

Among these drugs are *Rivastigmine*, a dual cholinesterase inhibitor, and *Neostigmine*, a longer-acting anticholinesterase (*Figure 32*).[217,218]

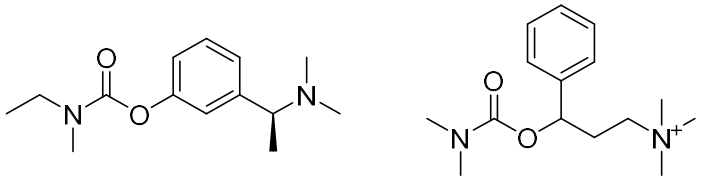

Rivastigmine **Neostigmine**

Figure 32. General chemical structure of Rivastigmine and Neostigmine.

Conversely, excessive activation of N-methyl-D-aspartate receptors (NMDARs) results in elevated calcium (Ca^{2+}) influx, which contributes to neuronal death and synaptic dysfunction. NMDAR antagonists counteract this process by preventing receptor overactivation and the subsequent Ca^{2+} overload, thereby helping to restore normal receptor function.[219]

Within this latter class, *Memantine* represents the primary therapeutic agent, often administered in combination with acetylcholinesterase inhibitors. It acts by blocking the NMDA receptor subtype of glutamate receptors, thereby preventing their overactivation and supporting the restoration of normal glutamatergic signaling (*Figure 33*).[220]

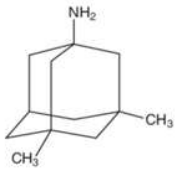

Memantine

Figure 33. General structure of Memantine.

Despite their therapeutic effects, these two classes of drugs are effective only in treating AD symptoms, but do not cure or prevent the disease.[221]

Similarly, therapies for Parkinson's disease (PD) are primarily aimed at restoring dopaminergic function. The main pharmacological treatments currently employed include **Levodopa**, a dopamine precursor typically administered in combination with peripheral dopa-decarboxylase inhibitors (such as Carbidopa or Benserazide), as well as **dopamine agonists**, including Pramipexole and Ropinirole (*Figure 34*).[222,223]

They effectively alleviate motor symptoms, yet they fail to address the fundamental neurodegenerative mechanisms. Prolonged administration of these drugs may also lead to adverse outcomes, including dyskinesias—characterized by abnormal involuntary movements—and fluctuations in symptom control. [224]

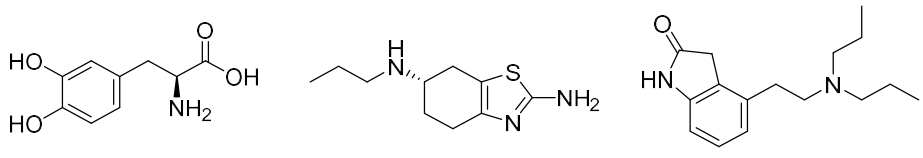

L-DOPA **Pramipexole** **Ropinirole**

Figure 34. General structure of pharmaceutical drugs now on therapy.

Consequently, research efforts have increasingly focused on identifying novel therapeutic strategies to enhance the management and slow the progression of these neurodegenerative disorders, which share overlapping pathophysiological mechanisms.[225,226]

Recently, **epigenetic therapy** has emerged as a promising therapeutic approach, showing great potential through the use of *histone deacetylase (HDAC) inhibitors* and other *epigenetic enzyme modulators*.[227]

8.1 EPIGENETIC MECHANISM

Epigenetic mechanisms encompass processes that modulate gene expression without altering the underlying DNA sequence. By regulating chromatin accessibility, these mechanisms can either promote or suppress transcriptional activity. When chromatin adopts a compacted configuration (heterochromatin), transcription is impeded, whereas a more relaxed structure (euchromatin) facilitates access of the transcriptional machinery to DNA.[228] Chromatin dynamics, in turn, are influenced both by intrinsic features of the DNA sequence and by post-translational modifications (PTMs) of histone proteins within the nucleosome.[229]

Consequently, epigenetic modifications encompass three principal mechanisms: DNA methylation, histone modifications, and noncoding ribonucleic acids (ncRNAs).[230] These modifications are enzymatically reversible and play diverse roles in both normal human physiology and disease pathophysiology.

8.2 HDAC INHIBITORS

Reversible histone acetylation and deacetylation play a central role in the regulation of gene expression. These processes are catalyzed by *histone acetyltransferases* (HATs) and *histone deacetylases* (HDACs), respectively [231,232]. Small-molecule HDAC inhibitors are important modulators of transcription, as they shift the cellular equilibrium towards a state of hyperacetylation. In neurodegenerative diseases, the homeostasis of histone acetylation is markedly disrupted, resulting in hypoacetylation. [233] The hyperacetylation induced by direct HDAC inhibition has been shown to exert neuroprotective effects.[234]

Histone deacetylases (HDACs) remove acetyl groups from histones, thereby promoting a more compact chromatin structure. They function as components of co-repressor complexes and are known to regulate multiple essential biological processes, including cell proliferation, differentiation, and development, through their interactions with various transcription factors and transcriptional co-regulators.[235]

HDACs are well characterized and grouped into four major classes based upon their homology to yeast histone deacetylases. The first class is made by HDACs *1,2,3* and *8*, that are predominantly localized in the nucleus and share homology with the yeast transcriptional regulator Rpd3 (reduced potassium deficiency 3) [236]. HDACs 1,2 and 3 are involved in cell proliferation and death [237], while HDAC 8 is found to be expressed in smooth muscle and plays a key role in muscle contractility.

The Class II HDACs share similarity with yeast Histone Deacetylase 1 (HD1) proteins and are further grouped into class IIa and Class IIb based on their structural features. The Class IIa includes HDACs *4*,*5*, *7*, and *9*, while Class IIb includes HDAC *6* and *10*. These HDACs have been found to travel back and forth between the nucleus and cytoplasm and seem to have a role in tissue specific developmental activities.[238]

Class IV includes only one atypical HDAC isoform 11: it is well expressed in the kidneys, testis and brain. HDAC11 has been identified to deacetylate histones along with some non-histone proteins, namely a nuclear hormone receptor, transcription factors and cytoskeletal elements.[239]

The Class I, II, and, IV HDACs are *zinc-dependent* and known as "classical" HDACs. In contrast, class III HDACs, commonly called sirtuins (SIRT 1-7), function as NAD-dependent HDACs and are similar to yeast SIR 2 (Silent Information Regulators 2). [240] Sirtuins are involved in regulation of metabolism, stress responses and aging.[241]

As shown in *Figure 35*, a general classification of HDAC enzymes is presented.

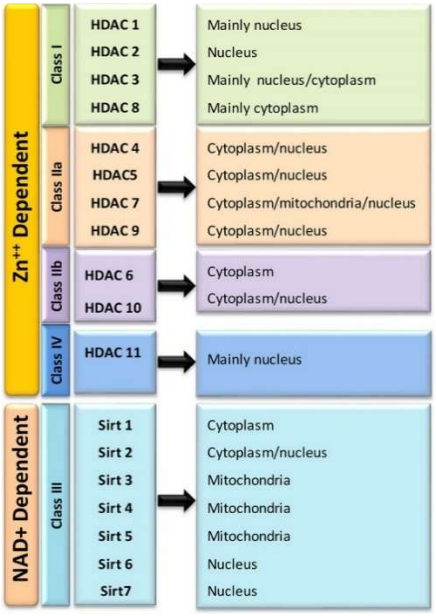

Figure 35. General classification of HDACs enzymes.

In recent years, **histone deacetylase inhibitors** (HDACi) have attracted considerable therapeutic interest. Initially, research focused primarily on the development of HDACi as *anticancer agents*.[242]

Several HDAC inhibitors, including **butyrate, trichostatin A** (TSA), **suberoylanilide hydroxamic acid** (SAHA), and **MS-275**, have been shown to inhibit cell proliferation and promote differentiation in various in vitro cancer models, including leukemia.

Notably, **SAHA (vorinostat, brand name Zolinza)** became the first HDACi approved by the FDA for the treatment of *cutaneous T-cell lymphoma*.

Currently, multiple HDACi are currently undergoing Phase I and Phase II clinical trials for cancer therapy,[243] and a summary of HDACi have been used in clinical trials for both neurological and oncological therapeties.

More recently, interest in HDACi has expanded to non-malignant disorders affecting the nervous system [244,245].

Targeting HDACs with HDACi holds therapeutic potential for a range of **neurological disorders**, including Huntington's disease, Alzheimer's disease, amyotrophic lateral sclerosis, seizure disorders, spinal muscular atrophy, Rett syndrome, stroke, Fragile X syndrome, and Rubinstein-Taybi syndrome. [246]

Histone deacetylase inhibitors (HDACi) have also shown considerable promise in the treatment of various psychiatric disorders, such as depression, drug addiction, schizophrenia, and anxiety disorders [247,248].

Under physiological conditions, the activities of histone acetyltransferases (HATs) and histone deacetylases (HDACs) are finely regulated within neuronal cells to maintain acetylation homeostasis. [249]

In *neurodegenerative disorders*, this delicate equilibrium is disrupted, leading to histone hypoacetylation. Pharmacological inhibition of HDACs restores hyperacetylation and has been associated with neuroprotective outcomes.

Beyond their ability to induce histone hyperacetylation, the neuroprotective properties of HDAC inhibitors are likely mediated through multiple mechanisms, including the activation of kinase signaling pathways in response to extracellular stimuli,[250] suppression of pro-apoptotic factors,[251] and attenuation of microglia-driven neuroinflammation,[252] as exemplified by the effects of valproic acid.

Accordingly, HDACs have emerged as compelling therapeutic targets for both neurological and psychiatric conditions. In preclinical studies, HDAC inhibition has been associated with a range of beneficial outcomes, such as enhanced neuroprotection and neurogenesis following traumatic brain

injury and ischemia, [251] restoration of learning and memory in neurodegeneration models,[253] promotion of neuronal differentiation and synaptic plasticity,[254] and the induction of antidepressant-like behaviors.[255]

8.3 HDACs INHIBITORS IN NEURODEGENERATIVE DISEASES

Recent evidence suggests that histone deacetylase inhibitors (HDACis) may offer promising therapeutic opportunities for the treatment of neurodegenerative disorders. Indeed, HDACs play a crucial role in neuronal survival, and alterations in their normal activity have been associated with cellular dysfunction and neurodegeneration.

8.3.1 HDACs INHIBITORS IN PARKINSON'S DISEASE

Although the pathogenesis of Parkinson's disease (PD) has not yet been fully elucidated, substantial evidence indicates that dopaminergic neuronal loss, [256-258] α-synuclein aggregation [259], metal ion accumulation [260], and oxidative stress [261] are key contributors to its development (Figure 36) [262]. Moreover, transcriptional dysregulation is frequently observed during the onset and progression of various neurodegenerative disorders of the central nervous system (CNS), including PD[263]. In this context, histone deacetylases (HDACs)—a major class of epigenetic regulators involved in transcriptional control—play a pivotal role in chromatin remodeling and gene expression by modulating histone acetylation status, and are therefore likely to participate in the pathogenic mechanisms underlying PD.[264]

For instance, HDACs and their associated epigenetic regulatory mechanisms have been proposed as potential therapeutic targets in PD [265-267]. Notably, a significant upregulation of HDAC2 expression has been observed in the microglial cells of the substantia nigra in individuals with PD. [268]
Among the 18 mammalian HDACs identified, individual isoforms exhibit distinct functional roles, exerting either neuroprotective or neurotoxic effects [269]. For example, activation of HDAC1 promotes neuroprotective activity in human neuronal models of neurodegeneration, but its interaction with HDAC3 looks like to contribute to a neurotoxic effect[270]; on the other hand, several Class II HDACs have been reported to exerto [271].

In particular, HDAC6 have been widely involved in neurodegeneration. Indeed, a transcriptome study of clinical PD samples gave a 1.6-fold higher level of HDAC6 expression in models of PD and a 1.65-fold higher level of histone acetyltransferase1 (HAT1) expression[272,273], consistent with elevated H3 histone acetylation levels reported in the above studies. [274,275]

In conclusion, current evidence indicates that HDAC1–3 and HDAC6 exert predominantly neurotoxic effects, whereas HDAC7, HDAC9, and HDAC10 appear to play neuroprotective roles based on their expression patterns in the brain.

Figure 36 provides a general summary of the HDACs involved in Parkinson's disease.

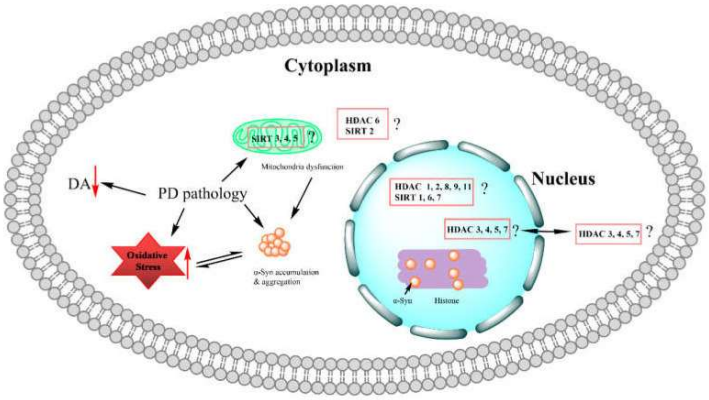

Figure 36. PD pathology and localizations of histone deacetylases. Current knowledge about the PD pathology mainly includes dopamine (DA) decrease, α-synuclein aggregation, oxidative stress, and mitochondrial dysfunction; whether histone deacetylases are linked with this pathogenesis in PD still remains to be explored and illustrated. This leaves a question mark for every histone deacetylase.

In a mouse model of PD induced by the dopaminergic toxin MPTP, treatment with the histone deacetylase (HDAC) inhibitor phenylbutyrate significantly attenuated dopamine loss and the degeneration of tyrosine hydroxylase–positive neurons in the substantia nigra.[276] Mutations in presynaptic α-synuclein are associated with familial forms of PD,[277] and α-synuclein has been shown to mediate neurotoxicity, with its cytoplasmic sequestration exerting protective effects in both cell culture and transgenic *Drosophila* models. Notably, HDAC inhibitors such as *Vorinostat* and *sodium butyrate* mitigate α-synuclein–induced toxicity and neuronal death in these models. [278]

Since an imbalance in lysine acetylation of both histone and non-histone proteins, together with the dysregulation of various histone deacetylase (HDAC) isoforms, may contribute to PD pathogenesis, considerable research efforts have been directed toward developing HDAC inhibitors for PD therapy (Figure 2) [279-283]. **Valproic acid**, a broad-spectrum (pan-) HDAC inhibitor, was among the first compounds shown to protect dopaminergic neurons and to mitigate lipopolysaccharide (LPS)-induced dopaminergic neurotoxicity in cellular models. [284,285]

Similarly, **sodium butyrate**, another pan-HDAC inhibitor structurally related to valproic acid, has been shown to exert beneficial effects against 6-OHDA–induced neurotoxicity and associated behavioral abnormalities. [286,287]

Suberoylanilide hydroxamic acid (SAHA), an HDAC inhibitor approved for cancer therapy, has been investigated for potential application in Parkinson's disease. In vitro PD models have shown that SAHA protects dopaminergic neurons from neurotoxin-induced damage. [288]

Collectively, these findings suggest that pan-HDAC inhibitors may exert a neuroprotective effect in PD. [289]

In parallel, **selective HDAC inhibitors** have been explored as potential therapeutic agents, highlighting the importance of targeting specific isoforms for improved efficacy and safety.

Selective HDAC inhibitors have shown promising neuroprotective effects in Parkinson's disease models. For example, **RGFP109**, which targets HDAC1 and HDAC3, alleviated L-DOPA–induced dyskinesia in MPTP-lesioned marmosets.[290] Similarly, the HDAC1/2 dual inhibitor **K560** and its derivative **K-856** demonstrated protective effects in both cellular and animal models of PD. [291,292]

Comparisons between Class I and Class II inhibitors indicated that inhibition of Class I HDACs, such as with **MS-275**, can prevent neuronal cell death by blocking HDAC3 binding, whereas Class IIa inhibition with LMK235, which selectively targets HDAC4 and HDAC5, protected dopaminergic neurons and prevented axonal degeneration caused by wild-type or A53T-mutant α-synuclein. [293,294]

These findings highlight the potential of isoform-selective HDAC inhibition as a therapeutic strategy in PD.

As illustrated in *Figure 37*, the HDAC inhibitors are presented.

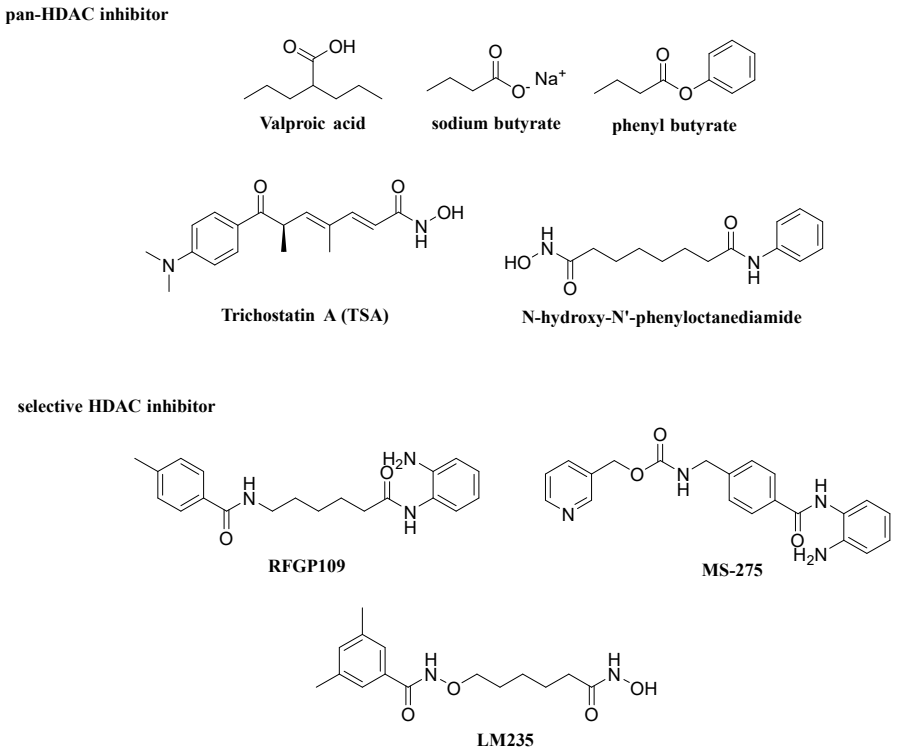

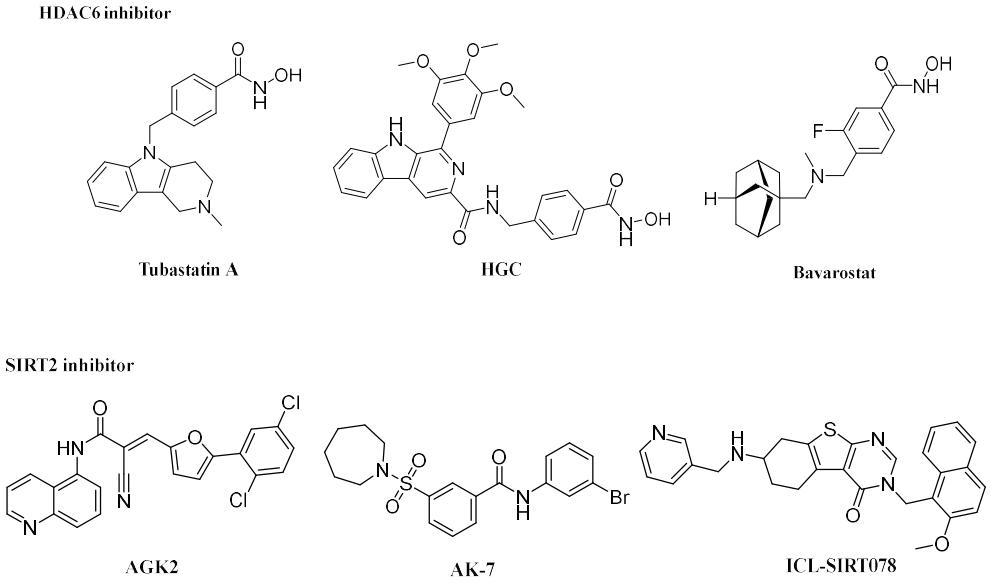

Figure 37. The structures of representative inhibitors of histone deacetylases used in PD study.

8.3.2 HDACs INHIBITORS IN ALZHEIMER'S DISEASE

Alzheimer's disease (AD) is the most common neurodegenerative disorder, accounting for 60–70% of dementia cases worldwide. [295] This progressive and irreversible condition is marked by gradually worsening memory loss, cognitive decline, and mood disturbances, which collectively lead to a profound deterioration in daily functioning. [296]

Alzheimer's disease (AD), a highly complex neurodegenerative disorder, is primarily characterized by two histopathological hallmarks: extracellular senile plaques composed of amyloid-beta (Aβ) aggregates and intraneuronal neurofibrillary tangles (NFTs) formed by hyperphosphorylated tau protein. [297,298]

The accumulation of these proteins disrupts neuronal connectivity, ultimately leading to cell death and brain atrophy. As the disease progresses, these pathological changes trigger additional cellular and molecular disturbances, including neuroinflammation, oxidative stress, excitotoxicity, blood–brain barrier dysfunction, and deficits in neurotransmitters such as acetylcholine. Collectively, these processes drive synaptic dysfunction and neuronal injury, underpinning the cognitive decline and clinical symptoms observed in AD patients. [299]

Several hypotheses have been proposed to explain the aetiology of Alzheimer's disease (AD) (Figure 1a–c). The most prominent include the amyloid cascade hypothesis, tau protein post-translational modifications (PTMs), chronic neuroinflammation, and dysfunction of cholinergic and glutamatergic

neurotransmission. Individually or in combination, these mechanisms contribute to the extensive neurodegeneration characteristic of AD.

While much research has focused on genetic factors in AD, growing evidence suggests that epigenetic dysregulation also contributes to its pathogenesis and progression. [299-301] Among epigenetic regulators, histone deacetylases (HDACs), which modulate gene transcription through chromatin remodeling, have been frequently implicated. The following discussion examines their potential role and impact in AD. [302]

Altered acetylation of non-histone proteins, such as α-tubulin, Hsp90, cortactin, c-fos, tau, and BDNF, is strongly linked to Alzheimer's disease, affecting processes like cell morphology, oxidative stress response, migration, and autophagy. [303,304]
Imbalances in HDAC levels and acetylation dynamics negatively impact learning and memory. [305] Moreover, reduced histone acetylation in AD and other neurodegenerative disorders is associated with decreased transcription of genes essential for cognitive function. [306-309]

The expression and distribution of HDACs vary across different regions of the human brain, directly influencing neuronal plasticity, memory, and behaviour. The first assessment of neuroepigenetic regulation in healthy individuals revealed that class I HDAC expression is higher in cortical grey matter than in white matter. Within grey matter, HDAC expression levels are lower in the hippocampus and amygdala, but higher in the putamen and cerebellum. Moreover, the expression profile of HDAC isozymes is altered in Alzheimer's disease.
For instance, in a study conducted on postmortem hippocampal samples from human brains, Graff et al. reported that while the expression levels of HDAC1 and HDAC3 remained unchanged, HDAC2 expression was significantly elevated, particularly during the early stages of the disease. [306]

Conversely, a study by Mahady et al. reported significantly increased expression of HDAC1, HDAC3, HDAC4, and HDAC6 across most stages of Alzheimer's disease in postmortem human frontal cortex samples. In contrast, HDAC2 expression showed no significant change, while SIRT1 expression was consistently reduced at all disease stages. [295]
These findings contrast with those reported by Anderson et al., who investigated the same brain region in human subjects. In their study, HDAC1 and HDAC2 expression levels were reduced by approximately 32%, whereas HDAC5 and HDAC6 expression increased by 47% and 31%, respectively, compared with control samples. [310]

Given the implication of epigenetic dysregulation in various neurological and psychiatric disorders, including Alzheimer's disease, HDACs have emerged as potential therapeutic targets. [287] As previously noted, histone acetylation is reduced in AD, contributing to several deleterious cellular mechanisms. Consequently, increasing research efforts are focusing on the use of HDAC inhibitors (HDACi) to restore acetylation levels and improve cognitive function, generating considerable scientific interest. [309]

HDAC inhibitors (HDACi) differ in their chemical structure, selectivity, and biological activity. Most currently available HDACi act as nonspecific, or pan-HDAC, inhibitors targeting all HDAC isozymes. In contrast, selective HDACi may inhibit multiple isozymes within a single class or act on a specific HDAC isoform only.

However, despite their promising potential, no HDACi have yet reached the market for central nervous system (CNS) disorders, with valproic acid representing the only exception. [285]

Figure 38 presents the HDAC inhibitors along with their selectivity.

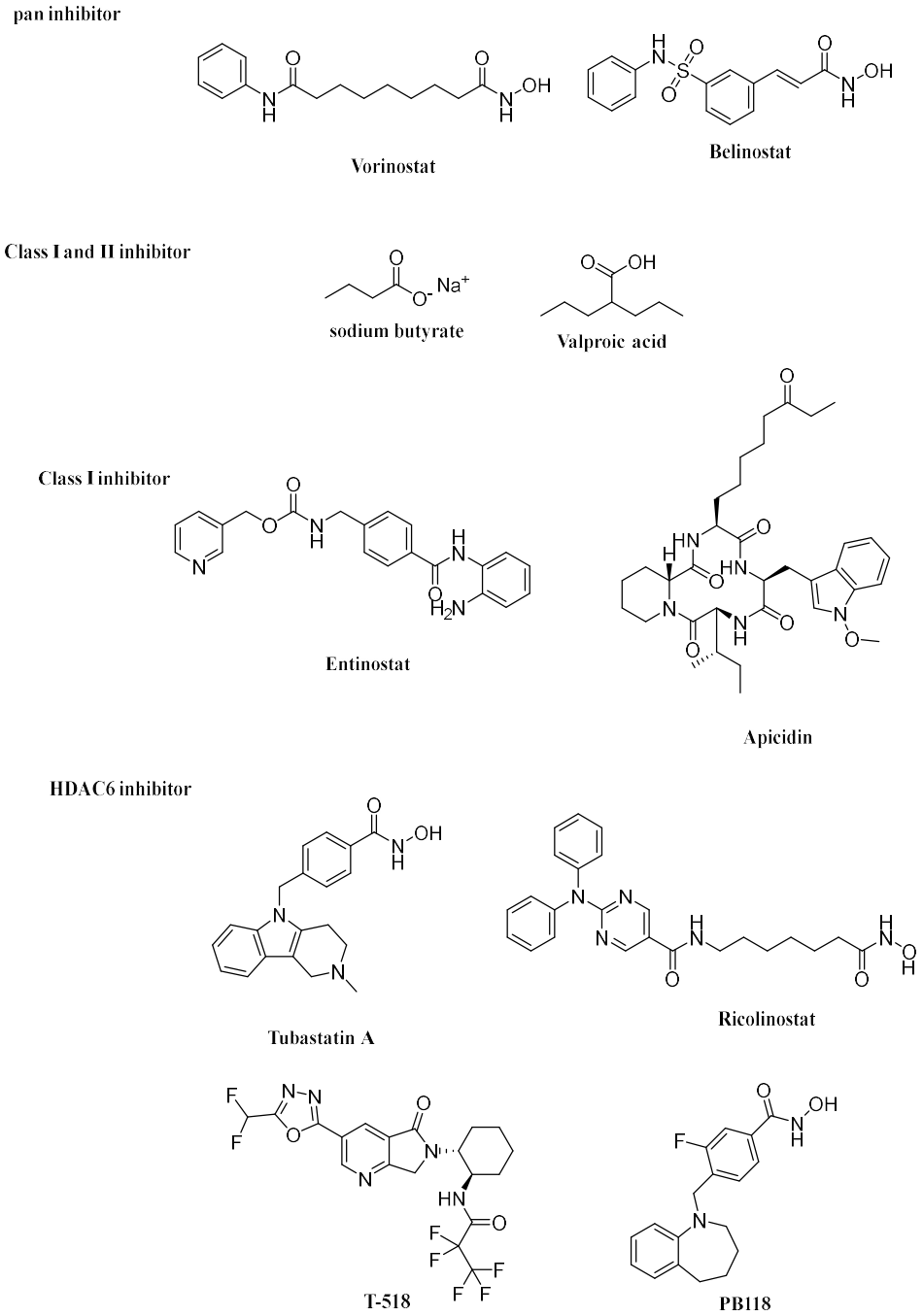

Figure 38. *The structures of representative inhibitors of histone deacetylases used in AD study.*

As previously reported, HDACi exhibit significant neuroprotective properties, positioning them as promising candidates for CNS disease therapy, due to the fact in preclinical studies, HDACi have been shown to exert neuroprotective effects, [311,312] restore learning and memory functions, promote neurogenesis and synaptic plasticity, enhance neuronal differentiation, and reduce oxidative stress. [313]

Several of these HDAC inhibitors (HDACi) have shown promising neuroprotective effects in Alzheimer's disease (AD) models. The selective HDAC6 inhibitors **Tubastatin A** and **ricolinostat**

(ACY-1215) improved behavioural deficits in AD mouse models, while the novel HDAC6 inhibitor PB118 enhanced microtubule stability, prevented neurofibrillary tangle formation, reduced Aβ production, and suppressed neuroinflammatory cytokines and chemokines in microglial and 3D human neural culture models. [314]

Valproic acid, a class I and II HDACi, demonstrated neuroprotective properties by promoting cell proliferation, increasing immature neuron density in the hippocampal dentate gyrus, and improving learning and memory in 3xTg-AD mice. [315] Similarly, **sodium butyrate** reduced amyloid-β plaque formation, while chronic administration of trichostatin A, another class I and II HDACi, decreased Aβ plaques and oligomers and ameliorated both short- and long-term cognitive deficits in APP/PS1 mice. [316]

On the other hand, the class I inhibitors **Entinostat** and **Apicidin** reduced Aβ accumulation, improved cellular function, and alleviated memory deficits through anti-inflammatory, antioxidant, and neuroprotective mechanisms. [317-319] Likewise, the class III inhibitor nicotinamide restored cognitive performance in 3xTg-AD mice by reducing tau phosphorylation and enhancing microtubule stability. [320]

8.4 NEW THERAPEUTICAL STRATEGY FOR NEURODEGENERATIVE DISEASES: MULTIVALENT DRUGS

Currently, research is highly active in the design and synthesis of novel molecules that may offer innovative strategies for the treatment of neurodegenerative diseases. Among these emerging approaches, the concept of **multivalent drugs** is emerging as particularly promising.

A **multivalent drug** is a therapeutic agent that can simultaneously bind to multiple sites or receptors on a cell surface, leading to stronger interactions and more potent effects than its single-binding counterparts.[321]

This strategy represents a highly promising approach in drug development, as it facilitates the design of a single therapeutic agent capable of simultaneously engaging multiple biological targets. Such an agent may provide both symptomatic relief and disease-modifying effects, thereby consolidating the benefits typically achieved through the administration of multiple medications into a single, more effective intervention.

This approach has the potential to enhance patient adherence, reduce the complexities associated with polypharmacy, and enable a more comprehensive management of multifactorial neurodegenerative disorders.

Drugs developed through this approach offer several notable advantages, including enhanced therapeutic efficacy, a reduced risk of toxicity, the avoidance of excessive suppression or overactivation of specific biological pathways, and improved patient adherence, ultimately contributing to a better overall quality of life. [322-324]

However, this approach is not without limitations. Multivalent ligands often exhibit larger molecular sizes, which can reduce bioavailability, and may display increased lipophilicity, leading to higher clearance rates. Additionally, the identification of suitable biological targets remains challenging. [324]

Although no rationally designed multi-target-directed ligand (MTDL) has yet obtained clinical approval, several hybrid molecules have demonstrated promising results in in vitro studies. [325]

In the last years, different multivalent molecules have been synthesized presenting the combination of different activities, as Cholinesterase and Aβ aggregation inhibition [326], AChE/BuChE inhibition, Aβ aggregation inhibition and anti-neuroinflammatory activity [327], ChE inhibitors, Aβ aggregation inhibitors and antioxidant [328,329].

Un example of drug that is actually on clinical phases, is **Vafidemstat**, produced by the Spanish company ORYZON: it (ORY-2001) is an oral small molecule that has been optimized for CNS

indications and that acts as a covalent inhibitor of the epigenetic enzyme Lysine Specific Demethylase-1, LSD1 (KDM1A).
The mechanism of action of this drug operates on multiple levels. It mitigates cognitive impairment, attenuates neuroinflammation, and exerts neuroprotective effects. [330]
In animal models, Vafidemstat not only restores memory function but also normalizes the heightened aggressiveness observed in SAMP8 mice, a model of accelerated aging and Alzheimer's disease (AD), while reducing social avoidance and enhancing sociability in rodents. Additionally, it demonstrates rapid, robust, and sustained efficacy in several preclinical models of multiple sclerosis (MS), where it diminishes neuroinflammation, modulates glial activity, provides neuroprotection, and preserves axonal integrity. [331]
The principal target of this drug is enzyme Lysine Specific Demethylase-1 (also called KDM1A): LSD1 plays a fundamental role in neurogenesis, neuronal differentiation and axonal navigation. LSD1 is the most abundant Lysine Demethylase in the prefontal cortex.
KDM1A plays multiple crucial roles in the brain: in fact, its activity is related to regulation of transcription, and its modulation can alleviate neuroinflammation and cognitive impairment. [332-334]

On the other hand, this compound exhibited strong inhibitory activity toward MAO-B. These enzymes catalyze the oxidative deamination of various monoamines and regulate key neurotransmitters such as dopamine, serotonin, and norepinephrine in the brain. Under physiological conditions, dopamine is mainly metabolized by MAO-A; however, with aging, MAO-B becomes the predominant enzyme responsible for this process. Indeed, several MAO-B inhibitors, such as rasagiline and selegiline, are currently used in the symptomatic treatment of Parkinson's disease.[335,336]
Vafidemstat is actually on III phase for treatment for psychiatric conditions like Borderline Personality Disorder (BDS), representing one of the first multivalent drugs.

Another particularly interesting therapeutic target is the inhibition of HDAC6, which appears to be overexpressed under pathological conditions, as previously mentioned in *paragraph 8.3.1* and *8.3.2*. One compound that has shown effective HDAC6 inhibition is **Tubastatin A**, which has demonstrated promising potential in reducing neuroinflammation.[337]

Concurrently, Paweł Zajdel and colleagues demonstrated that combining 5-HT6 receptor antagonism with D3 dopamine receptor (D3R) blockade in a single compound holds significant potential for the treatment of neurodegenerative diseases such as Alzheimer's and Parkinson's. This dual action confers neuroprotective effects, modulates neurotransmission, and improves cognitive function.[338,339]

The **5-HT6 receptor**, predominantly localized in brain regions associated with memory and learning, when blocked by antagonists, enhances the release of neurotransmitters such as acetylcholine and glutamate. This leads to improved synaptic signaling and neuronal plasticity, which may help counteract the cognitive deficits associated with Alzheimer's disease.[340]

On the other side, the **D3 dopamine receptor** (D3R) is primarily expressed in limbic brain regions associated with cognition and emotional behaviour. [341] D3R antagonists enhance dopaminergic signaling, which is particularly relevant in Parkinson's disease, where the loss of dopaminergic neurons contributes to both motor and cognitive symptoms. [342] Furthermore, these antagonists can activate intracellular signaling pathways that promote neuronal survival and neurogenesis, including the cyclin-dependent kinase 5 (Cdk5) and mammalian target of rapamycin (mTOR) pathways.[343,344]

The design of multivalent drug candidates represents a promising and increasingly influential frontier in the therapeutic landscape of neurodegenerative diseases. By engineering a single molecular entity capable of engaging multiple pharmacological targets implicated in disease onset and progression, it becomes possible to integrate symptomatic relief with a preventive therapeutic strategy. Such an approach holds particular promise when these targets converge on epigenetic mechanisms that govern neuronal resilience and vulnerability. Through the simultaneous modulation of complementary pathways, a multivalent compound may not only attenuate clinical manifestations but also intervene upstream in the molecular cascade that initiates and perpetuates neurodegeneration, thereby offering a more holistic and potentially transformative therapeutic paradigm.

8.5 AIM OF THE THESIS

Neurodegenerative diseases are currently among the most prevalent pathologies worldwide. These multifactorial disorders pose significant challenges for therapeutic intervention. At present, available treatments are primarily symptomatic, aiming to alleviate or manage clinical manifestations without halting disease progression or providing a preventive effect against neurodegeneration.

One strategy that has garnered increasing attention is the modulation of epigenetic mechanisms to prevent neurodegenerative processes. In particular, inhibitors of histone deacetylases (HDACs) have emerged as promising candidates in this context.

Another innovative therapeutic approach involves the design of multivalent molecules, which incorporate multiple pharmacophores to target different biological pathways simultaneously. Such molecules offer a unique opportunity to integrate symptomatic treatment with epigenetic modulation within a single compound, potentially applicable to both Alzheimer's and Parkinson's diseases.

During my thesis, I had the opportunity to conduct a research period in the laboratory of Professor Isabel Iriepa Canalda at the Universidad de Alcalá, collaborating on the development of a multivalent molecule as an innovative approach for neurodegenerative disorders.

The work aimed to develop and evaluate a new therapeutic approach for these pathologies, which currently lack treatments capable of substantially improving patients' quality of life.

The group with which I conducted my research collaboration at the University of Alcalá (Madrid) had published an article describing a novel molecule, **Contilisant**. This compound demonstrated strong multivalent activity, combining monoamine oxidase B (MAO-B) inhibition with histamine H3 receptor (H3R) antagonism, resulting in beneficial effects on dopamine regulation, representing a new opportunity for the treatment of Parkinson's disease (*Figure 39*). [345, 346]

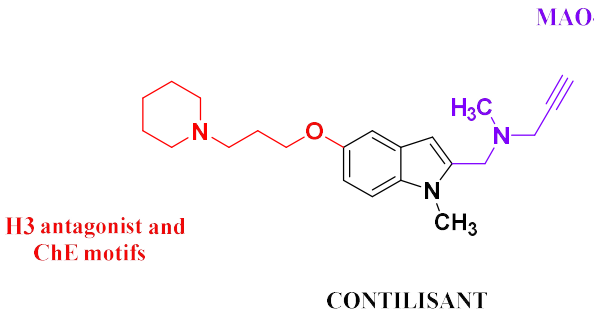

Figure 39. General structure of pharmacophoric points in Contilisant.

Contilisant has been shown to possess neuroprotective, non-toxic, antioxidant, and cell-permeable properties, exhibiting satisfactory in vitro pharmacological activity on selected biological targets

and effectively restoring LPS-induced cognitive impairment in an in vivo NRO test, an established animal model of Alzheimer's disease. These findings suggest the potential utility of H3R antagonists/inverse agonists for addressing AD-related cognitive deficits. However, despite their promise, clinical trials targeting H3R as a single target have (so far) been unsuccessful. [347]
The (piperidinopropyloxy)phenyl motif, present in compounds such as I (Figure 1), has been reported to confer antagonist properties at the Sigma 1 receptor (S1R). [348] S1R is involved in a wide range of biological processes, including Ca^{2+} signaling at the endoplasmic reticulum (ER), regulation of K^+, Ca^{2+}, Cl^-, and Na^+ ion channels at plasma and organelle membranes, maintenance of ER–mitochondria communication, and modulation of transcription factors. [349] Its role in learning and memory is well established, and S1R agonists have demonstrated antiamnesic effects across diverse pharmacological and pathological models, likely through enhancement of glutamatergic and cholinergic synapses and trophic factor activity, which are critical for memory processes. [350]
Several ligands with varying S1/2R affinities and agonist/antagonist profiles have been described in the past decade, [351-353] including donepezil, [354] although clear structure–activity relationship trends remain limited. S1R is also expressed in CNS structures involved in central sensitization mechanisms implicated in neuropathic pain. [355]
Contilisant has been confirmed as a permeable antioxidant with significant neuroprotective activity against multiple AD-relevant insults. As a novel tetratarget indole, it combines inhibitory activity against neurotransmitter-catabolizing enzymes (ChE, MAO) and H3R with high-affinity, selective agonism at S1R. This compound significantly restored $A\beta_{1-42}$-induced cognitive deficits in the radial arm-maze assay in an in vivo AD model, performing comparably or favorably relative to donepezil.[346]

Starting from the considerable pharmacological potential of Contilisant, the research group focused on elucidating the structural features of the molecule that could be optimized to enhance its biological activity. Through structure–activity relationship (SAR) studies on both Tubastatin A and Contilisant, correlations were established between target-specific activity and the presence as well as the spatial arrangement of distinct functional groups. For example, Tubastatin A exhibited pronounced inhibitory activity against HDAC6, an enzyme of significant interest in the modulation of epigenetic mechanisms. In contrast, Contilisant showed antagonistic activity at the H3 receptor, which could be attributed to the piperidine ring connected via a propylene linker to the central aromatic scaffold.
Building on these insights, two novel compounds were designed and synthesized, both derived from a common central scaffold while incorporating functional groups intended to engage distinct biological targets. As illustrated in Figure 40, **MTP100** and **MTP109** share the same pharmacophoric

groups—highlighted in blue and pink—designed to enhance interactions with the 5-HT6 receptor and to confer HDAC6 inhibitory activity, respectively. The primary distinction between the two molecules lies in the moiety intended to inhibit cholinesterases (ChE), depicted in red.

Both compounds were subsequently evaluated in vitro and in vivo, demonstrating promising activity against the intended biological targets and supporting their potential for further pharmacological development.

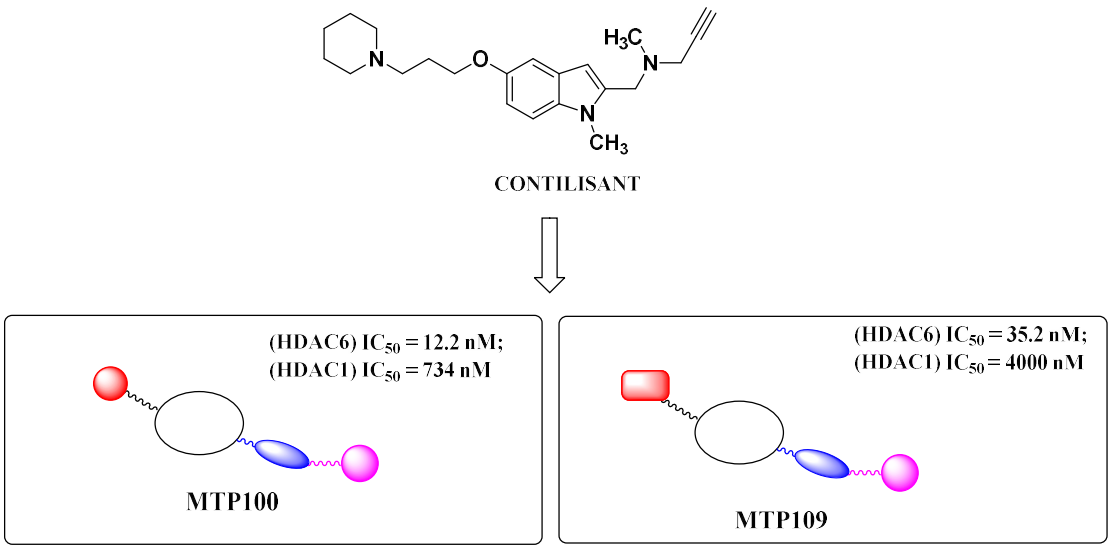

Figure 40. General structures of compounds MTP100 and MTP109, together with their respective IC_{50} values for HDAC1 and HDAC6 inhibition.

Starting from the therapeutic potential suggested by the biological activity of previously synthesized molecules, a modelling-based investigation was conducted to design a more structurally sophisticated derivative. This was achieved through the introduction of a more complex spacer, intended to broaden the molecule's biological profile and enable interaction with a wider range of targets. In particular, the design sought to incorporate pharmacophoric elements capable of engaging the **D3 receptor**, which is believed to play a pivotal role in restoring cognitive functions impaired in patients with Alzheimer's and Parkinson's diseases. *Figure 41* depicts a general schematic of the multivalent molecule. Since the corresponding article has not yet been published, the structure is presented solely in a schematic format.

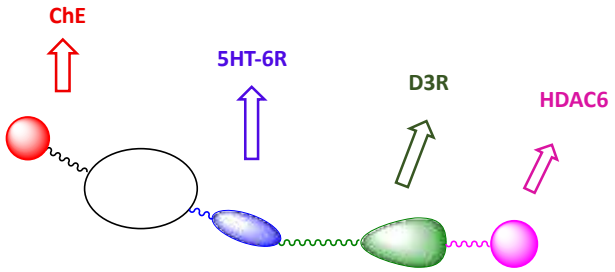

Figure 41. General structure of designed compound to obtain a multivalent drug.

The molecule depicted in *Figure 41* is built around a central core (white), serving as a privileged scaffold to which various pharmacophoric moieties have been strategically attached. These structural elements were carefully selected to engage multiple biological targets involved in both typical and atypical symptoms of Alzheimer's and Parkinson's diseases.

The red group is well established for its ability to inhibit **ChE**, thereby reducing the enzymatic degradation of acetylcholine. This leads to an increase in synaptic acetylcholine levels, which is associated with measurable improvements in cognitive function and contributes to the symptomatic relief characteristic of this class of agents.

A spacer (blue) was introduced, a feature previously shown to confer antagonistic activity toward the **5-HT6 receptor**. This interaction enhances synaptic signaling and neuronal plasticity, ultimately helping to alleviate cognitive deficits in Alzheimer's disease. [340]

The most notable structural innovation is the incorporation of an additional core (green), which molecular docking studies suggest facilitates interaction with the D3 receptor. Antagonism at this receptor promotes dopaminergic signaling, a mechanism particularly relevant to Parkinson's disease.[342] Furthermore, such antagonists are known to activate intracellular pathways supporting neuronal survival and neurogenesis, including those regulated by cyclin-dependent kinase 5 (Cdk5) and the mammalian target of rapamycin (mTOR). [343,344]

Finally, the pharmacophore (pink) was added to ensure **HDAC6 inhibition**, adding another layer to the molecule's multifunctional pharmacological profile.

Taken together, this designed molecule represents a highly promising multivalent candidate for a therapeutic strategy aimed not only at symptomatic relief but also at preventing neurodegeneration in Parkinson's and Alzheimer's diseases. A dedicated synthetic approach, specifically conceived to accommodate its structural complexity and multifaceted pharmacological properties, has been developed and is detailed in the following section.

8.6 SYNTHETIC STRATEGY

The synthetic route developed for the preparation of the final compound **78** was conceived according to a **convergent design**, selected to maximize overall efficiency and modularity. In line with this strategy, the two key fragments—**70** and **76**—were synthesized independently through distinct three-step sequences, and subsequently united through an amide-bond-forming reaction to afford intermediate **77**, which was finally converted into the target hydroxamic acid derivative **78**.

The preparation of fragment **70** was accomplished through *three consecutive synthetic transformations*. The sequence commenced with a nucleophilic substitution reaction between the commercially available *alkyl chloride* (**65**) and *phenolic derivate* (**66**). This reaction, proceeding under standard conditions, furnished the O-alkylated derivative **67**.
Subsequently, compound **67** was subjected to an *acyl nucleophilic substitution* under basic conditions with the commercial reagent **68**. This step introduced the molecular spacer designed to ensure optimal interaction with the **5-HT6 receptor**, progressively leading to the formation of intermediate **69**.
In the final step, the ester function of **69** was hydrolyzed under strongly basic conditions employing 2N KOH, allowing the release of the corresponding carboxylic acid and thereby affording fragment **70** in good overall yield.

In parallel, fragment **76** was prepared through an alternative three-step sequence. The initial transformation consisted of a nucleophilic substitution between the primary amine **71** and the alkyl bromide **72** in DMF, using triethylamine as a base. This reaction selectively provided the monoalkylated product **73**.
The subsequent step involved the acidic removal of the Boc protecting group from compound **73**, achieved by treatment with trifluoroacetic acid, thus generating amine **74** as its salt. This intermediate was then employed in a reductive amination with aldehyde **75**. Because compound **74** was present in its protonated form, the reaction was performed under basic conditions using TEA to regenerate the free amine. The reducing agent **$NaBH_4$** was added to complete the transformation, giving rise to fragment **76**.

With both fragments in hand, the convergent phase of the strategy was implemented. Fragment **70** and fragment **76** were coupled through an amide-bond-forming reaction using HATU as the coupling reagent and DIPEA as the base. Due to the relatively low acidity of the carboxylic group in fragment **70**, an excess of DIPEA (5 equivalents) was required to ensure efficient activation and coupling. This key transformation delivered intermediate **77**.

In the final step, compound **77** was treated with an acqueous solution of commercially available compound **78** to introduce the last pharmacophoric group.

While the final step toward the synthesis of the designed multivalent molecule remains to be optimized, the work conducted during this PhD has validated the overall strategy and afforded the crucial intermediates needed for its completion. Future efforts will focus on refining the final transformation to obtain the fully functionalized target structure.

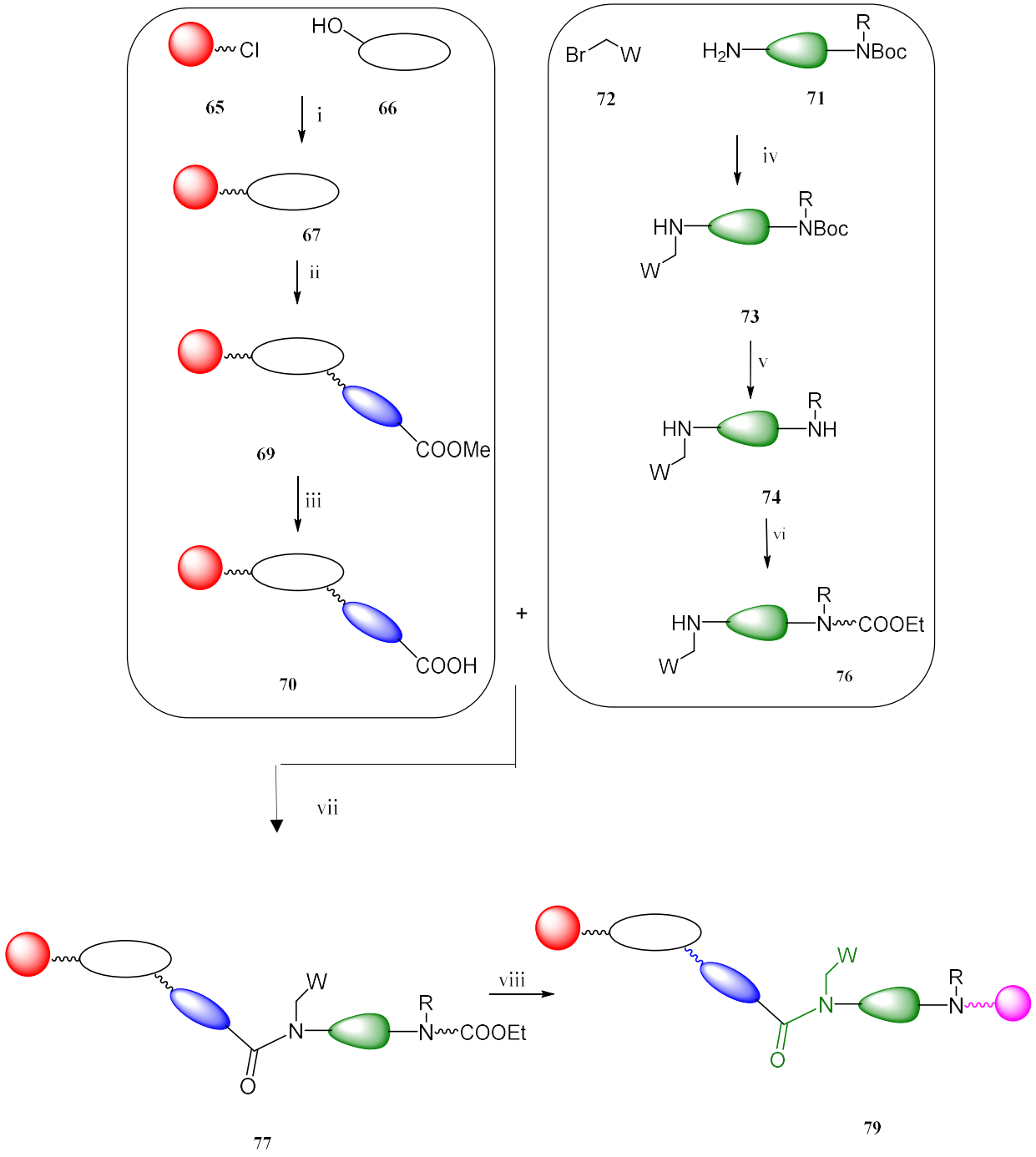

Experimental conditions:

i. K_2CO_3, $CHCl_3/H_2O$ (5:1), reflux 80°C, 24 hours.

ii., NaH 90%, anhydrous DMF, rt, 48 hours.

iii. KOH 2N, THF/EtOH (1:1), rt, 4 hours.

iv.TEA, anhydrous DMF, reflux 120°C, two

v., TFA, anhydrous DCM, rt, 16 hours.

vi. **75**, $NaBH_4$, anhydrous MeOH, rt, 1 hour.

vii. HATU, DIPEA, anhydrous DMF, rt, 72 hours.

viii. **78**, KOH, THF, 35°C, 24 hours.

Scheme 33. General synthetic strategy optimized for the synthesis of the designed compound **79**.

8.7 CONCLUSIONS

During my PhD at the University of Alcalá with Professor Isabel Iriepa Canalda's research group, it was possible to explore a novel and promising therapeutic approach for neurodegenerative diseases. These disorders, which are highly prevalent worldwide, are currently managed primarily with symptomatic therapies aimed at alleviating clinical manifestations and improving patients' quality of life. Existing drugs, however, neither halt disease progression nor prevent the underlying neurodegenerative processes.

One strategy that has attracted considerable attention is the modulation of epigenetic mechanisms. Epigenetic processes regulate gene expression without altering the underlying DNA sequence, primarily by controlling chromatin accessibility to either promote or suppress transcriptional activity. Among these, reversible histone acetylation and deacetylation play a central role and are catalyzed by histone acetyltransferases (HATs) and histone deacetylases (HDACs), respectively. [231,232]

Small-molecule HDAC inhibitors are important modulators of transcription, shifting the cellular equilibrium toward a hyperacetylated state. In neurodegenerative diseases, the balance of histone acetylation is often disrupted, resulting in hypoacetylation. [233] HDAC inhibition-induced hyperacetylation has been shown to exert neuroprotective effects. [234]

Notably, the inhibition of specific HDACs, such as HDAC6—which is overexpressed in Alzheimer's and Parkinson's diseases—represents a promising therapeutic strategy to prevent the activation of signaling cascades that lead to neurodegeneration.

An emerging approach to simultaneously address symptomatic relief and epigenetic modulation is the design of multivalent molecules. These compounds incorporate multiple pharmacophoric groups to engage different biological pathways concurrently, offering the possibility of integrating both symptomatic and disease-modifying effects within a single molecule for the treatment of Alzheimer's and Parkinson's diseases.

A novel synthetic strategy guided by molecular modeling studies was developed to generate such a multivalent molecule. This design allowed the incorporation of multiple pharmacophores into a single scaffold, including antagonistic activity toward the 5-HT6 receptor, D3 receptor antagonism, cholinesterases (ChE) inhibition, and HDAC6 inhibition as an epigenetic mechanism.

The synthetic approach employed was convergent: two key fragments (**70** and **76**) were independently synthesized and then coupled via an amide bond, followed by a final transformation to introduce the HDAC6-inhibitory group.

The resulting compound will be evaluated in biological assays to determine its affinity for the intended targets. In addition, its antioxidant and neuroprotective activities will be tested in vivo to assess its overall biological relevance and therapeutic potential.

8.8 EXPERIMENTAL PROCEDURE

8.8.1 Methods and materials

The progress of the reactions was monitored by Thin Layer Chromatography (TLC) using Macherey-Nagel Poligram SIL/UV 254 silica gel plates (0.25 mm thickness) and reversed-phase plates featuring an amino-modified silica stationary phase compatible with ultraviolet detection at 254 nm, and visualized by staining with an aqueous solution of potassium permanganate ($KMnO_4$, 2%).

The reactions were carried out using commercially available anhydrous solvents (DMF, THF, MeOH, EtOAc, DCM).

The progress of the reactions was monitored by ^1H NMR spectroscopy (300 MHz) after dissolving the crude reaction mixture in a deuterated solvent (DMSO-d_6, MeOD-d_4, or $CDCl_3$).

The molecular weights of the reaction products were verified using High-resolution mass spectrometry (HRMS).

Samples for mass spectrometric analysis were prepared by diluting the residue in non-halogenated organic solvents.

Purification of intermediate compounds was carried out via conventional column chromatography using Merck silica gel (230–240 mesh). The eluent phase consisted of mixtures of ethyl acetate and cyclohexane, dichloromethane and methanol/ methanol and ammonium hydroxide with proportions adjusted according to the polarity of the compound to be purified.

^1H NMR and ^{13}C NMR (DEPT) spectra were recorded on a VARIAN 400 MHz spectrometer. Samples for NMR analysis were prepared in $CDCl_3$, DMSO-d_6 or MeOD-d_4.

General procedure for synthesis of derivative 67

A mixture of commercially available compound **65** (1.5 equiv., 26.9 mmol), compound **66** (1 equiv., 17.9 mmol), and K_2CO_3 (3 equiv., 53.4 mmol) in chloroform/water (50:10 mL) was heated to reflux at 80 °C for 24 hours.

Upon cooling to room temperature, the reaction mixture was filtered under pressure, and the resulting solid was washed with dichloromethane (DCM). The combined filtrates were diluted with DCM and extracted three times with water. The organic layers were then pooled, washed with brine, dried over anhydrous Na_2SO_4, filtered, and concentrated under reduced pressure.

The crude product was purified by flash chromatography, eluting from ethyl acetate/hexane (1:4) to dichloromethane/methanol containing 10% NH_4OH (3%), affording compound **67** as a white solid.

General procedure for synthesis of derivative 69

To a solution of compound **67** (1 equiv., 4.16 mmol) in anhydrous DMF, cooled to 0 °C, NaH (90% oil dispersion) (2 equiv., 8.32 mmol) was added, and the mixture was allowed to warm to room temperature and stirred for one hour. Subsequently, commercially available compound **68** (1.5 equiv., 6.24 mmol), dissolved in DMF, was added, and the reaction mixture was stirred at room temperature for 48 hours.

The solvent was then removed under reduced pressure, and the resulting residue was extracted three times with dichloromethane/water. The combined organic layers were washed with brine, dried over anhydrous Na_2SO_4, filtered, and concentrated under reduced pressure.

Purification by flash chromatography, eluting from DCM to DCM/MeOH containing 10% NH_4OH (2.5%), afforded compound **69** as a white solid.

General procedure for synthesis of derivative 70

To a solution of compound **69** (1 equiv., 0.54 mmol) in THF/EtOH (1:1, 2 mL: 2 mL), a 2 N KOH solution (4 equiv., 2.16 mmol) was added dropwise, and the reaction mixture was stirred at room temperature for 4 hours. The progress of the reaction was monitored by NMR in DMSO until complete disappearance of the starting material.

The reaction mixture was then acidified with 5 N HCl to pH 2–3 and concentrated under reduced pressure. The resulting residue was crystallized from ethanol by heating to reflux for one hour and subsequently filtered. The solid obtained after drying afforded compound **70** as a pink solid.

General procedure for synthesis of derivative 73

Under an argon atmosphere, a solution of commercially available compound **71** (1 equiv., 2.68 mmol) in DMF (5 mL) was treated with TEA (1.2 equiv., 3.22 mmol) and alkyl bromide **72** (1 equiv., 2.68 mmol). The mixture was heated to reflux (120 °C) for two hours. After cooling to room temperature, the solvent was removed under reduced pressure, and the residue was diluted with an aqueous $NaHCO_3$ solution and adjusted to pH 8–9. The mixture was extracted three times with DCM.

The combined organic layers were washed with brine, dried over anhydrous Na_2SO_4, filtered, and concentrated under reduced pressure. Purification of the crude product by flash chromatography, eluting from hexane/ethyl acetate (9:1) to hexane/ethyl acetate (8:2), afforded compound **73** as a yellow oil.

General procedure for synthesis of derivative 74

Under an argon atmosphere, a solution of compound **73** (0.413 mmol, 1 equiv.) in DCM (2 mL) was treated dropwise with trifluoroacetic acid (10 equiv., 4.13 mmol) and stirred at room

temperature for 16 hours. The progress of the reaction was monitored by NMR, confirming the complete disappearance of the Boc protecting group. The solvent was removed under reduced pressure, and the residue was washed five times with DCM to remove any excess acid. Compound **74** was used directly in the subsequent step without further purification.

General procedure for synthesis of derivative 76

Under a nitrogen atmosphere, a solution of compound **74** (1 equiv., 0.63 mmol) in MeOH (2 mL) was treated dropwise with TEA (1 equiv., 0.63 mmol), followed by the addition of commercially available compound **75** (1.2 equiv., 0.72 mmol, 124.9 mg) dissolved in MeOH (2 mL). The reaction mixture was stirred at room temperature for 90 minutes.

At 0 °C, $NaBH_4$ was added gradually over 30 minutes, and the mixture was then stirred at room temperature for an additional 30 minutes. Any excess $NaBH_4$ was quenched with a few drops of distilled water, and the reaction mixture was concentrated under reduced pressure. The residue was diluted with ethyl acetate and extracted three times with water. The combined organic layers were washed with brine, dried over anhydrous Na_2SO_4, filtered, and concentrated under reduced pressure. Purification of the crude product by flash chromatography, eluting from ethyl acetate/hexane (1:4) to MeOH/DCM (0.5:9.5), afforded compound **76** as a fluorescent oil.

General procedure for synthesis of derivative 77

Under an argon atmosphere, a solution of compound **70** (50 mg, 0.104 mmol, 1 equiv.) in DMF (1 mL) was treated with HATU and DIPEA, and the mixture was stirred at room temperature for 25 minutes. Subsequently, compound **76**, dissolved in DMF (1 mL), was added dropwise, and the reaction mixture was stirred at room temperature for 3 days.

The solvent was removed under reduced pressure, and the residue was diluted with DCM and extracted three times with water. The combined organic layers were washed with brine, dried over anhydrous Na_2SO_4, filtered, and concentrated under reduced pressure. Purification of the crude product by flash chromatography, eluting from DCM to DCM/MeOH containing 10% NH_4OH (1.5%), afforded compound **77** as a yellow solid.

General procedure for synthesis of derivative 79

To a solution of aqueous compound **78** (28 equiv.) at 0°C, KOH (4 equiv.) was dissolved and compound **77** (1 equiv.) dissolved in THF was added. The reaction was stirred at room temperature for 16 hours. After that time, other 28 equiv. of 78 were added and the mixture was put at 35°C for 16 hours.

The final step of the synthetic route has not yet been completed and requires further optimization to achieve the desired transformation. Nonetheless, the work carried out established the feasibility of the convergent strategy and provided a solid foundation for the completion of the target molecule.

9 BIBLIOGRAPHY

1. Cooper GM. The Cell: A Molecular Approach. 2nd edition. Sunderland (MA): Sinauer Associates; 2000. Protein Degradation.
2. Glickman MH, Ciechanover A. The ubiquitin-proteasome proteolytic pathway: destruction for the sake of construction. Physiol Rev. 2002 Apr.
3. Alves-Rodrigues A, Gregori L, Figueiredo-Pereira ME. Ubiquitin, cellular inclusions and their role in neurodegeneration. Trends Neurosci. 1998 Dec.
4. Hoppe T. Multiubiquitylation by E4 enzymes: 'one size' doesn't fit all. Trends Biochem Sci. 2005 Apr.
5. Favaro M., Viviani E., In vivo characterization in flies of novel USP14 inhibitors.
6. Matteucci A., Lariccia V., Parkin-dependent regulation of the components of the mitochondrial calcium uniporter complex.
7. Adams J. The proteasome: structure, function, and role in the cell. Cancer Treat Rev. 2003 May.
8. Cappadocia L, Lima CD. Ubiquitin-like Protein Conjugation: Structures, Chemistry, and Mechanism. Chem Rev. 2018 Feb.
9. Zheng N, Schulman BA, Song L, Miller JJ, Jeffrey PD, et al. 2002. Structure of the Cul1-Rbx1-Skp1-F boxSkp2 SCF ubiquitin ligase complex. Nature 416: 703-9.
10. Fumiaki Yamao, Ubiquitin System: Selectivity and Timing of Protein Destruction, *The Journal of Biochemistry*, Volume 125, Issue 2, February 1999.
11. Maupin-Furlow JA, Wilson HL, Kaczowka SJ, Ou MS. Proteasomes in the archaea: from structure to function. Front Biosci. 2000 Sep.
12. Tanaka K. The proteasome: overview of structure and functions. Proc Jpn Acad Ser B Phys Biol Sci. 2009.
13. Burston SG, Clarke AR. Molecular chaperones: physical and mechanistic properties. Essays Biochem.
14. Stadtmueller BM, Kish-Trier E, Ferrell K, Petersen CN, Robinson H, Myszka DG, Eckert DM, Formosa T, Hill CP. Structure of a proteasome Pba1-Pba2 complex: implications for proteasome assembly, activation, and biological function. J Biol Chem. 2012 Oct.
15. Fu X, Inouye M, Shinde U. Folding pathway mediated by an intramolecular chaperone. The inhibitory and chaperone functions of the subtilisin propeptide are not obligatorily linked. J Biol Chem. 2000 Jun 2;275(22):16871-8.
16. Kusmierczyk AR, Hochstrasser M. Some assembly required: dedicated chaperones in eukaryotic proteasome biogenesis. Biol Chem. 2008 Sep;389(9):1143-51.
17. Schnell HM, Walsh RM, Rawson S, Hanna J. Chaperone-mediated assembly of the proteasome core particle - recent developments and structural insights. J Cell Sci. 2022 Apr.
18. Fricke B, Heink S, Steffen J, Kloetzel PM, Krüger E. The proteasome maturation protein POMP facilitates major steps of 20S proteasome formation at the endoplasmic reticulum. EMBO Rep. 2007 Dec;8(12):1170-5.
19. Nandi, D., Tahiliani, P., Kumar, A. *et al.* The ubiquitin-proteasome system. *J. Biosci.* 31, 137–155 (2006).
20. Zwickl P, Voges D, Baumeister W. The proteasome: a macromolecular assembly designed for controlled proteolysis. Philos Trans R Soc Lond B Biol Sci. 1999 Sep 29;354(1389):1501-11.
21. Ciechanover A. The ubiquitin-proteasome pathway: on protein death and cell life. EMBO J. 1998 Dec.
22. Saha A, Oanca G, Mondal D, Warshel A. Exploring the Proteolysis Mechanism of the Proteasomes. J Phys Chem B. 2020 Jul 9;124(27):5626-5635
23. Yasushi Saeki, Keiji Tanaka, Unlocking the Proteasome Door, Molecular Cell, Volume 27, Issue 6, 2007.

24. Rabl J, Smith DM, Yu Y, Chang SC, Goldberg AL, Cheng Y. Mechanism of gate opening in the 20S proteasome by the proteasomal ATPases. Mol Cell. 2008 May 9;30(3):360-8.
25. Kisselev AF, van der Linden WA, Overkleeft HS. Proteasome inhibitors: an expanding army attacking a unique target. Chem Biol. 2012 Jan 27;19(1):99-115.
26. Fricker LD. Proteasome Inhibitor Drugs. Annu Rev Pharmacol Toxicol. 2020 Jan 6;60:457-476. doi: 10.1146/annurev-pharmtox-010919-023603. Epub 2019 Sep 3.
27. Musgrove EA, Caldon CE, Barraclough J, Stone A, Sutherland RL. Cyclin D as a therapeutic target in cancer. Nat Rev Cancer. 2011 Jul.
28. Di Donato JA, Mercurio F, Karin M. NF-κB and the link between inflammation and cancer. Immunol Rev. 2012 Mar.
29. Park J, Cho J, Song EJ. Ubiquitin-proteasome system (UPS) as a target for anticancer treatment. Arch Pharm Res. 2020 Nov.
30. Wan L, Chen M, Cao J, Dai X, Yin Q, Zhang J, Song SJ, Lu Y, Liu J, Inuzuka H, Katon JM, Berry K, Fung J, Ng C, Liu P, Song MS, Xue L, Bronson RT, Kirschner MW, Cui R, Pandolfi PP, Wei W. The APC/C E3 ligase complex activator FZR1 restricts BRAF oncogenic function. Cancer Discov. 2017.
31. Senft D, Qi J, Ronai ZA. Ubiquitin ligases in oncogenic transformation and cancer therapy. Nat Rev Cancer. 2018.
32. Iwatsuki M, Mimori K, Ishii H, Yokobori T, Takatsuno Y, Sato T, Toh H, Onoyama I, Nakayama KI, Baba H, Mori M. Loss of FBXW7, a cell cycle regulating gene, in colorectal cancer: clinical significance. Int J Cancer. 2010.
33. Stevenson LF, Sparks A, Allende-Vega N, Xirodimas DP, Lane DP, Saville MK. The deubiquitinating enzyme USP2a regulates the p53 pathway by targeting Mdm2. EMBO J. 2007 Feb 21;26(4):976-86.
34. Kitamura H, Hashimoto M. USP2-Related Cellular Signaling and Consequent Pathophysiological Outcomes. Int J Mol Sci. 2021 Jan 26;22(3):1209.
35. Oliveira RI, Guedes RA, Salvador JAR. Highlights in USP7 inhibitors for cancer treatment. Front Chem. 2022 Sep 15;10:1005727.
36. Sun SC. CYLD: a tumor suppressor deubiquitinase regulating NF-kappaB activation and diverse biological processes. Cell Death Differ. 2010 Jan;17(1):25-34.
37. Shin JY, Muniyappan S, Tran N-N, Park H, Lee SB, Lee B-H. Deubiquitination Reactions on the Proteasome for Proteasome Versatility. *International Journal of Molecular Sciences*. 2020; 21(15):5312.
38. Shen M, Schmitt S, Buac D, Dou QP. Targeting the ubiquitin-proteasome system for cancer therapy. Expert Opin Ther Targets. 2013 Sep;17(9):1091-108.
39. Nunes AT, Annunziata CM. Proteasome inhibitors: structure and function. Semin Oncol. 2017 Dec.
40. Raedler LA. Ninlaro (Ixazomib): First Oral Proteasome Inhibitor Approved for the Treatment of Patients with Relapsed or Refractory Multiple Myeloma.
41. Chen D, Frezza M, Schmitt S, Kanwar J, Dou QP. Bortezomib as the first proteasome inhibitor anticancer drug: current status and future perspectives. Curr Cancer Drug Targets. 2011 Mar;11(3):239-53.
42. Roth P, Gorlia T, Reijneveld JC, de Vos F, Idbaih A, Frenel JS, Le Rhun E, Sepulveda JM, Perry J, Masucci GL, Freres P, Hirte H, Seidel C, Walenkamp A, Lukacova S, Meijnders P, Blais A, Ducray F, Verschaeve V, Nicholas G, Balana C, Bota DA, Preusser M, Nuyens S, Dhermain F, van den Bent M, O'Callaghan CJ,

Vanlancker M, Mason W, Weller M. Marizomib for patients with newly diagnosed glioblastoma: A randomized phase 3 trial. Neuro Oncol. 2024 Sep 5;26(9):1670-1682.

43. Kisselev AF, van der Linden WA, Overkleeft HS. Proteasome inhibitors: an expanding army attacking a unique target. Chem Biol. 2012 Jan 27;19(1):99-115.
44. Wang J, Fang Y, Fan RA, Kirk CJ. Proteasome Inhibitors and Their Pharmacokinetics, Pharmacodynamics, and Metabolism. Int J Mol Sci. 2021 Oct.
45. Alexei F. Kisselev, Wouter A. van der Linden, Herman S. Overkleeft, Proteasome Inhibitors: An Expanding Army Attacking a Unique Target, Chemistry & Biology, Volume 19, Issue 1, 2012, Pages 99-115, ISSN 1074-5521.
46. Michael Groll, Yutaka Koguchi, Robert Huber, Jun Kohno, Crystal structure of the 20 S proteasome:TMC-95A complex: a non-covalent proteasome inhibitor11Edited by I. A. Wilson, Journal of Molecular Biology, Volume 311, Issue 3, 2001, Pages 543-548.
47. Beck P, Dubiella C, Groll M. Covalent and non-covalent reversible proteasome inhibition. Biol Chem. 2012 Oct;393(10):1101-20.
48. Li-Qiang Han, Xia Yuan, Xing-Yu Wu, Ri-Dong Li, Bo Xu, Qing Cheng, Zhen-Ming Liu, Tian-Yan Zhou, Hao-Yun An, Xin Wang, Tie-Ming Cheng, Ze-Mei Ge, Jing-Rong Cui, Run-Tao Li, Urea-containing peptide boronic acids as potent proteasome inhibitors, European Journal of Medicinal Chemistry, Volume 125, 2017, Pages 925-939.
49. Gandolfi S, Laubach JP, Hideshima T, Chauhan D, Anderson KC, Richardson PG. The proteasome and proteasome inhibitors in multiple myeloma. Cancer Metastasis Rev. 2017 Dec.
50. Nakaya A, Fujita S, Satake A, Nakanishi T, Azuma Y, Tsubokura Y, Hotta M, Yoshimura H, Ishii K, Ito T, Nomura S. Impact of CRAB Symptoms in Survival of Patients with Symptomatic Myeloma in Novel Agent Era. Hematol Rep. 2017 Feb 23;9(1):6887.
51. Yan W, Wu Z, Zhang Y, Hong D, Dong X, Liu L, Rao Y, Huang L, Zhang X, Wu J. The molecular and cellular insight into the toxicology of bortezomib-induced peripheral neuropathy. Biomed Pharmacother. 2021 Oct.
52. Murai K, Kowata S, Shimoyama T, Yashima-Abo A, Fujishima Y, Ito S, Ishida Y. Bortezomib induces thrombocytopenia by the inhibition of proplatelet formation of megakaryocytes. Eur J Haematol. 2014 Oct;93(4):290-6.
53. Omar Alkharabsheh, M. Hasib Sidiqi, Mohammed A. Aljama, Morie A. Gertz, Arthur E. Frankel; The Human Microbiota in Multiple Myeloma and Proteasome Inhibitors. *Acta Haematol* 25 March 2020; 143 (2): 118–123.
54. Georgiopoulos G, Makris N, Laina A, Theodorakakou F, Briasoulis A, Trougakos IP, Dimopoulos MA, Kastritis E, Stamatelopoulos K. Cardiovascular Toxicity of Proteasome Inhibitors: Underlying Mechanisms and Management Strategies: *JACC: CardioOncology* State-of-the-Art Review. JACC CardioOncol. 2023 Feb.
55. Njomen E, Tepe JJ. Proteasome Activation as a New Therapeutic Approach To Target Proteotoxic Disorders. J Med Chem. 2019 Jul 25.
56. Hetz C; Glimcher LH Protein Homeostasis Networks in Physiology and Disease. Curr. Opin. Cell Biol 2011.
57. Frydman J Folding of Newly Translated Proteins in Vivo: The Role of Molecular Chaperones. Annu. Rev. Biochem 2001.
58. Douglas PM; Summers DW; Cyr DM Molecular Chaperones Antagonize Proteotoxicity by Differentially Modulating Protein Aggregation Pathways. Prion 2009.

59. Ji CH; Kwon YT Crosstalk and Interplay between the Ubiquitin-Proteasome System and Autophagy. Mol. Cells 2017.
60. Korolchuk VI; Mansilla A; Menzies FM; Rubinsztein DC Autophagy Inhibition Compromises Degradation of Ubiquitin-Proteasome Pathway Substrates. Mol. Cell 2009.
61. Halliwell B; Isacson O; Jenner P; McNaught KSP; Olanow CW Failure of the Ubiquitin-Proteasome System in Parkinson's Disease. Nat. Rev. Neurosci 2001.
62. Saez I; Vilchez D The Mechanistic Links Between Proteasome Activity, Aging and Age-Related Diseases. Curr. Genomics 2014.
63. Ostrowska H The Ubiquitin-Proteasome System: A Novel Target for Anticancer and Anti-Inflammatory Drug Research. Cell. Mol. Biol. Lett 2008.
64. Opattova A; Cente M; Novak M; Filipcik P The Ubiquitin Proteasome System as a Potential Therapeutic Target for Treatment of Neurodegenerative Diseases. Gen. Physiol. Biophys 2015.
65. Jung T; Grune T The Proteasome and Its Role in the Degradation of Oxidized Proteins. IUBMB Life 2008.
66. Grune T; Reinheckel T; Davies KJ Degradation of Oxidized Proteins in Mammalian Cells. FASEB J. 1997.
67. Grune T Oxidative Stress, Aging and the Proteasomal System. Biogerontology 2000.
68. Breusing N; Arndt J; Voss P; Bresgen N; Wiswedel I; Gardemann A; Siems W; Grune T Inverse
69. Correlation of Protein Oxidation and Proteasome Activity in Liver and Lung. Mech. Ageing Dev 2009.
70. Wang X; Yen J; Kaiser P; Huang L Regulation of the 26S Proteasome Complex During Oxidative Stress. Sci. Signaling 2010.
71. Lam YA; Pickart CM; Alban A; Landon M; Jamieson C; Ramage R; Mayer RJ; Layfield R Inhibition of the Ubiquitin-Proteasome System in Alzheimer's Disease. Proc. Natl. Acad. Sci. U.S.A 2000.
72. Perry G; Friedman R; Shaw G; Chau V Ubiquitin Is Detected in Neurofibrillary Tangles and Senile Plaque Neurites of Alzheimer Disease Brains. Proc. Natl. Acad. Sci. U. S. A 1987.
73. Hayes MT. Parkinson's Disease and Parkinsonism. Am J Med. 2019 Jul.
74. Iwai A, Masliah E, Yoshimoto M *et al.* The precursor protein of non-Aβ component of Alzheimer's disease amyloid is a presynaptic protein of the central nervous system. *Neuron* 1995.
75. Lowe J, Blanchard A, Morrell K, Lennox G, Reynolds L, Billett M, Landon M, Mayer RJ- Ubiquitin is a common factor in intermediate filament inclusion bodies of diverse type in man, including those of Parkinson's disease, Pick's disease, and Alzheimer's disease, as well as Rosenthal fibres in cerebellar astrocytomas, cytoplasmic bodies in muscle, and mallory bodies in alcoholic liver disease. J Pathol 1988.
76. Giasson BI, Lee VM, Parkin and the molecular pathways of parkinson's disease. Neuron, 2001.
77. Bedford L; Hay D; Devoy A; Paine S; Powe DG; Seth R; Gray T; Topham I; Fone K; Rezvani N; Mee M; Soane T; Layfield R; Sheppard PW; Ebendal T; Usoskin D; Lowe J; Mayer RJ Depletion of 26S Proteasomes in Mouse Brain Neurons Causes Neurodegeneration and Lewy-like Inclusions Resembling Human Pale Bodies. J. Neurosci 2008.
78. Liu Y, Hettinger CL, Zhang D, Rezvani K, Wang X, Wang H. The proteasome function reporter GFPu accumulates in young brains of the APPswe/PS1dE9 Alzheimer's disease mouse model. Cell Mol Neurobiol. 2014 Apr.
79. Bird TD. Genetic aspects of Alzheimer disease. Genet Med. 2008 Apr.
80. Selkoe D. J. (1991) The molecular pathology of Alzheimer's disease. *Neuron* 6.

81. Smith M. A., Taneda S., Richey P. L., Miyata S., Yan S.-D., Stern D., Sayre L. M., Monnier V. M. and Perry G. (1994) Advanced Maillard reaction end products are associated with Alzheimer disease pathology. *Proc. Natl Acad. Sci. USA* 91.
82. Keck S, Nitsch R, Grune T, Ullrich O. Proteasome inhibition by paired helical filament-tau in brains of patients with Alzheimer's disease. J Neurochem. 2003 Apr.
83. Ribeiro, F.C., Cozachenco, D., Heimfarth, L. *et al.* Synaptic proteasome is inhibited in Alzheimer's disease models and associates with memory impairment in mice. *Commun Biol* **6**, 1127 (2023).
84. Zhao, X. & Yang, J. Amyloid-B peptide is a substrate of the human 20S proteasome. *ACS Chem. Neurosci, 2010.*
85. Ding, M. & Shen, K. The role of the ubiquitin proteasome system in synapse remodeling and neurodegenerative diseases. *Bioessays* **30**, 1075–1083 (2008).
86. Woo, M.S. · Engler, J.B. · Friese, M.A., The neuropathobiology of multiple sclerosis, Nat. Rev. Neurosci. 2024.
87. Wilson, D.M. · Cookson, M.R. · Van Den Bosch, L., Hallmarks of neurodegenerative diseases, Cell. 2023.
88. Berriat, F. · Lobsiger, C.S. · Boillée, S., The contribution of the peripheral immune system to neurodegeneration, Nat. Neurosci. 2023.
89. Woo, M.S. · Ufer, F. · Rothammer, N., Neuronal metabotropic glutamate receptor 8 protects against neurodegeneration in CNS inflammation, J. Exp. Med. 2021.
90. Tai, Y.-H. · Engels, D. · Locatelli, G., Targeting the TCA cycle can ameliorate widespread axonal energy deficiency in neuroinflammatory lesions, Nat. Metab. 2023.
91. Jhelum, P. · Zandee, S. · Ryan, F., Ferroptosis induces detrimental effects in chronic EAE and its implications for progressive MS, Acta Neuropathol. Commun. 2023.
92. Jimenez-Blasco, D. · Agulla, J. · Lapresa, R., Weak neuronal glycolysis sustains cognition and organismal fitness, Nat. Metab. 2024.
93. Herrero-Mendez, A. · Almeida, A. · Fernández, E., The bioenergetic and antioxidant status of neurons is controlled by continuous degradation of a key glycolytic enzyme by APC/C–Cdh1, Nat. Cell Biol. 2009
94. Woo MS, Brand J, Bal LC, Moritz M, Walkenhorst M, Vieira V, Ipenberg I, Rothammer N, Wang M, Dogan B, Loreth D, Mayer C, Nagel D, Wagner I, Pfeffer LK, Landgraf P, van Ham M, Mattern KM, Winschel I, Frantz N, Sonner JK, Grosshans HK, Miguela A, Bauer S, Meurs N, Müller A, Binkle-Ladisch L, Salinas G, Jänsch L, Dieterich DC, Riedner M, Krüger E, Heppner FL, Glatzel M, Puelles VG, Engler JB, Nyengaard JR, Misgeld T, Kerschensteiner M, Merkler D, Meyer-Schwesinger C, Friese MA. The immunoproteasome disturbs neuronal metabolism and drives neurodegeneration in multiple sclerosis. Cell. 2025 Aug 21;188(17):4567-4585.e32. doi: 10.1016/j.cell.2025.05.029. Epub 2025 Jun 17.
95. Rousseau A, Bertolotti A. Regulation of proteasome assembly and activity in health and disease. Nat Rev Mol Cell Biol. 2018 Nov.
96. Khan TK, Nelson TJ. Protein kinase C activator bryostatin-1 modulates proteasome function. J Cell Biochem, 2018.
97. Khan TK, You Y, Nelson TJ, Kundu S, Pramanik SK, Das J. Modulation of proteasome activity by curcumin and didemethylcurcumin. J Biomol Struct Dyn. 2022 Nov.
98. Coleman, R. A.; Muli, C. S.; Zhao, Y.; Bhardwaj, A.; Newhouse, T. R.; Trader, D. J. Analysis of Chain Length, Substitution Patterns, and Unsaturation of AM-404 Derivatives as 20S Proteasome Stimulators. Bioorg. Med. Chem. Lett. 2019.

99. Sophia D. Staerz, Corey L. Jones, and Jetze J. Tepe, Design, Synthesis, and Biological Evaluation of Potent 20S Proteasome Activators for the Potential Treatment of α-Synucleinopathies, J. Med. Chem. 2022.
100. Deshmukh FK, Ben-Nissan G, Olshina MA, Füzesi-Levi MG, Polkinghorn C, Arkind G, Leushkin Y, Fainer I, Fleishman SJ, Tawfik D, Sharon M. Allosteric regulation of the 20S proteasome by the Catalytic Core Regulators (CCRs) family. Nat Commun. 2023 May.
101. Pepelnjak M, Rogawski R, Arkind G, Leushkin Y, Fainer I, Ben-Nissan G, Picotti P, Sharon M. Systematic identification of 20S proteasome substrates. Mol Syst Biol. 2024 Apr.
102. Motosugi R, Murata S. Dynamic Regulation of Proteasome Expression. Front Mol Biosci. 2019 May.
103. Mannhaupt G., Schnall R., Karpov V., Vetter I., Feldmann H. (1999). Rpn4p acts as a transcription factor by binding to PACE, a nonamer box found upstream of 26S proteasomal and other genes in yeast. FEBS Lett.
104. Xie Y., Varshavsky A. (2001). RPN4 is a ligand, substrate, and transcriptional regulator of the 26S proteasome: A negative feedback circuit. Proc. Natl. Acad. Sci. U.S.A. 98.
105. Wang X., Xu H., Ju D., Xie Y. (2008). Disruption of Rpn4-induced proteasome expression in Saccharomyces cerevisiae reduces cell viability under stressed conditions. Genetics 180, 1945–1953.
106. Diehl CJ, Ciulli A. Discovery of small molecule ligands for the von Hippel-Lindau (VHL) E3 ligase and their use as inhibitors and PROTAC degraders. Chem Soc Rev. 2022 Oct 3;51(19):8216-8257.
107. Leestemaker Y, de Jong A, Witting KF, Penning R, Schuurman K, Rodenko B, Zaal EA, van de Kooij B, Laufer S, Heck AJR, Borst J, Scheper W, Berkers CR, Ovaa H. Proteasome Activation by Small Molecules. Cell Chem Biol. 2017 Jun.
108. C.R. Berkers, F.W. van Leeuwen, T.A. Groothuis, V. Peperzak, E.W. van Tilburg, J. Borst, J.J. Neefjes, H. Ovaa, Profiling proteasome activity in tissue with fluorescent probes, Mol. Pharm., 4 (2007).
109. de Jong, A., Schuurman, K.G., Rodenko, B., Ovaa, H., and Berkers, C.R. (2012). Fluorescence-based proteasome activity profiling. Methods Mol. Biol. 803, 183–204.
110. Celia R. Berkers, Fijs W. B. van Leeuwen, Tom A. Groothuis, Victor Peperzak, Erica W. van Tilburg, Jannie Borst, Jacques J. Neefjes, and Huib Ovaa. Molecular Pharmaceutics 2007 4 (5), 739-748.
111. Dantuma NP, Lindsten K, Glas R, Jellne M, Masucci MG. Short-lived green fluorescent proteins for quantifying ubiquitin/proteasome-dependent proteolysis in living cells. Nat Biotechnol. 2000 May.
112. Verdoes M, Florea BI, Menendez-Benito V, Maynard CJ, Witte MD, van der Linden WA, van den Nieuwendijk AM, Hofmann T, Berkers CR, van Leeuwen FW, Groothuis TA, Leeuwenburgh MA, Ovaa H, Neefjes JJ, Filippov DV, van der Marel GA, Dantuma NP, Overkleeft HS. A fluorescent broad-spectrum proteasome inhibitor for labeling proteasomes in vitro and in vivo. Chem Biol. 2006 Nov.
113. Hanlin Wang, Zhaoxiao Wu, Yu Cao, Lixin Gao, Jiaan Shao, Yanmei Zhao, Jiankang Zhang, Yubo Zhou, Gang Wei, Jia Li, Huajian Zhu, Exploration of novel four-membered-heterocycle constructed peptidyl proteasome inhibitors with improved metabolic stability for cancer treatment, Bioorganic Chemistry, Volume 138, 2023, 106626, ISSN 0045-2068.
114. Pacifico S, Ferretti V, Albanese V, Fantinati A, Gallerani E, Nicoli F, Gavioli R, Zamberlan F, Preti D, Marastoni M. Synthesis and Biological Activity of Peptide α-Ketoamide Derivatives as Proteasome Inhibitors. ACS Med Chem Lett. 2019 Jun 6.
115. Zhou, Jiao; Sang, Xiaohong; Wang, Juan; Xu, Yan; An, Jing; Chu, Zhen Tao; Saha, Arjun; Warshel, Arieh; Huang, Ziwei. *"Elucidation of the α-Ketoamide Inhibition Mechanism: Revealing the Critical Role of the*

Electrostatic Reorganization Effect of Asp17 in the Active Site of the 20S Proteasome". ACS Catalysis, 2023, 13(21), 14368–14376.

116. Scharpé SL, Vanhoof GC, De Meester IA, Hendriks DF, van Sande ME, Muylle LM, Yaron A. Exopeptidases in human platelets: an indication for proteolytic modulation of biologically active peptides. Clin Chim Acta. 1991 Jan 15.
117. Yao JF, Yang H, Zhao YZ, Xue M. Metabolism of Peptide Drugs and Strategies to Improve their Metabolic Stability. Curr Drug Metab. 2018. LEGGITELO CHE è INTERESSANTE
118. Gokhale AS, Satyanarayanajois S. Peptides and peptidomimetics as immunomodulators. Immunotherapy. 2014.
119. Robello M, Barresi E, Baglini E, Salerno S, Taliani S, Settimo FD. The Alpha Keto Amide Moiety as a Privileged Motif in Medicinal Chemistry: Current Insights and Emerging Opportunities. J Med Chem. 2021 Apr.
120. Herman S Overkleeft, Pepijn R Bos, Brian G Hekking, Eva J Gordon, Hidde L Ploegh, Benedikt M Kessler. Solid phase synthesis of peptide vinyl sulfone and peptide epoxyketone proteasome inhibitors. 2000 May;17.
121. Guo N, Peng Z. MG132, a proteasome inhibitor, induces apoptosis in tumor cells. Asia Pac J Clin Oncol. 2013 Mar;9(1):6-11.
122. Kim YM, Kim HJ. Proteasome Inhibitor MG132 is Toxic and Inhibits the Proliferation of Rat Neural Stem Cells but Increases BDNF Expression to Protect Neurons. Biomolecules. 2020 Nov 2;10(11):1507.
123. Jones CL; Njomen E; Sjögren B; Dexheimer TS; Tepe JJ Small Molecule Enhancement of 20S Proteasome Activity Targets Intrinsically Disordered Proteins. ACS Chem. Biol 2017, 12, 2240–2247.
124. Trader DJ; Simanski S; Dickson P; Kodadek T Establishment of a Suite of Assays That Support the Discovery of Proteasome Stimulators. Biochim. Biophys. Acta, Gen. Subj 2017, 1861, 892–899.
125. Coleman RA; Trader DJ Development and Application of a Sensitive Peptide Reporter to Discover 20S Proteasome Stimulators. ACS Comb. Sci 2018, 20, 269–276.
126. Leestemaker Y; de Jong A; Witting KF; Penning R; Schuurman K; Rodenko B; Zaal EA; van de Kooij B; Laufer S; Heck AJR; Borst J; Scheper W; Berkers CR; Ovaa H Proteasome Activation by Small Molecules. Cell Chem. Biol 2017, 24, 725–736.
127. Coleman RA; Muli CS; Zhao Y; Bhardwaj A; Newhouse TR; Trader DJ Analysis of Chain Length, Substitution Patterns, and Unsaturation of AM-404 Derivatives as 20S Proteasome Stimulators. Bioorg. Med. Chem. Lett 2019, 29, 420–423.
128. Njomen E, Tepe JJ. Proteasome Activation as a New Therapeutic Approach To Target Proteotoxic Disorders. J Med Chem. 2019 Jul 25;62(14):6469-6481.
129. Kisselev AF; Goldberg AL Monitoring Activity and Inhibition of 26S Proteasomes with Fluorogenic Peptide Substrates In Ubiquitin and Protein Degradation, Part A; Methods in Enzymology; Academic Press, 2005; Vol. 398, pp 364–378.
130. Kisselev AF; Akopian TN; Castillo V; Goldberg AL Proteasome Active Sites Allosterically Regulate Each Other, Suggesting a Cyclical Bite-Chew Mechanism for Protein Breakdown. Mol. Cell 1999, 4, 395–402.
131. Njomen E; Osmulski PA; Jones CL; Gaczynska M; Tepe JJ Small Molecule Modulation of Proteasome Assembly. Biochemistry 2018, 57, 4214–4224.
132. Jonathan J M Landry, Paul Theodor Pyl, Tobias Rausch, Thomas Zichner, Manu M Tekkedil, Adrian M Stütz, Anna Jauch, Raeka S Aiyar, Gregoire Pau, Nicolas Delhomme, Julien Gagneur, Jan O Korbel, Wolfgang Huber, Lars M Steinmetz, The Genomic and Transcriptomic Landscape of a HeLa Cell Line, *G3 Genes|Genomes|Genetics*, Volume 3, Issue 8, 1 August 2013, Pages 1213–1224.

133. Landry, J. J. M., Pyl, P. T., Rausch, T., Zichner, T., Tekkedil, M. M., Stütz, A. M., … & Steinmetz, L. M. (2013). *The Genomic and Transcriptomic Landscape of a HeLa Cell Line*. **G3: Genes, Genomes, Genetics**, 3(8), 1213-1224.
134. Fiolek TJ, Keel KL, Tepe JJ. Fluspirilene Analogs Activate the 20S Proteasome and Overcome Proteasome Impairment by Intrinsically Disordered Protein Oligomers. ACS Chem Neurosci. 2021 Apr 21;12(8):1438-1448.
135. Jasper H.L. Claessen, Lenka Kundrat, Hidde L. Ploegh, Protein quality control in the ER: balancing the ubiquitin checkbook, Trends in Cell Biology, Volume 22, Issue 1, 2012, Pages 22-32, ISSN 0962-8924.
136. Słabicki M, Yoon H, Koeppel J, Nitsch L, Roy Burman SS, Di Genua C, Donovan KA, Sperling AS, Hunkeler M, Tsai JM, Sharma R, Guirguis A, Zou C, Chudasama P, Gasser JA, Miller PG, Scholl C, Fröhling S, Nowak RP, Fischer ES, Ebert BL. Small-molecule-induced polymerization triggers degradation of BCL6. Nature. 2020 Dec.
137. Krönke J, Udeshi ND, Narla A, Grauman P, Hurst SN, McConkey M, Svinkina T, Heckl D, Comer E, Li X, Ciarlo C, Hartman E, Munshi N, Schenone M, Schreiber SL, Carr SA, Ebert BL. Lenalidomide causes selective degradation of IKZF1 and IKZF3 in multiple myeloma cells. Science. 2014 Jan 17.
138. Liu X, Zhang Y, Hu Z, Li Q, Yang L, Xu G. The Catalytically Inactive Mutation of the Ubiquitin-Conjugating Enzyme CDC34 Affects its Stability and Cell Proliferation. Protein J. 2018 Apr.
139. Ardley HC, Robinson PA (2005) E3 ubiquitin ligases. Essays Bio-chem 41:15–30.
140. Butz N, Ruetz S, Natt F, Hall J, Weiler J, Mestan J, Ducarre M, Grossenbacher R, Hauser P, Kempf D, Hofmann F (2005) The human ubiquitin-conjugating enzyme Cdc34 controls cellular proliferation through regulation of p27 Kip1 protein levels. Exp Cell Res 303:482–493.
141. Eliseeva E, Pati D, Diccinanni MB, Yu AL, Mohsin SK, Margolin JF, Plon SE (2001) Expression and localization of the CDC34 ubiquitin-conjugating enzyme in pediatric acute lymphoblastic leukemia. Cell Growth Differ 12:427–433.
142. Chauhan D, Li G, Hideshima T, Podar K, Shringarpure R, Mitsiades C, Munshi N, Yew PR, Anderson KC (2004) Blockade of ubiquitin-conjugating enzyme CDC34 enhances anti-myeloma activity of Bortezomib/Proteasome inhibitor PS-341. Oncogene 23:3597–3602.
143. Tanaka K, Kondoh N, Shuda M, Matsubara O, Imazeki N, Ryo A, Wakatsuki T, Hada A, Goseki N, Igari T, Hatsuse K, Aihara T, Horiuchi S, Yamamoto N, Yamamoto M (2001) Enhanced expression of mRNAs of antisecretory factor-1, gp96, DAD1 and CDC34 in human hepatocellular carcinomas. Biochim Biophys Acta 1536:1–12.
144. Ceccarelli DF, Tang X, Pelletier B, Orlicky S, Xie W, Plantevin V, Neculai D, Chou YC, Ogunjimi A, Al-Hakim A, Varelas X, Koszela J, Wasney GA, Vedadi M, Dhe-Paganon S, Cox S, Xu S, Lopez-Girona A, Mercurio F, Wrana J, Durocher D, Meloche S, Webb DR, Tyers M, Sicheri F. An allosteric inhibitor of the human Cdc34 ubiquitin-conjugating enzyme. Cell. 2011 Jun 24.
145. Rechsteiner M, Hill CP. Mobilizing the proteolytic machine: cell biological roles of proteasome activators and inhibitors. Trends Cell Biol. 2005 Jan.
146. Oxford Dictionary of Biochemistry and Molecular Biology, Oxford University Press Inc.: New York 2000.
147. Tan X, Osmulski PA, Gaczynska M. Allosteric regulators of the proteasome: potential drugs and a novel approach for drug design. Curr Med Chem. 2006.
148. Coffino P, Cheng Y. Allostery Modulates Interactions between Proteasome Core Particles and Regulatory Particles. Biomolecules. 2022 May 30;12(6):764.

149. Groll M, Huber R, Moroder L. The persisting challenge of selective and specific proteasome inhibition. J Pept Sci. 2009 Feb;15(2):58-66.
150. Bajorek M, Glickman MH. Keepers at the final gates: regulatory complexes and gating of the proteasome channel. Cell Mol Life Sci. 2004 Jul.
151. P. Beck, T.A. Lansdell, N.M. Hewlett, J.J. Tepe, M. Groll Angew. Chem. Int. Ed., Engl. (2015)
152. S. Ozcan, A. Kazi, F. Marsilio, B. Fang, W.C. Guida, J. Koomen, H.R. Lawrence, S.M. Sebti J. Med. Chem., 56 (2013), p. 3783
153. N. Gallastegui, P. Beck, M. Arciniega, R. Huber, S. Hillebrand, M. Groll Angew. Chem. Int., Ed. Engl., 51 (2012), p. 247.
154. T.A. Lansdell, M.A. Hurchla, J. Xiang, S. Hovde, K.N. Weilbaecher, R.W. Henry, J.J. Tepe ACS Chem. Biol., 8 (2013), p. 578.
155. L. Azevedo, T. Lansdell, J. Ludwig, D. Woloch, D. Cogan, G. Patten, M. Kuszpit, J. Fisk, R.A. Mosey, J.J. Tepe J. Med. Chem., 56 (2013), p. 5974
156. N. Basse, M. Montes, X. Marechal, L. Qin, M. Bouvier-Durand, E. Genin, J. Vidal, B.O. Villoutreix, M. Reboud-Ravaux J. Med. Chem., 53 (2010), p. 509
157. M. Hasegawa, Y. Yasuda, M. Tanaka, K. Nakata, E. Umeda, Y. Wang, C. Watanabe, S. Uetake, T. Kunoh, M. Shionyu, R. Sasaki, I. Shiina, T. Mizukami Eur. J. Med. Chem., 71 (2014), p. 290.
158. Hajri M, Esteve MA, Khoumeri O, Abderrahim R, Terme T, Montana M, Vanelle P. Synthesis and evaluation of in vitro antiproliferative activity of new ethyl 3-(arylethynyl)quinoxaline-2-carboxylate and pyrido[4,3-b]quinoxalin-1(2H)-one derivatives. Eur J Med Chem. 2016 Nov 29.
159. Salman Ahmad Khan, Kishwar Saleem, Zaheer Khan, Synthesis, characterization and in vitro antibacterial activity of new steroidal thiazolo quinoxalines, European Journal of Medicinal Chemistry, Volume 42, Issue 1,2007,Pages 103-108.
160. Lawrence, H. R.; Kazi, A.; Luo, Y.; Kendig, R.; Ge, Y.; Jain, S.; Daniel, K.; Santiago, D.; Guida, W. C.; Sebti, S. M. Bioorg. Med. Chem. 2010, 18, 5576.
161. Xiaoming Li, Tabitha E. Wood, Remco Sprangers, Gerrit Jansen, Niels E. Franke, Xinliang Mao, Xiaoming Wang, Yi Zhang, Sue Ellen Verbrugge, Hans Adomat, Zhi Hua Li, Suzanne Trudel, Christine Chen, Tomasz L. Religa, Nazir Jamal, Hans Messner, Jacqueline Cloos, David R. Rose, Ami Navon, Emma Guns, Robert A. Batey, Lewis E. Kay, Aaron D. Schimmer, Effect of Noncompetitive Proteasome Inhibition on Bortezomib Resistance, *JNCI: Journal of the National Cancer Institute*, Volume 102, Issue 14, 21 July 2010, Pages 1069–1082.
162. A. Burguete, E. Pontiki, D. Hadjipavlou-Litina, S. Ancizu and R. Villar, et al., Synthesis and Biological evaluation of New Quinoxaline Derivatives as Antioxidant and Anti-Inflammatory Agents, Chem. Biol. Drug Des., 2011, 77, 255–267.
163. M. S. Gomaa, Abdulghany H. A. Ahmed, S. M. El Rayes, Ibrahim A. I. Ali, Walid Fathalla, Mansour S. Alturki, Abdulaziz Hassan Al Khzem, Atiah H. Almalki, Mohammed F. Aldawsari, F. H. Pottoo, Firdos A. Khan, Mohd Amir, Synthesis and antiproliferative activity of 2-oxo-3-phenylquinoxaline derivatives and related compounds against colon cancer, RSC Advances, Volume 14, Issue 48, 2024, Pages 35679-35695.
164. McDaniel TJ, Lansdell TA, Dissanayake AA, Azevedo LM, Claes J, Odom AL, Tepe JJ. Substituted quinolines as noncovalent proteasome inhibitors. Bioorg Med Chem. 2016 Jun 1;24(11):2441-2450. doi: 10.1016/j.bmc.2016.04.005. Epub 2016 Apr 2.

165. Brown, D.J. In The Heterocycles Compounds: The Quinoxalines Supplement II; Taylor-Wipf, Ed.; John Wiley & Sons, Inc: Hoboken, 2004.
166. Carta A, Piras S, Loriga G, Paglietti G. Chemistry, biological properties and SAR analysis of quinoxalinones. Mini Rev Med Chem. 2006 Nov.
167. Sanna, P.; Carta, A.; Loriga, M.; Zanetti, S.; Sechi, L. Farmaco, 1998, 53, 455.
168. Sanna, P.; Carta, A.; Loriga, M.; Zanetti, S.; Sechi, L. Farmaco, 1999, 54, 161.
169. Sanna, P.; Carta, A.; Loriga, M.; Zanetti, S.; Sechi, L. Farmaco, 1999, 54, 169.
170. Carta, A.; Loriga, M.; Zanetti, S.; Sechi, L. Farmaco, 2003, 58, 1251.
171. Carta, A.; Sanna, P.; Loriga, M.; Setzu, M.G.; La Colla, P.; Loddo, R. Farmaco, 2002, 57, 19.
172. Young, S.D.; Britcher, S.F.; Tran, L.O.; Payne, L.S.; Lumma, W.C.; Lyle, T.A.; Huff, J.R.; Anderson, P.S.; Olsen, D.B.; Carroll, S.S. Antimicrob. Agents Chemother., 1995, 39, 2602.
173. Patel, M.; Ko, S.S.; Mchugh, R.J.; Markwalder, J.A.; Srivastava, A.S., Cordova, B.C.; Klabe, R.M.; Erickson-Viitanen, S.; Trainor, G.L.; Seitz, S.P. Bioorg. Med. Chem. Lett., 1999, 9, 2805.
174. Patel, M.; Mchugh, R.J.; Cordova, B.C.; Klabe, R.M.; Erickson- Viitanen, S.; Trainor, G.L.; Ko, S.S. Bioorg. Med. Chem. Lett., 1999, 9, 3221.
175. Drugs Fut., 1999, 24, 201.
176. Kleim, J.-P.; Bender, R.; Billhard, U.M.; Meischner, C.; Reiss, G.; Rosner, M.; Winkler, I.; Paessens, A. Antimicrob. Agents Che-mother., 1993, 37, 1659.
177. Drugs Fut., 2000, 25, 24.
178. Ahren, B.; Simmonsson, E.; Larsson, H.; Landin-Olsson, M.; Torheirsson, H.; Jansson, P.A.; Sanqqvist, M.; Bavenholm, P.; Efendic, S.; Eviksson, J. W.; Dickinson, S.; Holmes, D. Diabetes Care, 2002, 25, 869.
179. Cheon HG, Lee CM, Kim BT, Hwang KJ. Lead discovery of quinoxalinediones as an inhibitor of dipeptidyl peptidase-IV (DPP-IV) by high-throughput screening. Bioorg Med Chem Lett. 2004 May 17.
180. Alamanni, M.C.; Pirisino, G.; Savelli, F.; Sparatore, F.; Manca, P.; Satta, M. Farmaco, 1981, 36, 359.
181. Pirisino, G.; Alamanni, M.C.; Savelli, F.; Sparatore, F.; Manca, P.; Satta, M. Farmaco, 1983, 38, 359.
182. Savelli, F.; Pirisino, G.; Alamanni, M.C.; Manca, P.; Satta, M. Farmaco, 1983, 38, 869.
183. Sparatore, A.; Boido-Canu, C.; Sparatore, F.; Manca, P.; Satta, M. Farmaco, 1985, 40, 303.
184. Sparatore, A.; Vaccai, A.; Boido V.; Sparatore, F. Farmaco, 1995, 50, 217.
185. Ries, U.J.; Priepke, H.W.M.; Hauel, N.H.; Handschuh, S.; Mihm, G.; Stassen, J.M.; Wienen, W.; Nar, H. Bioorg. Med. Chem. Lett., 2003, 13, 2297.
186. Willardssen, J.A.; Dudley, D.A.; Cody, W.L.; Chi, L.; McClanahan, T.B.; Mertz, T.E.; Potoczak, R.E.; Narasimhan, L.S.; Holland, D.R.; Rapundalo, S.T.; Edmunds, J. J. Med. Chem., 2004, 47, 4089.
187. El-Adl K, Sakr HM, Yousef RG, Mehany ABM, Metwaly AM, Elhendawy MA, Radwan MM, ElSohly MA, Abulkhair HS, Eissa IH. Discovery of new quinoxaline-2(1H)-one-based anticancer agents targeting VEGFR-2 as inhibitors: Design, synthesis, and anti-proliferative evaluation. Bioorg Chem. 2021 Sep.
188. Koizumi S, Irie T, Hirayama S, Sakurai Y, Yashiroda H, Naguro I, Ichijo H, Hamazaki J, Murata S. The aspartyl protease DDI2 activates Nrf1 to compensate for proteasome dysfunction. eLife. 2016.
189. Ibtisam I, Kisselev AF. Early recovery of proteasome activity in cells pulse-treated with proteasome inhibitors is independent of DDI2. Elife. 2024 Apr 15.
190. Wang A, Abulaiti X, Zhang H, Su H, Liu G, Gao S, Li L. Cancer Cells Evade Stress-Induced Apoptosis by Promoting HSP70-Dependent Clearance of Stress Granules. Cancers (Basel). 2022 Sep 25.

191. Boukamp, P., Petrussevska, R.T., Breitkreutz, D., Hornung, J., Markham, A., & Fusenig, N.E. (1988). *Normal keratinization in a spontaneously immortalized aneuploid human keratinocyte cell line*. *Journal of Cell Biology*, 106(3), 761–771.

192. Jung T; Grune T The Proteasome and Its Role in the Degradation of Oxidized Proteins. IUBMB Life 2008, 60, 743–752.

193. Grune T; Reinheckel T; Davies KJ Degradation of Oxidized Proteins in Mammalian Cells. FASEB J. 1997, 11, 526–534.

194. Sitte N; Merker K; Grune T Proteasome-Dependent Degradation of Oxidized Proteins in MRC-5 Fibroblasts. FEBS Lett. 1998, 440, 399–402.

195. Reinheckel T; Sitte N; Ullrich O; Kuckelkorn U; Davies KJ; Grune T Comparative Resistance of the 20S and 26S Proteasome to Oxidative Stress. Biochem. J 1998, 335, 637–642.

196. Wang X; Yen J; Kaiser P; Huang L Regulation of the 26S Proteasome Complex During Oxidative Stress. Sci. Signaling 2010, 3, ra88.

197. Bedford L; Hay D; Devoy A; Paine S; Powe DG; Seth R; Gray T; Topham I; Fone K; Rezvani N; Mee M; Soane T; Layfield R; Sheppard PW; Ebendal T; Usoskin D; Lowe J; Mayer RJ Depletion of 26S Proteasomes in Mouse Brain Neurons Causes Neurodegeneration and Lewy-like Inclusions Resembling Human Pale Bodies. J. Neurosci 2008, 28, 8189–8198.

198. Liu Y; Hettinger CL; Zhang D; Rezvani K; Wang X; Wang H The Proteasome Function Reporter GFPu Accumulates in Young Brains of the APPswe/PS1dE9 Alzheimer's Disease Mouse Model. Cell. Mol. Neurobiol 2014, 34, 315–322.

199. Albanese V, Pedriali G, Fabbri M, Ciancetta A, Ravagli S, Roccatello C, Guerrini R, Morciano G, Preti D, Pinton P, Pacifico S. Design and synthesis of 1,4,8-triazaspiro[4.5]decan-2-one derivatives as novel mitochondrial permeability transition pore inhibitors. J Enzyme Inhib Med Chem. 2025 Dec;40(1):2505907.

200. Myeku N, Metcalfe MJ, Huang Q, Figueiredo-Pereira M. Assessment of proteasome impairment and accumulation/aggregation of ubiquitinated proteins in neuronal cultures. Methods Mol Biol. 2011;793:273-96.

201. Gilda JE, Nahar A, Kasiviswanathan D, Tropp N, Gilinski T, Lahav T, Alexandrovich D, Mandel-Gutfreund Y, Park S, Shemer S. Proteasome gene expression is controlled by coordinated functions of multiple transcription factors. J Cell Biol. 2024 Aug 5.

202. Brunner, J. *Photoaffinity labeling—An overview.* Annu. Rev. Biochem. 1993, 62, 483–514.

203. Westheimer, The photolysis of diazoacetylchymotrypsin. A. Singh, E. R. Thornton, F. H. 1962. J Biol Chem. vol. 237:3006-8.

204. Sadakane, Y. Hatanaka Y., Photochemical fishing approaches for identifying target proteins and elucidating the structure of a ligand-binding region using carbene-generating photoreactive probes, 2006. Anal Sci. vol. 22(2):209-18.

205. Lapinsky DJ, Johnson DS. Recent developments and applications of clickable photoprobes in medicinal chemistry and chemical biology. Future Med Chem. 2015;7(16):2143-71.

206. Smith E, Collins I. Photoaffinity labeling in target- and binding-site identification. Future Med Chem. 2015;7(2):159-83.

207. Kolb HC, Sharpless KB. The growing impact of click chemistry on drug discovery. Drug Discov Today. 2003 Dec 15;8(24):1128-37.

208. Liu J., Liu C., He W. *Fluorophores and Their Applications as Molecular Probes in Living Cells*. Current Organic Chemistry, 2013, 17(6): 564–579.
209. Martin JB. Molecular basis of the neurodegenerative disorders. N Engl J Med. 1999 Jun 24.
210. Hague SM, Klaffke S, Bandmann O. Neurodegenerative disorders: Parkinson's disease and Huntington's disease. J Neurol Neurosurg Psychiatry. 2005 Aug.
211. Mattson MP. Apoptosis in neurodegenerative disorders. Nat Rev Mol Cell Biol. 2000 Nov.
212. Lamptey RNL, Chaulagain B, Trivedi R, Gothwal A, Layek B, Singh J. A Review of the Common Neurodegenerative Disorders: Current Therapeutic Approaches and the Potential Role of Nanotherapeutics. Int J Mol Sci. 2022 Feb 6.
213. Chen C. Fronting the twin challenges: Alzheimer's and Parkinson's disease. Arch Alzheimers Parkinsons Dis. 2024;1(1):1-3.
214. Breijyeh Z, Karaman R. Comprehensive Review on Alzheimer's Disease: Causes and Treatment. Molecules. 2020 Dec 8;25(24):5789.
215. Eldufani J, Blaise G. The role of acetylcholinesterase inhibitors such as neostigmine and rivastigmine on chronic pain and cognitive function in aging: A review of recent clinical applications. Alzheimers Dement (N Y). 2019 Jun 4;5:175-183.
216. Lahiri D.K., Chen D.M., Lahiri P., Bondy S., Greig N.H. Amyloid, cholinesterase, melatonin, and metals and their roles in aging and neurodegenerative diseases. Ann New York Acad Sci. 2005;1056:430–449.
217. Ballard C.G. Advances in the treatment of Alzheimer's disease: benefits of dual cholinesterase inhibition. Eur Neurol. 2002;47:64–70.
218. Taylor P. 12th ed. Macmillan; New York: 2011. Anticholinesterase agents. Goodman & Gilman's The Pharmacological Basis of Therapeutics; pp. 239–254.
219. Wang R., Reddy P.H. Role of glutamate and NMDA receptors in Alzheimer's disease. J. Alzheimer's Dis. Jad. 2017;57:1041–1048.
220. Kuns B., Rosani A., Varghese D. StatPearls. StatPearls Publishing; Treasure Island, FL, USA: 2020. [(accessed on 8 December 2020)]. Memantine.
221. Kishi T, Matsunaga S, Oya K, Nomura I, Ikuta T, Iwata N. Memantine for Alzheimer's disease: an updated systematic review and meta-analysis. Journal of Alzheimer's Disease. 2017 Jan 1;60(2):401-25.
222. LeWitt PA. Levodopa therapy for Parkinson's disease: Pharmacokinetics and pharmacodynamics. Mov Disord. 2015 Jan;30(1):64-72.
223. Yamamoto M, Schapira AH. Dopamine agonists in Parkinson's disease. Expert Review of Neurotherapeutics. 2008 Apr 1;8(4):671-7.
224. YY Szeto J, JG Lewis S. Current treatment options for Alzheimer's disease and Parkinson's disease dementia. Current Neuropharmacology. 2016 May 1;14(4):326-38.
225. Ganguly G, Chakrabarti S, Chatterjee U, Saso L. Proteinopathy, oxidative stress and mitochondrial dysfunction: cross talk in Alzheimer's disease and Parkinson's disease. Drug Design, Development and Therapy. 2017 Mar 16:797-810.
226. Jiang T, Sun Q, Chen S. Oxidative stress: A major pathogenesis and potential therapeutic target of antioxidative agents in Parkinson's disease and Alzheimer's disease. Progress in Neurobiology. 2016 Dec 1;147:1-9.
227. Coppedè F. The potential of epigenetic therapies in neurodegenerative diseases. Front Genet. 2014 Jul 14;5:220. doi: 10.3389/fgene.2014.00220.

228. Stuart M. Raleigh, Chapter 2 - Epigenetic processes—An overview, Editor(s): Stuart M. Raleigh, In Translational Epigenetics, Epigenetics of Exercise and Sports, Academic Press, Volume 25, 2021, Pages 23-3
229. Ghosh P, Saadat A. Neurodegeneration and epigenetics: A review. Neurologia (Engl Ed). 2023 Jul-Aug;38(6):e62-e68.
230. Villa C, Stoccoro A. Epigenetic Peripheral Biomarkers for Early Diagnosis of Alzheimer's Disease. Genes (Basel). 2022 Jul 22;13(8):1308.
231. Icardi, L., De Bosscher, K., Tavernier, J. (2012). The HAT/HDAC interplay: Multilevel control of STAT signaling. Cytokine Growth Factor Rev. 23.
232. Rousseaux, S., Khochbin, S. (2015). Histone Acylation beyond Acetylation: Terra Incognita in Chromatin Biology. Cell J. 17.
233. Saha, R. N., Pahan, K. (2005). HATs and HDACs in neurodegeneration: a tale of disconcerted acetylation homeostasis. Cell Death Differ 13 (4), 539–550.
234. Shukla S, Tekwani BL. Histone Deacetylases Inhibitors in Neurodegenerative Diseases, Neuroprotection and Neuronal Differentiation. Front Pharmacol. 2020 Apr 24.
235. Haberland, M., Montgomery, R. L., Olson, E. N. (2009). The many roles of histone deacetylases in development and physiology: implications for disease and therapy. Nat. Rev. Genet. 10 (1), 32–42.
236. De Ruijter, A. J. M., van Gennip, A. H., Caron, H. N., Kemp, S., van Kuilenburg, A. B. P. (2003). Histone deacetylases (HDACs): characterization of the classical HDAC family. Biochem. J. 370 (3), 737–749.
237. Wiech, N., Fisher, J., Helquist, P., Wiest, O. (2009). Inhibition of Histone Deacetylases: A Pharmacological Approach to the Treatment of Non-Cancer Disorders. CTMC 9 (3), 257–271.
238. Bjerling, P., Silverstein, R. A., Thon, G., Caudy, A., Grewal, S., Ekwall, K. (2002). Functional Divergence between Histone Deacetylases in Fission Yeast by Distinct Cellular Localization and In Vivo Specificity. Mol. Cell. Biol. 22 (7), 2170–2181.
239. Yang, X.-J., Seto, E. (2008). The Rpd3/Hda1 family of lysine deacetylases: from bacteria and yeast to mice and men. Nat. Rev. Mol. Cell Biol. 9 (3), 206–218.
240. Wiech, N., Fisher, J., Helquist, P., Wiest, O. (2009). Inhibition of Histone Deacetylases: A Pharmacological Approach to the Treatment of Non-Cancer Disorders. CTMC 9 (3), 257–271.
241. Michan, S., Sinclair, D. (2007). Sirtuins in mammals: insights into their biological function. Biochem. J. 404 (1), 1–13.
242. Kazantsev, A. G., Thompson, L. M. (2008). Therapeutic application of histone deacetylase inhibitors for central nervous system disorders. Nat. Rev. Drug Discovery 7 (10), 854–868.
243. Marks, P., Xu, W.-S. (2009). Histone deacetylase inhibitors: Potential in cancer therapy. J. Cell. Biochem 107, 600–608.
244. Konsoula, Z., Barile, F. A. (2012). Epigenetic histone acetylation and deacetylation mechanisms in experimental models of neurodegenerative disorders. J. Pharmacol. Toxicolog. Methods 66 (3), 215–220.
245. Ziemka-Nalecz, M., Jaworska, J., Sypecka, J., Zalewska, T. (2018). Histone Deacetylase Inhibitors: A Therapeutic Key in Neurological Disorders? J. Neuropathol. Exp. Neurol. 77 (10), 855–870.
246. Chuang, D.-M., Leng, Y., Marinova, Z., Kim, H.-J., Chiu, C.-T. (2009). Multiple roles of HDAC inhibition in neurodegenerative conditions. Trends Neurosci. 32 (11), 591–601.
247. Butler, R., Bates, G. P. (2006). Histone deacetylase inhibitors as therapeutics for polyglutamine disorders. Nat. Rev. Neurosci. 7 (10), 784–796.

248. Guidotti, A., Dong, E., Kundakovic, M., Satta, R., Grayson, D. R., Costa, E. (2009). Characterization of the action of antipsychotic subtypes on valproate-induced chromatin remodeling. Trends Pharmacol. Sci. 30 (2), 55–60.
249. Saha, R. N., Pahan, K. (2005). HATs and HDACs in neurodegeneration: a tale of disconcerted acetylation homeostasis. Cell Death Differ 13 (4), 539–550.
250. Hao, Y. (2004). Mood Stabilizer Valproate Promotes ERK Pathway-Dependent Cortical Neuronal Growth and Neurogenesis. J. Neurosci. 24 (29), 6590–6599.
251. Kim, H. J., Rowe, M., Ren, M., Hong, J. S., Chen, P. S., Chuang, D. M. (2007). Histone Deacetylase Inhibitors Exhibit Anti-Inflammatory and Neuroprotective Effects in a Rat Permanent Ischemic Model of Stroke: Multiple Mechanisms of Action. J. Pharmacol. Exp. Ther. 321 (3), 892–901.
252. Peng, G.-S., Li, G., Tzeng, N.-S., Chen, P.-S., Chuang, D.-M., Hsu, Y.-D., et al. (2005). Valproate pretreatment protects dopaminergic neurons from LPS-induced neurotoxicity in rat primary midbrain cultures: role of microglia. Mol. Brain Res. 134 (1), 162–169.
253. Dash, P. K., Orsi, S. A., Moore, A. N. (2009). Histone deactylase inhibition combined with behavioral therapy enhances learning and memory following traumatic brain injury. Neuroscience 163 (1), 1–8.
254. Vecsey, C. G., Hawk, J. D., Lattal, K. M., Stein, J. M., Fabian, S. A., Attner, M. A., et al. (2007). Histone deacetylase inhibitors enhance memory and synaptic plasticity via CREB:CBP-dependent transcriptional activation. J. Neurosci. 27 (23), 6128–6140.
255. Schroeder, F. A., Lin, C. L., Crusio, W. E., Akbarian, S. (2007). Antidepressant-Like Effects of the Histone Deacetylase Inhibitor, Sodium Butyrate, in the Mouse. Biol. Psychiatry 62 (1), 55–64.
256. Raza C., Anjum R., Shakeel N.U.A. Parkinson’s disease: Mechanisms, translational models and management strategies. Life Sci. 2019;226:77–90.
257. Kordower J.H., Olanow C.W., Dodiya H.B., Chu Y., Beach T.G., Adler C.H., Halliday G.M., Bartus R.T. Disease duration and the integrity of the nigrostriatal system in Parkinson’s disease. Pt 8Brain. 2013;136:2419–2431.
258. Kalia L.V., Lang P.E. Parkinson’s disease. Lancet. 2015;386:896–912. doi: 10.1016/S0140-6736(14)61393-3.
259. Peng C., Trojanowski J.Q., Lee V.M. Protein transmission in neurodegenerative disease. Nat. Rev. Neurol. 2020;16:199–212.
260. Mezzaroba L., Alfieri D.F., Colado Simão A.N., Reiche E.M.V. The role of zinc, copper, manganese and iron in neurodegenerative diseases. Neurotoxicology. 2019;74:230–241.
261. Puspita L., Chung S.Y., Shim J.W. Oxidative stress and cellular pathologies in Parkinson’s disease. Mol. Brain. 2017;10:53.
262. Przedborski S. The two-century journey of Parkinson disease research. Nat. Rev. Neurosci. 2017;18:251–259.
263. Abeliovich A., Gitler A.D. Defects in trafficking bridge Parkinson’s disease pathology and genetics. Nature. 2016;539:207–216.
264. Li Y, Gu Z, Lin S, Chen L, Dzreyan V, Eid M, Demyanenko S, He B. Histone Deacetylases as Epigenetic Targets for Treating Parkinson's Disease. Brain Sci. 2022 May 21;12(5):672. doi: 10.3390/brainsci12050672. Erratum in: Brain Sci. 2025 Mar 24;15(4):335.
265. Harrison, I. F., Dexter, D. T. (2013). Epigenetic targeting of histone deacetylase: Therapeutic potential in Parkinson's disease? Pharmacol. Ther. 140 (1), 34–52.

266. Sharma, S., Taliyan, R. (2015a). Targeting histone deacetylases: a novel approach in Parkinson's disease. Parkinson's Dis. 2015, 303294–303294.
267. Hegarty, S. V., Sullivan, A. M., O'Keeffe, G. W. (2016b). The Epigenome as a therapeutic target for Parkinson's disease. Neural Regeneration Res. 11 (11), 1735–1738.
268. Tan, Y., Delvaux, E., Nolz, J., Coleman, P. D., Chen, S., Mastroeni, D. (2018). Upregulation of histone deacetylase 2 in laser capture nigral microglia in Parkinson's disease. Neurobiol. Aging 68, 134–141.
269. Thomas E.A., D'Mello S.R. Complex neuroprotective and neurotoxic effects of histone deacetylases. J. Neurochem. 2018;145:96–110.
270. Patnaik D., Pao P.C., Zhao W.N., Silva M.C., Hylton N.K., Chindavong P.S., Pan L., Tsai L.-H., Haggarty S.J. Exifone Is a Potent HDAC1 Activator with Neuroprotective Activity in Human Neuronal Models of Neurodegeneration. ACS Chem. Neurosci. 2021;12:271–284.
271. Mazzocchi M., Collins L.M., Sullivan A.M., O'Keeffe G.W. The class II histone deacetylases as therapeutic targets for Parkinson's disease. Neuronal Signal. 2020;4:NS20200001.
272. Gebremedhin K.G., Rademacher D.J. Histone H3 acetylation in the postmortem Parkinson's disease primary motor cortex. Neurosci. Lett. 2016;627:121–125.
273. Dijkstra A.A., Ingrassia A., de Menezes R.X., van Kesteren R.E., Rozemuller A.J.M., Heutink P., van de Berg W.D.J. Evidence for Immune Response, Axonal Dysfunction and Reduced Endocytosis in the Substantia Nigra in Early Stage Parkinson's Disease. PLoS ONE. 2015;10:e0128651.
274. Park G., Tan J., Garcia G., Kang Y., Salvesen G., Zhang Z. Regulation of Histone Acetylation by Autophagy in Parkinson Disease. J. Biol. Chem. 2016;291:3531–3540.
275. Harrison I.F., Smith A.D., Dexter D.T. Pathological histone acetylation in Parkinson's disease: Neuroprotection and inhibition of microglial activation through SIRT 2 inhibition. Neurosci. Lett. 2018;666:48–57.
276. Gardian, G., Yang, L., Cleren, C., Calingasan, N. Y., Klivenyi, P., Beal, M. F. (2004). Neuroprotective Effects of Phenylbutyrate Against MPTP Neurotoxicity. NMM 5 (3), 235–242.
277. Gasser, T. (2001). Genetics of Parkinson's disease. J. Neurol. 248, 833–840.
278. Kontopoulos, E., Parvin, J. D., Feany, M. B. (2006). α-synuclein acts in the nucleus to inhibit histone acetylation and promote neurotoxicity. Hum. Mol. Genet. 15 (20), 3012–3023.
279. Gupta R., Ambasta R.K., Kumar P. Pharmacological intervention of histone deacetylase enzymes in the neurodegenerative disorders. Life Sci. 2020;243:117278.
280. Mohd Murshid N., Aminullah Lubis F., Makpol S. Epigenetic Changes and Its Intervention in Age-Related Neurodegenerative Diseases. Cell Mol. Neurobiol. 2022;42:577–595.
281. Wang R., Sun H., Wang G., Ren H. Imbalance of Lysine Acetylation Contributes to the Pathogenesis of Parkinson's Disease. Int. J. Mol. Sci. 2020;21:7182.
282. Teijido O., Cacabelos R. Pharmacoepigenomic Interventions as Novel Potential Treatments for Alzheimer's and Parkinson's Diseases. Int. J. Mol. Sci. 2018;19:3199.
283. Harrison I.F., Dexter D.T. Epigenetic targeting of histone deacetylase: Therapeutic potential in Parkinson's disease? Pharmacol. Ther. 2013;140:34–52.
284. Wu X., Chen P.S., Dallas S., Wilson B., Block M.L., Wang C.-C., Kinyamu H., Lu N., Gao X., Leng, Y., et al. Histone deacetylase inhibitors up-regulate astrocyte GDNF and BDNF gene transcription and protect dopaminergic neurons. Int. J. Neuropsychopharmacol. 2008;11:1123–1134.

285. Chen P.S., Wang C.C., Bortner C.D., Peng G.-S., Wu X., Pang H., Lu R.-B., Gean P.-W., Chuang D.-M., Hong J.-S. Valproic acid and other histone deacetylase inhibitors induce microglial apoptosis and attenuate lipopolysaccharide-induced dopaminergic neurotoxicity. Neuroscience. 2007;149:203–212.
286. Rane P., Shields J., Heffernan M., Guo Y., Akbarian S., King J.A. The histone deacetylase inhibitor, sodium butyrate, alleviates cognitive deficits in pre-motor stage PD. Neuropharmacology. 2012;62:2409–2412.
287. Sharma S., Taliyan R., Singh S. Beneficial effects of sodium butyrate in 6-OHDA induced neurotoxicity and behavioral abnormalities: Modulation of histone deacetylase activity. Behav. Brain Res. 2015;291:306–314.
288. Chen S.H., Wu H.M., Ossola B., Schendzielorz N., Wilson B., Chu C., Chen S., Wang Q., Zhang D., Qian L., et al. Suberoylanilide hydroxamic acid, a histone deacetylase inhibitor, protects dopaminergic neurons from neurotoxin-induced damage. Br. J. Pharmacol. 2012;165:494–505.
289. Kidd S.K., Schneider J.S. Protection of dopaminergic cells from MPP+-mediated toxicity by histone deacetylase inhibition. Brain Res. 2010;1354:172–178.
290. Johnston T.H., Huot P., Damude S., Fox S.H., Jones S.W., Rusche J.R., Brotchie J. RGFP109, a histone deacetylase inhibitor attenuates L-DOPA-induced dyskinesia in the MPTP-lesioned marmoset: A proof-of-concept study. Parkinsonism Relat. Disord. 2013;19:260–264.
291. Choong C.J., Sasaki T., Hayakawa H., Yasuda T., Baba K., Hirata Y., Uesato S., Mochizuki H. A novel histone deacetylase 1 and 2 isoform-specific inhibitor alleviates experimental Parkinson's disease. Neurobiol. Aging. 2016;37:103–116.
292. Hirata Y., Sasaki T., Kanki H., Choong C.-J., Nishiyama K., Kubo G., Hotei A., Taniguchi M., Mochizuki H., Uesato S. New 5-Aryl-Substituted 2-Aminobenzamide-Type HDAC Inhibitors with a Diketopiperazine Group and Their Ameliorating Effects on Ischemia-Induced Neuronal Cell Death. Sci. Rep. 2018;8:1400.
293. Mazzocchi M., Goulding S.R., Wyatt S.L., Collins L.M., Sullivan A.M., O'Keeffe G.W. LMK235, a small molecule inhibitor of HDAC4/5, protects dopaminergic neurons against neurotoxin and α-synuclein-induced degeneration in cellular models of Parkinson's disease. Mol. Cell Neurosci. 2021;115:103642.
294. Formisano L., Guida N., Laudati G., Mascolo L., Di Renzo G., Canzoniero L.M.T. MS-275 inhibits aroclor 1254-induced SH-SY5Y neuronal cell toxicity by preventing the formation of the HDAC3/REST complex on the synapsin-1 promoter. J. Pharmacol. Exp. Ther. 2015;352:236–243.
295. World Health Organization, Global action plan on the public health response to dementia (2017–2025), WHO (2017), p. 44.
296. De Ture MA, Dickson DW. The neuropathological diagnosis of Alzheimer's disease. Mol Neurodegener. 2019 Aug 2;14(1):32.
297. Márcia Pereira, Maria Teresa Cruz, Ana Fortuna, Joana Bicker, Restoring the epigenome in Alzheimer's disease: advancing HDAC inhibitors as therapeutic agents, Drug Discovery Today, Volume 29, Issue 7, 2024, 104052, ISSN 1359-6446.
298. Zhu X, Wang S, Yu L, Jin J, Ye X, Liu Y, Xu Y. HDAC3 negatively regulates spatial memory in a mouse model of Alzheimer's disease. Aging Cell. 2017 Oct;16(5):1073-1082.
299. Villa C, Stoccoro A. Epigenetic Peripheral Biomarkers for Early Diagnosis of Alzheimer's Disease. Genes (Basel). 2022 Jul 22;13(8):1308.
300. Liu P, Liu X, Yang H (2019), "Evaluation of the marine economic development quality in Qingdao based on entropy and grey relational analysis". Marine Economics and Management, Vol. 2 No. 1 pp. 29–38.

301. Sharma VK, Mehta V, Singh TG. Alzheimer's Disorder: Epigenetic Connection and Associated Risk Factors. Curr Neuropharmacol. 2020;18(8):740-753.
302. Wey HY, Gilbert TM, Zürcher NR, She A, Bhanot A, Taillon BD, Schroeder FA, Wang C, Haggarty SJ, Hooker JM. Insights into neuroepigenetics through human histone deacetylase PET imaging. Sci Transl Med. 2016 Aug 10;8(351):351ra106.
303. Guan JS, Haggarty SJ, Giacometti E, Dannenberg JH, Joseph N, Gao J, Nieland TJ, Zhou Y, Wang X, Mazitschek R, Bradner JE, DePinho RA, Jaenisch R, Tsai LH. HDAC2 negatively regulates memory formation and synaptic plasticity. Nature. 2009 May 7;459(7243):55-60.
304. Kim C, Choi H, Jung ES, Lee W, Oh S, Jeon NL, Mook-Jung I. HDAC6 inhibitor blocks amyloid beta-induced impairment of mitochondrial transport in hippocampal neurons. PLoS One. 2012;7(8):e42983.
305. Mahady L, Nadeem M, Malek-Ahmadi M, Chen K, Perez SE, Mufson EJ. Frontal Cortex Epigenetic Dysregulation During the Progression of Alzheimer's Disease. J Alzheimers Dis. 2018;62(1):115-131.
306. Gräff J, Rei D, Guan JS, Wang WY, Seo J, Hennig KM, Nieland TJ, Fass DM, Kao PF, Kahn M, Su SC, Samiei A, Joseph N, Haggarty SJ, Delalle I, Tsai LH. An epigenetic blockade of cognitive functions in the neurodegenerating brain. Nature. 2012 Feb 29;483(7388):222-6.
307. Lu X, Wang L, Yu C, Yu D, Yu G. Histone Acetylation Modifiers in the Pathogenesis of Alzheimer's Disease. Front Cell Neurosci. 2015 Jun 16;9:226.
308. Carlomagno Y, Chung DC, Yue M, Castanedes-Casey M, Madden BJ, Dunmore J, Tong J, DeTure M, Dickson DW, Petrucelli L, Cook C. An acetylation-phosphorylation switch that regulates tau aggregation propensity and function. J Biol Chem. 2017 Sep 15;292(37):15277-15286.
309. Gräff J, Tsai LH. The potential of HDAC inhibitors as cognitive enhancers. Annu Rev Pharmacol Toxicol. 2013;53:311-30. doi: 10.1146/annurev-pharmtox-011112-140216.
310. Anderson KW, Chen J, Wang M, Mast N, Pikuleva IA, Turko IV. Quantification of histone deacetylase isoforms in human frontal cortex, human retina, and mouse brain. PLoS One. 2015 May 11;10(5):e0126592.
311. McQuown SC, Barrett RM, Matheos DP, Post RJ, Rogge GA, Alenghat T, Mullican SE, Jones S, Rusche JR, Lazar MA, Wood MA. HDAC3 is a critical negative regulator of long-term memory formation. J Neurosci. 2011 Jan 12;31(2):764-74.
312. Wu Y, Hou F, Wang X, Kong Q, Han X, Bai B. Aberrant Expression of Histone Deacetylases 4 in Cognitive Disorders: Molecular Mechanisms and a Potential Target. Front Mol Neurosci. 2016 Nov 1;9:114.
313. Parmigiani RB, Xu WS, Venta-Perez G, Erdjument-Bromage H, Yaneva M, Tempst P, Marks PA. HDAC6 is a specific deacetylase of peroxiredoxins and is involved in redox regulation. Proc Natl Acad Sci U S A. 2008 Jul 15;105(28):9633-8.
314. Zhang L, Liu C, Wu J, Tao JJ, Sui XL, Yao ZG, Xu YF, Huang L, Zhu H, Sheng SL, Qin C. Tubastatin A/ACY-1215 improves cognition in Alzheimer's disease transgenic mice. J Alzheimers Dis. 2014;41(4):1193-1205.
315. Zeng Q, Long Z, Feng M, Zhao Y, Luo S, Wang K, Wang Y, Yang G, He G. Valproic Acid Stimulates Hippocampal Neurogenesis via Activating the Wnt/β-Catenin Signaling Pathway in the APP/PS1/Nestin-GFP Triple Transgenic Mouse Model of Alzheimer's Disease. Front Aging Neurosci. 2019 Mar 26;11:62.
316. Fernando WMADB, Martins IJ, Morici M, Bharadwaj P, Rainey-Smith SR, Lim WLF, Martins RN. Sodium Butyrate Reduces Brain Amyloid-β Levels and Improves Cognitive Memory Performance in an Alzheimer's Disease Transgenic Mouse Model at an Early Disease Stage. J Alzheimers Dis. 2020;74(1):91-99.

317. Zhang ZY, Schluesener HJ. Oral administration of histone deacetylase inhibitor MS-275 ameliorates neuroinflammation and cerebral amyloidosis and improves behavior in a mouse model. J Neuropathol Exp Neurol. 2013 Mar;72(3):178-85.
318. Marinho D, Ferreira IL, Lorenzoni R, Cardoso SM, Santana I, Rego AC. Reduction of class I histone deacetylases ameliorates ER-mitochondria cross-talk in Alzheimer's disease. Aging Cell. 2023 Aug;22(8):e13895.
319. Luo B, Chen J, Zhou GF, Xie XY, Tang J, Wen QX, Song L, Xie SQ, Long Y, Chen GJ, Hu XT. Apicidin attenuates memory deficits by reducing the Aβ load in APP/PS1 mice. CNS Neurosci Ther. 2023 May;29(5):1300-1311.
320. Green KN, Steffan JS, Martinez-Coria H, Sun X, Schreiber SS, Thompson LM, LaFerla FM. Nicotinamide restores cognition in Alzheimer's disease transgenic mice via a mechanism involving sirtuin inhibition and selective reduction of Thr231-phosphotau. J Neurosci. 2008 Nov 5;28(45):11500-10.
321. Chittasupho C. Multivalent ligand: design principle for targeted therapeutic delivery approach. Ther Deliv. 2012 Oct;3(10):1171-87.
322. Chandni Pathak, Uma D. Kabra, A comprehensive review of multi-target directed ligands in the treatment of Alzheimer's disease, Bioorganic Chemistry, Volume 144, 2024, 107152, ISSN 0045-2068.
323. L.M. Espinoza-Fonseca, The benefits of the multi-target approach in drug design and discovery, Bioorg. Med. Chem. 14 (2006) 896–897.
324. L. Blaikie, G. Kay, P.K. Lin, Current and emerging therapeutic targets of Alzheimer's disease for the design of multi-target directed ligands, Med. Chem. Comm. 10 (12) (2019) 2052–2072.
325. D. Mu˜noz-Torrero, Multitarget anti-Alzheimer hybrid compounds: do they work in vivo? Design of Hybrid Mol. Drug Devel. (2017) 167-192.
326. S.S. Gujral, A. Shakeri, L. Hejazi, P.P. Rao, Design, synthesis and structure-activity relationship studies of 3 phenylpyrazino [1, 2-a] indol-1 (2H)-ones as amyloid aggregation and cholinesterase inhibitors with antioxidant activity, Eur. J. Med. Chem. Reports 6 (2022) 100075.
327. P.F. Lamie, M.M. Abdel-Fattah, J.N. Philoppes, Design and synthesis of new indole drug candidates to treat Alzheimer's disease and targeting neuro- inflammation using a multi-target-directed ligand (MTDL) strategy, Enzyme, Inhib. Med. Chem. 37 (1) (2022) 2660–2678.
328. G.F. Makhaeva, N.V. Kovaleva, N.P. Boltneva, E.V. Rudakova, S.V. Lushchekina, T.Y. Astakhova, I.V. Serkov, A.N. Proshin, E.V. Radchenko, V.A. Palyulin, J. Korabecny, Bis-amiridines as acetylcholinesterase and butyrylcholinesterase cholinesterase and monoamine oxidase inhibitors, J. Mol. Struct. 1271 (2023) 134138.
329. D. Vicente-Zurdo, N. Rosales-Conrado, M.E. Le´on-Gonz´alez, L. Brunetti, L. Piemontese, A.R. Pereira-Santos, S.M. Cardoso, Y. Madrid, S. Chaves, M. A. Santos, Novel rivastigmine derivatives as promising multi-target compounds for potential treatment of Alzheimer's disease, Biomedicines 10 (7) (2022) 1510.
330. Maes et al, PLOS ONE 15(5): e0233468.
331. ORYZON, Vafidemstat,
332. Maiques-Diaz A, Somervaille TCP. LSD1: biologic roles and therapeutic targeting. Epigenomics. 2016;8:1103–1116.
333. Hirano K, Namihira M. New insight into LSD1 function in human cortical neurogenesis. Neurogenesis. 2016;3:e1249195.

334. Swahari V, West AE. Histone demethylases in neuronal differentiation, plasticity, and disease. Curr Opin Neurobiol. 2019;59:9–15.
335. Jost WH. A critical appraisal of MAO-B inhibitors in the treatment of Parkinson's disease. J Neural Transm (Vienna). 2022 Jun;129(5-6):723-736.
336. Peedicayil, J., & Grayson, D. R. (2025). Vafidemstat: a lysine-specific demethylase 1A inhibitor that shows promise for treating neuropsychiatric disorders. Epigenetics Reports, 3(1).
337. Song Y, Qin L, Yang R, Yang F, Kenechukwu NA, Zhao X, Zhou X, Wen X, Li L. Inhibition of HDAC6 alleviating lipopolysaccharide-induced p38MAPK phosphorylation and neuroinflammation in mice. Pharm Biol. 2019 Dec;57(1):263-268.
338. Grychowska K, Chaumont-Dubel S, Kurczab R, Koczurkiewicz P, Deville C, Krawczyk M, Pietruś W, Satała G, Buda S, Piska K, Drop M, Bantreil X, Lamaty F, Pękala E, Bojarski AJ, Popik P, Marin P, Zajdel P. Dual 5-HT6 and D3 Receptor Antagonists in a Group of 1H-Pyrrolo[3,2-c]quinolines with Neuroprotective and Procognitive Activity. ACS Chem Neurosci. 2019 Jul 17;10(7):3183-3196.
339. Grychowska K, Satała G, Kos T, Partyka A, Colacino E, Chaumont-Dubel S, Bantreil X, Wesołowska A, Pawłowski M, Martinez J, Marin P, Subra G, Bojarski AJ, Lamaty F, Popik P, Zajdel P. Novel 1H-Pyrrolo[3,2-c]quinoline Based 5-HT6 Receptor Antagonists with Potential Application for the Treatment of Cognitive Disorders Associated with Alzheimer's Disease. ACS Chem Neurosci. 2016 Jul 20;7(7):972-83.
340. Amodeo DA, Peterson S, Pahua A, Posadas R, Hernandez A, Hefner E, Qi D, Vega J. 5-HT6 receptor agonist EMD386088 impairs behavioral flexibility and working memory. Behav Brain Res. 2018 Sep 3;349:8-15.
341. Millan MJ, Dekeyne A, Gobert A, Brocco M, Mannoury la Cour C, Ortuno JC, Watson D, Fone KCF. Dual-acting agents for improving cognition and real-world function in Alzheimer's disease: Focus on 5-HT6 and D3 receptors as hubs. Neuropharmacology. 2020 Oct 15;177:108099.
342. Yang P, Perlmutter JS, Benzinger TLS, Morris JC, Xu J. Dopamine D3 receptor: A neglected participant in Parkinson Disease pathogenesis and treatment? Ageing Res Rev. 2020 Jan;57:100994.
343. Chen PC, Lao CL, Chen JC. The D(3) dopamine receptor inhibits dopamine release in PC-12/hD3 cells by autoreceptor signaling via PP-2B, CK1, and Cdk-5. J Neurochem. 2009 Aug;110(4):1180-90.
344. Salles MJ, Hervé D, Rivet JM, Longueville S, Millan MJ, Girault JA, Mannoury la Cour C. Transient and rapid activation of Akt/GSK-3β and mTORC1 signaling by D3 dopamine receptor stimulation in dorsal striatum and nucleus accumbens. J Neurochem. 2013 May;125(4):532-44.
345. Łażewska D, Olejarz-Maciej A, Reiner D, Kaleta M, Latacz G, Zygmunt M, Doroz-Płonka A, Karcz T, Frank A, Stark H, Kieć-Kononowicz K. Dual Target Ligands with 4-tert-Butylphenoxy Scaffold as Histamine H3 Receptor Antagonists and Monoamine Oxidase B Inhibitors. Int J Mol Sci. 2020 May 12;21(10):3411.
346. Bautista-Aguilera ÓM, Budni J, Mina F, Medeiros EB, Deuther-Conrad W, Entrena JM, Moraleda I, Iriepa I, López-Muñoz F, Marco-Contelles J. Contilisant, a Tetratarget Small Molecule for Alzheimer's Disease Therapy Combining Cholinesterase, Monoamine Oxidase Inhibition, and H3R Antagonism with S1R Agonism Profile. J Med Chem. 2018 Aug 9;61(15):6937-6943.
347. Sadek, B.; Saad, A.; Sadeq, A.; Jalal, F.; Stark, H. Histamine H3 receptor as a potential target for cognitive symptoms in neuro- psychiatric diseases. Behav. Brain Res. 2016, 312, 415−430.
348. Lan, Y.; Chen, Y.; Cao, X.; Zhang, J.; Wang, J.; Xu, X.; Qiu, Y.; Zhang, T.; Liu, X.; Liu, B.-F.; Zhang, G. Synthesis and biological evaluation of novel sigma-1 receptor antagonists based on pyrimidine scaffold as agents for treating neuropathic pain. J. Med. Chem. 2014, 57, 10404−10423.

349. Nguyen, L.; Lucke-Wold, B. P.; Mookerjee, S. A.; Cavendish, J. Z.; Robson, M. J.; Scandinaro, A. L.; Matsumoto, R. R. Role of sigma-1 receptors in neurodegenerative diseases. J. Pharmacol. Sci. 2015, 127, 17−29.
350. Maurice, T.; Goguadze, N. Role of σ1 receptors in learning and memory and Alzheimer's disease-type dementia. Adv. Exp. Med. Biol. 2017, 964, 213−233.
351. Sguazzini, E.; Schmidt, H. R.; Iyer, K. A.; Kruse, A. C.; Dukat, M. Reevaluation of fenpropimorph as a σ1 receptor ligand: structure- affinity relationship studies at human 1 receptors. Bioorg. Med. Chem. Lett. 2017, 27, 2912−2919.
352. Donnier-Maré chal, M.; Carato, P.; Larchanche, P.-E.; Ravez, S.; Boulahjar, R.; Barczyk, A.; Oxombre, B.; Vermersch, P.; Melnyk, P. Synthesis and pharmacological evaluation of benzamide derivatives as potent and selective sigma-1 protein ligands. Eur. J. Med. Chem. 2017, 138, 964−978.
353. Díaz, J. L.; Cuberes, R.; Berrocal, J.; Contijoch, M.; Christmann, U.; Ferná ndez, A.; Port, A.; Holenz, J.; Buschmann, H.; Laggner, C.; Serafini, M. T.; Burgueñ o, J.; Zamanillo, D.; Merlos, M.; Vela, J. M.; Almansa, C. Synthesis and biological evaluation of the 1-arylpyrazole class of σ1 receptor antagonists: identification of 4-{2- [5-methyl-1-(naphthalen-2-yl)-1H-pyrazol-3-yloxy]ethyl}morpholine (S1RA, E-52862). J. Med. Chem. 2012, 55, 8211−8224.
354. Meunier, J.; Ieni, J.; Maurice, T. The anti-amnesic and neuroprotective effects of donepezil against amyloid β25-35 peptide- induced toxicity in mice involve an interaction with the σ1 receptor. Br. J. Pharmacol. 2006, 149, 998−1012.
355. Alonso, G.; Phan, V.; Guillemain, I.; Saunier, M.; Legrand, A.; Anoal, M.; Maurice, T. Immunocytochemical localization of the sigma1 receptor in the adult rat central nervous system. Neuroscience 2000, 97, 155−170.